Mean and Fluctuating Pressures on an Automotive External Rear View Mirror

A thesis submitted for the
Degree of Masters of Engineering

By

Rajneesh Jaitlee

School of Aerospace, Mechanical and Manufacturing Engineering
RMIT University
Melbourne
Australia

March 2006

Abstract

The primary function of an automobile rear View Mirror is to provide the driver with a clear vision interpretation of all objects to the rear and side of the vehicle. The rear View Mirror is a bluff body and there are several problems associated with the rear View Mirror. These include buffeting, image distortion (due to aerodynamically induced and structural vibration), aerodynamically induced noise (due to cavities and gaps) and water and dirt accumulation on Mirror glass Surface. Due to excessive glass vibration, the rear View Mirror may not provide a clear image. Thus, vibrations of Mirror can severely impair the driver's vision and safety of the vehicle and its occupants. The rear View Mirrors are generally located close to the A-pillar region on the side window. A conical vortex forms on the side window close to A-pillar due to A-pillar geometry and the presence of side rear View Mirror and flow separation from it makes the airflow even more complex.

The primary objective of this work is to study the aerodynamic pressures on Mirror Surface at Various speeds to determine the effects of aerodynamics on to Mirror vibration. Additionally, the Mirror was modified by Shrouding around the external periphery to determine the possibility of minimisation of aerodynamic pressure fluctuations and thereby vibration. The Shrouding length used for the analysis was of 24mm, 34mm and 44mm length. The mean and fluctuating pressures were measured using a production rear side View Mirror fitted to a ¼ quarter production passenger car in RMIT Industrial Wind Tunnel. The tests were also conducted in semi-isolation condition to understand influence of the A-pillar geometry. The mean and fluctuating pressures were converted into non-dimensional pressure coefficients (Cp and Cprms) and the frequency content of the fluctuating pressure was analysed. The results show that the fluctuating aerodynamic pressures are not uniformly distributed over an automobile Mirror Surface. The highest magnitude of fluctuating pressure for the standard Mirror was found at the central bottom part of the Mirror Surface. The highest magnitude of fluctuating pressure for the modified Mirror was found at the central top part of the Mirror Surface. As expected, the modification has significant effect on the magnitude of fluctuating pressure. The results show that an increase of Shrouding length reduces the magnitude of the fluctuating pressure. The frequency-based analysis was done to understand the energy characteristics of the flow, particularly to its phase, since it is the out of phase components

that usually cause Mirror rotational vibration. The spectral analysis showed that the magnitude of the energy distribution reduces with increase of shrouding length throughout the frequency range. Flow visualisation was also used to supplement the pressure data.

The effects of yaw angles were not included in this study, however, are thought to be worthy of further investigation. On road testing and the variation of mirror locations might have some effects on the fluctuating pressures. These need to be investigated in the future work. The quarter model used in this study was a car specific. However, for more generic results, a simplified model with variable geometry can be used in future study.

1.1 Acknowledgements

I want to express my whole-hearted thanks and gratitude to my first supervisor Dr. Firoz Alam for his guidance, efforts, encouragement, advice and assistance. I am also thankful to my second supervisor Associate Professor Simon Watkins for his feedback, assistance and encouragement through out the course of project. Without their advice, expert assistance and encouragements, this project would never have been possible.

I also acknowledge the assistance of the workshop technical staff, Mr. Brett Vincent and especially to Mr. Gilbert Atkins at the School of Aerospace, Mechanical and Manufacturing Engineering, RMIT University for their assistance with the equipment facilities and wind tunnel usage. I would also like to thank the Commonwealth Government of Australia for providing financial assistance to me for this work.

I also owe a heartfelt thanks to my fellow post graduate friends especially to Mr. Suhaib Mohammad Ali and Mr. Kaneslingam for their assistance and advice during my testing in RMIT Industrial Wind Tunnel and thesis writing. Their moral and mental support throughout the year was invaluable and greatly contributed to the work presented.

Last but not least, I'd like to thank my parents Mr K L Jaitlee and Mrs Tripta Jaitlee for their encouragement, inspiration and patience during the time it took to complete my thesis. Finally, I would also like to express my sincere appreciation to my fiancé Dr. Aarti Sharma for her encouragement, inspiration and tolerance during the time it took to complete this work.

DECLARATION

I, Rajneesh Jaitlee, hereby submit the thesis titled Mean and Fluctuating Pressures on an Automotive External Rear View Mirror for the degree of Master of Engineering and certify that except where due acknowledgement has been made, the work is that of the candidate alone; the work has not been submitted previously, in whole or in part, for any other academic award and that the content of the thesis is the result of work which has been carried out since the official commencement of the approved research program.

RAJNEESH JAITLEE

March 2006

Table of Contents

Figures **Page No.**

List of Figures

Chapter 1 – Introduction

Chapter 2 - Facilities, Equipment and Data Processing

Chapter 3 – Quarter Model Testing

Chapter 4 – Semi - Isolation Testing

Chapter 5 – Results and Discussion

Appendix A

Quarter Model

Appendix B

Semi- Isolation Model

Appendix C

PSD Comparison for Point 47

Appendix E

Mirror Housing Surface Mean Pressure Coefficient (Cp)

Appendix F

Mirror Housing Surface Mean Pressure Coefficient (Cp)

List of Tables

1.1.1 Chapter 3 – Quarter Model Testing

1.1.2 Chapter 4- Semi-Isolation Testing

1.1.3 Chapter 5- Results and Discussion

Nomenclature

S_t:	Strouhal number
ω:	Frequency of Vortices
l:	Length scale
V:	Fluid Velocity
Re:	Reynolds number
ρ:	Fluid Density
μ:	Viscosity
L:	Characteristic Length
U:	Velocity
f_n:	Natural Frequency
F:	Forcing Factor
k:	Stiffness of system
x:	Displacement
m:	Mass of the Dynamic System
k:	Stiffness of the System.
Hz:	Hertz

Chapter 1
Introduction

1. Introduction

Wind noise is critical passenger discomfort attribute due to its high intensity and low frequency. Generally, wind noise contributes to the pressure variation that's being developed on the surface of the automobile due to its motion. However, rear view mirror and side glass of an automobile represents a problematic and interesting area to the vehicles manufacturer. Automotive industry in today's world is highly competitive and new technologies along with their engineers are looking to improve the vehicle designs, which results to reduce the cost and simultaneously improve its productivity and safety features. In this chapter, the background to the research topic with its rationale is described and initiated. The objective and scope are mentioned in the later part of this chapter.

1.1 Background

The airflow around a road vehicle is very complex especially at high speeds. When the vehicle is moving, it displaces air to the surrounding and creates a wind resistive motion against direction of motion of vehicle known as aerodynamic drag. A moving car dissipates the airhead so that the air is forced to flow from the front end to the back of the car. Figure 1.1 shows as car move forward air accelerate at the front end (hood side) in order to maintain the volumetric displacement. However when the air moves over the roof the air movement will be at its maximum but it causes reduction in the air pressure in that region. When the air moves at the end section (trunk) of the car, its pressure rises causing the air molecules to move closer to the car body. Thus the pressure over much of the vehicle surface fluctuates with time due to complex vehicle's geometry and crosswinds while in motion. The air velocity and pressure reaches to their highest and lowest values at the top of the front windscreen, towards the rear of roof and when there is change in shape where the screen tilts downwards there is reduction in air speed which causes rise in pressure. A schematic of flow pattern over the passenger car is shown in Figure 1.2

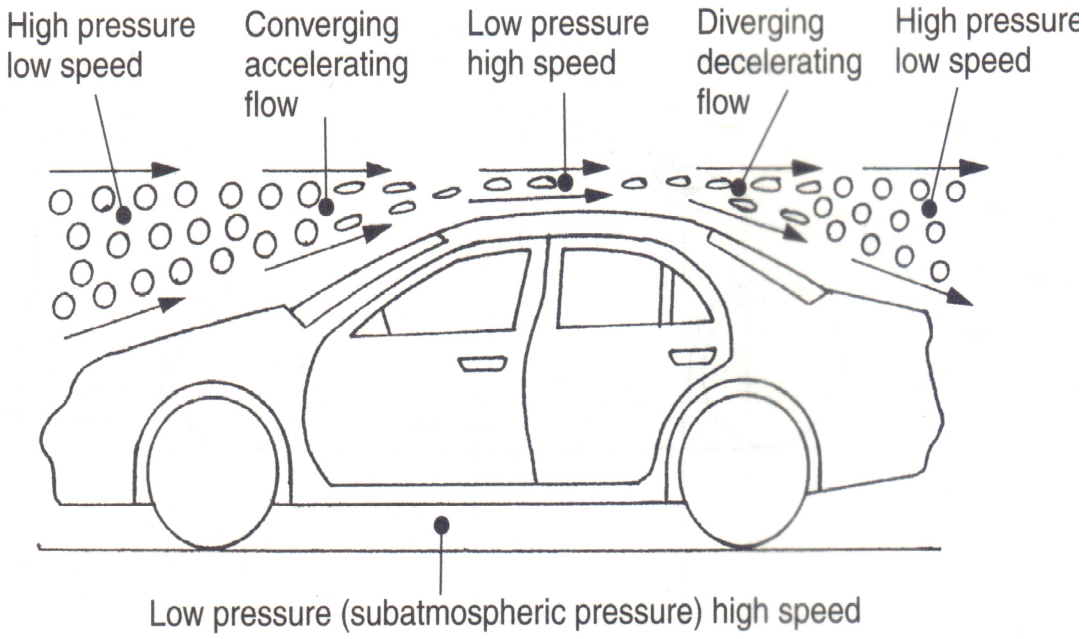

Figure 1.1: Relative air speed and pressure condition over the surface of a moving car (Heisler, 2002)

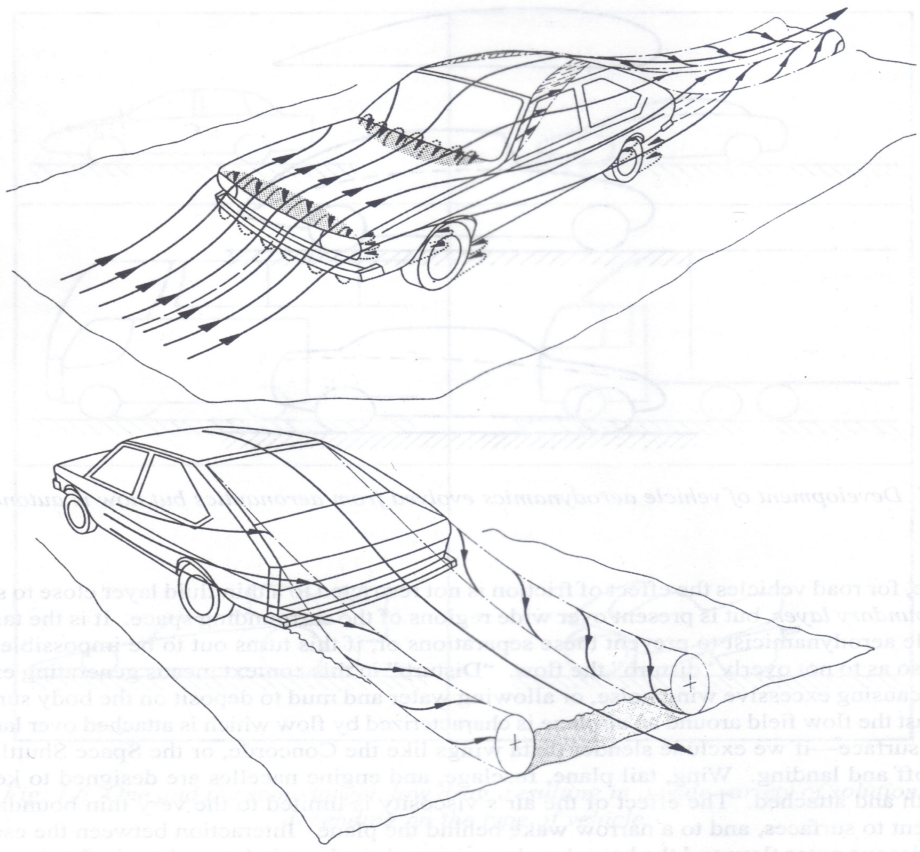

Figure 1.2: A schematic flow pattern around a passenger car, Hucho (1999)

In today's world due to continuos technological improvements we are able to reduce aerodynamic drag by streamlining the car shapes. However, passenger comfort becomes an essential criterion for marketing. Comfort is now the most influential and dominating field of research in vehicle aerodynamics. Aerodynamics in road vehicles have become an important part in automobiles industry as it encompasses vehicle performance, comfort, safety, stability, cooling and visibility, see Figure 1.3.

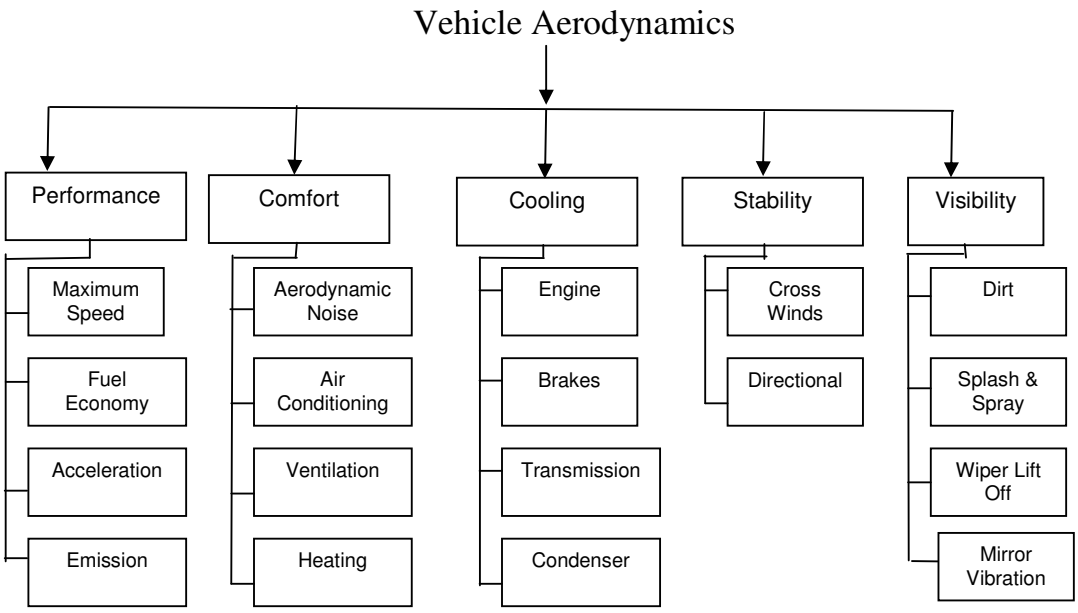

Figure 1.3: Spectrum of Vehicle Aerodynamics (Adapted from Hucho, 1999)

1.2 Bluff Body Aerodynamics

A bluff body has a non-streamlined shape that produces considerable wind resistance when immersed in a moving air. It has regions of separated flow over a large portion of the surface, which results in a high-pressure drag and a large wake region. The flow over a bluff body is unsteady and causes vortex formation and vortex shedding. Vortex shedding not only depends on the external shape of the object but also on parameter like turbulence, surface roughness and Reynolds's number. Hucho (1998) stated vortex shedding of the rear view mirror of an automobile is believed to have a substantial effect due to airflow-induced vibration. Bluff bodies are widely encountered in many engineering applications and design problems. These include in many every day to day situation such as wind/structures, interaction on buildings,

transportation, and sports. Industrial applications include mixing, turbines and cooling of electrical components; automobile application includes flow past the rear view mirror.

An automobile rear view mirror is considered as a bluff body. Rear view mirror is sometimes also called a wing mirror. The primary function of automobile rear view mirrors is to provide visual information to the driver about surroundings outside the vehicle, such that the driver does not divert his attention away from the vehicle's motion. The rear view mirror has surface irregularities located in a region of local high-speed flow, which causes high wind noise levels. Moreover, the location of the wing mirrors is in a very complex environment. Automobile manufacturers invest significant resources into research and developments towards optimisation of airflow over the vehicles to reduce drag resulting in decrease of fuel consumption with an increase in efficiency and to reduce aerodynamically generated noise, vibration and harshness (NVH). The focus in this area is on improving the comfort level for the occupants, along with enhancing the safety aspects of the vehicle at the same time. The aesthetics of an automobile remains the predominant attraction force behind consumer's sales, followed by safety, comfort and performance. However, for marketing purpose the automobile shape and design is important factor that comprises of aesthetics, safety, comfort, and performance. Therefore, it is a challenge for automotive manufacturers to continuously improve qualities in vehicle design including mirror, whilst enhancing the aesthetic appeal of products as criterion.

Rear view mirrors of an automobile have high drag coefficients in relation to their individual frontal area. The overall drag contribution from the pair of rear view mirrors on a passenger car is in the order of 0.01, which is negligible to the car body. The mirror unit on the passenger cars is streamlined and the mirror housing section that faces the approaching air is shaped in order to minimise flow separation and aerodynamic drag. The flow separation at the mirror housing can be periodic that produces oscillating mirror load, which can cause severe vibration on mirror face, resulting in image blurring. The wing mirror also have long, wide wake that disturbs the flow on the side surface of car. The airflow over the wing mirror is turbulent, when the airflow approaches the body it separates that causes formation of vortices and wake region. It is due to this turbulent flow that the wake pressure will change resulting in pressure fluctuation on the mirror glass surface. The vortices formed are called as Von Karmen Vortex and can be characterised by the Strouhal number (S_t). The bluff mirror fore

body with the mirror is placed at its flat cut-off base and attachment to the A-pillar area, which produces a long separation bubble extending downstream with the ensuing high turbulence unsteady flow persisting along almost the entire length of car. Continuous aerodynamically induced noise from the wake of the mirror does not directly affect the safety of the vehicle. However, it is distortion of the reflected image from the wing mirror that causes a safety concern at higher speeds. It is due to the fact that mirror face experience rotational motion rather than translational motion.

1.2.1 Bluff body and Flow Separation

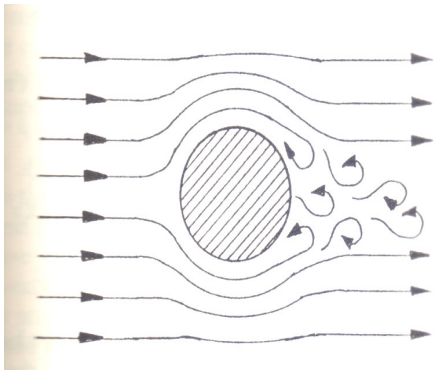

a.) Circular Section

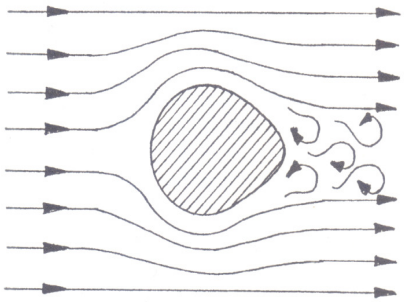

b.) Circular/Lobe Section

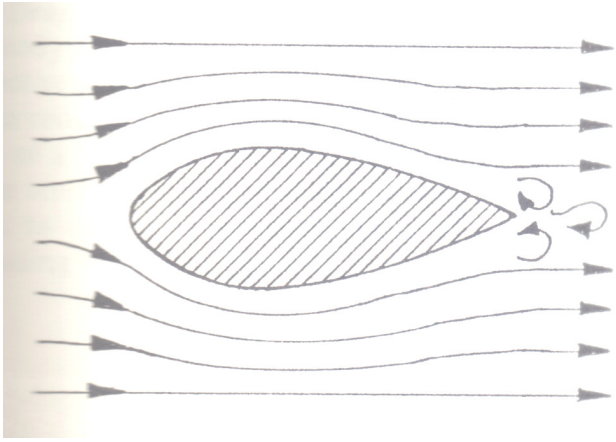

c.) Aerofoil Section

Figure 1.4: Some examples of bluff body aerodynamics (Heisler, 2002)

Figure 1.4 shows some basic cross sections for the bluff bodies. The flow pattern over the bluff body is highly dependent on the Reynolds number (*Re)* which is a dimensionless parameter and is defined as the ratio of the inertial forces to the viscous forces.

$$\mathrm{Re} = \frac{\rho UL}{\mu} \quad \ldots \qquad \ldots \quad (1.1)$$

Where,

ρ: fluid density

μ: viscosity

L: characterized length

U: velocity

At high Reynolds number the inertial forces are large relative to the viscous forces causing rapid fluctuation in the fluid, whereas at low Reynolds number the viscous forces are more dominant over the inertial forces. The flow at low Reynolds number (<1) is described as creeping flow. In this case the flow remains laminar and fully attached over the entire body. However, at slightly higher Reynolds number (4<Re<40) separated eddies are generated behind the bluff body. The vortex shedding occurs within a certain range of Reynolds number regime (80<Re<200), during which unsteady wake exhibits from bluff body. Above Reynolds number 150-vortex shedding is a 2-dimensonal phenomenon as it exhibits 2-dimensional characteristics. Gerrad (1996) identified different ways of vortex shedding:

a) Oblique shedding
b) Dislocation of vortices
c) Looping of vortices

In case of Reynolds number <200, eddies are laminar and are shed at distinct frequency. As the Reynolds number increases beyond 400, transition to turbulence occurs at the separation point. Figure 1.5, shows the different flow patters at various Reynolds number (Re).

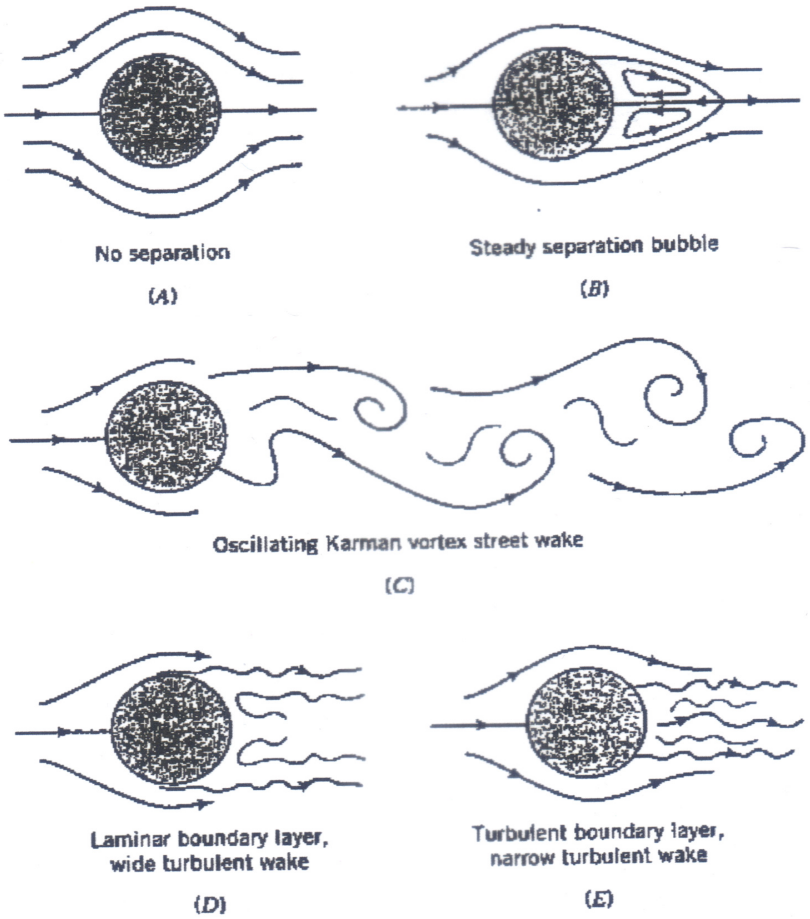

Figure 1.5: Typical flow patterns past cylinder at various Reynolds's Numbers (Munson et al, 1998)

1.3 Mirror Aerodynamic

The flow around the mirror causes aerodynamic noise. The physical reason is periodic flow separation due to its location in complex environment near A-pillar. In the region of periodic flow separation, vortices are shed which move downstream in a wake and can be observed for a long distance. The flow field is unsteady due to periodic vortex shedding which can be expressed as Strouhal number (S_t). Vortices are typically shed when Strouhal number is approximately 0.2. The Strouhal number is a dimensionless parameter, which measures the ratio of inertia forces due to unsteadiness of flow to the inertia forces due to changes in velocity from point to point the flow field.

$$S_t = \frac{\omega l}{V} \qquad \ldots (1.2)$$

Where,

ω: Frequency of vortices

l: length scale

V: fluid velocity

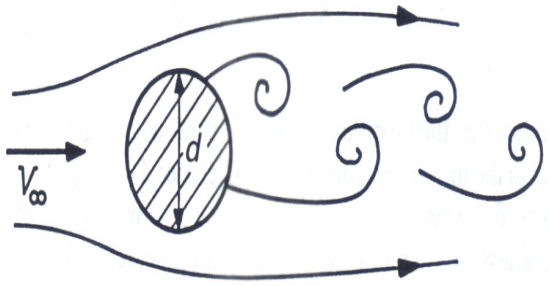

Figure 1.6: Schematic view of periodic vortex shedding from circular cylinder.

1.4 Sources of Mirror Vibration

There are three different types of vibration that cause mirror to vibrate and results in image blurring at high speeds, see Figure 1.7.

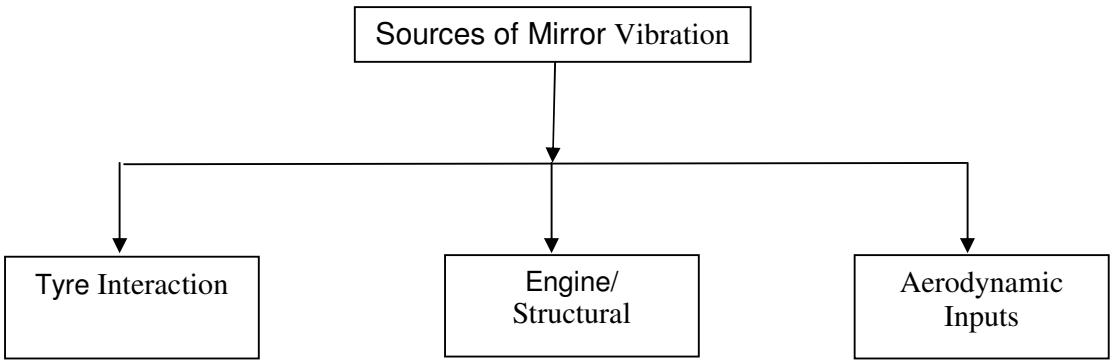

Figure 1.7: Types of Mirror vibration

1.4.1 Road Induced Vibration

The road-induced vibration is caused directly from the contact of tyres with road surface. Road surface and obstructions such as potholes, bumps, uneven surface cause these vibration which severally affect the mirror vibration. The frequency of road-induced vibration is very low.

1.4.2 Mechanically Induced Vibration

Mechanically induced vibrations originate due to the vibration in the engines, moving of mechanically coupled transmissions etc. The natural frequency (f_n) of a structure including the wing mirror can be mathematically defined in equation (1.3). Mechanically induced structure vibration can be due to periodic vortex shedding, as the frequency of the peak level is proportional to the local air speed. The vibration can also be due to buffeting of housing caused by change in external flow approaching mirror (Watkins 2004)

$$f_n = \frac{1}{2\pi}\sqrt{\frac{k}{m}} \quad \text{Hz} \qquad \ldots (1.3)$$

Where,

m=mass of the dynamic system

k = stiffness of the system.

Moreover, vibrations in mirror can be a forcing function. A simple dynamic system with a forcing function is described in the equation (1.4)

$$m\ddot{x} + kx = F \qquad \ldots (1.4)$$

Where,

F: Forcing Factor

k: Stiffness of system

x: Displacement

1.4.3 Aerodynamic Vibration

Movement of air causes aerodynamically induced vibration over the mirror surface at high speeds due to its complex location and geometry. The main aerodynamic influences in automobiles on this airflow include: the shape of the vehicle bonnet, the geometry of the A-pillar region, and the location of the wing mirrors. Things like polar moment of inertia, damping coefficient of mirror and plate, flow angles, turbulence and angular stiffness characteristics are some of the design specific concern that contribute to the pressure fluctuations across the surface of the wing mirror glass. Vortex shedding, turbulent buffeting, base pressure fluctuation and separated flows also cause the aerodynamically induced vibration. The aesthetics of the mirror geometry will affect its size, direction and wake properties that will interact with complex A-pillar flow. The aerodynamic forces acting on the mirror housing are internally transferred through to the mirror structure and later to the glass. Fluctuating moments on the mirror glass arise due to the differences in internal pressure in the mirror housing (i.e. inside shell housing) and the fluctuating base pressure on the glass surface. The resulting motion of the mirror glass is a combination of all the inputs and their individual transfer and admittance functions to the mirror glass. Therefore, it is considerable complexity in a full analysis of the rotational response of the mirror. Wing mirrors are fixed onto a mounting plate behind which is a pivot, from which vibration is transferred to and from the mirror. Image blurring arises from a rotational vibration of the mirror glass that differs with respect to that of time. A modern external mirror typically consists of a plastic housing or shell, on which two DC motors are mounted from inside, connected together with screw threads at its pivot, with a support of a backing plate. The reflective glass (referred to as the mirror) is later on mounted over this backing plate and screw threads permit adjustments to suite driver's visibility at different viewing angles. Figure 1.8 shows the schematic of mirror vibration due to all inputs.

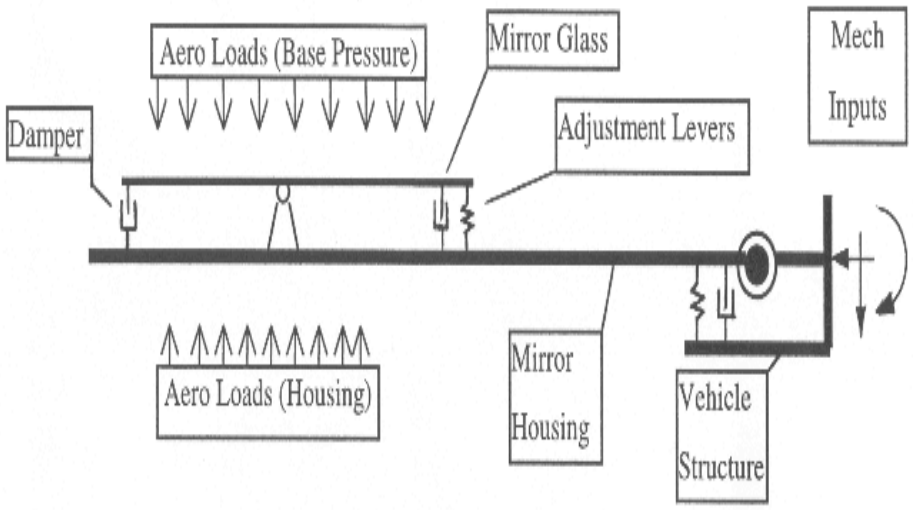

Figure 1.8: Schematic of mirror vibration due to all inputs (Oswald, 1999)

The location of mirror attachment is in a complex area as the structural geometry of the A-pillar has significant influence on flow pattern in this area. The flow around the A-pillar is very complex due to the formation of the conical vortex that expands and travels towards the roof on the side window studied by Alam (2000).

Alam et al. (1998) experimented with various vehicle velocities at different yaw angles and found some Reynolds number dependency at low velocity. They observed a larger separation on the leeward side with associated velocity drop and increased turbulence intensity. Alam (200) extended the test on various windshield radiuses to see its effects on A-pillar flow behaviour. It was found that fluctuating pressure have strong dependence on A-pillar radius. Alam also found the surface mean and fluctuating pressure coefficients are independent of Reynolds number at high velocities and maximum pressure fluctuation occurs between areas of separation and reattachment of A-pillar vortex.

Oswald (1999) showed during wind tunnel and on-road testing conducted that wing mirror vibration above 20Hz was primarily the result of aerodynamic inputs, rather than mechanical origin. He suggested that the levels of angular rotation of the wing mirror above 20Hz were very similar to that of wind tunnel tests, whereas below 20Hz, on-road tests showed significantly higher vibrations in the wing mirror. However, from this he concluded that

influence of aerodynamic input were more prevalent above 20Hz. This was due to the fact that because no mechanical vibrations were present during wind tunnel testing, as the vehicle was stationary and with the engine off. The Figure 1.9 illustrates test results for vibrational spectra of a mirror at different yaw angles at 100 km/h. Yaw angle (ψ) can be defined as the difference between the relative velocity and the vehicle centre line.

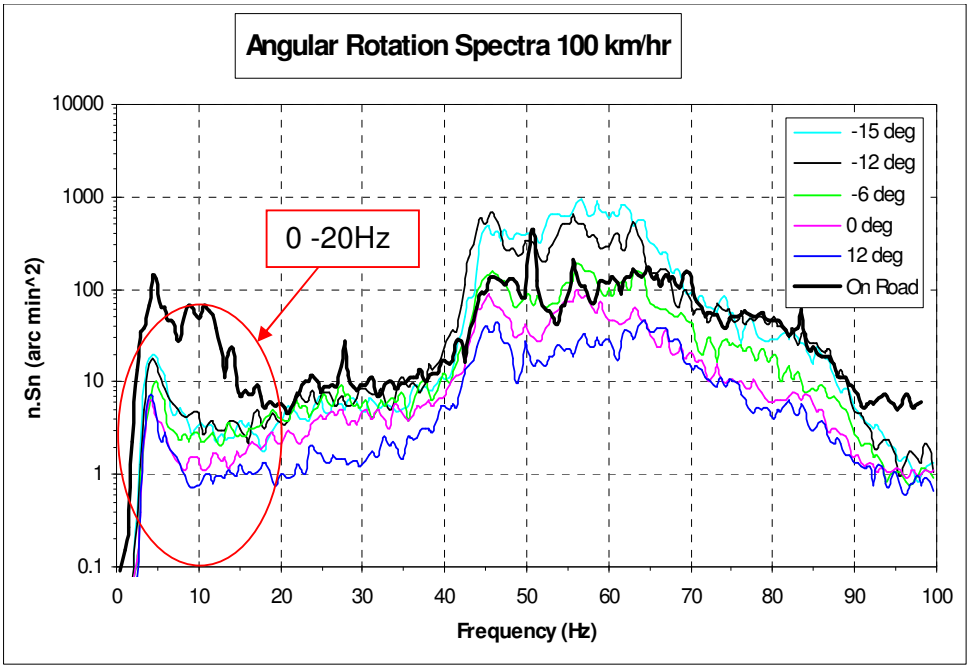

Figure 1.9: Angular Rotation Spectra at 100 km/h (Oswald, 1999)

Watkins (SAE, 2004) studied the cause of the aerodynamically induced vibration, is through to a mix of turbulent buffeting arising from the unsteadiness in A-pillar vortex and base pressure fluctuations in the wake of the mirror acting on mirror glass. However at higher speeds, vibration in rear view mirror is due to the rotational motion of the mirror glass. Aerodynamic inputs on mirror housing, causes flow to be turbulent around A-pillar due to the A-pillar vortex and base pressure fluctuations. It is this turbulent flow that causes mirror vibration by buffeting the mirror housing. In general the airflow accelerates around the side and top of the car to the point of maximum frontal areas, and then decelerates as it closes around the vehicle. Generally at low frequency, road inputs are dominant factors whereas at high frequency the aerodynamics inputs play a vital role in mirror vibration. However, a small rotation about either its vertical or horizontal axis causes blurring of an image. It is a combination of all inputs on the mirror glass along with its transfer function that causes mirror

glass to vibrate. Moreover, fluctuating moments on the mirror glass can also be due to pressure difference between the mirror housing and the base pressure fluctuations.

On road and wind tunnel test were carried out and indicate considerable amount of aerodynamically induced vibration especially at frequencies of 30Hz and above (Watkins 1997). The peak in wind tunnel spectra of 4-5 Hz is considered to arise from the solid body vibration of car and was aerodynamically induced. However, tests for mirror translation and rotation both clearly showed that airflow is the main cause of mirror glass vibration at typically for on road high speeds for frequencies above 30Hz and may have strong effect at frequencies below it.

1.4.3.1 Flows around A-Pillar and Wing Mirror Location

Hucho (1998) found that the flow separations around the A-pillar produced an increase in drag of up to 2-5%. Hucho (1998) found that when pair of wing mirrors is used on a vehicle, total contribution of the two mirrors to the overall drag coefficient of the vehicle was estimated to be within the order of 0.01. However, airflow around A-pillar (region between windscreen and side glass) is very complex, non-uniform and turbulent with its turbulence intensities reaching 40% close to the side glass depending upon the yaw angles, Watkins et al. (1999).

Generally in the A-pillar region the local flow velocity tends to be at its highest and decelerates in downstream direction with enhanced turbulence intensity. The presence of wing mirror gave rise to rather complicated flow patter resulting in rapid pressure fluctuations within the wing mirror region. These fluctuations cause vibration on the mirror housing and across the mirror surface. The flow over wing mirror is unsteady and causes vortex formation and vortex shedding. It has a region of separated flow over a large portion of the surface, which results in a high-pressure drag force and a large wake region. This also gives rise to wide trailing wakes & pressure fluctuations across the rear of the mirror housing, and subsequently, vibrations across the front mirror glass through the mirror unit. Since it is exposed to flow separation around the A-pillar of the vehicle, it further compounds changes in the flow at different yaw angle. Enormous study and experiments were conducted showing the flow A-pillar (see Alam (2000), Haruna (1990), Popat (1991), and Zimmer (2004))

Stapleford and Carr (1971) revealed that external flow around car have large areas of separated flow and reattached flow by using a rectangular block at different yaw angles. A conical vortex is formed around this region that causes flow separation in A- pillar region and it travels upstream and downstream along the side window glass of the car to the roofline where it expands.

Watanabe et al. (1978) found that significant levels of aerodynamically induced noise and vibration were a result of flow separation around this region. They found that the highest fluctuating pressure was at the reattachment point of the separated flow. From their investigation it is unveiled that due to the A-pillar edge a high circumferential velocity vortex develops at the junction of the A-pillar and the vehicle bonnet. This complex flow pattern subsequently travels up the side of the vehicle windows causing the main aerodynamic flow to separate from the vehicle (Figure 1.10)

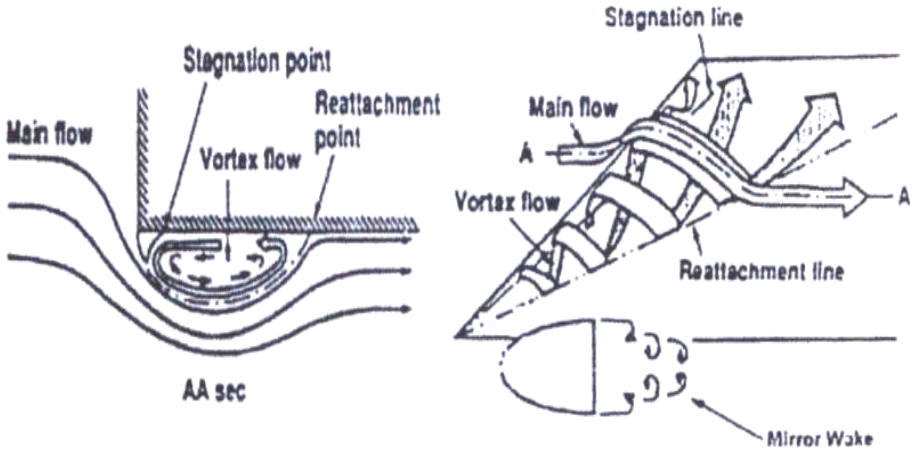

Figure 1.10: Flow-field around A-pillar (Watanabe et. al., 1978)

Other influence on the A-Pillar geometry includes the angle of windscreen and the subsequent airflow over the front part of the vehicle that contributes to this vortex. Haruna et al. (1990) studied the flow beyond the side window surface by measuring the surface pressure fluctuations along the window (Figure1.11). Homsi however concluded that separation region is dependent on the yaw angle and noted from the flow visualisation that re-attachment line with yaw angles clearly shifted resulting in wider separation when the yaw angles have been changed to -10˚.

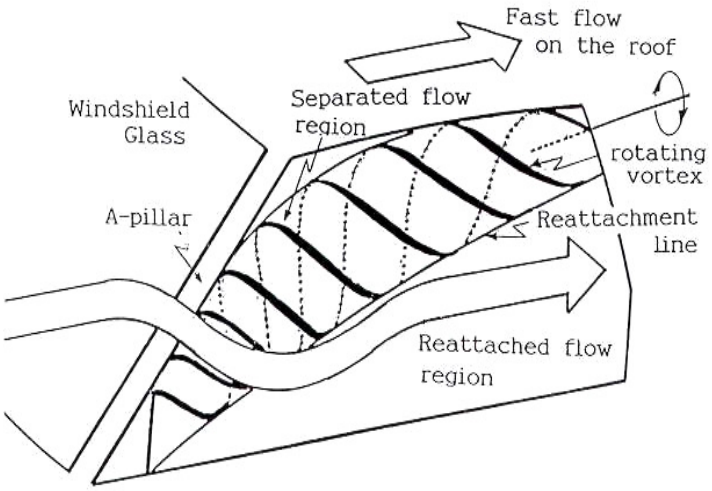

Figure 1.11: A-pillar flow pattern (Source: Haruna, 1990)

Popat (1991) strongly suggested that these geometric variables had significant effects on the flow into the A-Pillar region. Popat (1991) also analysed effects of windshield angle on the A-pillar vortex and flow-induced noise by measuring static and dynamic pressure measurements around A-pillar. From his pressure measurements at several positions he found that flow in A-pillar region is Reynolds number (Re) dependent & the highest fluctuating pressure was produced for yaw angles 40˚, this angle also has lowest mean pressure measurements.

Neienaltowska (1993) studied the velocity fluctuations on the side window with upstream velocity. The study performed measurements of fluctuating pressure around several points around A-pillar and local velocity for full-scale passenger car. His study couldn't establish any coherent relationship between fluctuating pressures and the local velocity and he concluded A-pillar region as turbulent and can be a cause of aerodynamically induced noise.

Ahuja (1996) carried an investigation to determine the importance of heights of A-pillar to the fluctuating pressure levels (FPL's) over the side glass of an automobile with and without mirror. He concluded that in the presence of side mirror, A-pillar height contributes a low frequency FPL in the region just downstream of A-pillar. Moreover, mirror is a very significant contributor to the low frequency energy of fluctuating pressure levels. The frequency at which the mirror contributes the FPL's was found to be a function of A-pillar height.

Homsi and Narain (1998) did vibration testing on body mounted plastic mirror and observed that during testing the side view mirror was vibrating excessively around 70mph. However, they concluded at these speeds the frequency of the flow induces unsteady forces that were close to the natural frequency of the mirror causing the mirror to vibrate and therefore obscuring the driving view. The vortex shedding behind the mirror is responsible for the unsteady forces acting on the mirror. The frequency of the vortex shedding depends on the geometry of the mirror and the angle of impingement of the incoming air. Vortex shedding is the source of the unsteady pressure field on the mirror. However, he concluded by suggesting a geometric modification and effective approach to control vibration caused by vortex shedding

Oswald (1999) studied movements of the mirrored surface of the wing mirror in 6 D.O.F and concluded that for a flat reflective surface (mirror glass), small translational movements in the plane of the surface did not alter the perceived image, and this can remain same for rotations about the axis perpendicular to the surface. Also, Oswald (1999) concludes that in general most objects are typically over 10 meters away from the wing mirror, and mirror movement usually within the order of 1mm; the object will generally stay within the depth of field and bear no adverse effects on the driver's functionality. Refocusing of the eyes is needed where a mirror surface produces slight shift in distance of image that causes translational movement perpendicular to the mirror surface

1.5 Human Peripheral Vision

Human eyes play an important role in interpreting reflected images from the automobiles mirror while driving. The human eyes ability of perceiving visual information is frequency sensitive i.e. it interacts differently at different frequencies. For example, at low frequencies the human eye translates visual stimuli as one continuous image, but on other hand at higher frequencies cause the image to become distorted, leading the brain to encounter difficulties in interpreting the information. The rear view mirror can move up to six degree of freedom. If the mirror glass is to move in a translational direction i.e. along the line of vision, then in that case the image will be distorted rather than blurring, which can be a safety concern for driver at high speeds. However, if the mirror glass is to rotate, which it may at high frequency then

in that case it may be a blur. The vibrating characteristics of the mirror depend on its frequency and magnitude due to structural or aerodynamic inputs. Therefore, a clear understanding of human visual concept is necessary to appreciate the level of sensitivity required when assessing the vibration of vehicle wing mirrors.

A number of analytical experiment tests were performed in the past to measure human eye interaction with the mirror and its effects on driving performance. A lot of factors in performance of mirror, time taken in distraction from front view of vision, distance of judgement and accuracy of drivers have been studied and well documented. Generally, while driving short observation is made by the driver in wing mirrors is often at the periphery of view; it is also relevant to consider the range of human peripheral vision. SAE (1995, J985, Vision factors consideration in rear view mirror design) highlights that human binocular field of vision is 60 degrees on either side of our forward line of sight, with our ability to perceive detail diminishes as an object moves further into our peripheral region of vision as shown below in Figure 1.12. The paper also explains that the further a mirror is placed away from the driver's sight of perception it reduces the driver's sight from forward traffic while looking in the rear view mirror.

Experimental tests using rear view mirrors have been conducted and the research shows the complex behaviour interaction of driver and the mirror. However, the use of rear wing mirror has been broken down into head rotation movements, eye movements and lateral movements. The research has also been done in measuring the other aspects of changing effects of the colour of reflected image to enable objects to be clearly identified. Mourant et al. (1974) measured the drivers glance to the outside rear view mirror during manoeuvre and found out that a majority of drivers take 0.5 to 1.2 seconds to respond, which was later agreed by Nagata and Kuriyama (1985). Bhinse et al. (1981) conducted the study on associated body movements while performing different tasks during viewing mirrors. The studies show the lateral movement of the head increase while absence of vehicle traffic. Therefore, the location of vehicle wing mirrors, and its optimal location has received considerable study by past researchers. Moreover, horizontal head movement consideration is about 45˚ to left and right of the front line of sight, whereas 50˚ is agreed for up and down movement. In order to maximise the visual efficiency and to reduce driver fatigue the rear vision unit should be well placed within the driver's binocular field of view while looking straight ahead. Therefore, it is

a compromise for location of rear view mirror because of its location in complex flow along with human eye scenario.

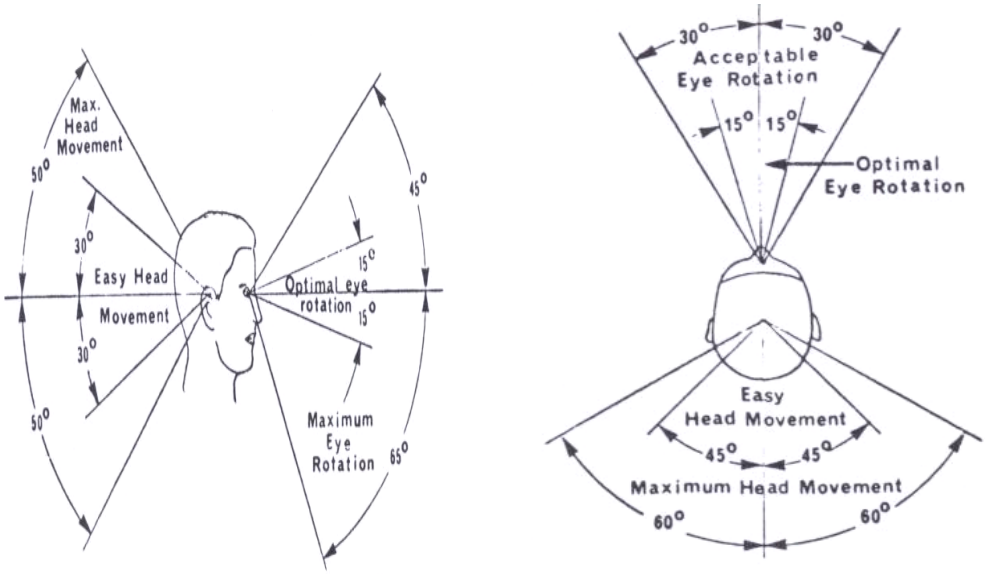

Figure 1.12: Human peripheral vision (SAE, 1995)

1.6 Conclusions from prior work

Effective and efficient rear view vision from external mirrors is a compromise at high speed due to rotational vibration of the mirror glass. The possible causes of mirror vibration are reviewed, including road inputs to the vehicle body and a variety of aerodynamic inputs. The latter included vibrations of the entire vehicle body, vibrations of the mirror "shell", the turbulent flow field due to the A-pillar vortex (and to a lesser extent the approach flow) and base pressure fluctuations. The location and functionality of vehicle wing mirrors are major contributors towards good driver visibility; however vibrations of the wing mirrors can severely impair the driver's vision and thus, the safety of the vehicle and its occupants. Manufacturers have achieved significant improvements in clarity through better mounting techniques of the mirror to the vehicle. However, wing mirror vibration still remains a major concern for the automotive industry, particularly at high speeds.

Mirror vibration is a combination of a range of factors such as structural vibration due to power train, road surface roughness and aerodynamic vibration. Mirror vibration due to engine and power train is well studied and documented. However, the aerodynamic input on

mirror vibration is not well studied and understood. No significant publication can be cited in the public domain. There is a gap in knowledge of mirror vibration due to pressure fluctuations. The proposed study will address the aerodynamic input in semi-isolation of other sources of vibration. The housing of mirror is very complex and located near the A- pillar region where flow is relatively complex and strong flow separation occurs in the A-pillar region. The presence of mirror in the complex A-pillar vortex makes the flow more complex. Therefore, a detailed study of fluctuating pressures around the mirror can give a good indication of aerodynamic input on mirror vibration and optimal location of the mirror housing.

1.7 Objectives and Scope of Investigation

The primary objectives of this research are to:

- To measure fluctuating pressures around the mirror to understand the aerodynamic input to mirror vibration.
- To find the combined effects of mirror housing and the shrouding effects.
- To measure the axis of rotation along which the image blurring occurs (vertical, horizontal and diagonal)
- What are the aerodynamic inputs that cause the mirror vibration (mirror housing and glass surface) and at what frequency are they dominant.
- Practical modifications possible for decreasing the pressure fluctuation around the wing mirror and mirror in isolation condition.
- Comparing the flow and pressure variation around the wing mirror with quarter model and in semi-isolation condition.

Chapter 2

Facilities, Equipment and Data Processing

Brief descriptions of the facilities, equipments and data processing methodology that will be used for this work are described in the following sub sections:

2.1 RMIT University Industrial Wind Tunnel

The testing for aerodynamic effects on wing mirror was carried out in full-sized RMIT Industrial Wind Tunnel using a quarter model of the 1998 Ford Falcon AU, where the vehicle is held stationary and the relative air velocity is generated via a fan. RMIT Industrial Wind Tunnel is a closed loop type, where the fan continually circulates the air. The maximum speed of the tunnel is 145 km/h. The rectangular test section dimension is 2 x 3 x 9 (m) with a turntable attached to yaw at different angles. The turning vanes of the wind tunnel are acoustically treated to reduce the background noise. The wind tunnel has turbulent intensity of 1.8% for free stream. This closed loop type tunnel is also known as Gottingen type wind tunnel. (Generally 3 different types of wind tunnel test sections are commonly used for automobile testing. They are-3/4 open jet section, closed wall section and slotted wall section). The advantages of Gottingen type wind tunnel are its low power requirement, low cost of drive unit, low operating cost. However, it has some disadvantages too due to its length and large settling chamber and the cost of tunnel duct are high (Hucho, 1998)

Wind tunnel testing provides a simulation better than the on road testing. Since in this testing only the aerodynamic effects needs to be considered so the test would be carried out only in the Wind Tunnel instead of on road testing. However, wind tunnel testing is more prohibitive than testing on-road due to the high associated costs of operation and maintenance. The wind tunnel provides a simulation close to that of flow over the prototype vehicle. The accuracy of the results depends on the accuracy of the models, wind speed, blockage ratio and data acquisition used. In the wind tunnel test, tyres, engine and other mechanical source of vibration and noise are discarded and speed of the airflow can be maintained constant. Moreover the effects of the yaw angle can also be done to simulate effects of the atmospheric winds. The advantage of having total control over the environmental conditions available

within wind tunnels, allows for tests to be controlled and repeated with greater ease. Moreover for understanding the aerodynamic problem and its improvement requires good incremental data, productive vehicle improvement can be achieved with 14% blockage ratio in a wind tunnel. A plane view of the RMIT Industrial wind tunnel is shown in Figure 2.1.

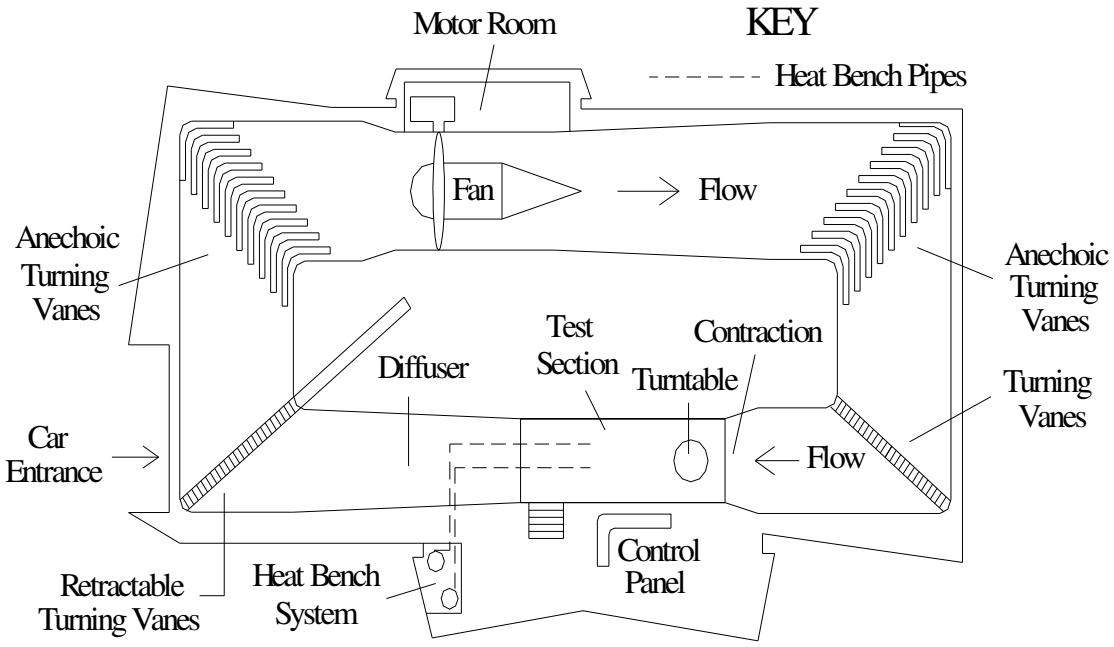

Figure 2.1: Schematic of RMIT Industrial Wind Tunnel

2.1.1 Wind Tunnel Blockage Ratio

Blockage occurs in wind tunnel airflow for limited size during the testing of relatively large models. The blockage is defined as the ratio of the frontal area of the model to the area of the test section. Hucho (1998) cites that the ratio of 0.10 is reasonable for automotive application using open jet wind tunnel. As mentioned above the blockage ratio of less than 10% is needed, but sometimes far larger ratio is used like for aeronautical engineering testing blockage ratio is less than 5%. In automotive engineering testing this value can be achieved by very few wind tunnels. Merker and Wiedemann (1996) proposed Cd correction factor for open jet wind tunnels. The correction form of the equation is

$$q_{corr} / q_m = (1 + \varepsilon_s + \varepsilon_n + \varepsilon_c) \qquad \ldots (2.1)$$

Where:

q_{corr} = Corrected dynamic pressure

q_m = measured dynamic pressure

ε_s = induced velocity due to jet expansion

ε_n = induced velocity due to nozzle effect

ε_c = induced velocity due to collector effect

The presence of the testing prototype in test section blocks the incoming airflow and causes increase in the pressure on the tunnel walls. For this reason sometimes open section wind tunnels or tunnels with slotted walls are used. Correction for blockage has been an active subject of research in today's world.

2.1.2 Wind Tunnel Correction

When the vehicle travels on road it travels through space, which is unlimited in all directions compared to that of wind tunnel. In the wind tunnels, cross section and the length of its airstream are limited. It is due to the proximity in the wind tunnel that the flow around vehicle modifies due to tunnel walls and boundary layer, when compared to that of unlimited space available on road. However, the test condition is never the same as the operational conditions. Among the most known effects there are the scale effects, airflow blockage due to the presence of model in the test section and wall boundary layers. Wind tunnel requires special analysis and data acquisition systems (Refer Appendix D).

2.2 Testing Vehicle

The test models were a hollow quarter model of Ford Falcon Au, 1998 that was provided by Ford Motor Company of Australia to the Department of Mechanical and Manufacturing Engineering RMIT University, Bundoora East Campus. The reason of using a quarter models as compared to the full-scale model was to see the effects of blockage. The quarter model will shows the similar effects to that of full-scale car inside the wind tunnel. The quarter model was kept 3.4m away from the front test section and was kept next to the side tunnel wall in order to minimise any airflow disturbances coming inside the testing vehicle. Figure 2.2 - 2.3

shows the front and side view of the testing vehicle. Figure 2.4 shows the quarter model inside the RMIT Industrial Wind Tunnel with dimensions.

Figure 2.2: Front View of Ford Falcon

Figure 2.3: Side view of quarter Model

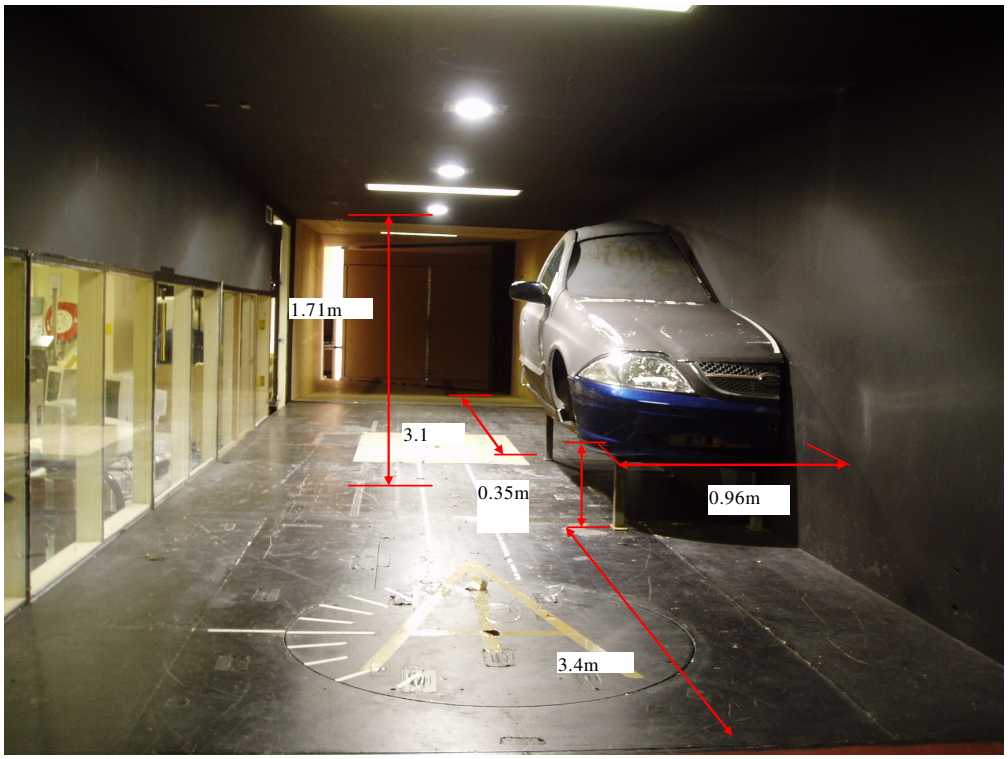

Figure 2.4: Ford Falcon AU model inside the RMIT Industrial Wind Tunnel

2.3 Rear View Mirror

Schefenacker Australia is world's leading automotive manufacturer in designing and developing high quality technical and visual products. The company has provided a pair of right hand side rear view mirror for the Ford Falcon AU model. Figure 2.5 shows the schematic diagram of the rear view mirror for Ford Falcon AU used in the RMIT Industrial Wind Tunnel testing. Figure 2.6 shows the inside mechanism of mirror on which the reflective glass of mirror mounts over the mounting plate of the motor mechanism.

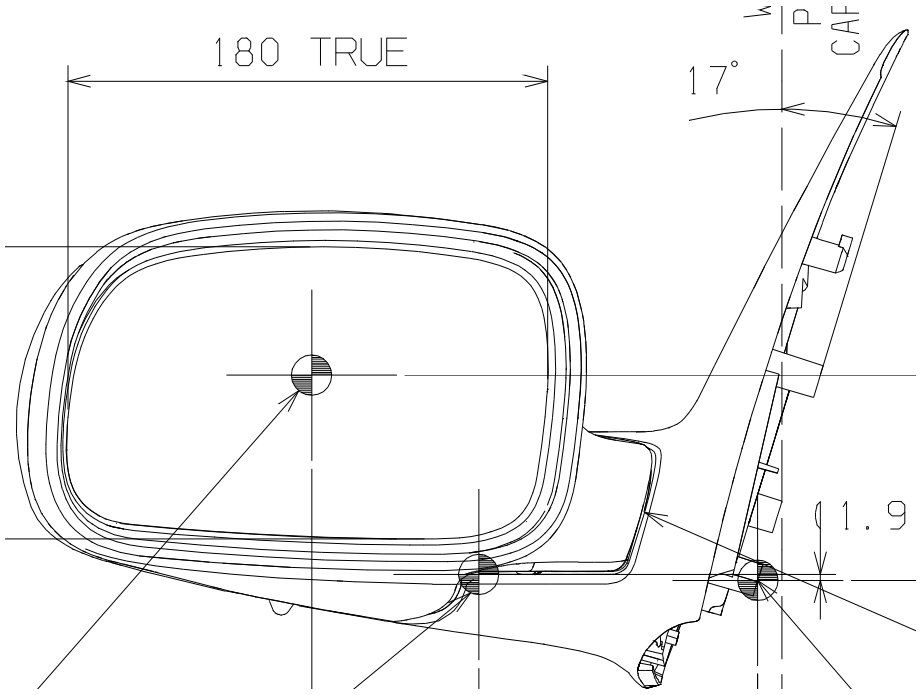

Figure 2.5: Schematic drawing for the Schefenacker Rear View Mirror

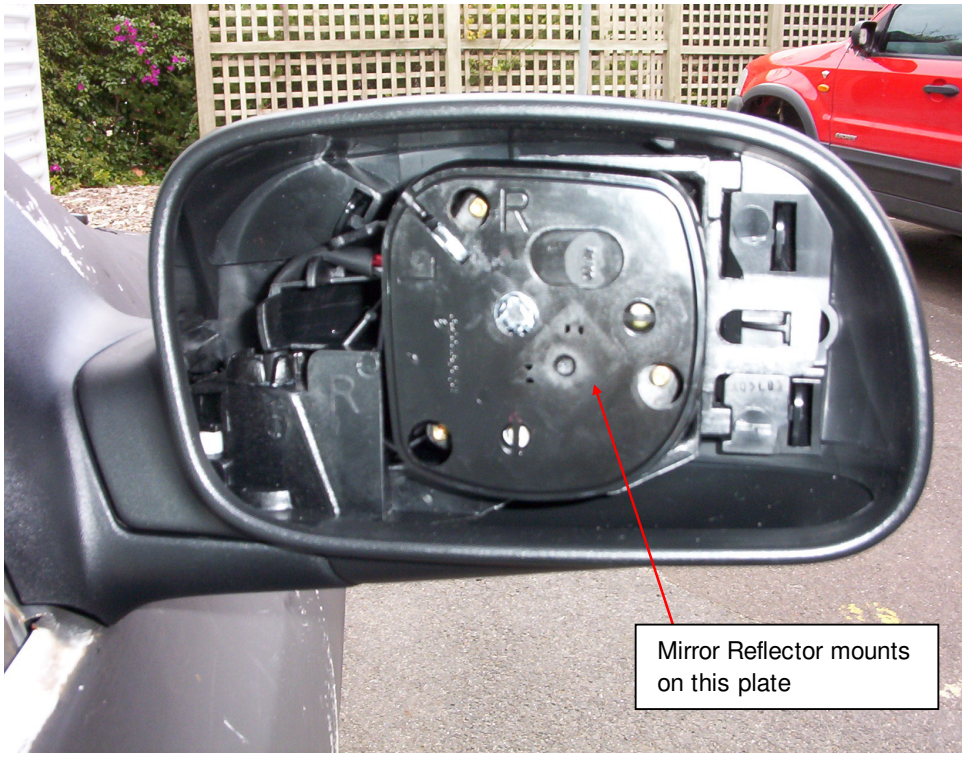

Figure 2.6: Inside of Schefenacker rear view mirror

2.4 Instrumentation of Pressure Measurements

2.4.1 Pressure: An Overview

Pressure is an important and vital measurement in many engineering flow systems as it determines the flow measurement's accuracy of the system. Pressure is a stress and defined as force per unit area exhibited in a fluid medium. With the change in pressure, compressible fluids like gases will change its density properties. On the other hand it's not the same for the liquids, as they don't change their physical properties with change in pressure. Effectively measuring and sensing these operating parameters is a difficult task. In a fluid medium, pressure at a given point of reference is classified as a compression stress and its direction of flow is independent.

2.4.2 Pressure Transducer

A pressure transducer is a device that converts pressure into its equivalent electrical analogue signal. This conversion of pressure into an electrical signal is achieved by physical deflection of diaphragm. When a pressure is applied to the pressure transducer it produces a deflection to its diaphragm, which introduces strain to the gages. This strain will then produce an electrical resistance change proportional to the pressure. The pressure transducer comprises of a semiconductor material such as silicon, in real physical problem pressure transducers are used widely to measure gauge, absolute and differential pressure due to their sensitivity, reliability and precession to measure a wide range of pressure. The most common method used earlier to measure pressure was by manometer (comprising U-tubes with one end closed, containing mercury as medium) and mechanical deflection devices (tubes, diaphragms or bellows). Manometers are commonly used to measure pressure from small to moderate range only. The fluid pressure inside the manometer is used to measure the pressure difference.

2.4.3 Dynamic Pressure Measurement System (DPMS)

In order to measure time-accurate surface pressures on the mirror model, a Dynamic Pressure Measurement System (DPMS) was used manufactured by Turbulent Flow Instrumentation (TFI). The mean and fluctuating pressure measurements were analysed with DPMS. It is a multi channel pressure measurement system and can measure the fluctuating pressure around 1000Hz.

DPMS system senses the distortion with help of tubing or external source like hypodermic tube, which is connected to the pressure, taps on the multi channel models. When the pressure is sensed from a desired location, it is then send with the help of rubber or plastic tubing on to the diaphragm inside the pressure transducer, which in return transfers the signals to the Data Acquisition used. It also measures the range of pressure measurements including the mean and fluctuating pressure at any point. The system corrects for distortions in the pressure tubing to provide linearised frequency response over the entire operating range. Real-time frequency spectra from any pressure taps can also be viewed from the data obtained for data acquisition.

2.5 Components of DPMS

DPMS comprises of the following. Each of these components will be discussed in the following subsections:

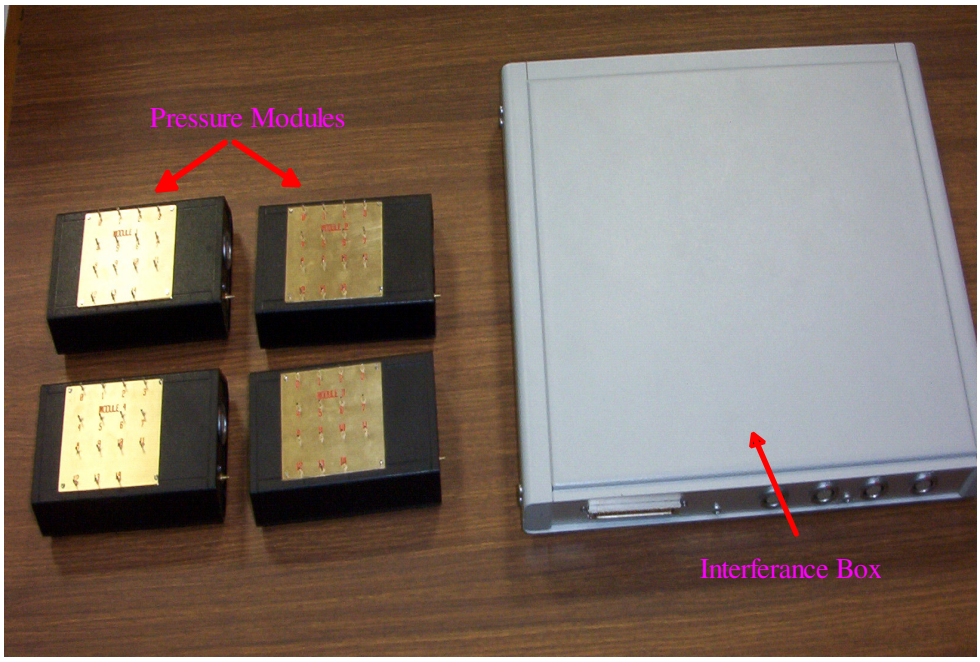

Figure 2.7: Components of Dynamic Pressure Measurement System (DPMS)

2.5.1 Data Acquisition System

It is a used for instrumentation of data processing in real time format. It also enables flow mapping and simple static calibration. The system allows us to view real time frequency analysis with a multiple use of different pressure modules used for surface pressure measurement.

2.5.2 DPMS - Hardware

The DPMS comprises of two main components: the pressure modules and an interference box. These two components are discussed in the following subsections.

2.5.2.1 Pressure Modules

Each pressure module contains 15 pressure taps channels. Each module has a pressure transducer for each channel. All of the pressure modules are connected to the interface box, which provides power and multiplexes the inputs to the data acquisition system. Software correction of the phase lag between channels provides quasi-simultaneous sampling without the need of a true simultaneous-sampling data acquisition system. The size of one module comprising of 16-channel is 110 x 65 x 30 mm. However, the pressure modules should be located close to the measurement points to minimise the length of tubing between the pressure module and the pressure taps. Reducing the length of tubing increases the available frequency response. Each pressure module has a pressure port for each transducer; a reference pressure port is used to measure atmospheric pressure and LED is present to indicate when power is available and an output connector

2.5.2.2 Interface Box

A 64-channel interface box, which measures approximately 280 x 220 x 40 mm, is attached to one end of the pressure module and other end to the computer. Connectors on the interface box include inputs for each pressure module and a single output connector to the data acquisition system. Power source to the interface box, and hence the pressure modules, is supplied by the data acquisition system or a separate 5 V power supply. The interface box is connected to the data acquisition system, which consists of a National Instruments E-series data acquisition card. Interface boxes are available for 64, 128 and 256 channels.

2.6 Operation of DMPS

The DPMS is similar to other pressure measurement systems but features one main difference; the amplitude and phase distortion effects of tubing are corrected to produce time accurate, time-varying pressure measurements. This makes the DPMS a true dynamic pressure measurement system, with the potential of measuring pressure fluctuations in excess of several kHz, even with large channel counts. During data acquisition, either time or frequency

data can be displayed in real time via the supplied Device Control software, or the data can be saved for later analysis.

2.7 Experimental Set-up and Data Processing

In order to measure the mean and fluctuating pressures on mirror surface, a new production mirror was obtained from Schefenacker, a world leader of mirror manufacture. The glass of the mirror was replaced with an aluminium plate (2.4 mm thickness) and the mirror case was made thoroughly hollow from inside for passage of pressure tubes and slightly modified in order to hold the aluminium plate. There are 51 holes made on aluminium plate in a grid pattern (keeping equidistant from x and y coordinates). The outer diameter of the silicon tubing used in the pressure taps is 2.4 mm and inner diameter of 0.9mm. The space between the two holes are 25 mm horizontally and 13 mm vertically. The mirror face replaced by aluminium plate was pressure tapped with the silicon rubber tubing. The silicon rubber tubing was connected to four pressure sensor modules, each having 15 channels individually. All pressure sensor modules are connected to an interface box that provides power and multiplexes the inputs to the data acquisition system. As mentioned before for measurement of pressure, is carried out from a reference pressure. However, for our analysis this reference pressure was taken from the bottom of the wind tunnel by inserting pressure tubing under the wind tunnel floor, which was connected to each of these pressure modules.

The DPMS data acquisition software provided mean, rms, minimum and maximum pressure value of each pressure port on mirror. By entering dimensions (diameter and length) of the tubing used, the data were linearised to correct for tubing response in order to obtain accurate dynamic pressure measurements. The instrumented mirror was attached with a quarter model (an earlier production model) Ford Falcon 1998 model that was described before and placed in the working section of RMIT Industrial Wind Tunnel. The quarter model used to reduce the blockage ratio and to have representative vehicle geometry and airflow pattern around the mirror. The Figure 2.8, below shows the schematic layout of the pressure measurement of the rear view mirror.

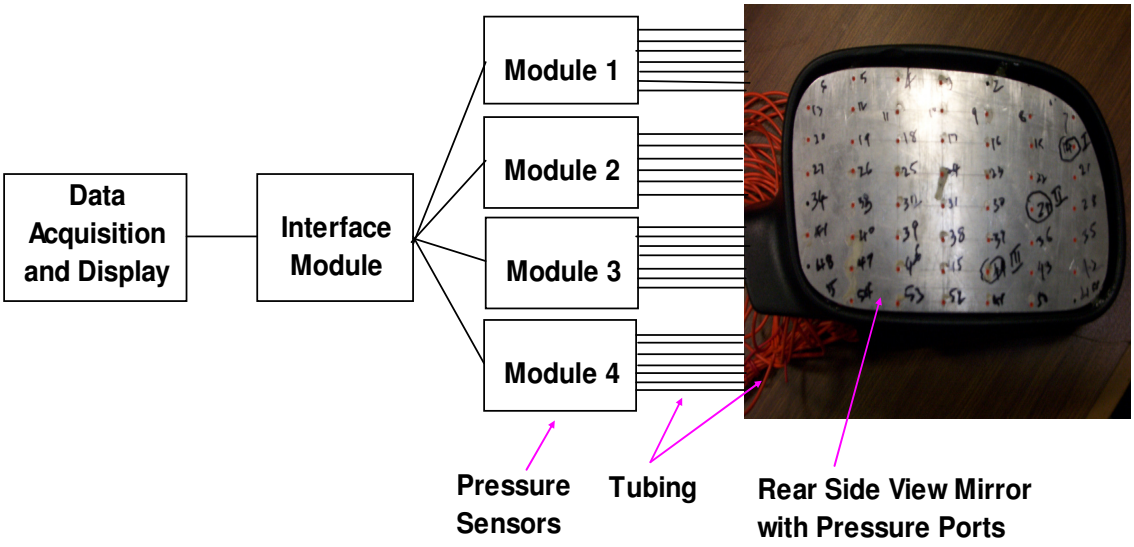

Figure 2.8: Pressure Measurement System Layout

The DPMS was used to scan the surface mean pressure. The pressures on the mirror plate were picked up by the individual pressure holes on the base plate and were fed to pressure sensor through the tubes. In this analysis we have used non – dimensional parameters of the mean (Cp) and standard deviation (STD). The fluctuating pressure coefficient Cp and Cprms were analysed as shown below:

$$\text{Mean Pressure Coefficient (Cp)} = \frac{Mean\,\text{Pr}\,essure}{\frac{\rho V\infty^2}{2}}$$

$$\text{Fluctuating Pressure Coefficients (Cprms)} = \frac{\text{Standard Deviation}}{\frac{\rho V\infty^2}{2}}$$

The time-averaged pressure distribution was converted into non-dimensional pressure coefficients (Cp) using the following relations:

$$Cp = \frac{P_m - P_\infty}{\frac{\rho V\infty^2}{2}} \qquad \ldots (2.2)$$

Where, P_m is the surface pressure at the point of measurement (time averaged pressure), P_∞ is the free stream static pressure and V_∞ is the free stream velocity. The relationship in equation (2.2) can be arranged in terms of velocity (ignoring turbulent losses):

$$Cp = \frac{1 - V_m^2}{V_\infty^2} \quad \text{... (2.3)}$$

The pressure coefficient is an important parameter in fluid mechanics as it identifies the nature of flow. If the local velocity (V_m) is larger than the free stream velocity ($V\infty$) the Cp becomes negative. It should be noted this relationship breaks down in wake of bluff body when turbulent losses can be significant.

2.8 Non - Dimensional Parameter (Cp and Cprms)

Wing mirror as classified before is a bluff body. The aerodynamic loads exerted on the bluff body immersed in the airflow are produced by normal and tangential stress over the surface. The resultant load components due to these stresses gave rise to force and moment's coefficient. The pressure *p* acting over the surface is defined as the pressure coefficient (Cp):

$$Cp = \frac{p - p_{ref.}}{\frac{1}{2}\rho U^2} \quad \text{… (2.4)}$$

The wing mirror is generally located around A-pillar and the flow around that region is complex and 3-dimensional. Due to its complexity sound level in vehicle cabin along with the mirror vibration affects the flow around A-pillar. Previous study done by Buchheim et. al. (1982) & Wantabe et. al. (1978) illustrates the relationship between pressure fluctuations on side window of the automobile along with its cabin interior noise level. However magnitude and frequency of the fluctuating pressure can be determined by non-dimensional parameters such as Strouhal number ($S_t = \frac{f.D}{U}$) where: *f, D & U* are the frequency, length of noise source and fluid velocity & fluctuating pressure coefficient ($C_p = \frac{P_{std.}}{\frac{1}{2}\rho U^2}$) where $P_{std.}$ is the standard deviation of the fluctuating pressure & $\frac{1}{2}\rho U^2$ is the dynamic head of the fluid. Another non-dimensional parameter Reynolds Number (Re) is defined as the ratio of the inertial force to the viscous force and is defined by the following formula ($\text{Re} = \frac{\rho UL}{\mu}$) where

ρ is the fluid density, μ is the absolute viscosity, L is the characteristic length & U is the velocity

2.9 Experimental Set Up of Mirror

The aerodynamic induced testing was done in RMIT Industrial Wind Tunnel. The tests were conducted using:

2.9.1 Quarter model – using Ford Falcon AU model

2.9.2 Semi - Isolation testing

2.9.1 Quarter Model

The quarter model of ford falcon 1998 AU model was used in the testing. The rear side view mirror provided by Schfenacker Australia, was clamped to these models to measure the mean (Cp) and pressure fluctuation (Cprms).

Figure 2.9: Quarter Model inside RMIT Industrial Wind Tunnel

The mean and fluctuating pressures were measured at a range of speeds (60 to 120 km/h with an increment of 20 km/h) at zero yaw angles. The mirror was tested as standard configuration first and then modified configuration. Adding a 10 mm (24mm, 34mm and 44mm) shrouding on the mirror periphery made the mirror modified.

2.9.2 Semi-Isolation Mirror

During this testing the wing mirror was mounted on the centre table of the RMIT Industrial wind tunnel with the help of M12 spindle. The length of the spindle from the wind tunnel floor was about 500mm high. The wing mirror was mounted over a collar, which was held by fine wires (fishing line) providing enough tension to prevent from moving. Moreover, wing mirror was also bolted from inside to hold the movement of mirror at high speeds. The pressure transducer was mounted on the wind tunnel floor inside a wooden box, which was covered on top with cardboard to provide the aerofoil shape in order to have a smooth flow (minimising disturbance). The reason for doing this testing was to minimise the blockage effects inside the wind tunnel as it doesn't include any model inside the test section. The schematic layout of this testing is shown in Figures 2.10 and 2.11

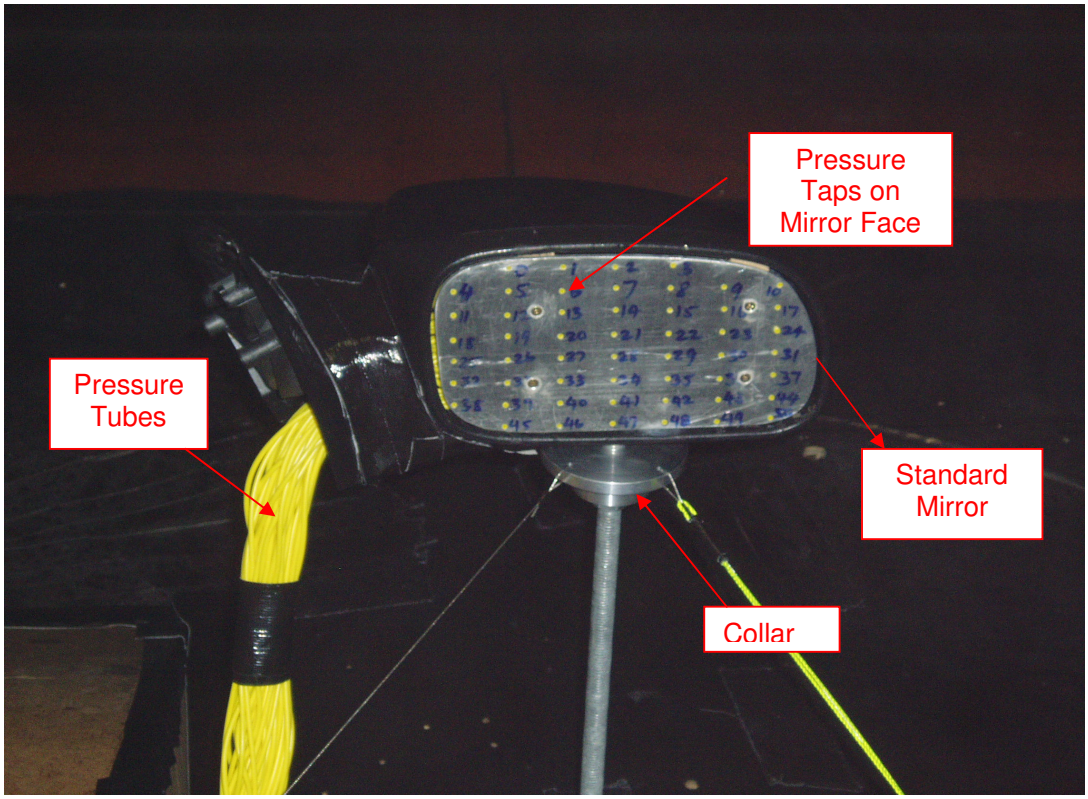

Figure 2.10: Front View of the Semi-isolation Case for Standard Mirror Test

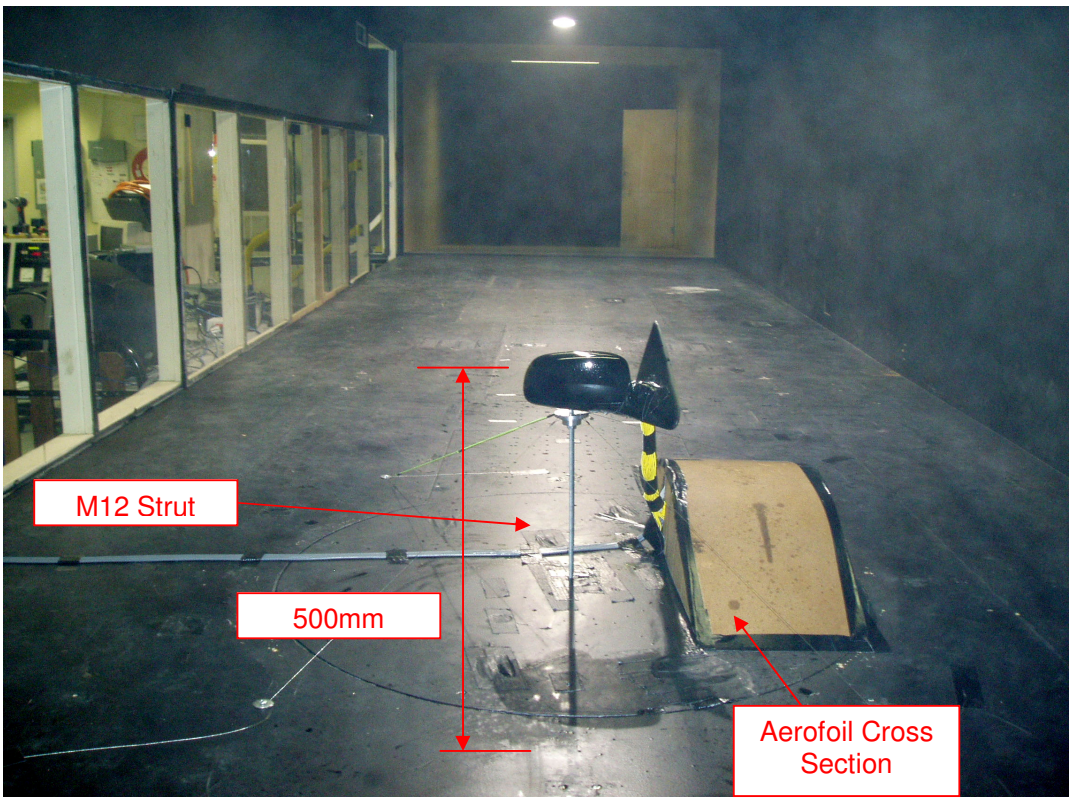

Figure 2.11: Back View of the Semi-isolation Case for Standard Mirror Test

2.10 Wing Mirror Modification – Shrouding Effects

The tests were carried out with the help of quarter model of ford falcon and in semi-isolation condition. The test was conducted at same speeds of 60 km/h, 80 km/h, and 100 km/h and120 km/h. The test also included the effects of shrouding. The shrouds included in the case of the testing carries from 24mm to 44mm with increment of 10 mm each. The shroud was made up of very thin wooden piece of very small thickness and was rounded across the outer periphery of the mirror housing in order to visualise the fluctuating pressure.

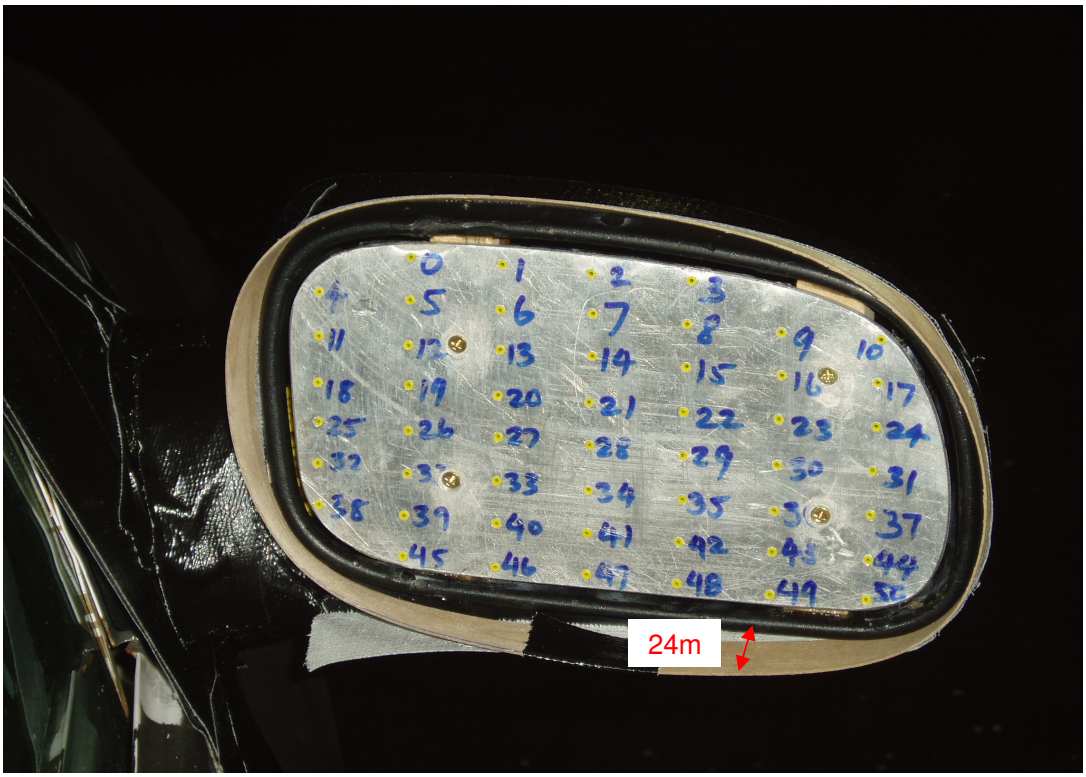

Figure 2.12: Shrouding of 24mm

Figure 2.13: Shrouding of 34mm

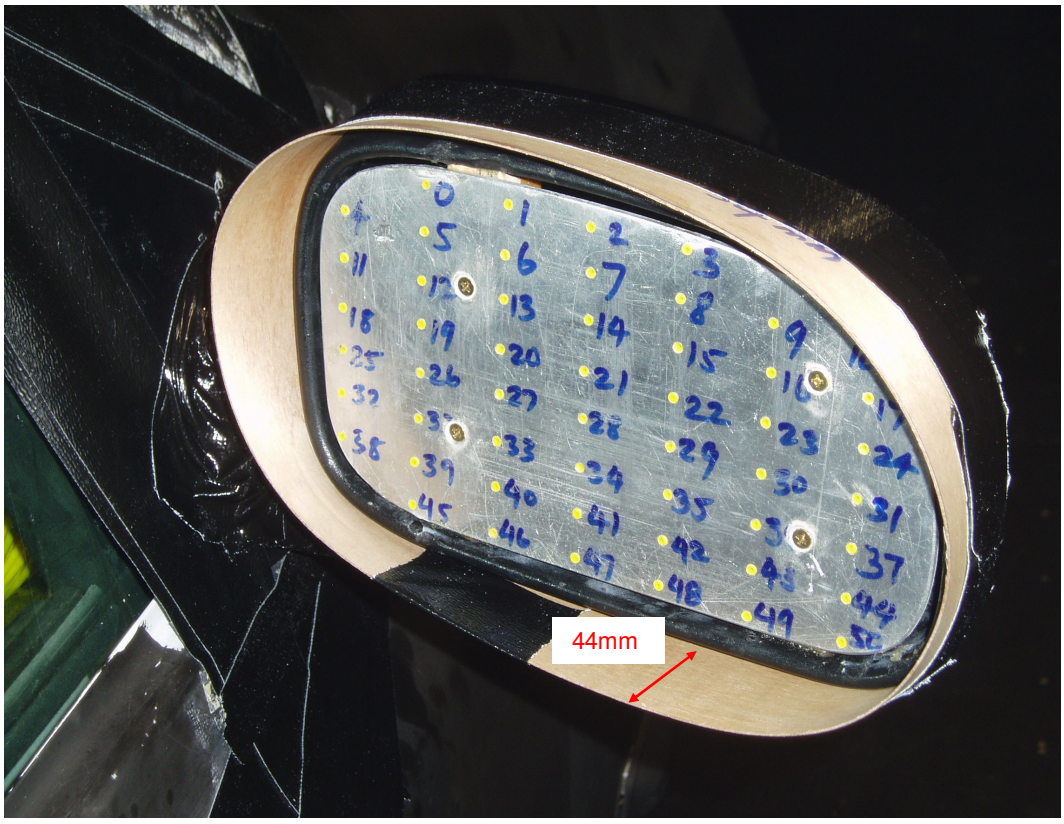

Figure2.14: Shrouding of 44mm

2.11 Pressure Leak Test

Prior taking and analysing the data reading from the pressure taps on the pressure modules the leak test was conducted to check for any leaks, blockage present inside the rubber tubes used to transfer pressure form the surface. Another reason to do it is to double-check whether the right pressure taps is connected to its individual tap in pressure module. Figure 2.15 below shows the schematic layout of the pressure leak system. A constant pressure was applied to the injection syringe manually. The plastic tube was attached to the output end of the inclined manometer, which was further connected to the T-section. Through the T-section one ends goes to the injection syringe where a constant pressure is applied through hand. The other end of the plastic tube is free to check for leaks inside the rubber tubes individually. During this analysis the pressure taps are connected to the pressure modules, which is further connected to the interference box. With the help of the data acquisition system we can monitor the pressure fluctuation on the wind tunnel system with the help of DPMS software.

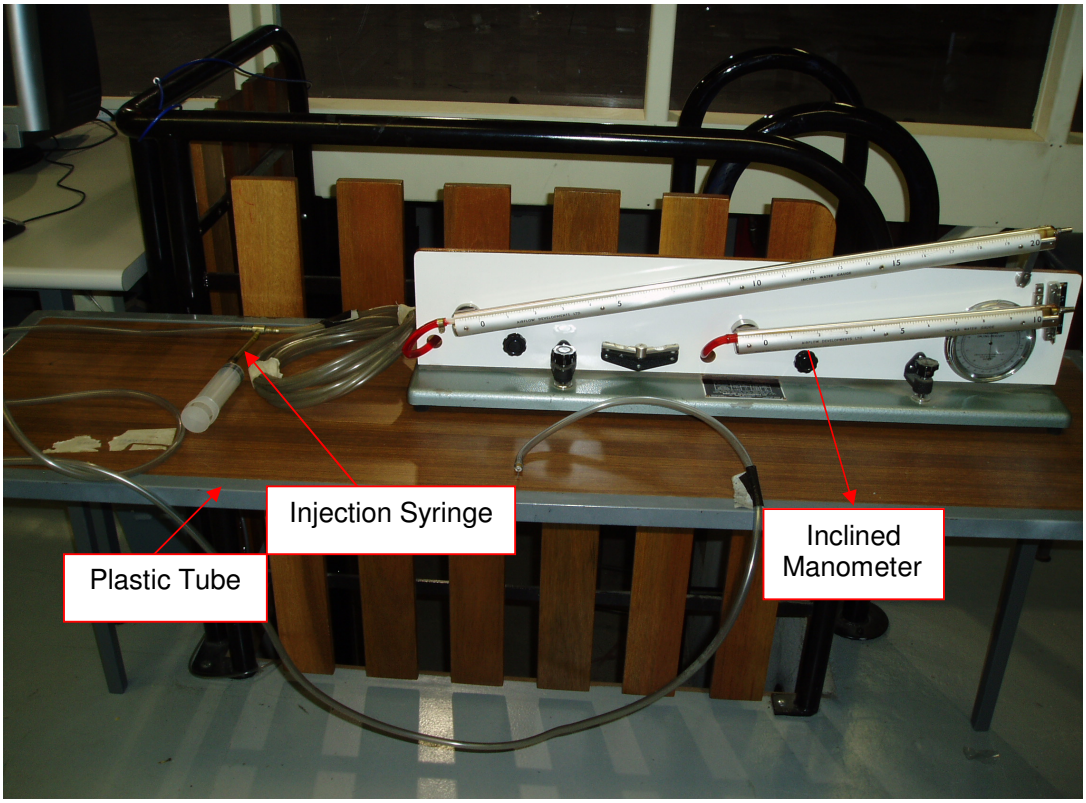

Figure 2.15: Inclined Manometer used for Pressure Leak Testing

When the desired pressure is applied to the individual pressure tap, we can measure the pressure from the inclined manometer along with can see the change in pressure at individual pressure tap on the DPMS software. The leaks can be detected from the system when the applied desired pressure drops down considerably inside the manometer along with the drop in the DPMS. Accordingly the checks were done so as to maintain the system from the leaks and blockage of tubing to get desired results. This is an important step as it may cause the error for the data to be analysed later. Figures 2.16 to 2.17 show the components of the pressure leaks test.

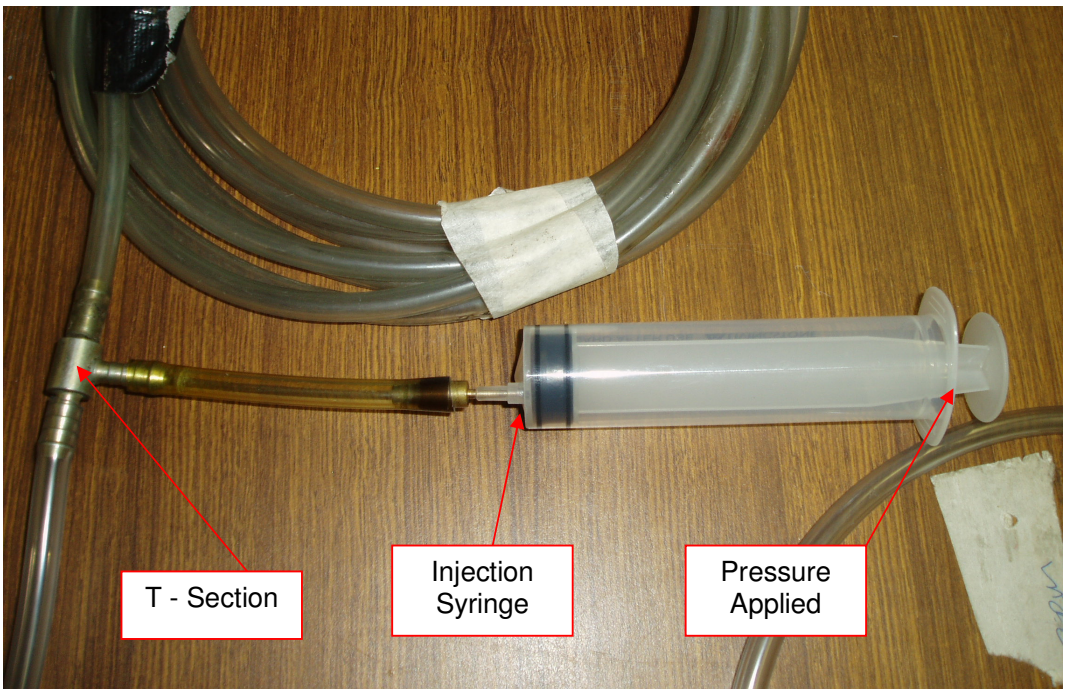

Figure 2.16: Injection Syringe connected with T -section to Plastic Tube

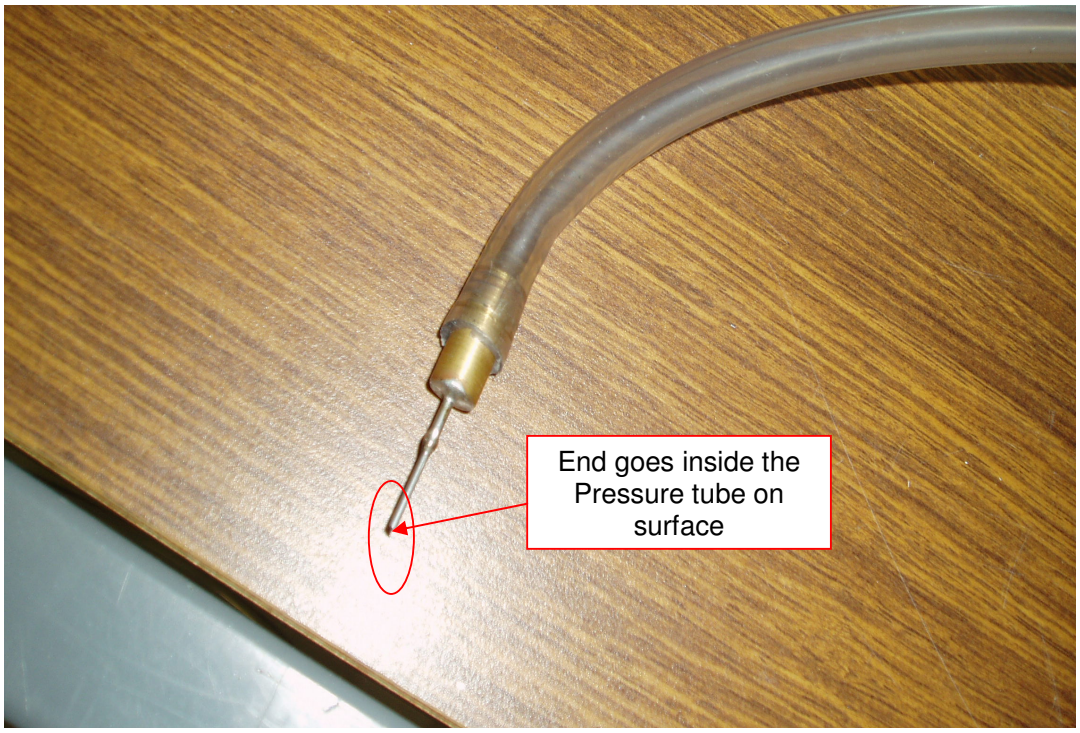

Figure 2.17: Hypodermic end inserted inside the Pressure Tubing at the surface

In the next chapter these individual cases will be elaborated along with their results and the discussion.

Chapter 3

Quarter Model Testing

As mentioned in Chapter 2, the test was carried out on quarter model scale of the Ford Falcon. This model was chosen to investigate the influence of surface mean and fluctuating pressures in order to understand flow patterns of pressure distribution on wing mirror face. The Ford Falcon model was hollow from inside and kept as simple as possible without the added complication of the wheels, wheel arches and engine compartment. The test results of the quarter model have been described only for every speed only for fluctuating pressure coefficients (Cprms) in this chapter. The mean pressure (Cp) results for 60 km/h, 80 km/h, 100 km/h and 120 km/h are presented in the Appendix A.

3.1 Experimental Layout

Two pairs of pressure modules were mounted on the inner side of the door of quarter model. The silicon tubing was then connected to the pressure transducer through the hole between the mirror assembly points with the car section (near A- pillar region) and was connected to their corresponding point on each module section.

The tests were conducted at 60 km/h, 80 km/h, 100 km/h and 120 km/h with 0˚ yaw angle. Prior to testing each individual pressure tap on the aluminium plate was checked for leak with the help of a inclined manometer as mentioned before to detect any blockage and also to verify that right pressure tap is attached to right channel number of pressure transducer module. Figure 3.1 shows the schematic view for the experimental set-up.

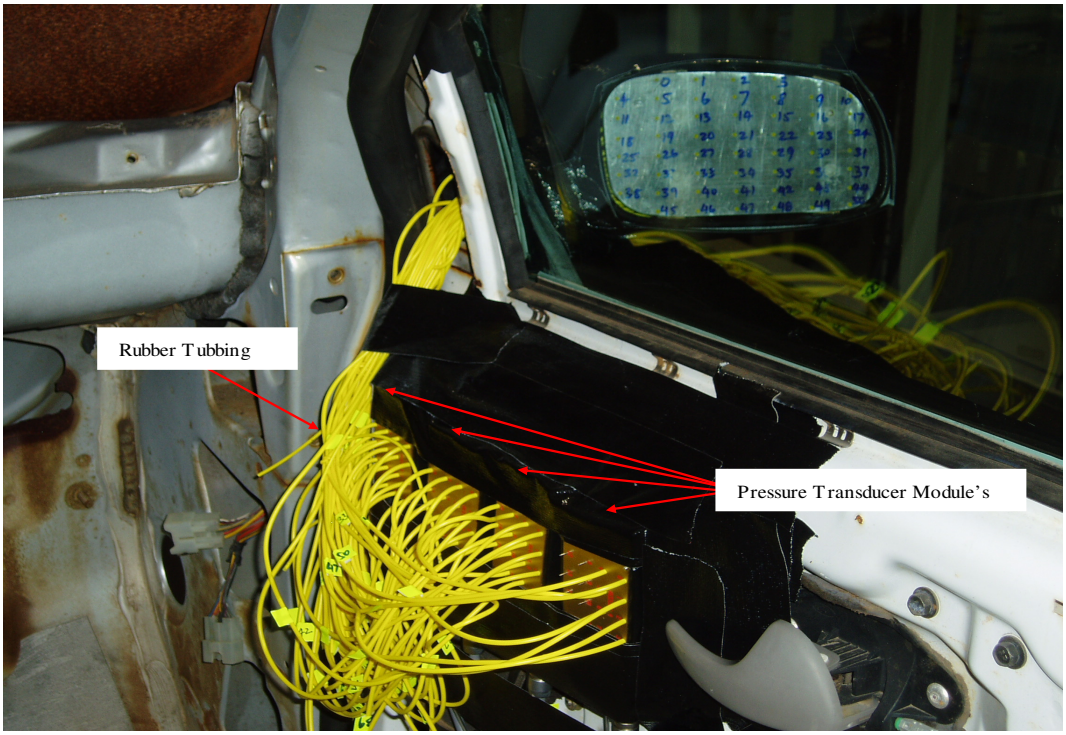

Figure 3.1: Schematic View of Pressure Taps

3.2 Testing Methodology

The tests were conducted on the standard mirror and shrouded mirror (24mm shroud, 34mm shroud, 44mm shroud). The shrouds were made of the thin sheet wooden sheet of 0.7mm thickness and wrapped around the mirror's external periphery with the help of cloth tape. Figures 3.2 - 3.3 shows the of schematic representation standard mirror case that was tested with quarter model in RMIT Industrial Wind Tunnel. The individual cases are discussed later in this chapter and the results are displayed only for 100 km/h, for other speeds refer to the Appendix A. The dynamic pressure of the each individual cases were noted individually and later used to non-dimensionalised the parameters in order to obtain the surface mean pressure Coefficients (Cp) and fluctuating pressure coefficients (Cprms)

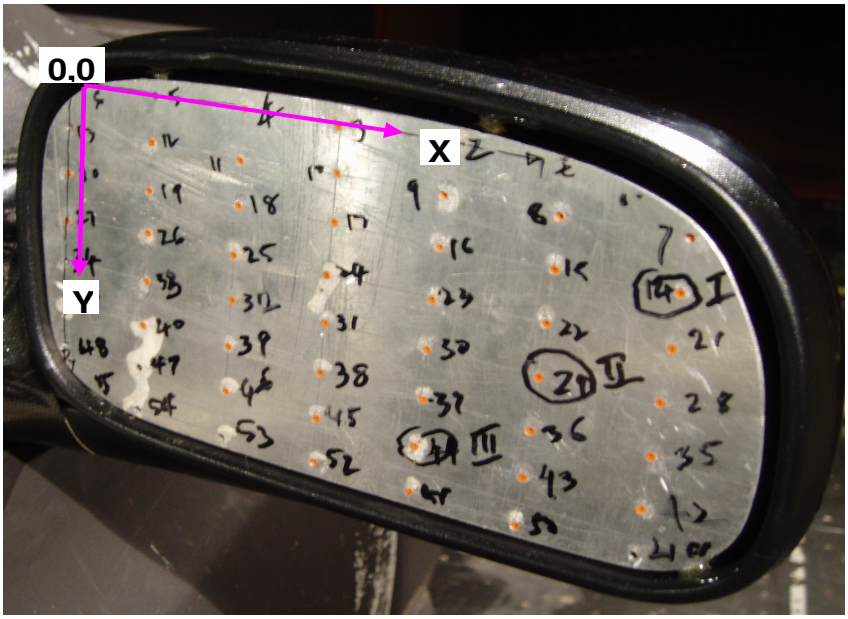

Figure 3.2: Schematic of Data Representation in Relation to Mirror Geometry

P.S - It may be mentioned that in contour plots, the extreme top left and right, and bottom left data points need to be ignored as these points are beyond the mirror geometry. These points are shown here for the sake of grid formation only due to the complex shape of mirror surface. The origin of the plot is located at the top left hand corner position (e.g., Position 1). The x-distance is horizontal and y-distance is vertically down (see Figure 3.3).

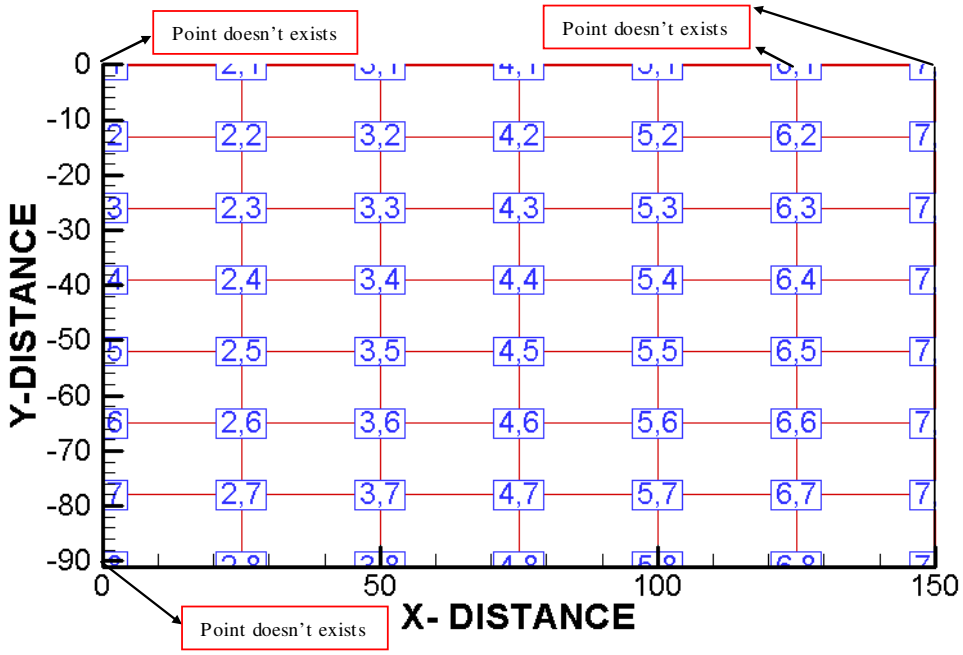

Figure 3.3: Representation of Data Points on Mirror Surface

This chapter comprises of the following sub-sections:

- Standard Mirror
- Modified Mirror – Shrouding
- Modified Bottom Flange - Shrouding
- Mirror Housing

3.3 Standard Mirror

The testing was done using a quarter model of Ford Falcon 1998 AU available in RMIT University. The quarter model provided to the Department of RMIT University from the Ford Company, Australia. The Standard mirror was modified internally in order to accommodate the silicon tubing, see Figure 3.5. The Aluminium plate replaced the mirror face and the distance was kept in accordance to that of the production mirror from the front end of the mirror. The Figure 3.6 shows the detail view of the standard mirror in order to accommodate the silicon tubing along with the modification made in order to fix the Aluminium plate. The mirror was modified internally in order to accommodate the Aluminium plate to replace the wing mirror's face. The inside motor mechanism of the mirror was removed in order to make room for the silicon tubing used to measure the pressure measurement on the face of mirror, which causes vision distortion to the driver at high speeds.

Figure 3.4: Standard Wing Mirror

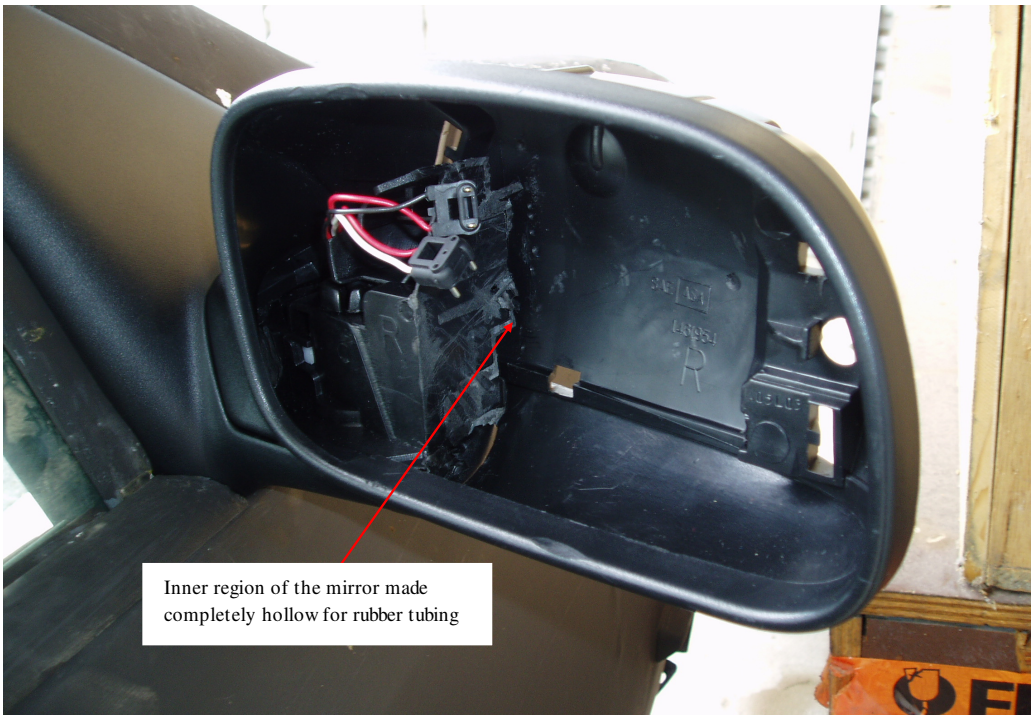

Figure 3.5: Modified Mirror Interior Region

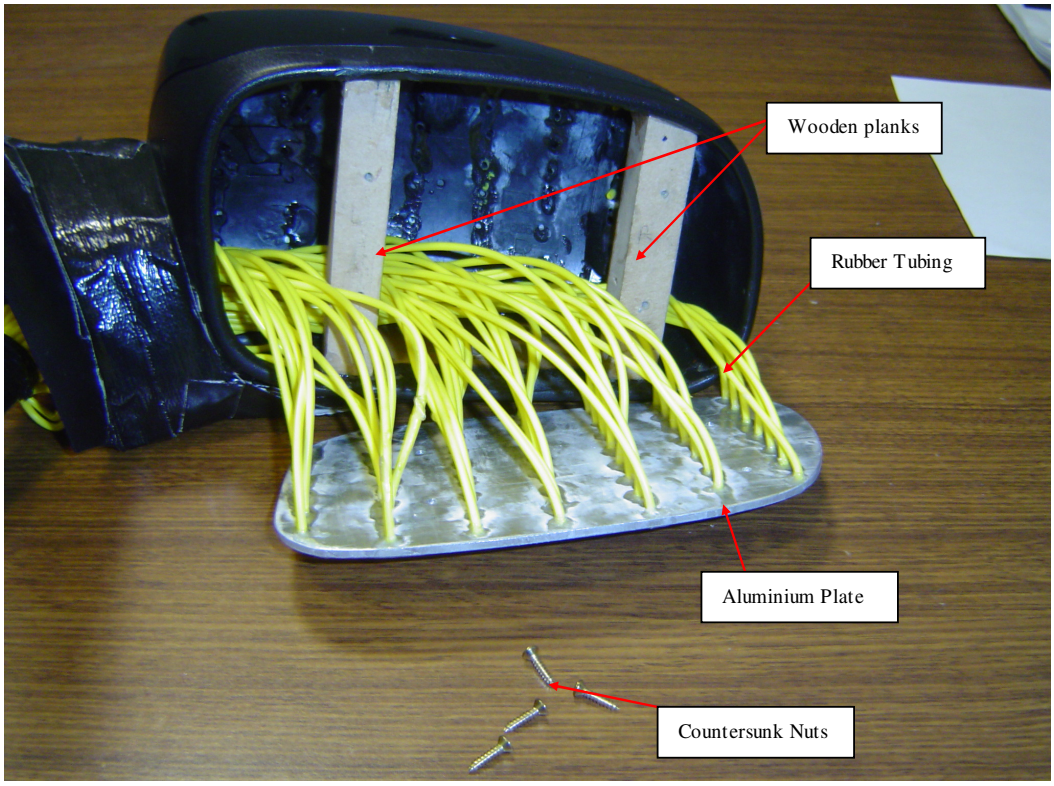

Figure 3.6: Aluminium plate with the Silicon Tubing

3.4. Results of Quarter Model

The maximum fluctuating pressure Coefficients was measured at the bottom right part of the mirror surface at all speeds tested. However, with the increase of speed, the magnitude of fluctuating pressures increases. This fluctuating pressure shifts from the far end bottom section of the mirror face towards the bottom central part of the mirror surface. The contour and 3-D plots are shown in Figures 3.7 – 3.10 and 2-D contour plots are shown in Figures 3.11 – 3.14 for the speeds of 60 km/h, 80 km/h, and 100 km/h and 120 km/h for standard mirror for Surface Mean Pressure Coefficient (Cp) and Fluctuating Pressure Coefficient (Cprms). 3-D and contour plots clearly show that the fluctuating pressure is not uniformly distributed on mirror surface rather concentrated at lower central part of the mirror surface due to the strong flow separation from the edge. Generally the higher the magnitude of fluctuating pressure, the greater possibility of generating intermittent force and aerodynamic noise.

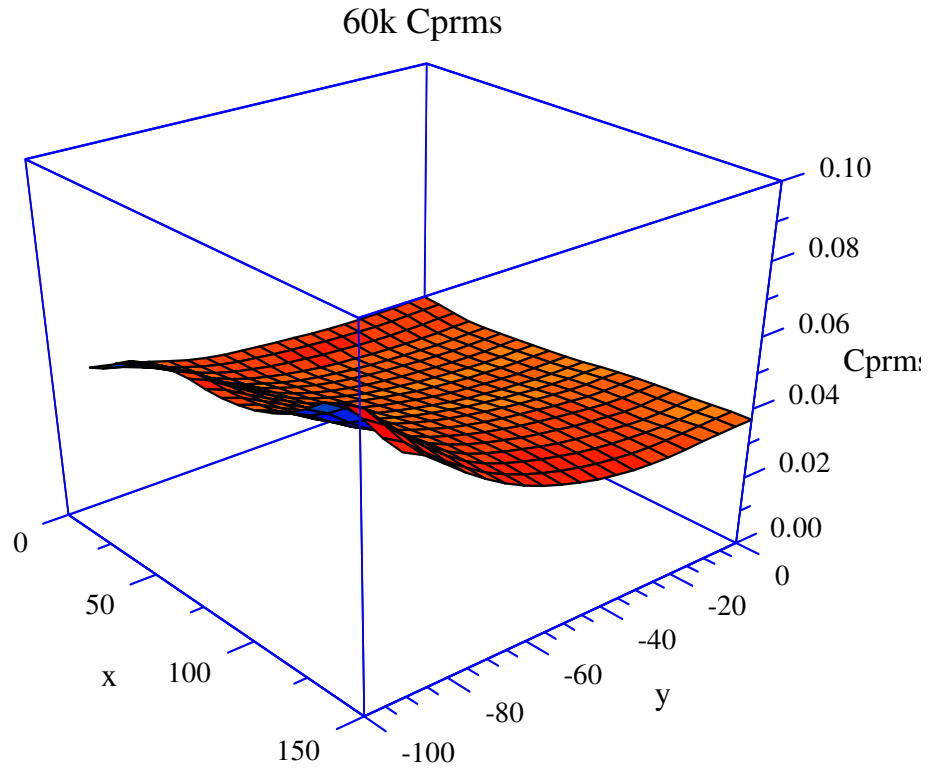

Figure 3.7: Fluctuating Pressure Coefficients (Cprms) -3D - 60 km/h

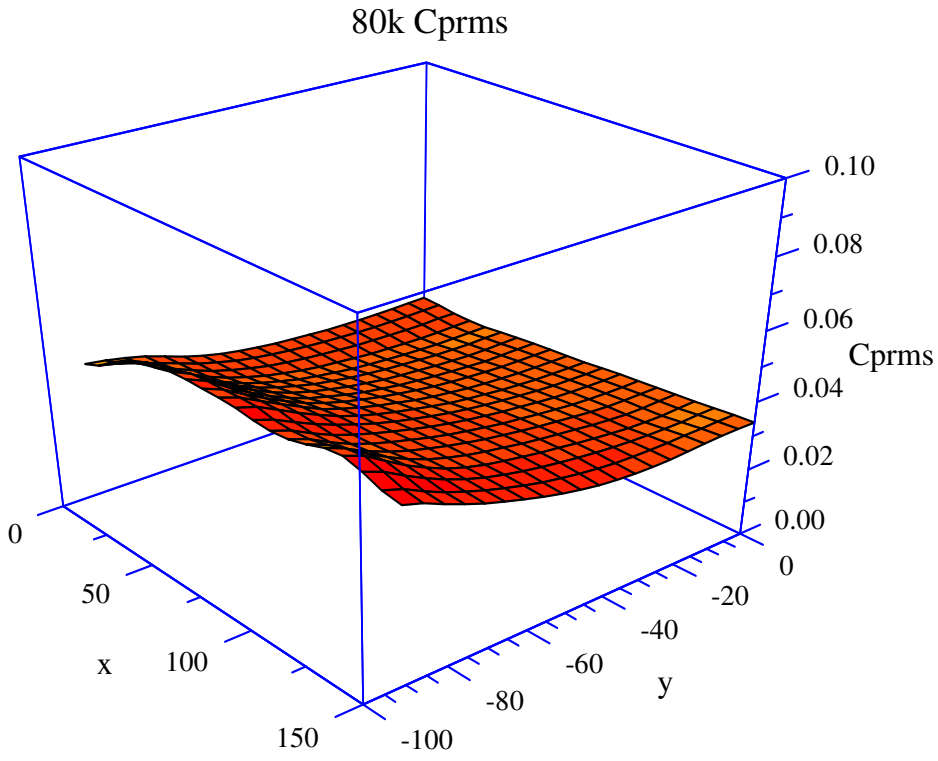

Figure3.8: Fluctuating Pressure Coefficients (Cprms) -3D - 80 km/h

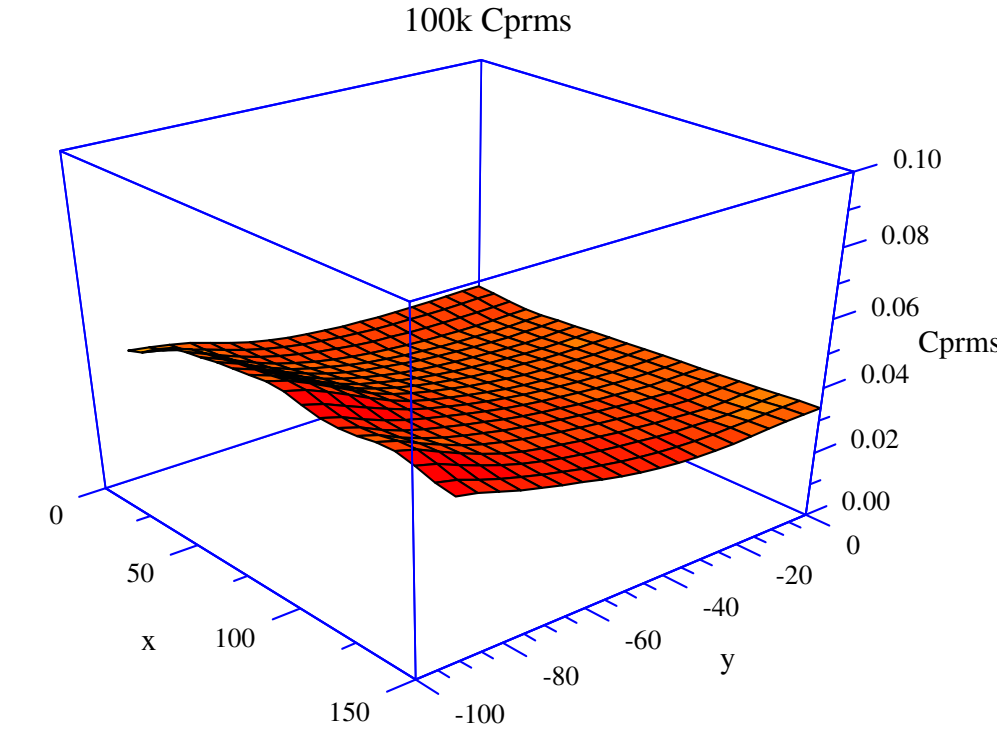

Figure 3.9: Fluctuating Pressure Coefficients (Cprms) -3D -100 km/h

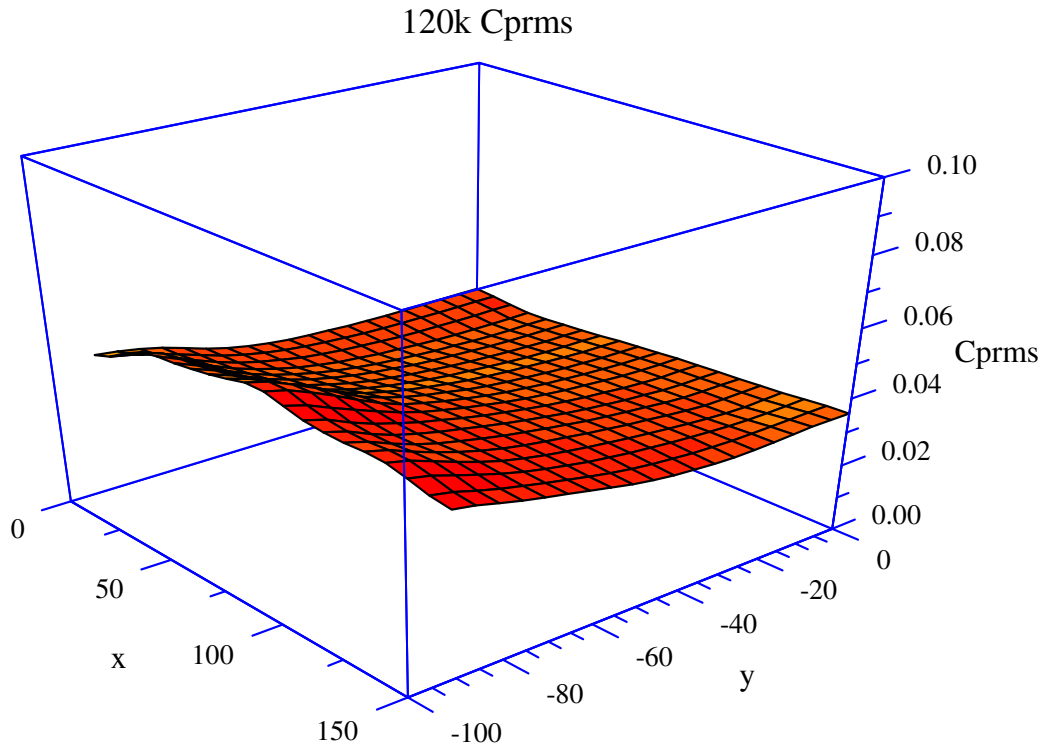

Figure 3.10: Fluctuating Pressure Coefficients (Cprms) -3D -120 km/h

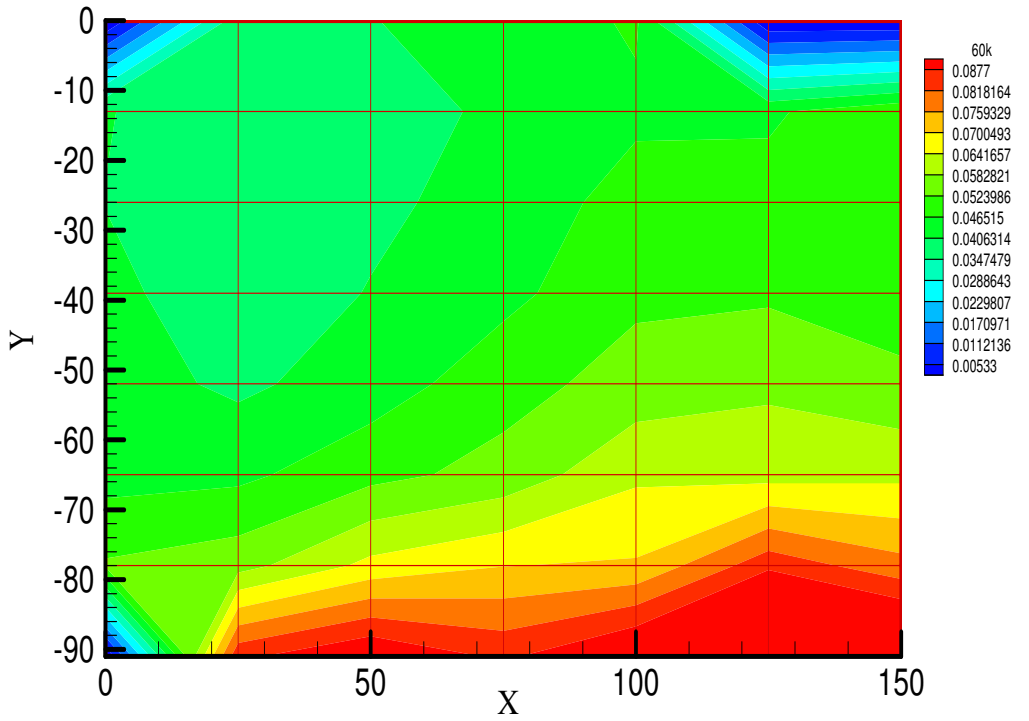

Figure 3.11: Fluctuating Pressure Coefficients (Cprms) -2D -60 km/h

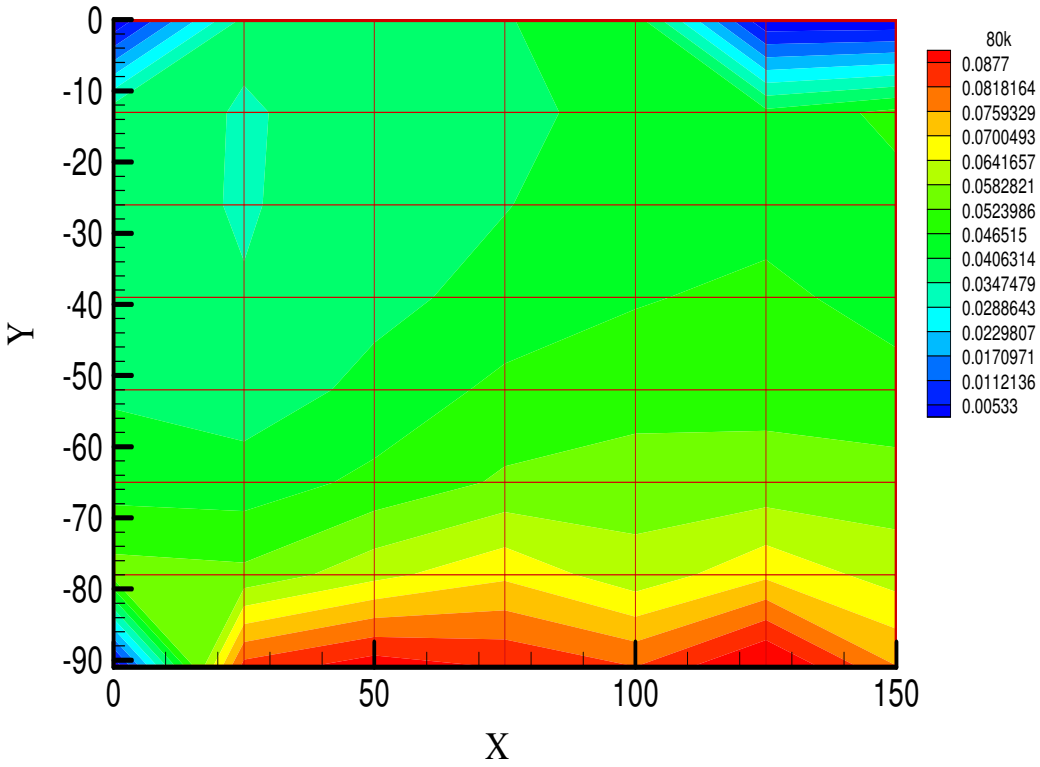

Figure 3.12: Fluctuating Pressure Coefficients (Cprms) -2D -80 km/h

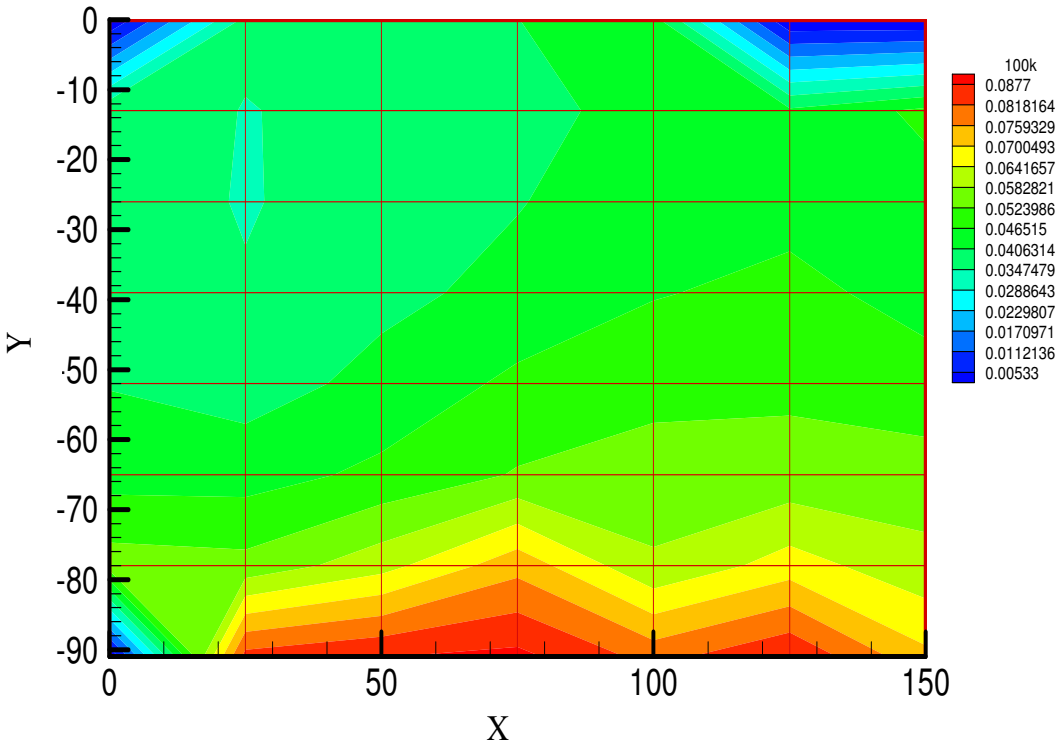

Figure 3.13: Fluctuating Pressure Coefficients (Cprms) -2D -100 km/h

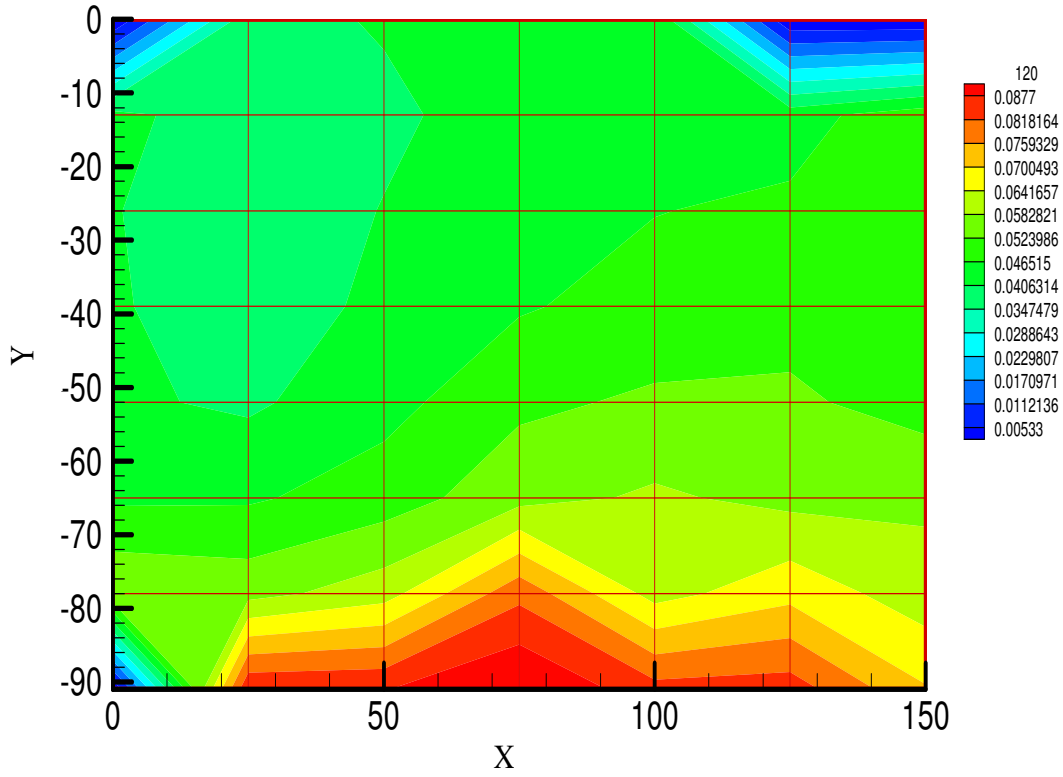

Figure 3.14: Fluctuating Pressure Coefficients (Cprms) -2D -120 km/h

3.5 Modified Mirror

The modification of the standard mirror is done by attaching thin plywood to its external periphery in order to see the effects of the air pressure on mirror's surface by comparing it with standard mirror. The three shrouding lengths used were of lengths: 24mm, 34mm and 44mm. the results of each shrouding length are discussed in the next 3 subsections.

3.5.1 24 mm Shroud

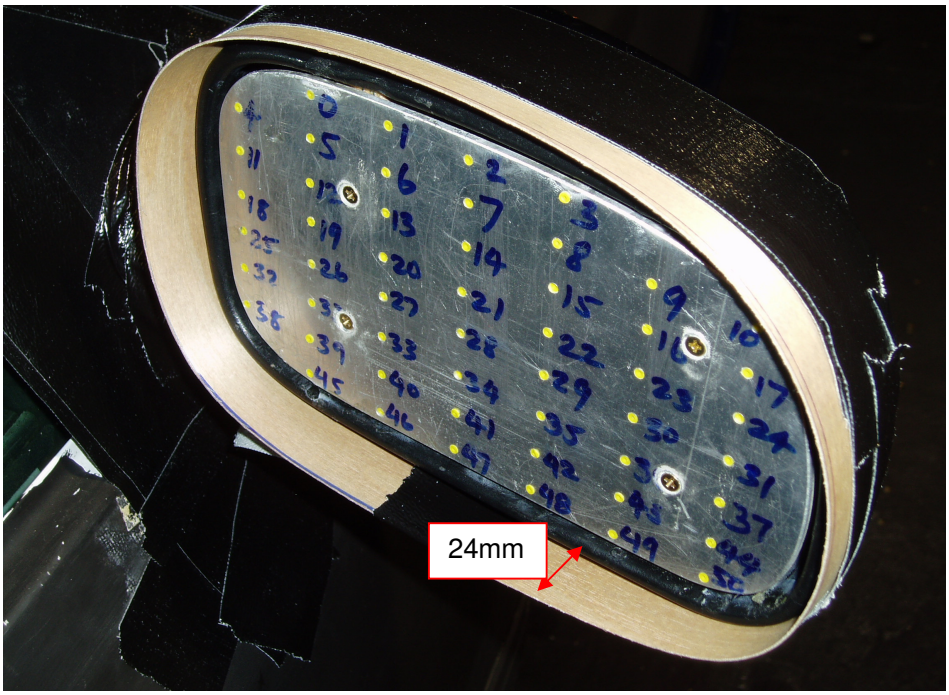

Figure 3.15: 24mm Shrouding

The standard mirror was firstly modified to 24mm shroud to see the edge effects on mirror surface pressure fluctuations. The contours of the fluctuating pressure (Cp rms) for 2-D and 3-D plots are shown in Figures 3.16 – 3.23 for all speeds for 24mm. In standard mirror case the general trend of highest fluctuating pressure was observed at the bottom central part of the mirror face as the speed was increased. In 24mm shroud case this trend has reversed due to recirculation on the mirror face due to mirror geometry been changed on the external periphery. This may be due to recirculating of the vortex on the mirror face. However, due to the addition of the shrouding lengths it is observed that the vortex around the mirror face dissipated at a distance larger that being observed in case of standard mirror. Moreover, it is

also due to fact of complex airflow from the root of the mirror that meets the flow from the top, bottom and side ways of the mirror periphery that changes the location of Cp rms from bottom to top position on the mirror face. Moreover, it was also noted that with the introduction of the shrouding the bottom area fluctuating pressure was eliminated as that was observed in case of standard mirror. The general trend of maximum fluctuating pressures was noted at the top central part of the mirror face. However, at the far end, the top section of the mirror, the highest fluctuating pressure was measured, which is believed to be due to the mirror shell housing and the recirculation of airflow around the edges.

3.5.1.1 Results of 24mm Shroud

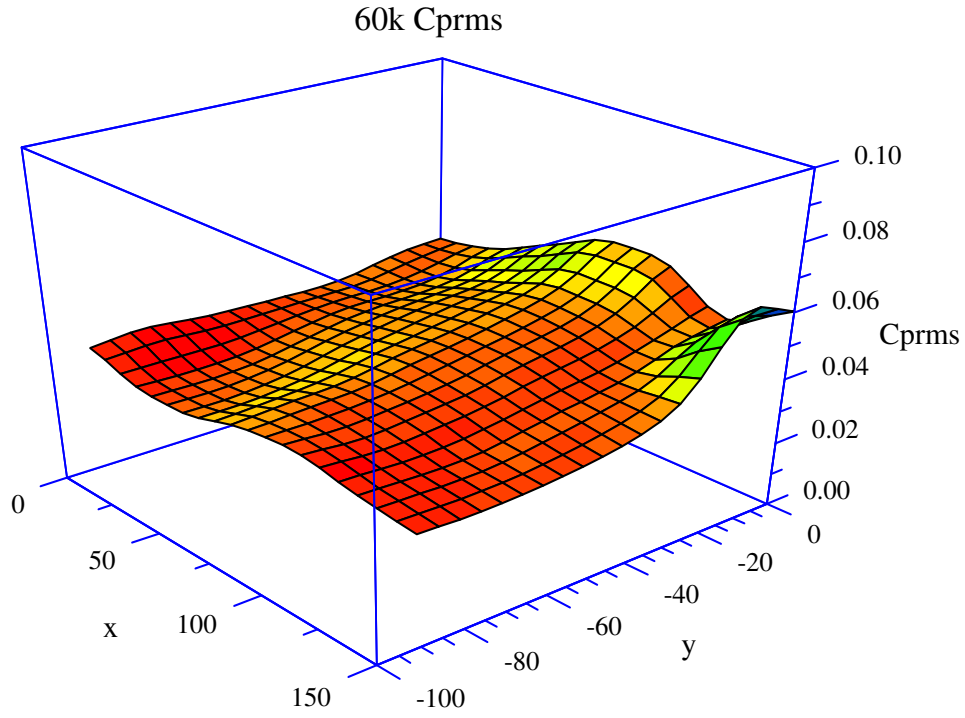

Figure 3.16: Fluctuating Pressure Coefficients (Cprms) -3D - 60 km/h

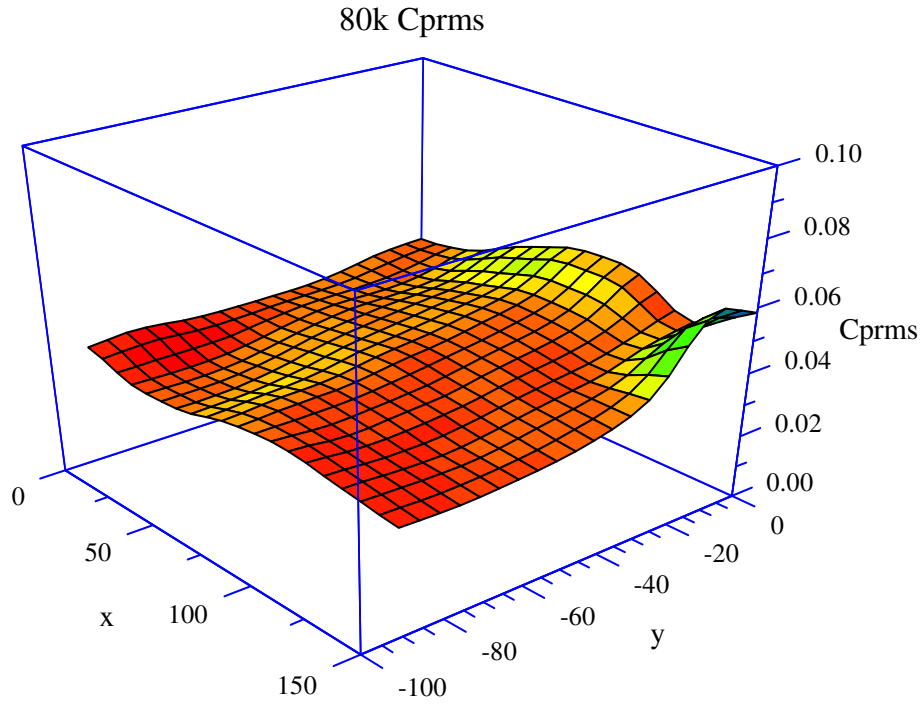

Figure 3.17: Fluctuating Pressure Coefficients (Cprms) -3D - 80 km/h

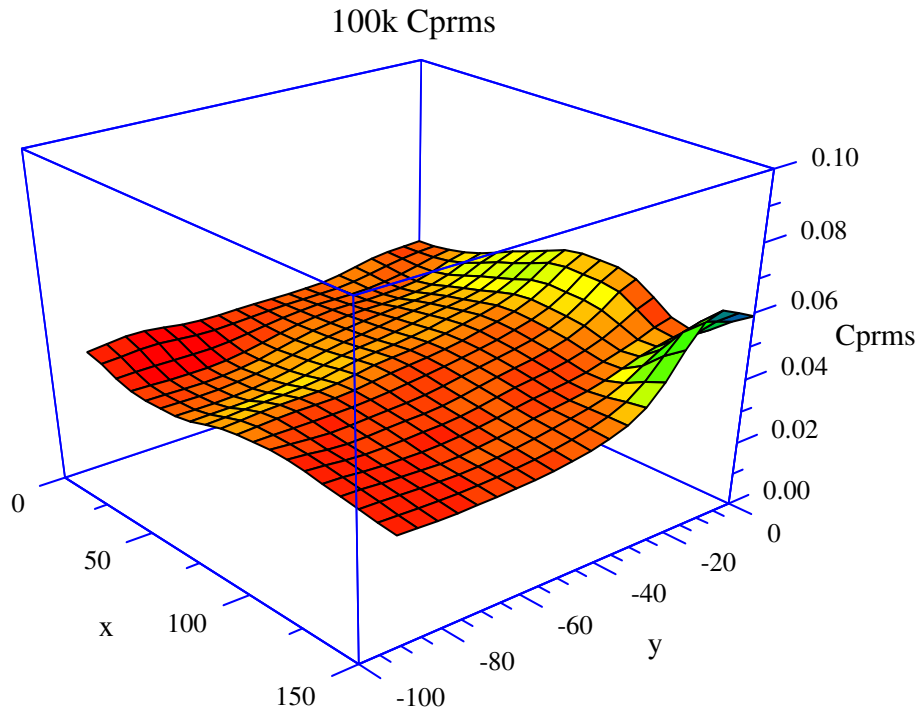

Figure 3.18: Fluctuating Pressure Coefficients (Cprms) -3D -100 km/h

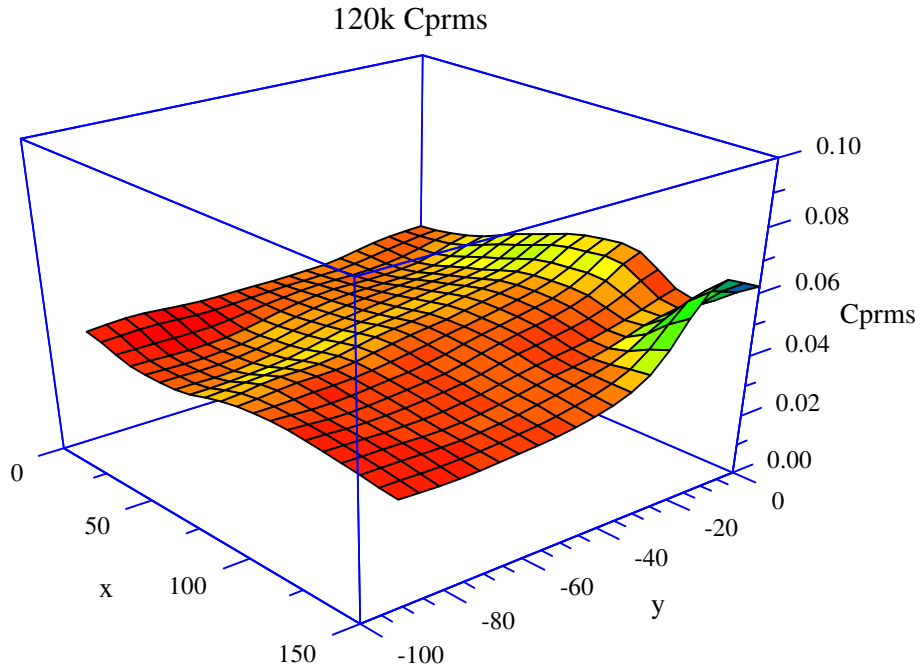

Figure 3.19: Fluctuating Pressure Coefficients (Cprms) -3D - 120 km/h

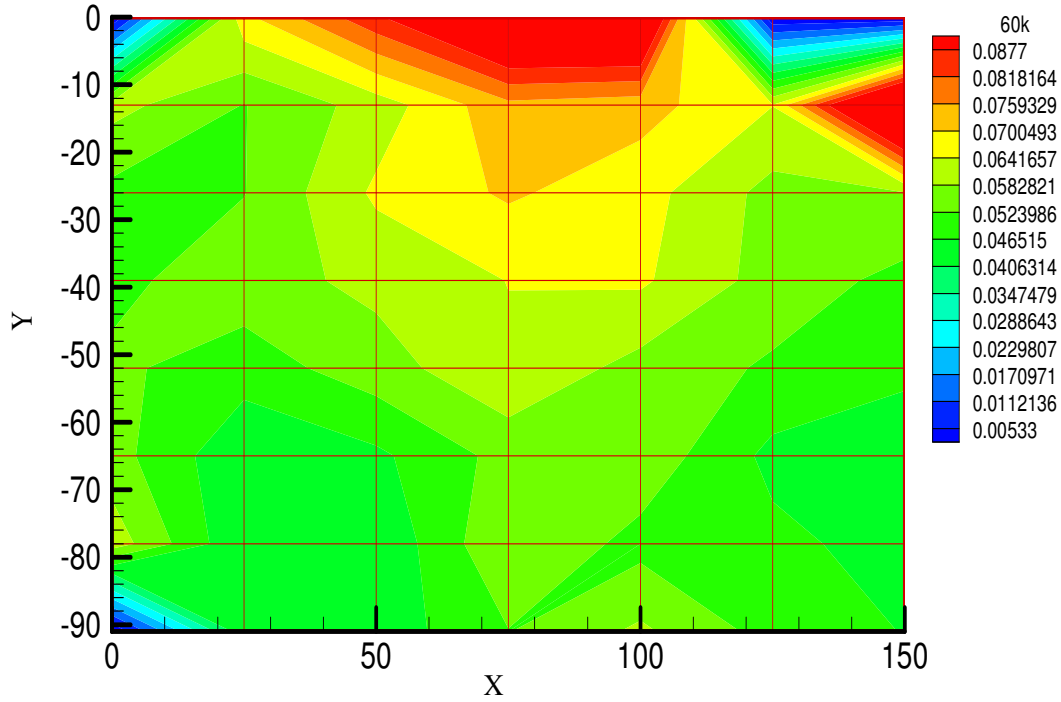

Figure 3.20: Fluctuating Pressure Coefficients (Cprms) - Contours - 60 km/h

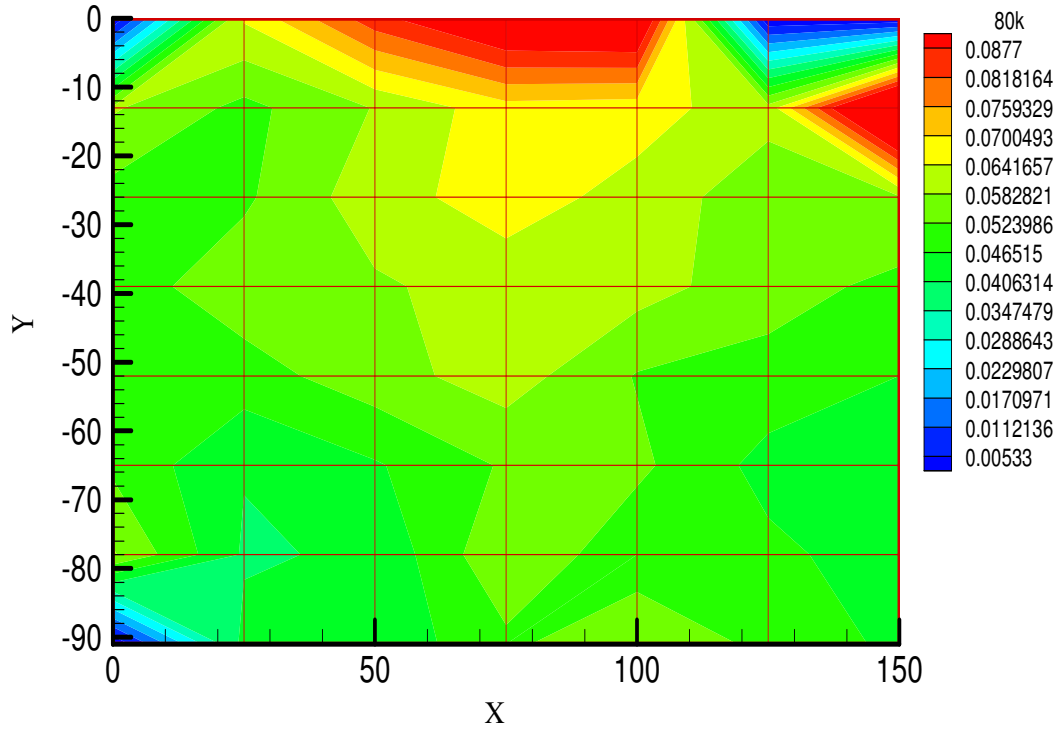

Figure 3.21: Fluctuating Pressure Coefficients (Cprms) - Contours - 80 km/h

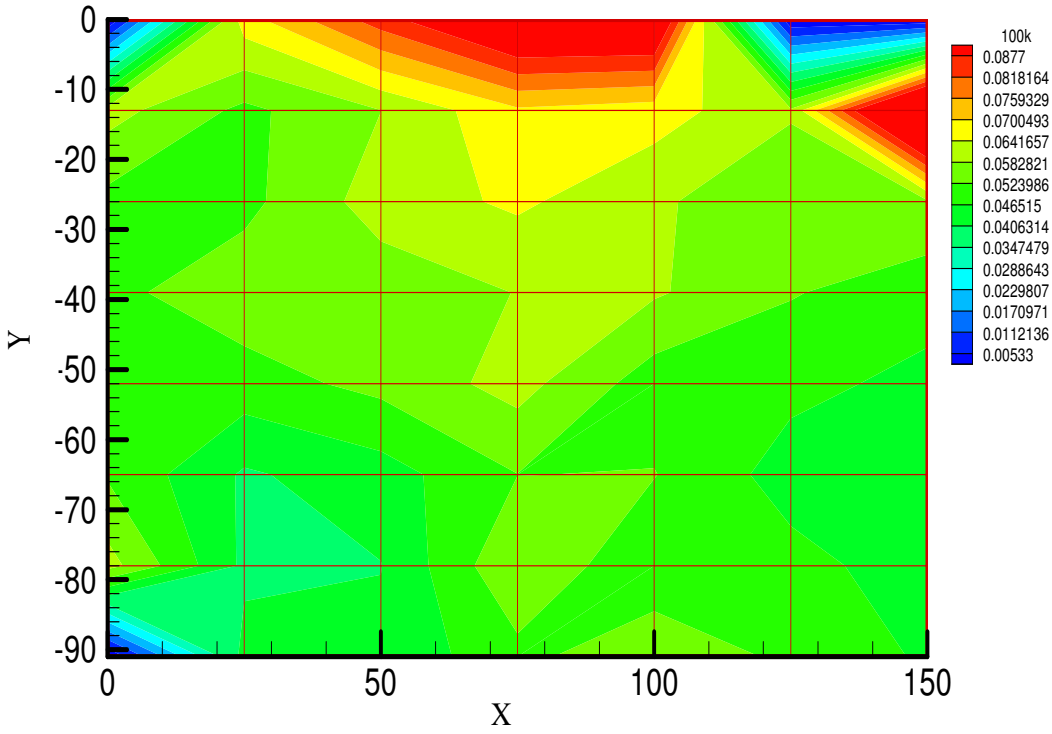

Figure 3.22: Fluctuating Pressure Coefficients (Cprms) - Contours - 100 km/h

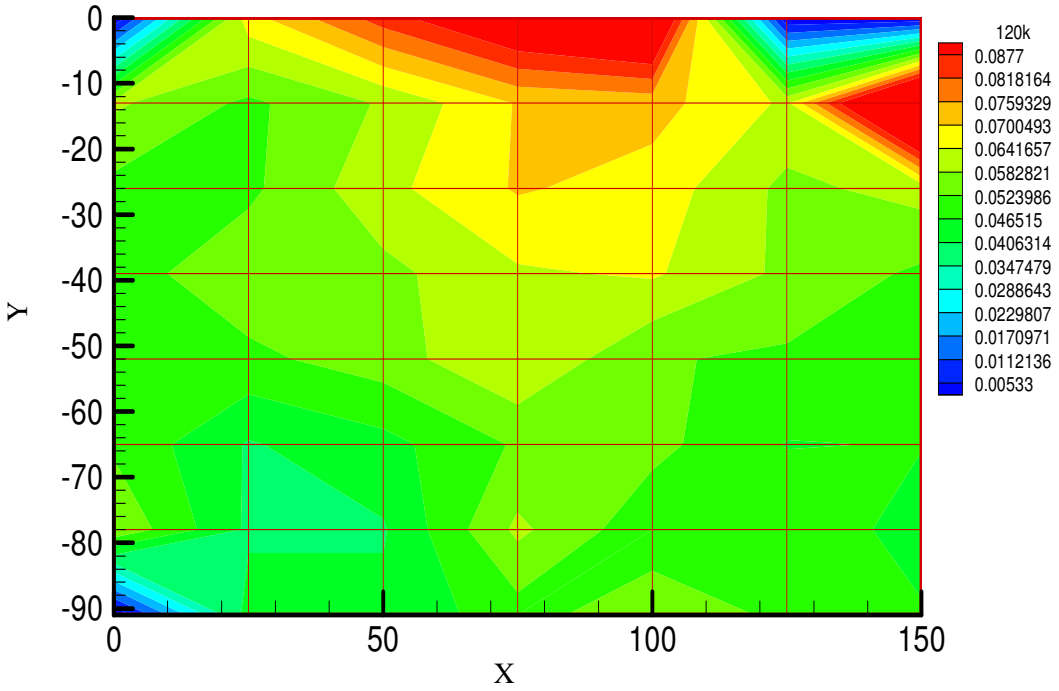

Figure 3.23: Fluctuating Pressure Coefficients (Cprms) - Contours - 120 km/h

3.5.2 34mm Shroud

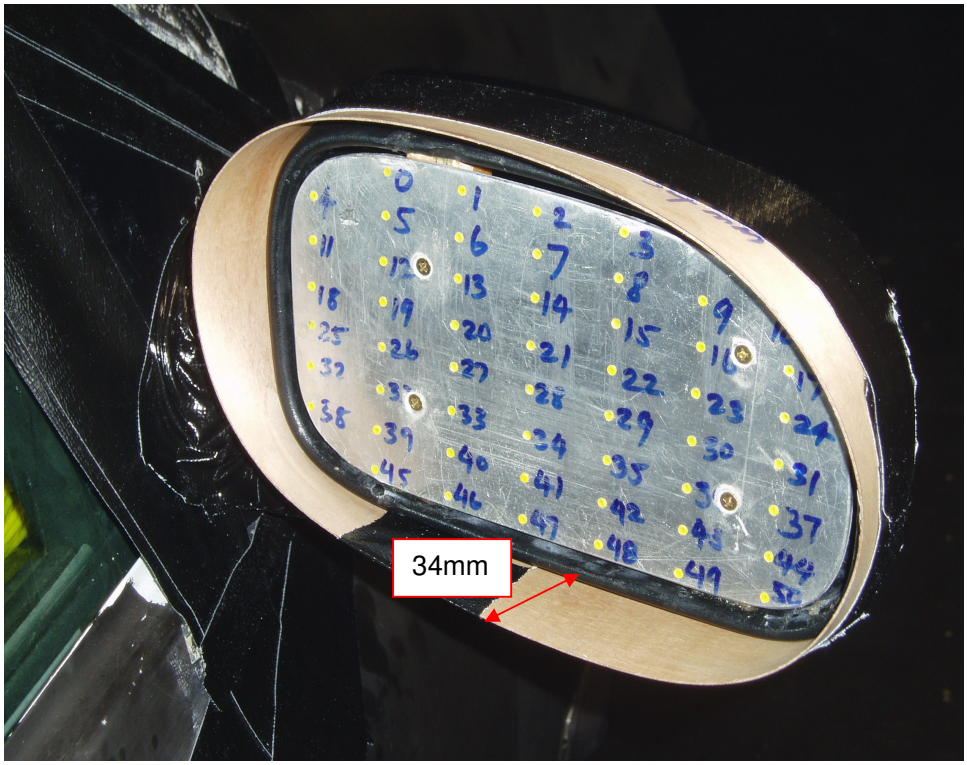

Figure 3.24: 34mm Shroud

The standard mirror was later modified to 34mm shroud as shown in Figure 3.24, to see the effects on mirror surface pressure fluctuations. The contours of fluctuating pressure (Cprms) for 2-D and 3-D plots are shown in Figures 3.25 – 3.32 for all speeds of 34mm shroud. As seen above from the graphs of the 24mm shroud that the maximum Fluctuating Pressure coefficient is at the top central part of the mirror top flange, but in case of the 34mm shrouds the magnitude of this fluctuating pressure coefficient has decreased on the same point. Moreover, the drop was also achieved on the bottom central part of the mirror face showing the effects of this shrouding on the mirror face. However, from the graphs shown below it is believed that shrouding plays an important role in the drop of pressure on mirror face. In general when the air flows over the mirror face it travels further down the mirror face due to shrouding and then breaks down resulting in drop in magnitude of pressure fluctuation on mirror face. However, the magnitude of the fluctuating pressure coefficient on the upper far end section of the mirror section causes in drop of fluctuating pressure due to increase in the length of shrouding which indicates that shrouding has an impact on the mirror face.

3.5.2.1 Results of 34mm Shroud

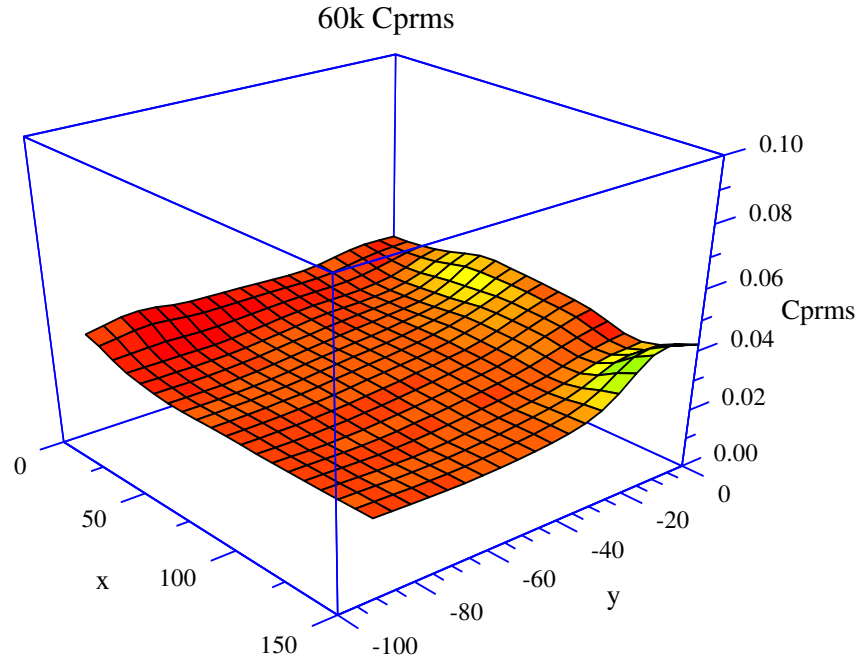

Figure 3.25: Fluctuating Pressure Coefficients (Cprms) -3D - 60 km/h

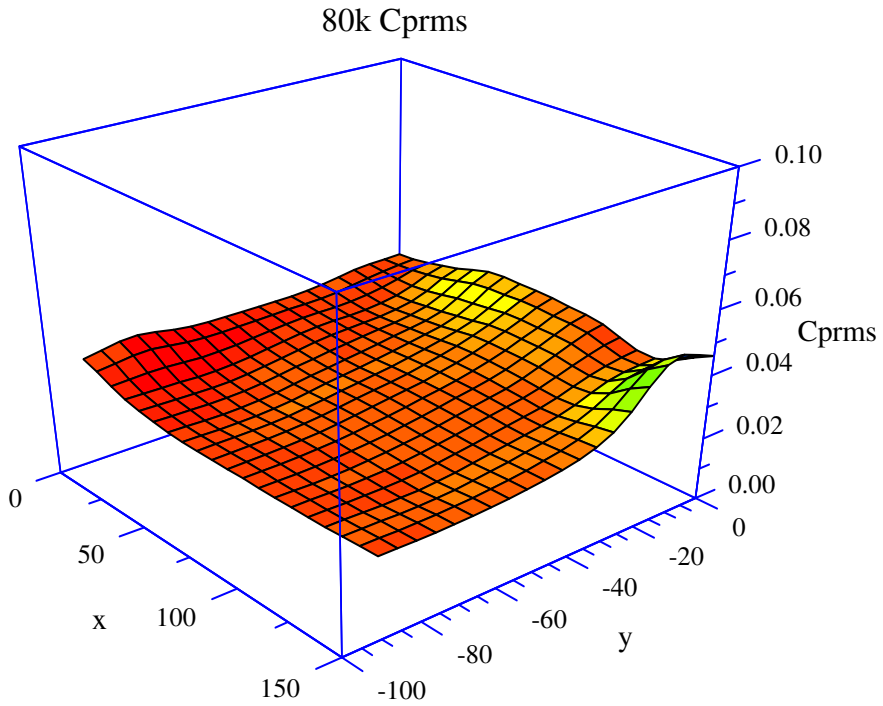

Figure 3.26: Fluctuating Pressure Coefficients (Cprms) -3D - 80 km/h

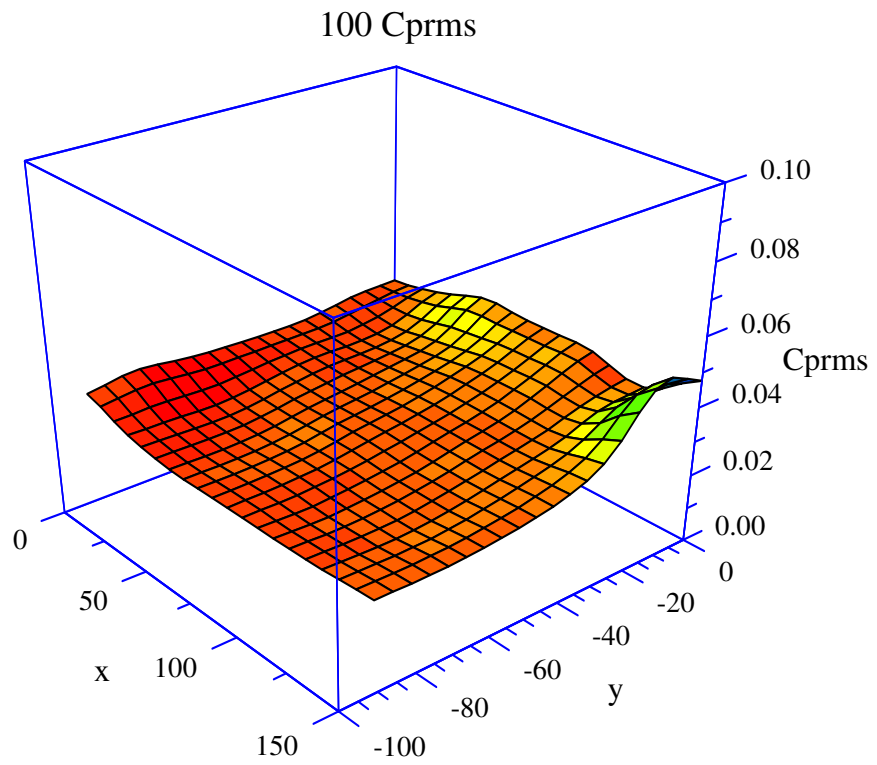

Figure 3.27: Fluctuating Pressure Coefficients (Cprms) -3D - 100 km/h

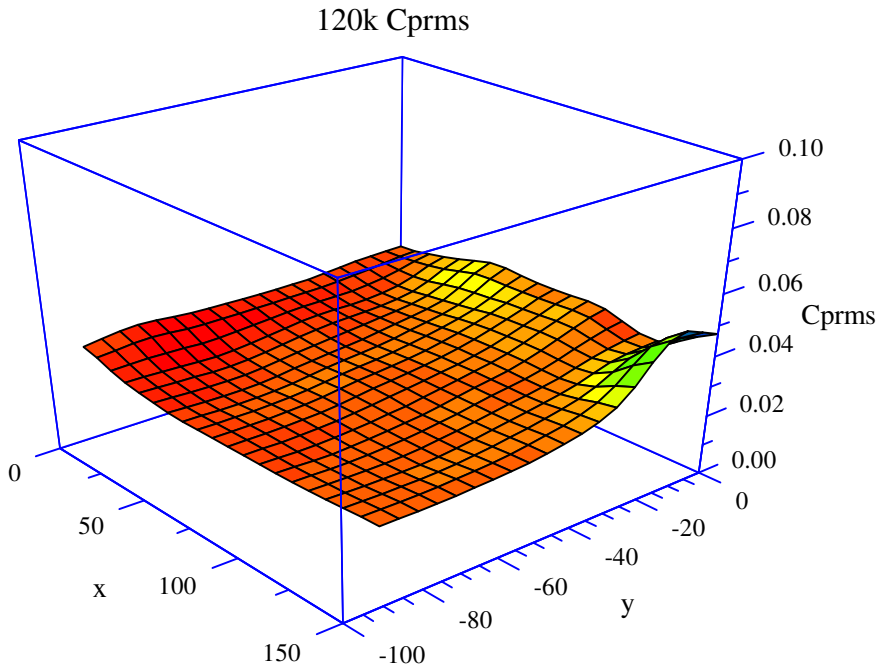

Figure3.28: Fluctuating Pressure Coefficients (Cprms) -3D - 120 km/h

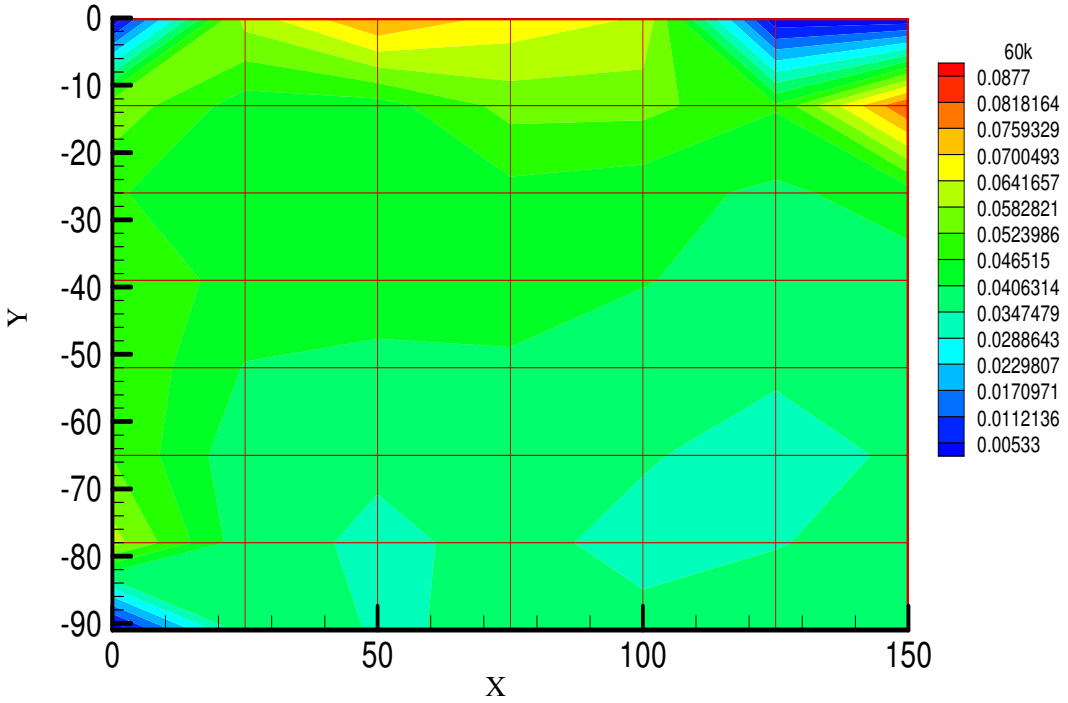

Figure 3.29: Fluctuating Pressure Coefficients (Cprms) - Contours - 60 km/h

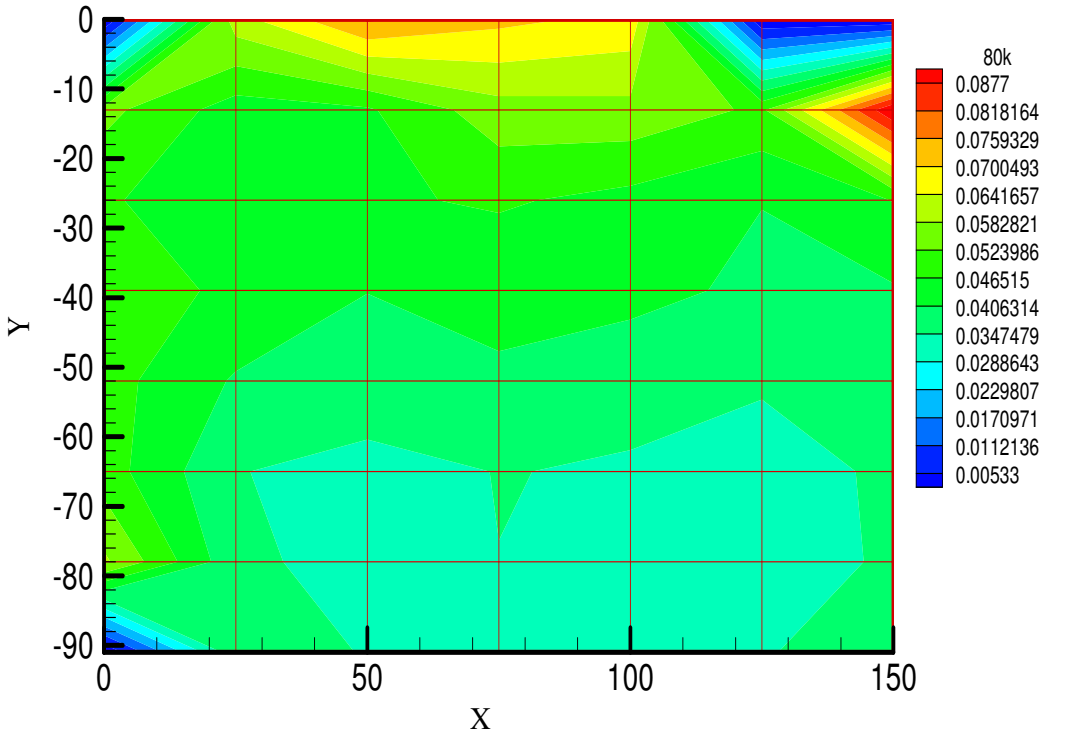

Figure 3.30: Fluctuating Pressure Coefficients (Cprms) - Contours - 80 km/h

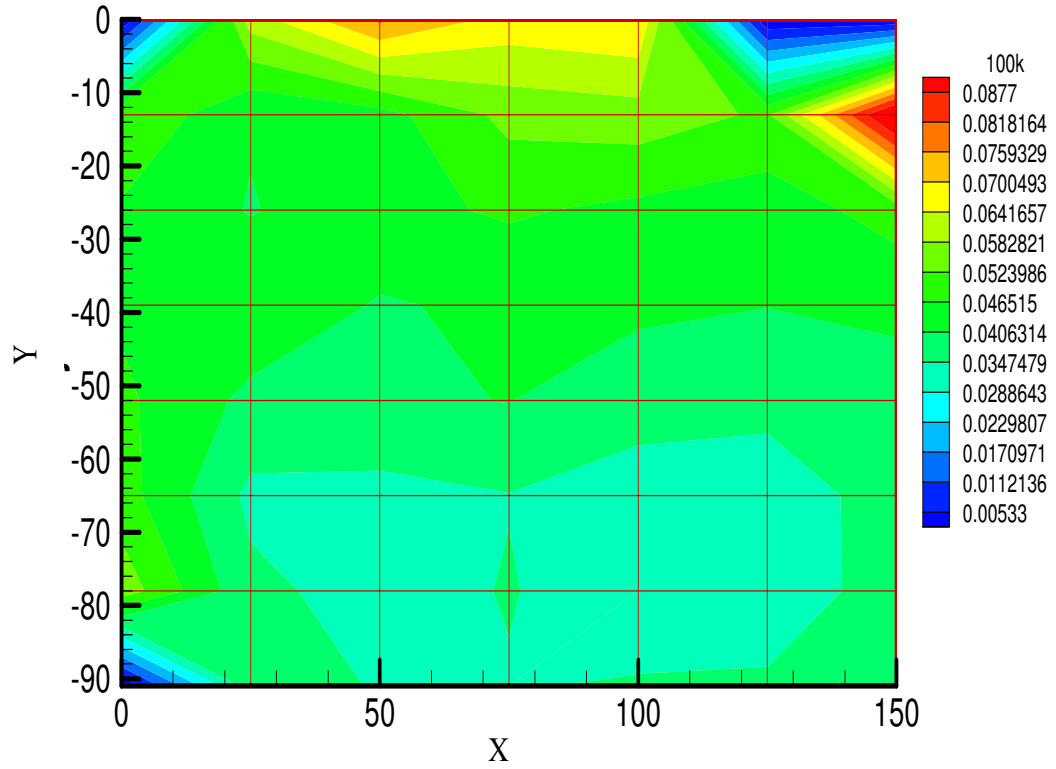

Figure 3.31: Fluctuating Pressure Coefficients (Cprms) - Contours - 100 km/h

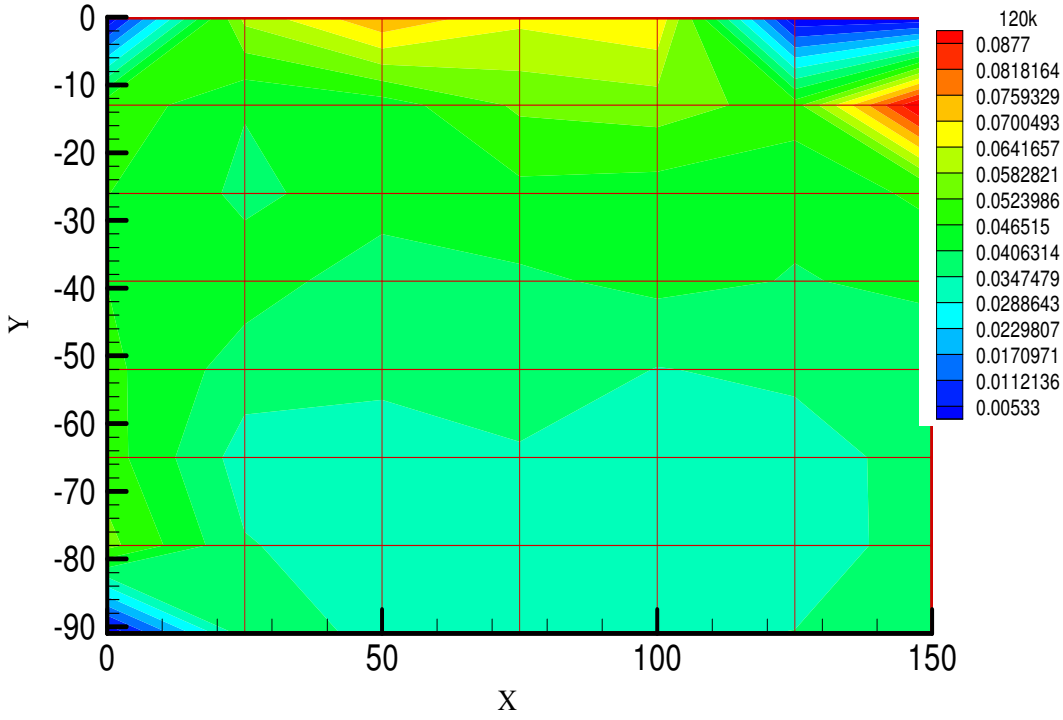

Figure 3.32: Fluctuating Pressure Coefficients (Cprms) - Contours - 120 km/h

3.5.3 44mm Shroud

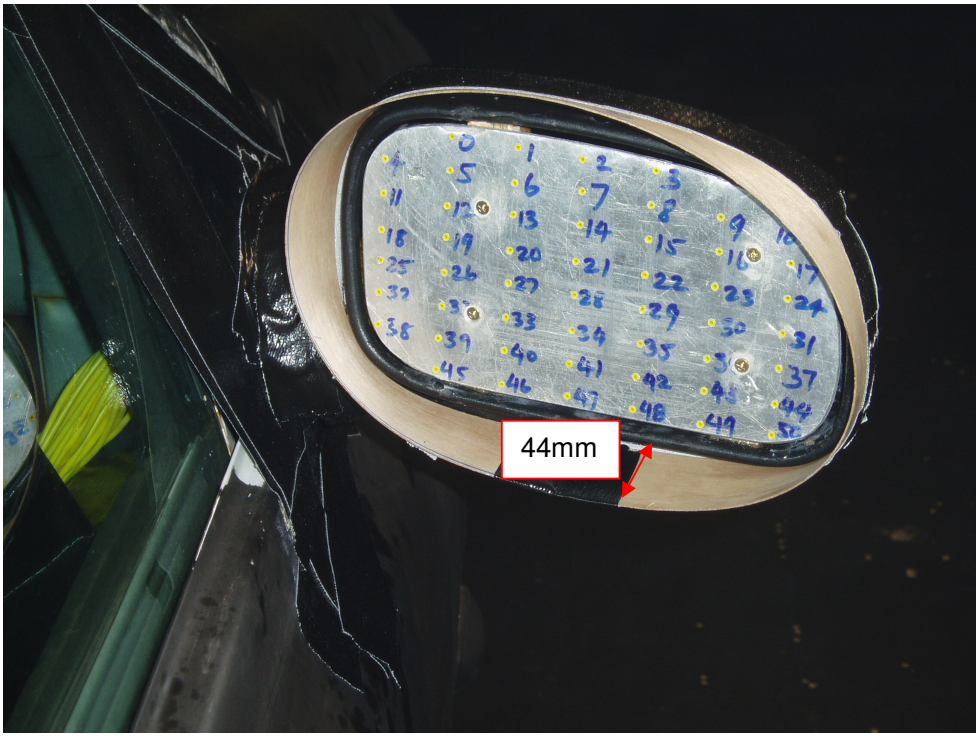

Figure 3.33: 44mm Shrouding

The standard mirror was lastly modified to 44mm shroud as shown in Figure 3.33, to see the effects on mirror surface pressure fluctuations. The contour and 3-D plots are shown in Figures 3.34– 3.41 for the speeds of 100 km/h for 44mm shroud for fluctuating pressure Coefficient (Cprms). As seen from the 24mm and 34mm shroud it is believed that the shrouding has its effects of the pressure variation on the mirror face. With 44mm shrouding we can see that the magnitude of the pressure drops further down as observed with the 24mm and 34mm shroud. We can observe the further drop in the pressure at the bottom part of the mirror face along with elimination of the high Fluctuating Pressure coefficient that was observed on the top face of the mirror flange. It can be noticed that with 44mm shroud there is a drop on the face of the mirror surface as vortex shedding is observed further away from the face of the mirror. The maximum effect in pressure variation was achieved with the 44 mm shrouding length.

3.5.3.1 Results of 44mm Shroud

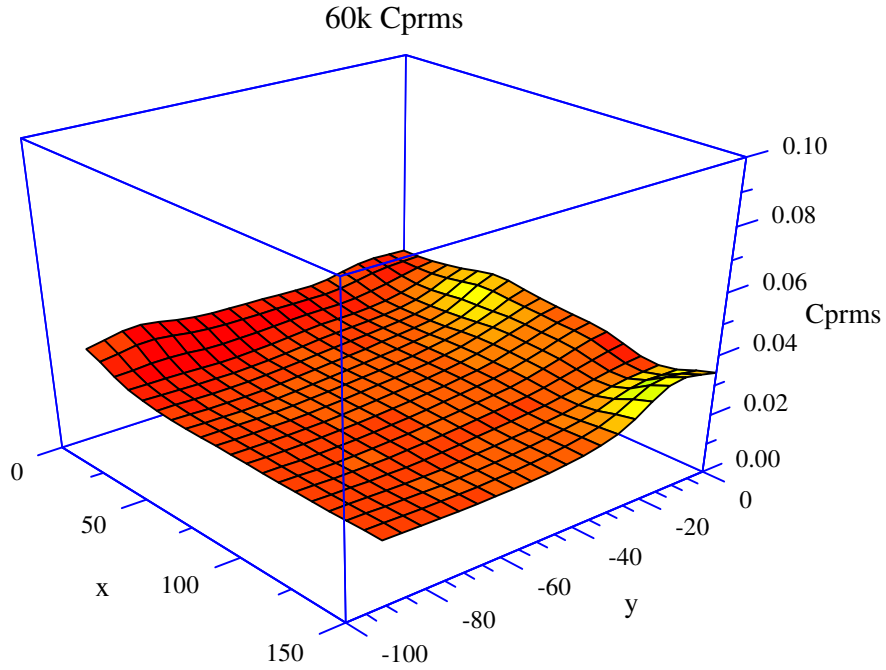

Figure 3.34: Fluctuating Pressure Coefficients (Cprms) -3D - 60 km/h

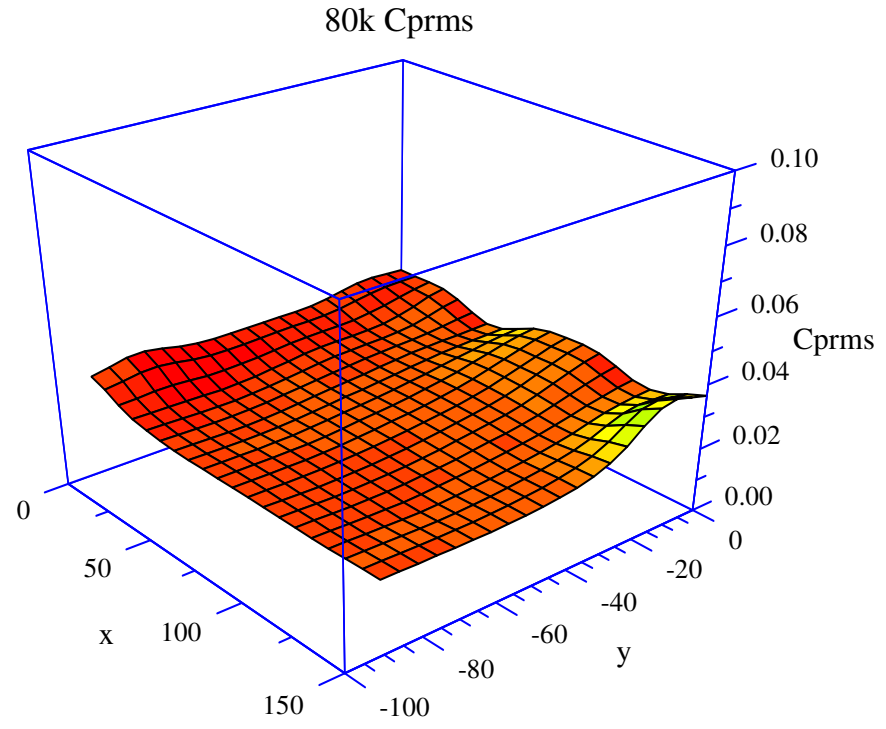

Figure3.35: Fluctuating Pressure Coefficients (Cprms) -3D - 80 km/h

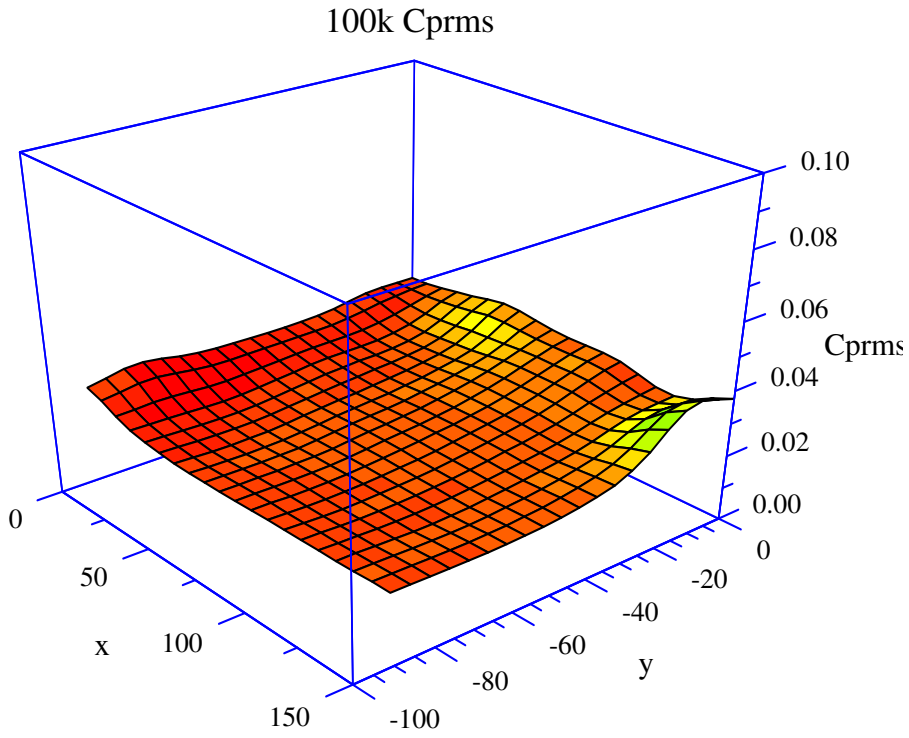

Figure 3.36: Fluctuating Pressure Coefficients (Cprms) -3D - 100 km/h

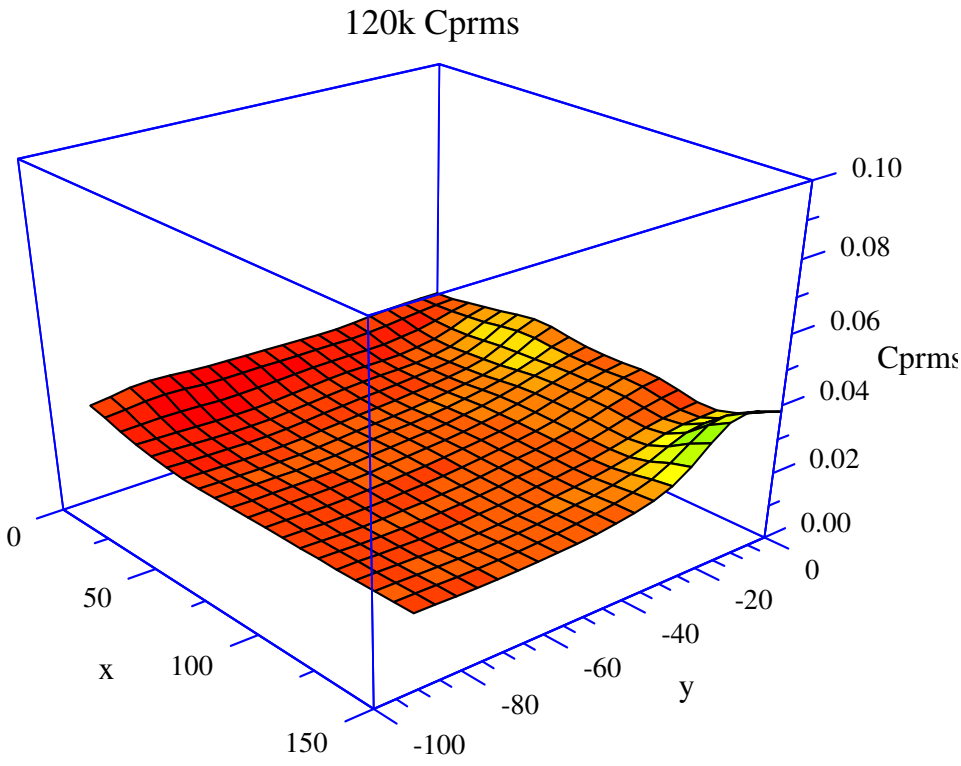

Figure 3.37: Fluctuating Pressure Coefficients (Cprms) -3D - 120 km/h

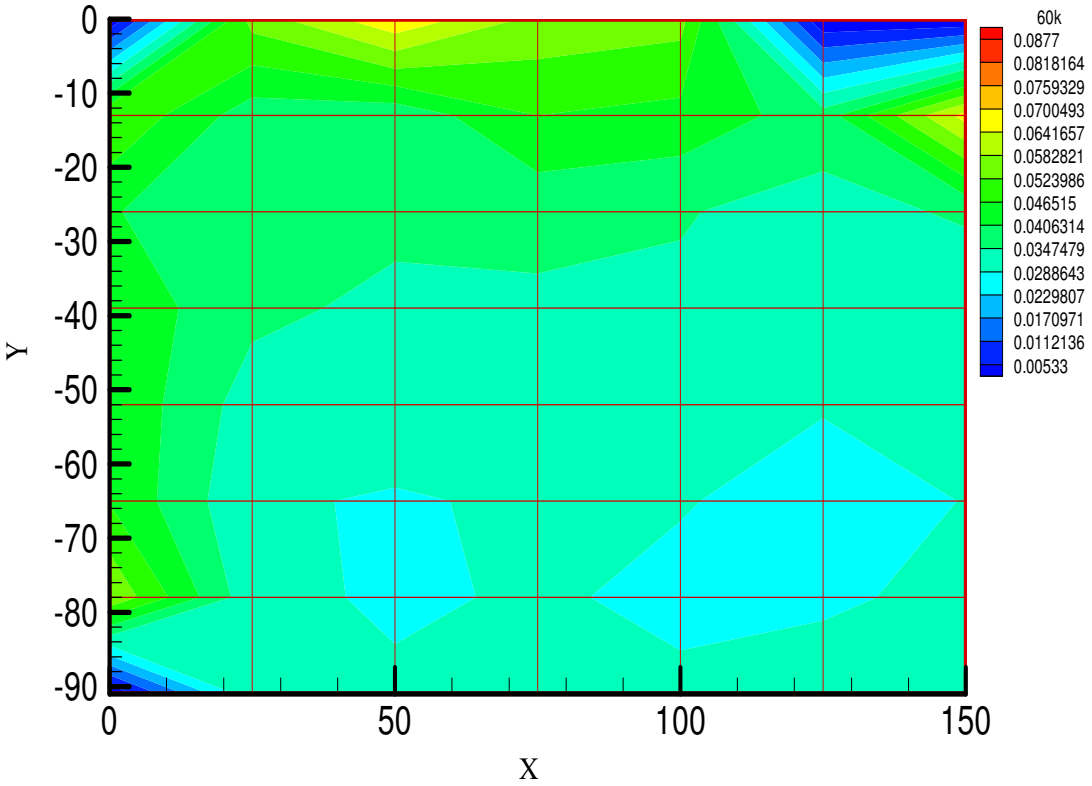

Figure 3.38: Fluctuating Pressure Coefficients (Cprms) – 2D -60 km/h

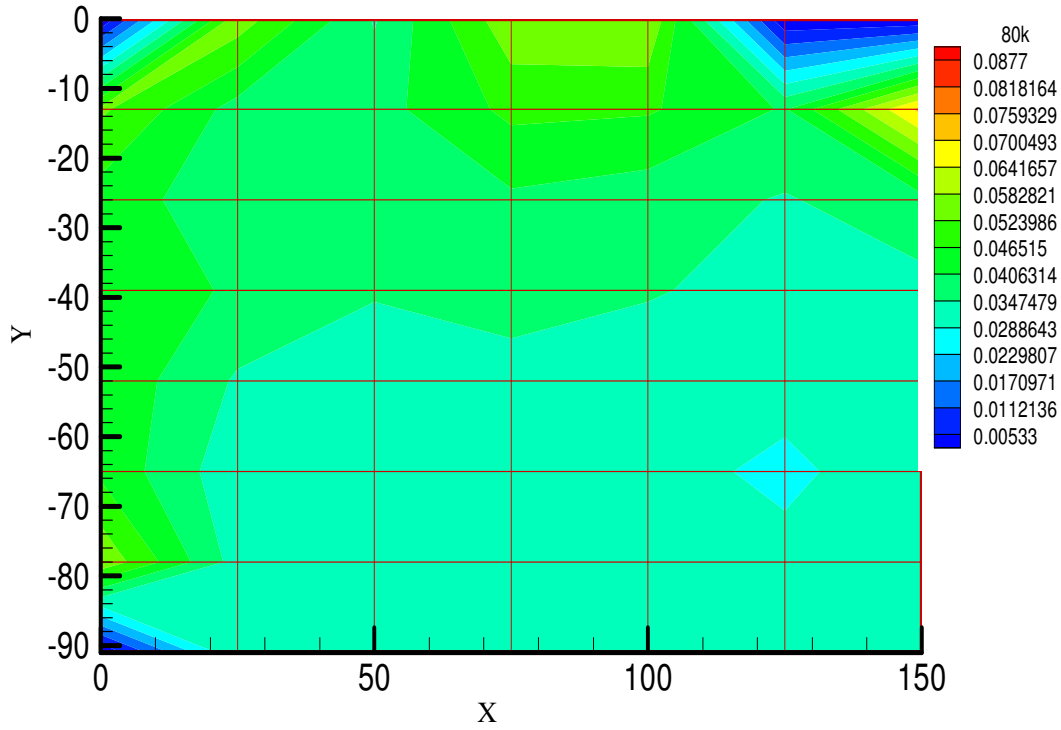

Figure 3.39: Fluctuating Pressure Coefficients (Cprms) – 2D -80 km/h

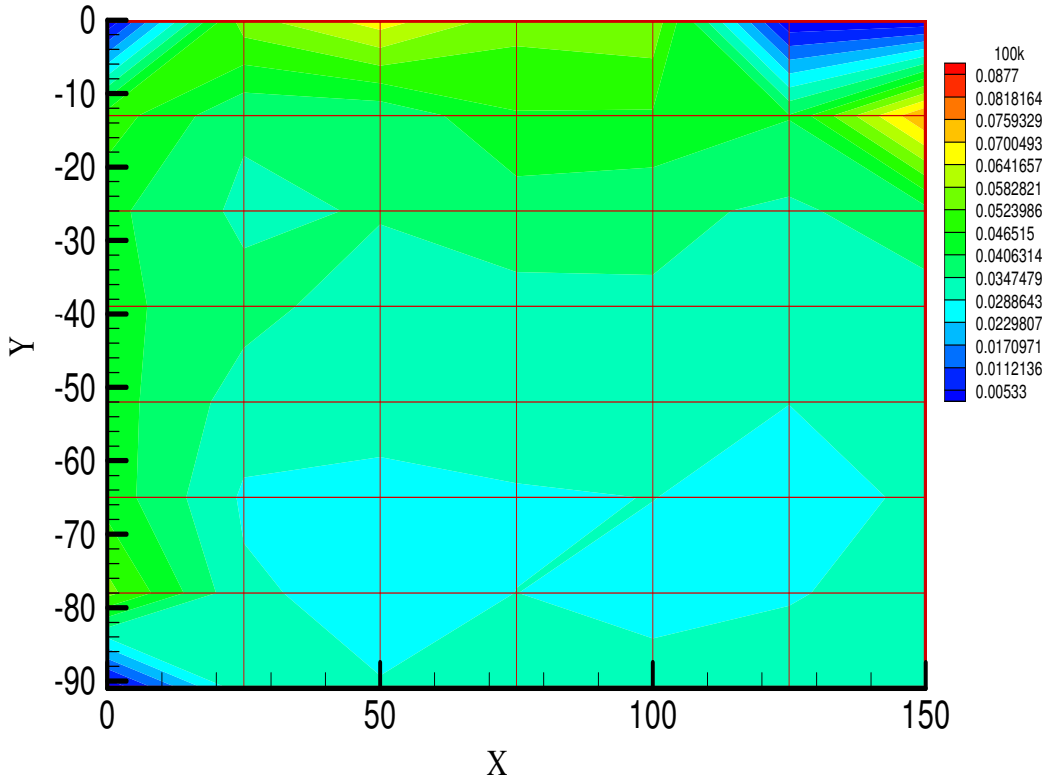

Figure 3.40: Fluctuating Pressure Coefficients (Cprms) – 2D -100 km/h

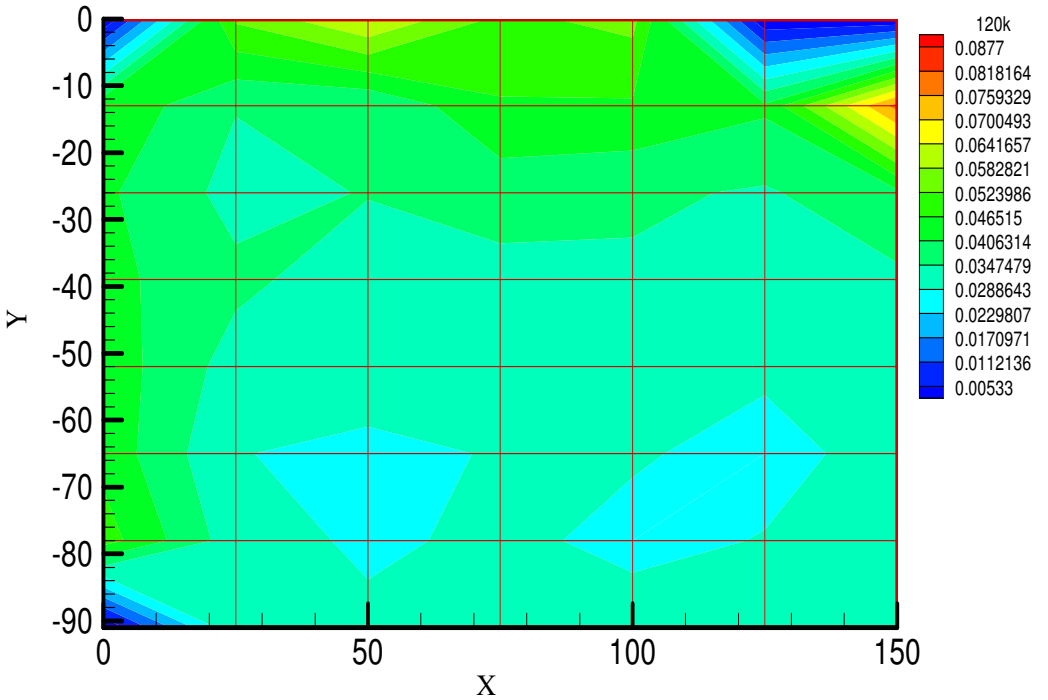

Figure 3.41: Fluctuating Pressure Coefficients (Cprms) – 2D -120 km/h

3.6 Shell Housing Data

Figure 3.42: Pressure Taps Arrangement on the Mirror Housing

The pressure measurement was also carried out on the mirror housing in order to find out the pressure distributon over the mirror housing, see Figure 3.42. However, for this pressure taps were done on the mirror housing keeping the horizontal and vertical distance the same as done in case of the mirror face. The testing for the mirror housing was carried only for 60 km/h, 80km,hr, 100 km/h but not at 120 km/h. This is due to the limitation of the DPMS software which was showing warning of over-rage voltage values at speeds from 100 km/h. So it was suggested to take the data only upto 100 km/h as higher speeds may cause problem within the software. Figures 3.43 to 3.48 shows the fluctuating pressure coefficient contours (Cprms) respectively. However, from the surface mean pressure graphs (Cp) the magnitude of high surface pressure is measured near to the car body, see Appendix E. However, the magnitude of pressure goes on decreasing as it travels towards the far end section of the mirror housing. The stagnation point (Cp=1) of the mirror shell housing can be measured at bottom central point of the mirror housing. However, from the fluctuating pressure coefficients (Cprms) it is believed that the pressure variation is dropped as it travels from the car body side to the far end section of the mirror housing (far away from the car body). There is also abrupt drop in

the pressure while we approach towards the far end section of the car, this can be due to the error or limitation of the over ranging voltage that was measured at those points. However, the DPMS used for the testing was having a maximum of ± 20Volts as the voltage limitation while conducting the wind tunnel testing. It can be noticed from the graphs that the Cp is higher measured near to the car body A-pillar section which is due to complex flow attained in that region. The mirror acts as a bluff body and also due to complex airflow high magnitude of surface pressure was measured near to the car body.

3.6.1 Results of Shell Housing Data

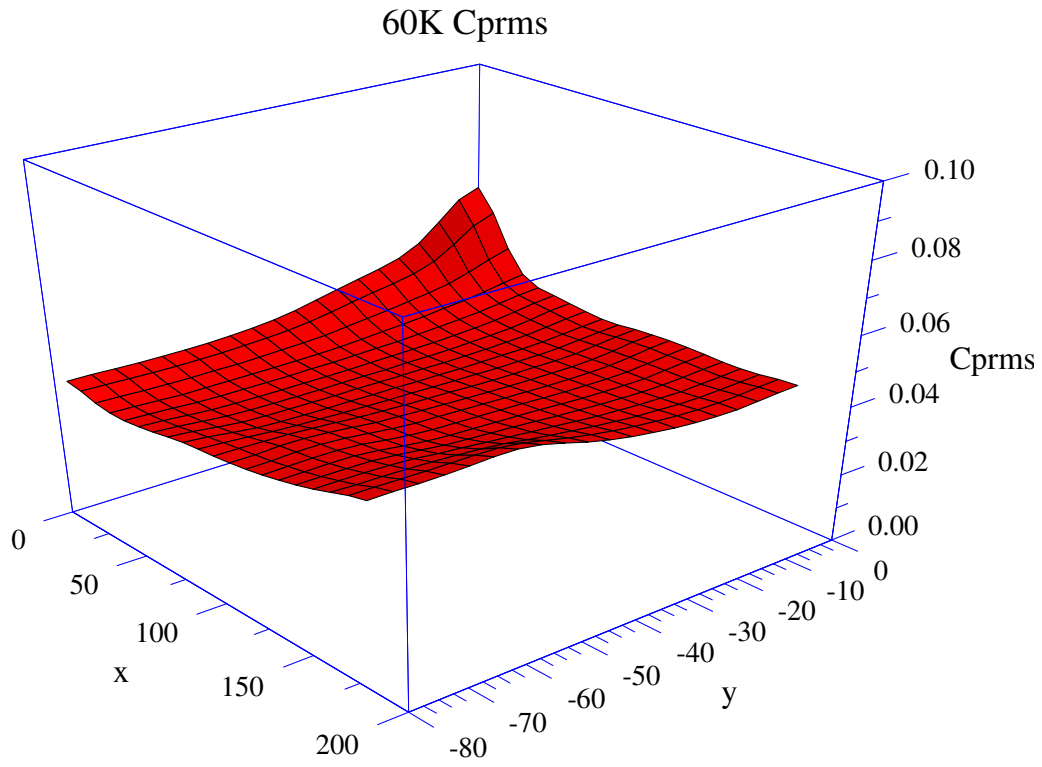

Figure 3.43: Fluctuating Pressure Coefficients (Cprms) -3D - 60 km/h

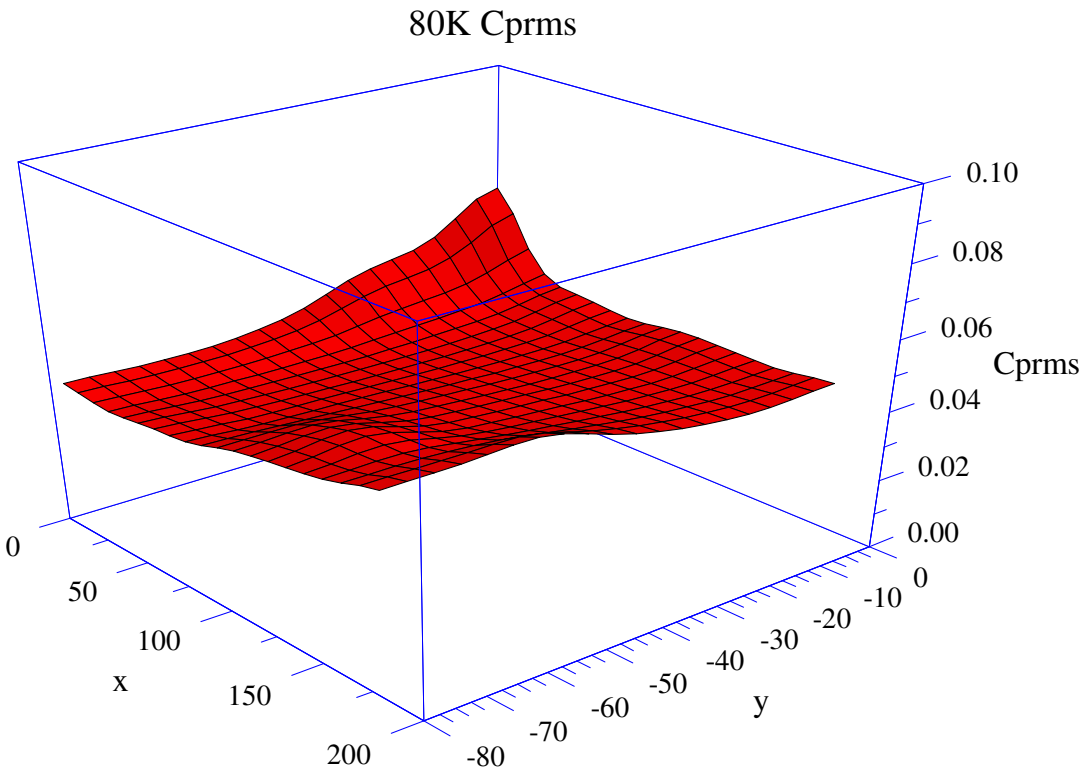

Figure 3.44: Fluctuating Pressure Coefficients (Cprms) -3D - 80 km/h

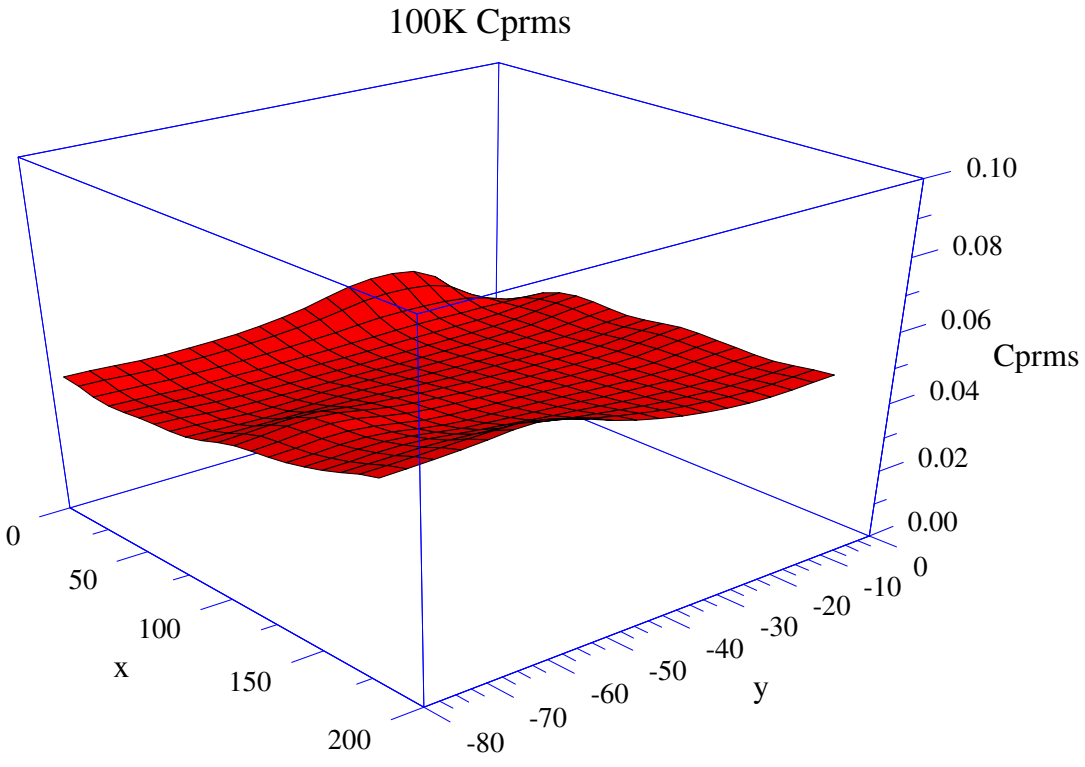

Figure 3.45: Fluctuating Pressure Coefficients (Cprms) -3D - 100 km/h

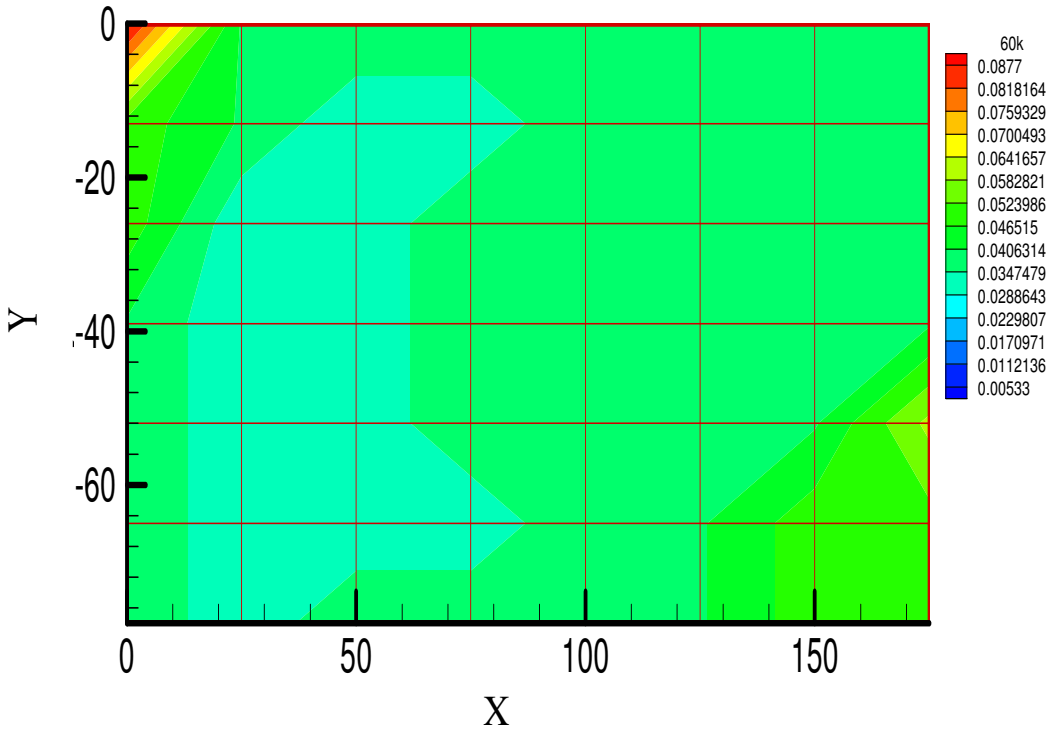

Figure 3.46: Fluctuating Pressure Coefficient Contours (Cprms) 60 km/h

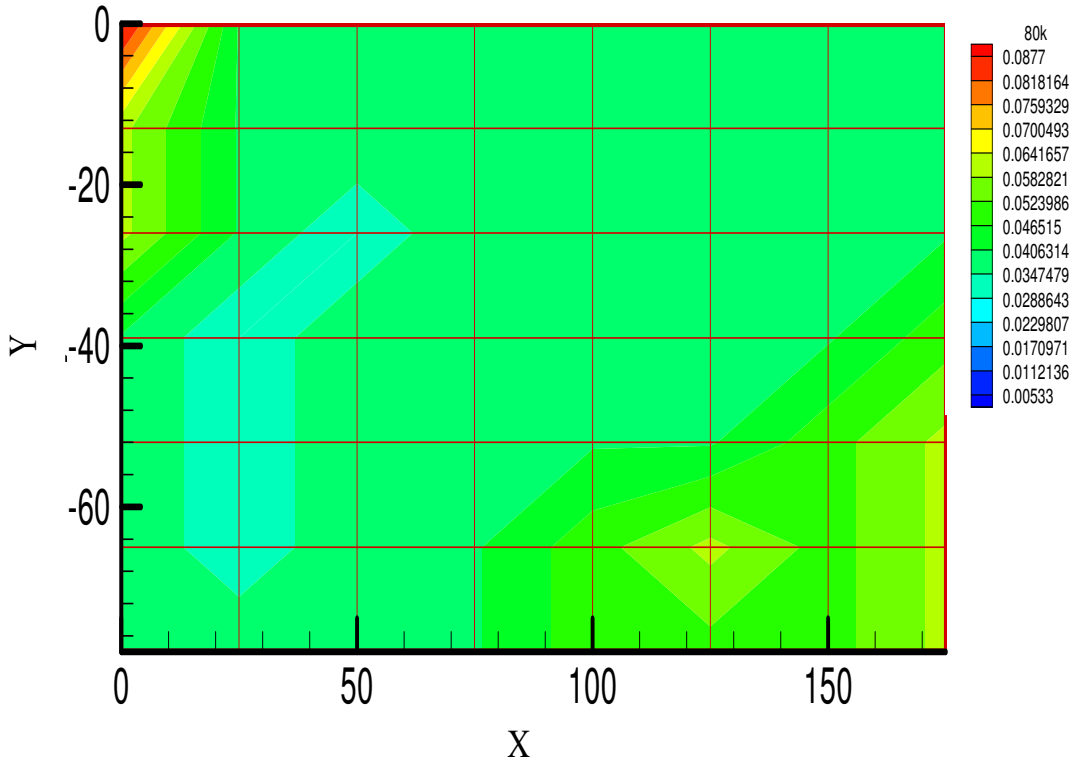

Figure 3.47: Fluctuating Pressure Coefficient Contours (Cprms) 80 km/h

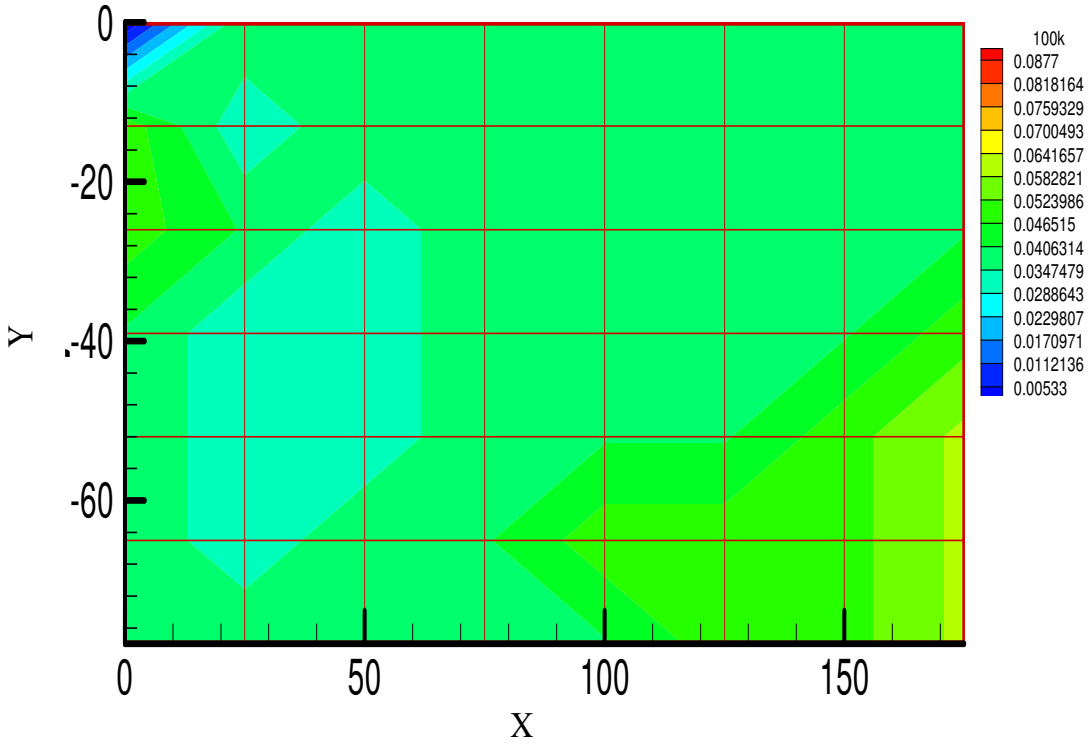

Figure 3.48: Fluctuating Pressure Coefficient Contours (Cprms) 100 km/h

3.7 Bottom Flange Modified for Streamlined flow

The 24 mm shroud as discussed before has later been modified at the bottom flange of the shrouding. The modification was done with addition of external substance to hold the 24mm shroud at the bottom flange so that the flow around that flange is streamlined in order to visualise the edge effects. The flow at the bottom flange of the 24mm shroud was checked with help of wool taps before the desired results were taken analysis. The fluctuating pressure contours 2-D plots are shown in Appendix F for all speeds for 24mm shroud for surface mean pressure coefficient (Cp). The plots for fluctuating pressure coefficient (Cprms).shows that there is drop in magnitude of the pressure when compare to the graphs of the 24mm Shroud as shown in Figures 3.49 to 3.52. The Cprms contour plots also shows the drop in pressure in the top flange of the mirror face when compared to that of 24mm shroud. The graphs also show that due to streamline at the bottom flange the mirror wake formed at mirror face is not that strong as was observed in case of 24mm shroud. It also shows that the flow passed through the mirror doesn't interact with the complex A-pillar and also the high fluctuating pressure coefficient observed in case of 24mm shroud far away from the car body also vanishes off due

to streamlining. This also showed that if mirror geometry is streamlined from the any flange, it will make huge change in implication on the pressure flow over the mirror face. We can also make an assumption that streamlining of mirror housing also has effects on mirror face and should also be taken into consideration while making any further changes or modifications.

3.7.1 Results of Bottom Flange Modified for Streamlined flow

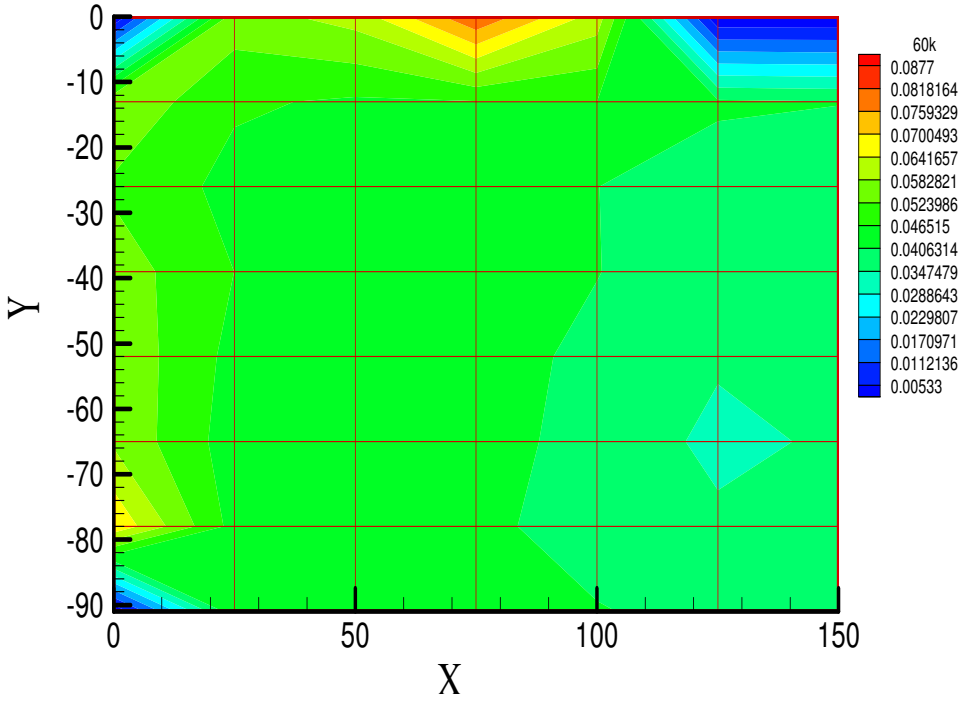

Figure 3.49: Fluctuating Pressure Coefficient Contours (Cprms) 60 km/h

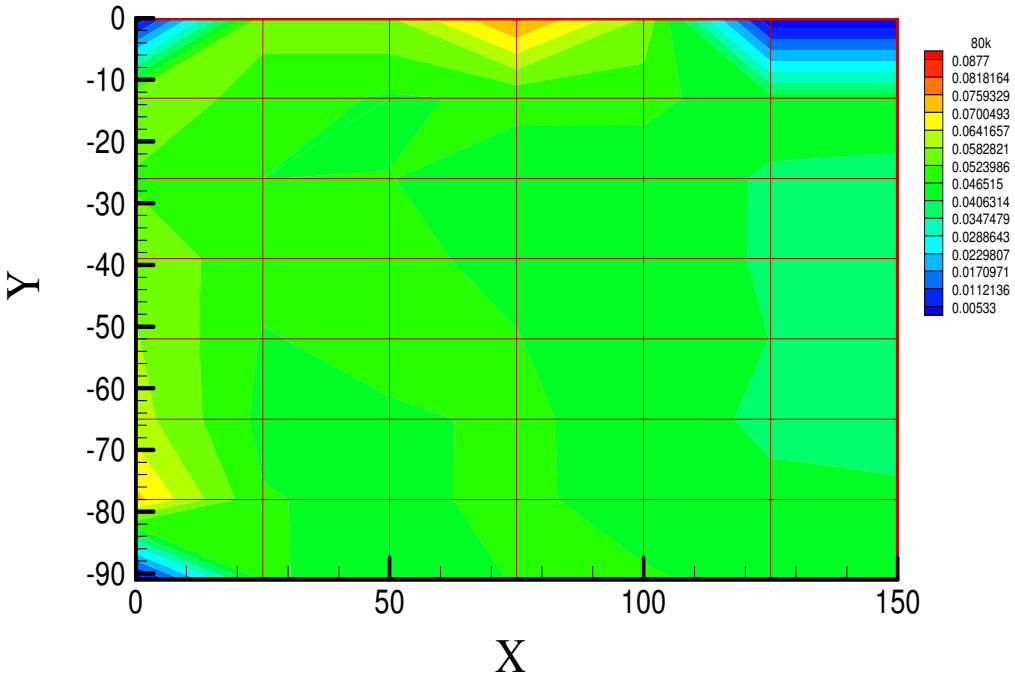

Figure 3.50: Fluctuating Pressure Coefficient Contours (Cprms) 80 km/h

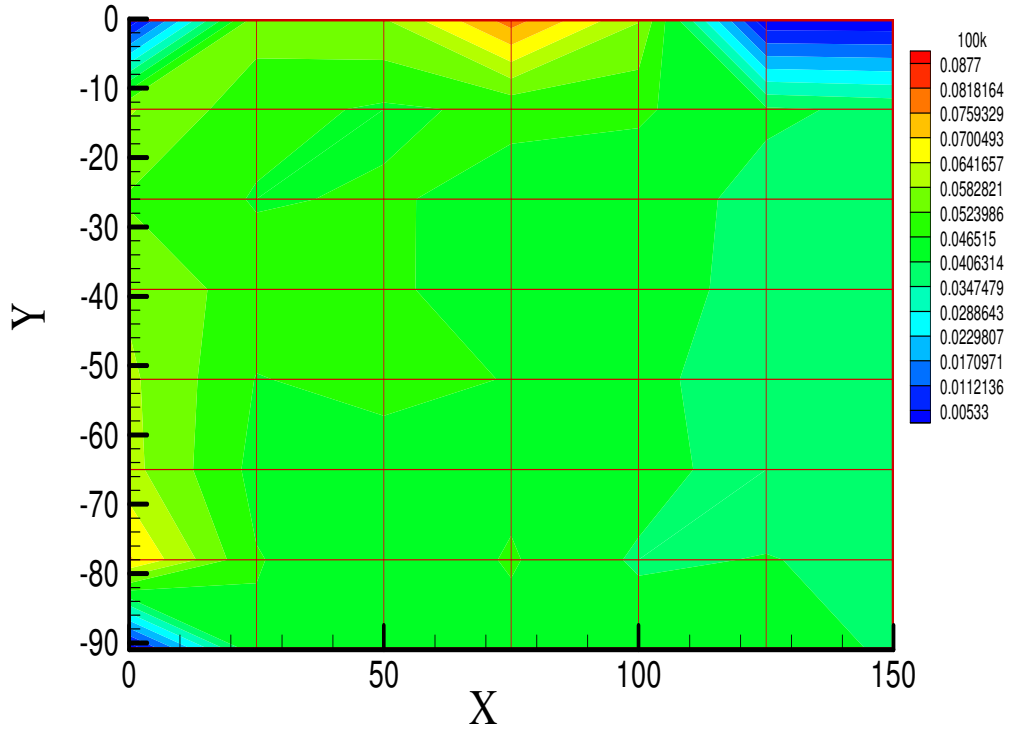

Figure 3.51: Fluctuating Pressure Coefficient Contours (Cprms) 100 km/h

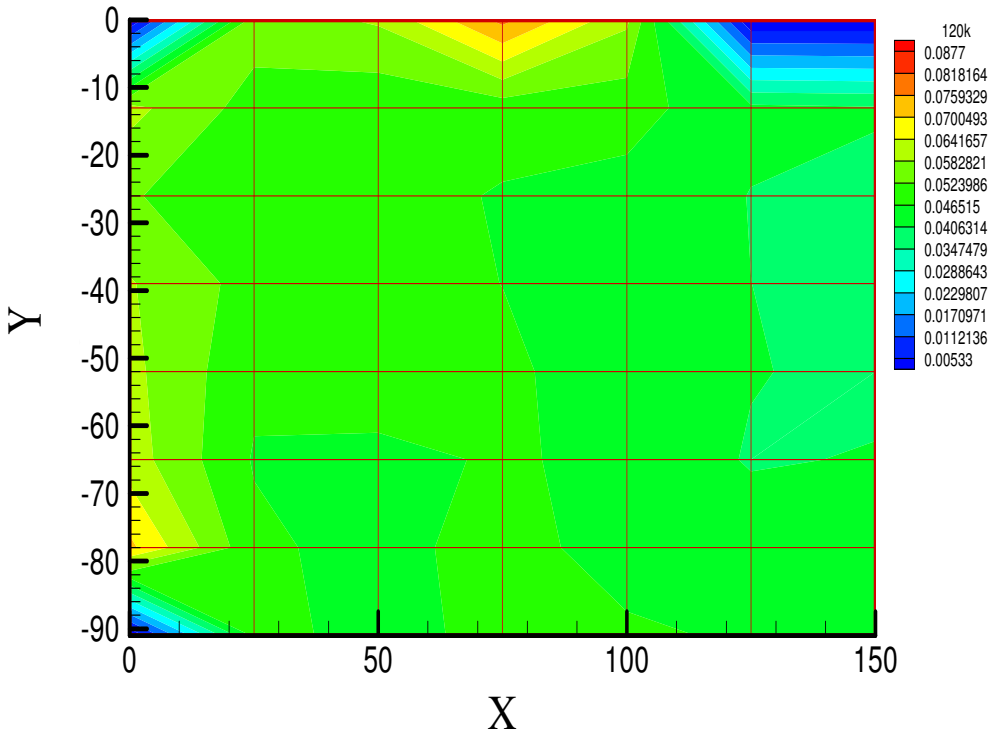

Figure 3.52: Fluctuating Pressure Coefficient Contours (Cprms) 120 km/h

3.8 Power Spectral Density Plot (PSD)

In this section the energy graphs of the highest fluctuating pressure are plotted for the highest fluctuating pressure coefficients for each individual case at different speeds. In case of standard mirror the maximum fluctuating pressure coefficients were observed near to bottom section of the mirror (point 47). However, this was not the case when shrouding of 24mm, 34mm and 44mm were done and it is noted that the trend have reversed and the maximum fluctuating pressure coefficients (Cpmrs) was observed in the top section of the mirror face (point 3). Figure 3.53 to Figure 3.60 shows the energy graphs for highest fluctuating pressure coefficients respectively. These Figures show that there is significant variation in energy distribution for the standard and modified mirror with quarter model at high speeds. The spectral plots show that the magnitude of energy distribution reduces with the increase of shrouding length through out the frequency range.

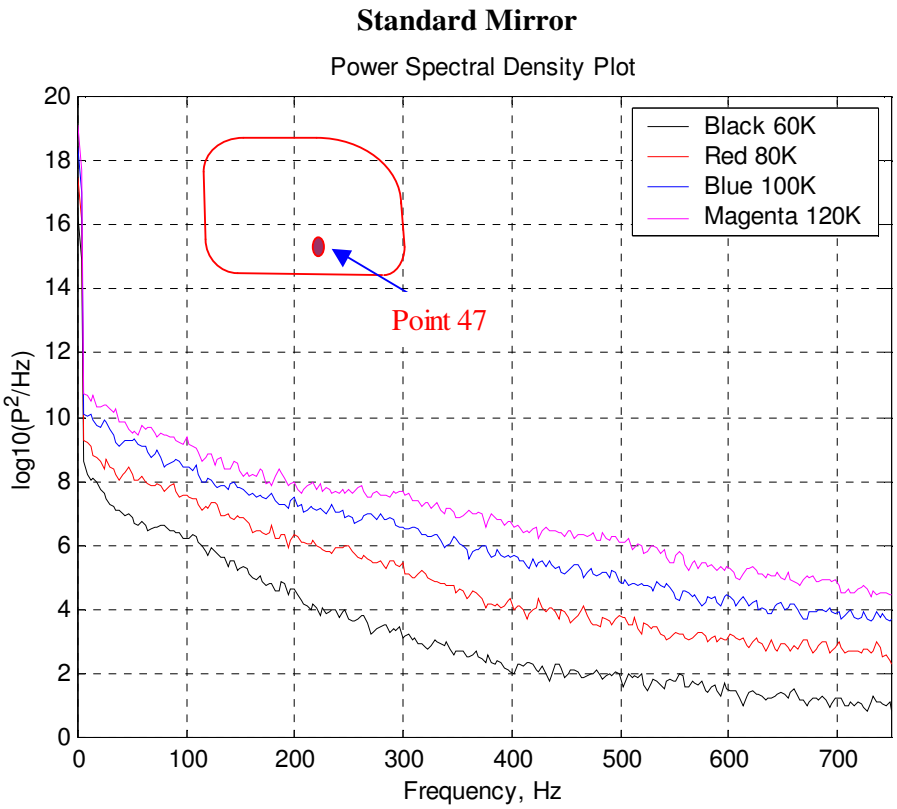

Figure 3.53: Highest Cprms at point 47

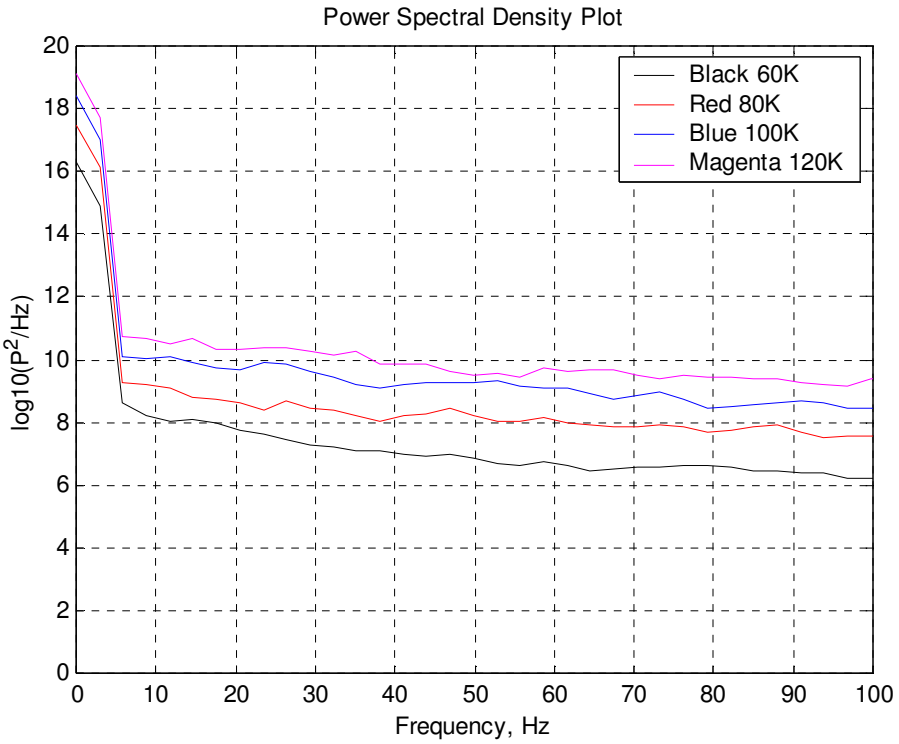

Figure 3.54: Zoom View of Highest Cprms 0-100Hz

24mm shroud

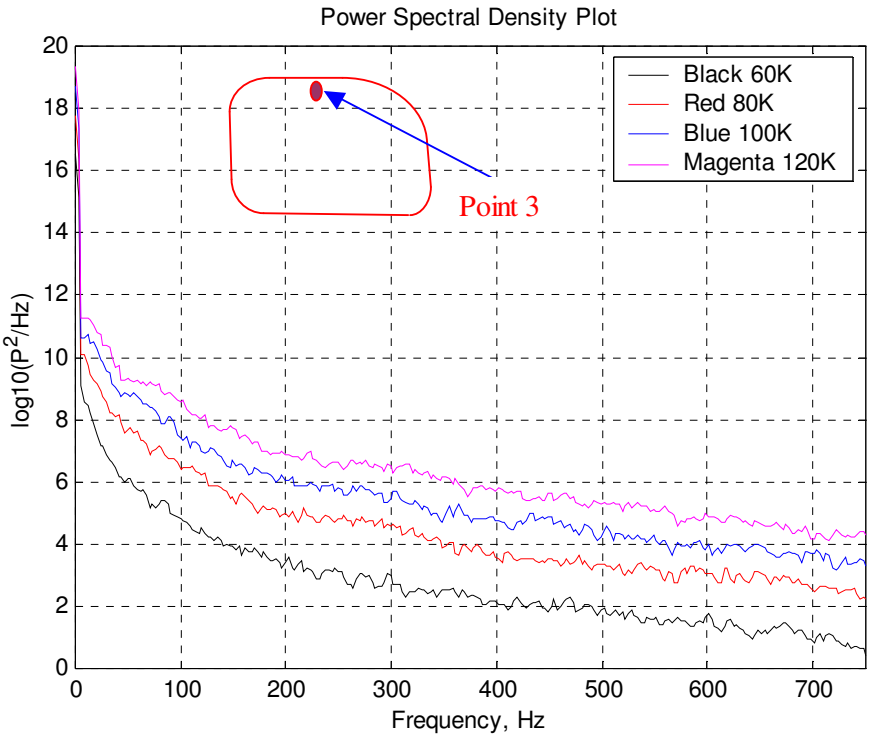

Figure 3.55: Highest Cprms at point 50

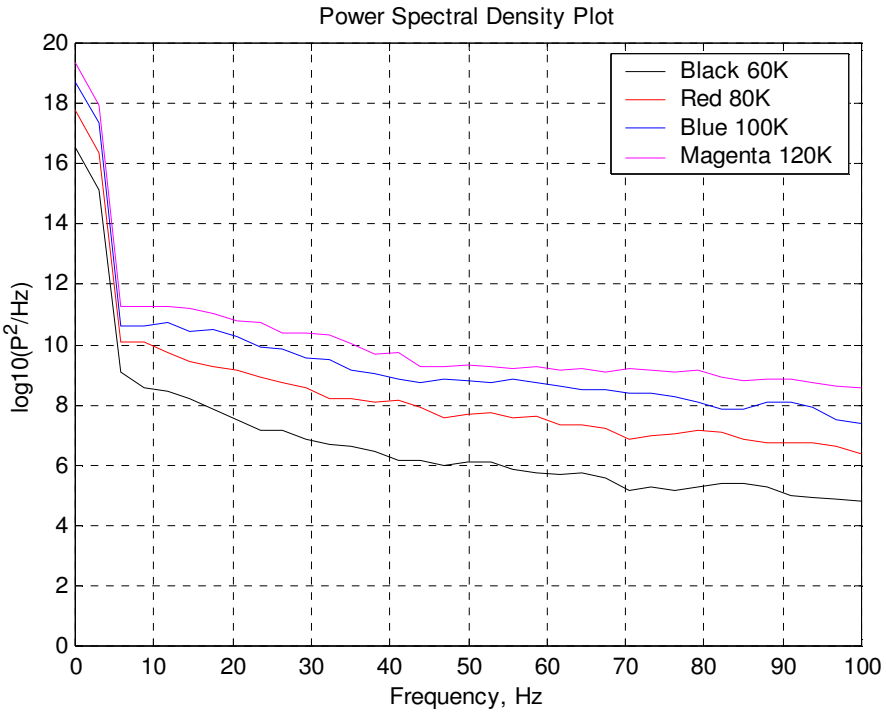

Figure 3.56: Zoom View of Highest Cprms 0-100Hz

34mm shroud

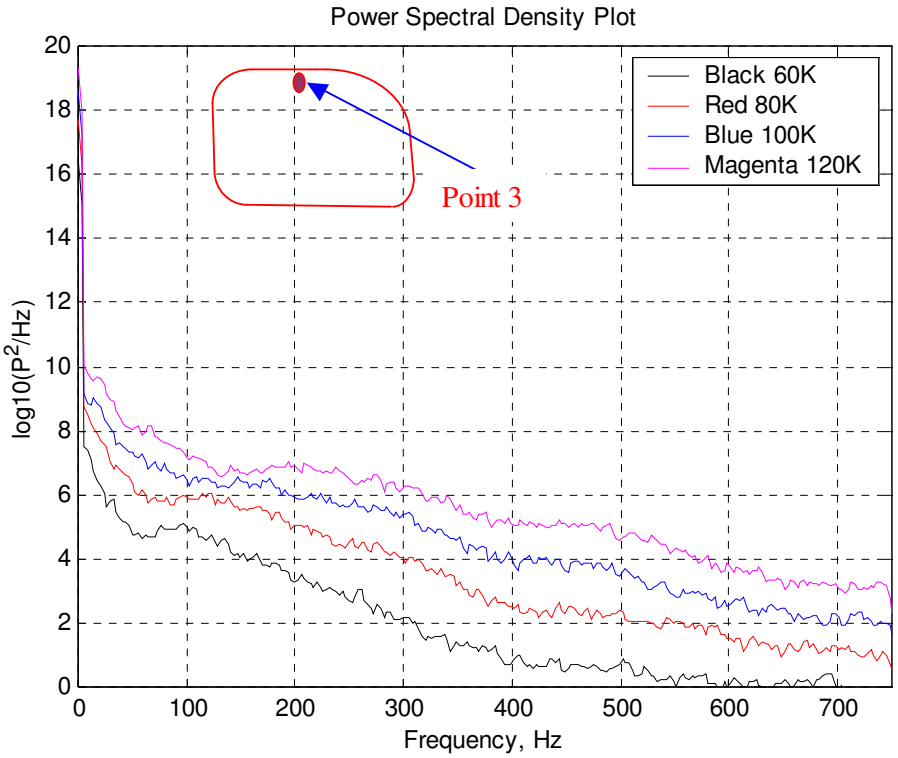

Figure 3.57: Highest Cprms at point 50

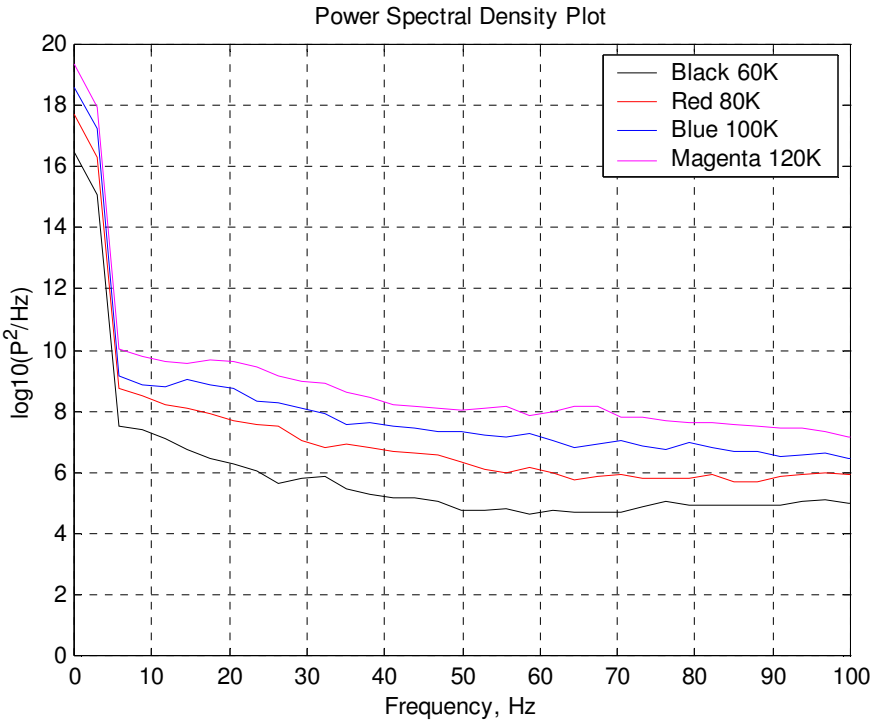

Figure 3.58: Zoom View of Highest Cprms 0-100Hz

44mm shroud

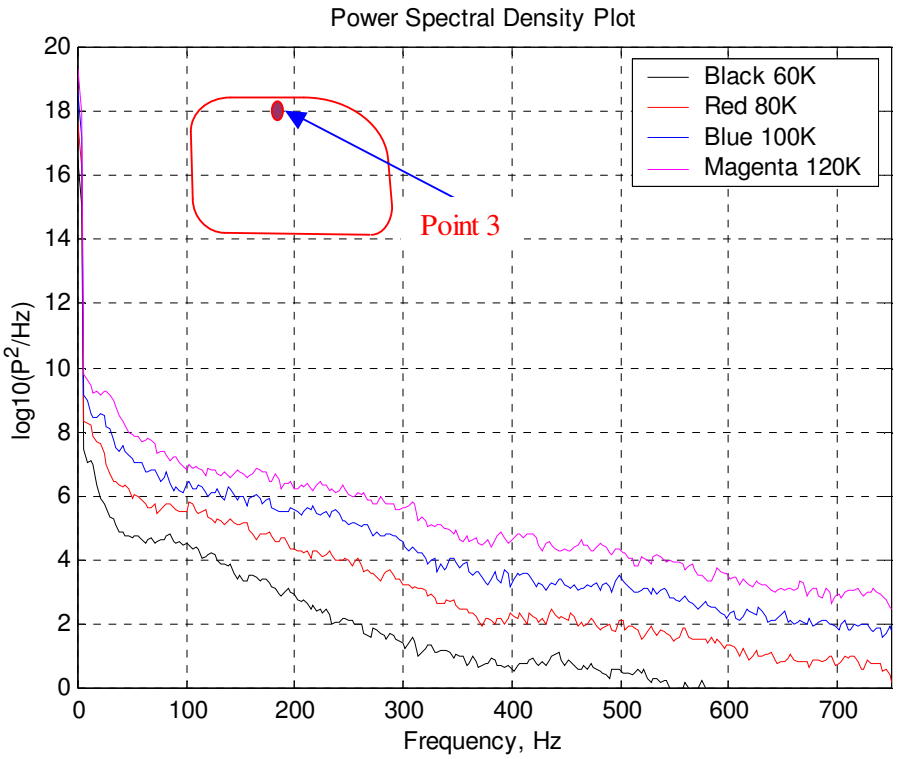

Figure 3.59: Highest Cprms at point 50

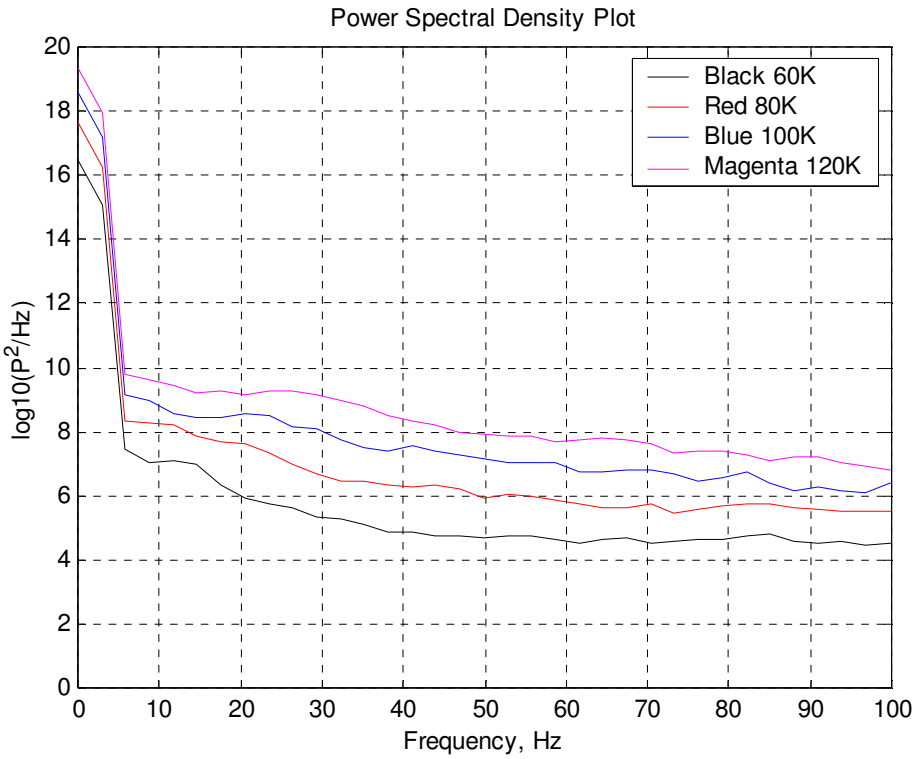

Figure 3.60: Zoom View of Highest Cprms 0-100Hz

Table 3.1 to 3.3 shows the comparison of results for the various frequency (40 Hz, 50 Hz, and 70Hz) ranges for the data presented in the graphs above for quarter model condition.

Comparison of Results for Quarter Model at 40 Hz

Table 3.1: Energy comparison for various shrouding lengths

Speeds Points →	Standard Mirror (Point 47)	24mm Shroud (Point 3)	34mm Shroud (Point 3)	44mm Shroud (Point 3)
60 km/h	7.00	6.25	5.00	5.00
80 km/h	8.25	8.10	6.50	6.25
100 km/h	9.25	8.50	7.50	7.75
120 km/h	9.85	8.75	8.25	8.25

Comparison of Results for Quarter Model at 50 Hz

Table 3.2: Energy comparison for various shrouding lengths

Speeds Points →	Standard Mirror (Point 47)	24mm Shroud (Point 3)	34mm Shroud (Point 3)	44mm Shroud (Point 3)
60 km/h	6.75	6.10	5.00	4.75
80 km/h	8.15	7.75	6.25	6.00
100 km/h	9.25	9.00	7.25	7.25
120 km/h	9.50	9.25	8.05	8.00

Comparison of Results for Quarter Model at 70 Hz

Table 3.3: Energy comparison for various shrouding lengths

Speeds Points →	Standard Mirror (Point 47)	24mm Shroud (Point 3)	34mm Shroud (Point 3)	44mm Shroud (Point 3)
60 km/h	6.25	5.25	4.50	4.50
80 km/h	7.75	7.00	5.90	5.75
100 km/h	8.75	8.25	7.00	6.75
120 km/h	9.50	9.00	7.90	7.75

3.9 Flow Visualisation

In this section the flow visualisation of the mirror for different shroud length for quarter model has been shown. Figures 3.61 to 3.70 show the shrouding length for standard, 24mm, 34mm and 44mm shroud length.

3.9.1 Standard Mirror

Figure 3.61: Flow over side face of Mirror

Figure 3.62: Flow around the Root showing Recirculation

3.9.2 24mm Shroud

Figure 3.63: Flow around Bottom Flange

Figure 3.64: Flow around Bottom Shroud Flange

3.9.3 34mm Shroud

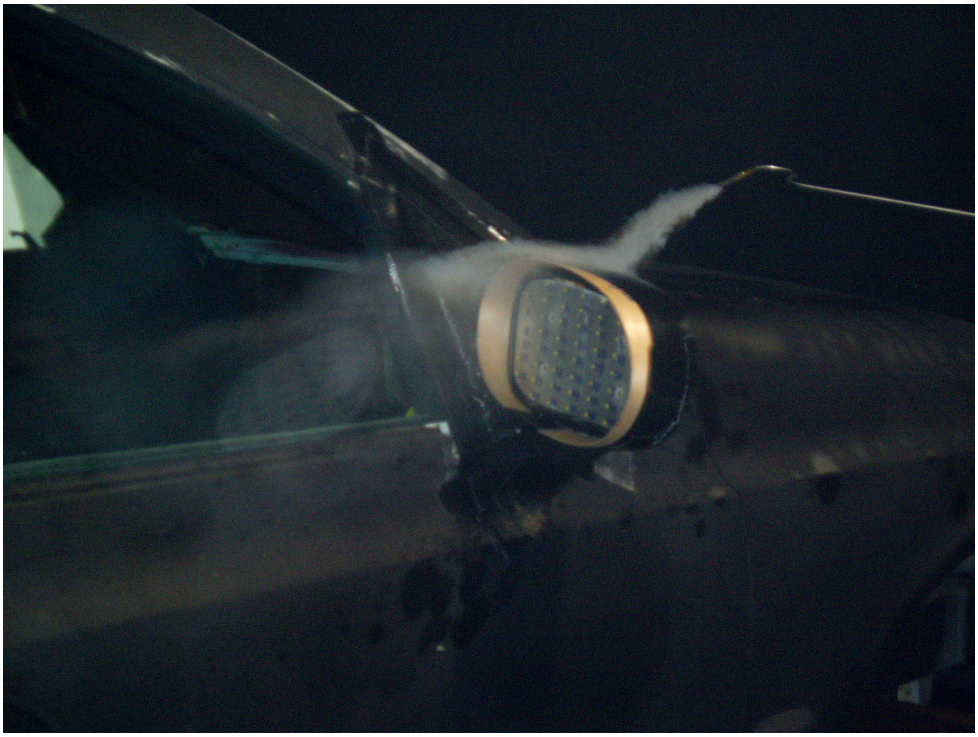

Figure 3.65: Flow around Top Flange of Shroud

Figure 3.66: Flow over the Mirror Face

3.9.4 44mm Shroud

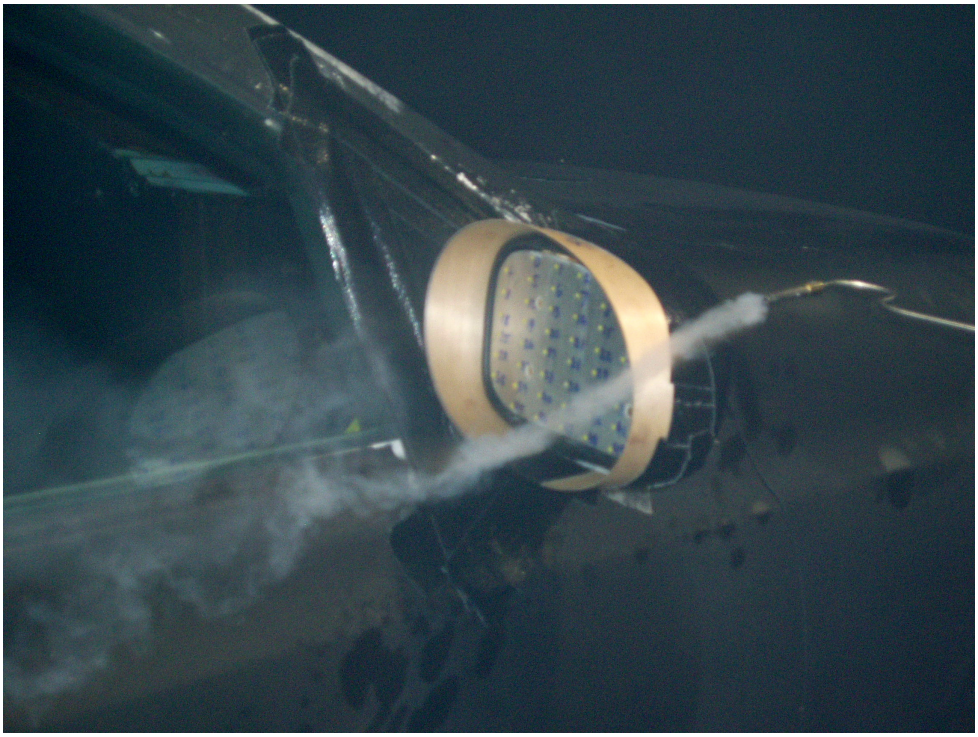

Figure3.67: Flow over Side Flange of the Mirror

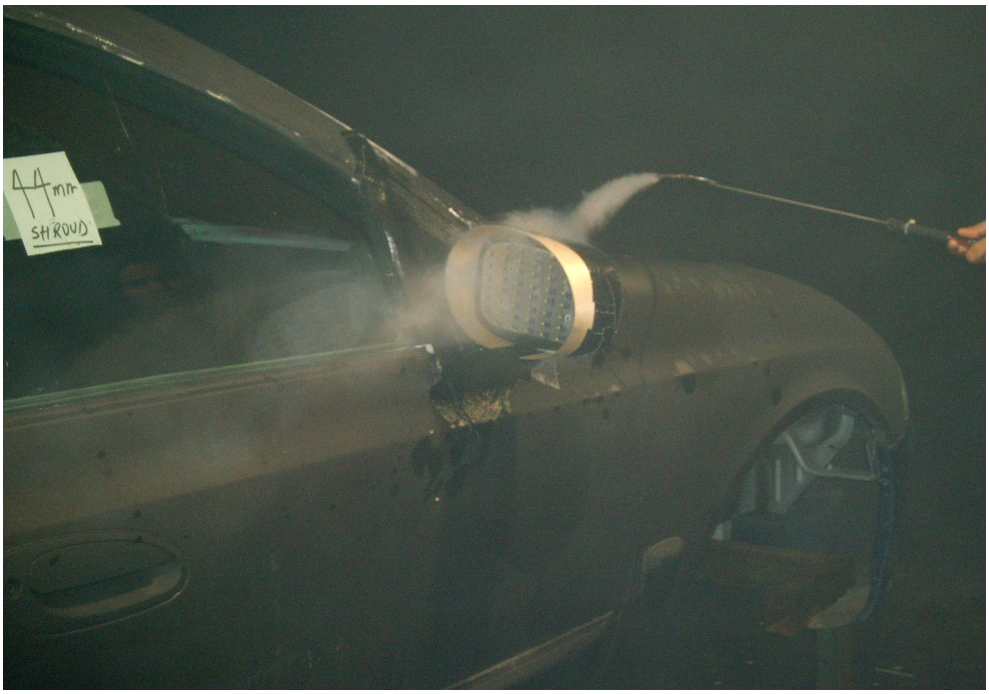

Figure 3.68: Flow over Top Flange of the Mirror

3.9.5 Mirror Housing

Figure 3.69: Flow Separation around Mirror Housing

Figure 3.70: Flow Separation around Mirror Face

Chapter 4

Semi-Isolation Testing

4.1 Introduction

The mirror was tested in Semi-Isolation of quarter model car to see the variation of results compared to the mirror with quarter model. During this testing, the Quarter model of Ford Falcon was not included while testing and the mirror was kept in semi-isolation condition. The mirror was kept at central position from either of the sidewalls of the wind tunnel. A wooden box was manufactured in the RMIT, Mechanic Engineering workshop to accommodate the pair of pressure modules a rectangular box was manufactured and was externally covered with a cardboard to provide an aerofoil cross-section. The aerofoil section was chosen mainly due to its aerodynamic shape in order to minimise any losses due to obstruction in airflow from the external source. This testing was chosen in order to understand the effects of blockage as well as A-pillar region effects as was done with the help of quarter model inside the wind tunnel. Figure 4.1 shows the schematic representation of layout

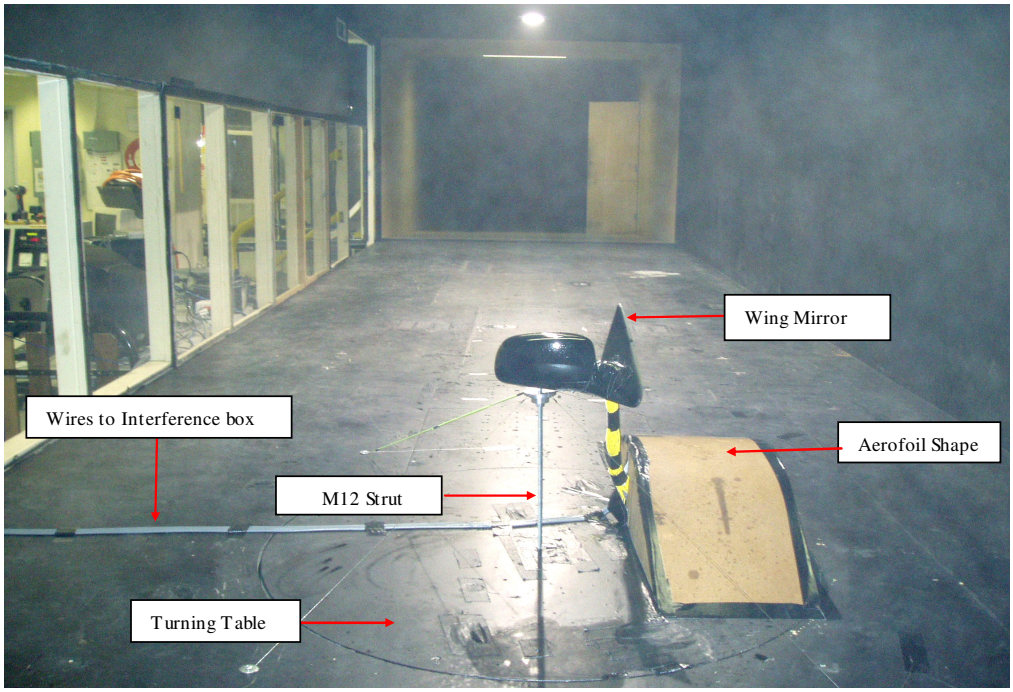

Figure 4.1 Back view of Semi-Isolation

4.2 Experimental Layout

The mirror was mounted on the spindle. The length of the spindle from the wind tunnel floor was about 500mm high from the tunnel floor. The wing mirror was mounted over a collar, which was held by fine wires (fishing wire) that provided enough tensions to prevent from moving in either direction. Moreover, wing mirror was also bolted from inside to hold the movement of mirror at high speeds. The pressure transducer was mounted on the wind tunnel floor inside a wooden box, which was covered on top with cardboard to provide the aerofoil shape in order to have a smooth flow (minimising disturbance). The reason for doing this testing was to minimise the blockage effects inside the wind tunnel as it doesn't include any model inside the test section.

Tests were conducted at 60 km/h, 80 km/h, 100 km/h and 120 km/h with 0˚ yaw angle. Prior to the testing each individual pressure taps on the aluminium plate was checked for leak with the help of a manometer as mentioned before to detect any blockage and also to verify that right pressure tap is attached to right channel number of pressure transducer module. The test also includes the effects of shrouding as was done with quarter model testing; similar shrouds were used of 24mm, 34mm and 44 mm individually at different speeds.

Once the set-up is complete the pressure taps were zeroed for initialising inside the wind tunnel to remove the effects of any voltage offset. This was done for all different cases of testing and while conducting the testing the dynamic pressure head for individual speeds was noted as it varied from one speed to another. The dynamic head was measured with the help of the pito-static tube mounted inside the wind tunnel at the entry of the airflow. The data acquisition system was attached to this tube to measure the pressure head, which also measures the temperature inside the tunnel. The flow visualisation was also carried out at low speeds for Semi-isolation condition and is shown in detail in Appendix [A3]. With the help of DPMS system surface means (Cp) and fluctuating pressure (Cprms) measurements were recorded and analysed.

The mean and fluctuating pressure was converted into non- dimensional parameter such as mean pressure coefficients (Cp) and fluctuating pressure coefficient (Cprms) by diving by the

dynamic pressure head (q) at each individual speeds. The plots of the Cp and Cprms were constructed in 3-dimensional and contour plots. The surface mean pressure coefficient (Cp) and the fluctuating pressure coefficients (Cprms) measurements for each speed case are described in the following subsections.

4.3 Standard Mirror

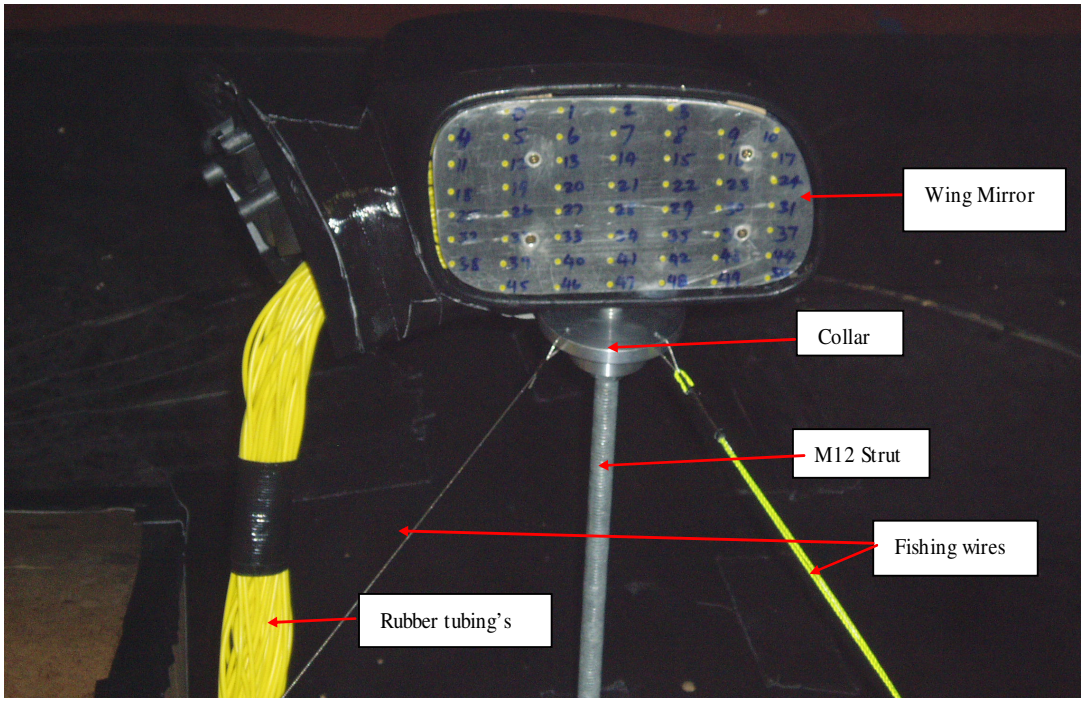

Figure 4.2 Front Semi-Isolation schematic views

3-D graphs shows that fluctuating pressure is not uniformly distributed on the mirror surface and maximum fluctuating pressure is observed across the right side of bottom part of the mirror face as was seen in case of quarter model. Figures 4.3 to Figures 4.10 show the fluctuating pressure coefficients (Cprms) for the standard mirror in isolation. The magnitude of fluctuating pressure increases with speed. The Figures indicate that the fluctuating pressure (Cprms) is highest at the bottom right hand corner of the mirror face. With the increase in speeds, its magnitude increases and at 100 km/h the fluctuating pressure tends to moves towards the centre of the mirror. At 120 km/h the fluctuating pressure coefficient moves at the bottom centre section of the mirror face and causes decrease in the pressure variation

around the corner end. It is believed that the fluctuation is concentrated largely at the bottom section of the mirror part than the top part of the mirror face.

4.3.1 Results of Standard Mirror

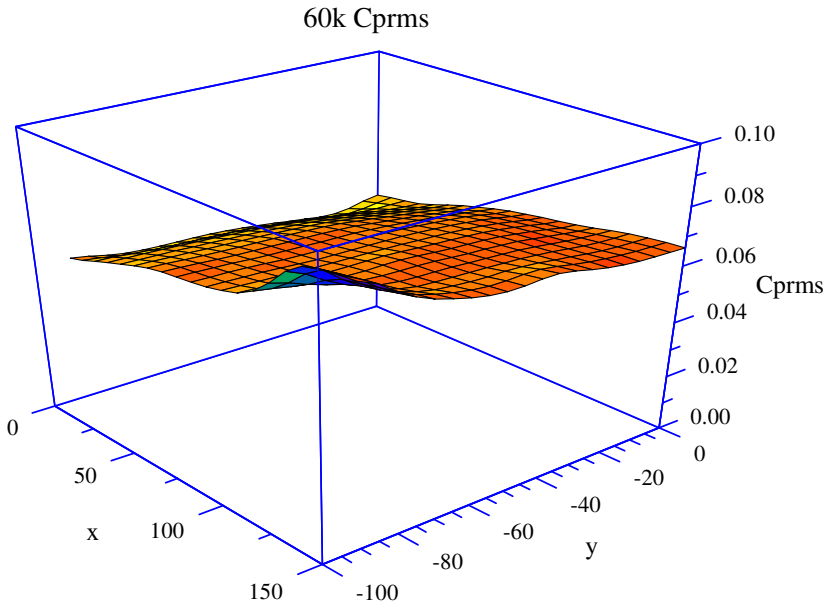

Figure 4.3: Fluctuating Pressure Coefficients (Cprms) -3D - 60 km/h

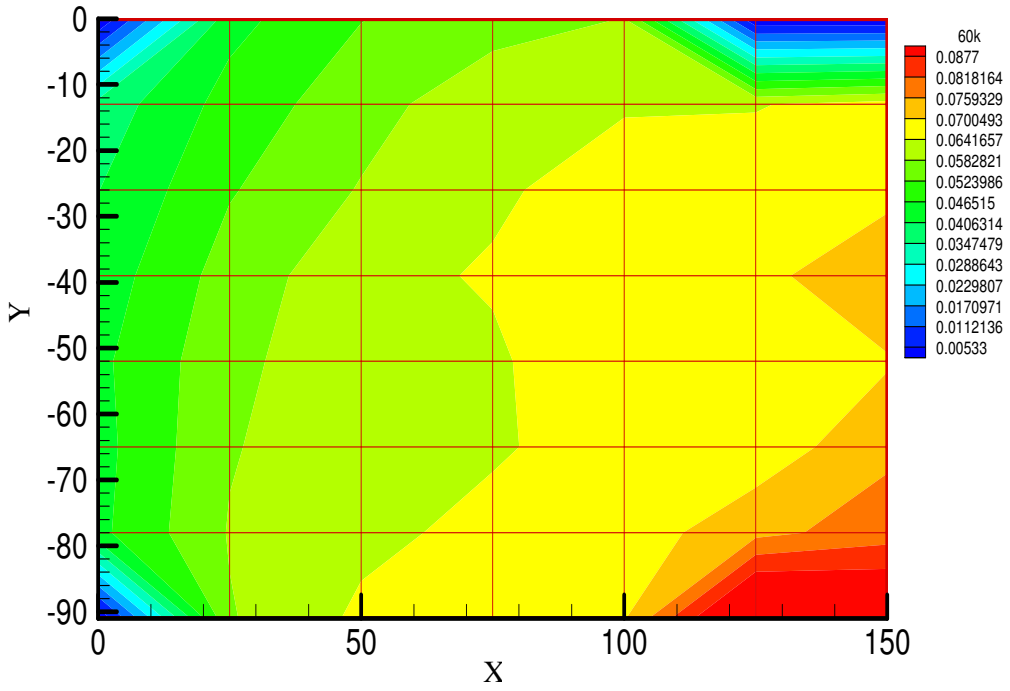

Figure 4.4: Fluctuating Pressure Coefficients (Cprms) - Contours - 60 km/h

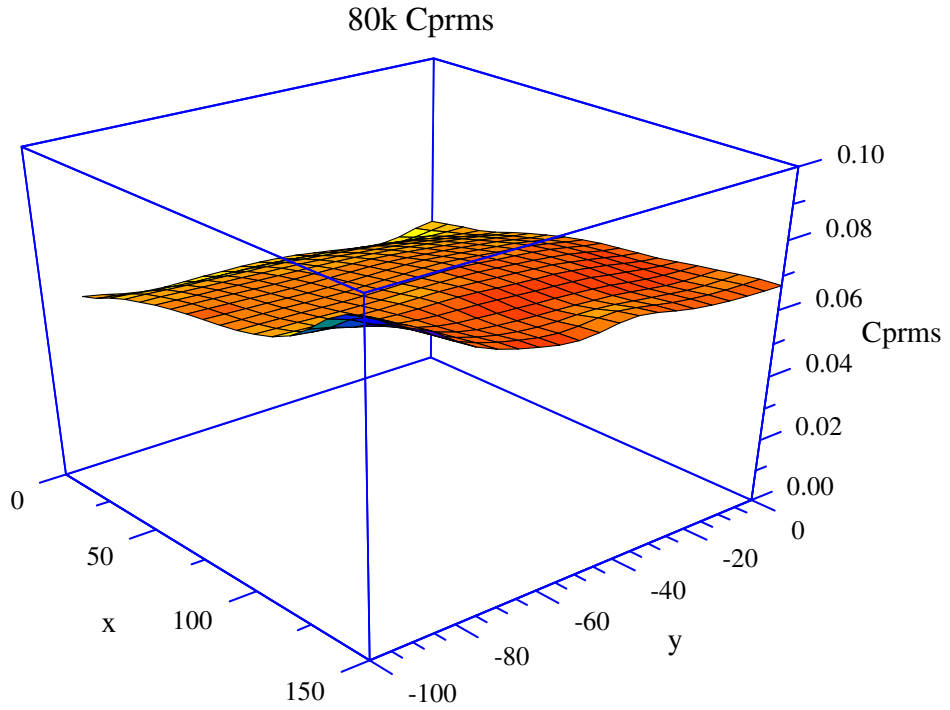

Figure 4.5: Fluctuating Pressure Coefficients (Cprms) -3D -80 km/h

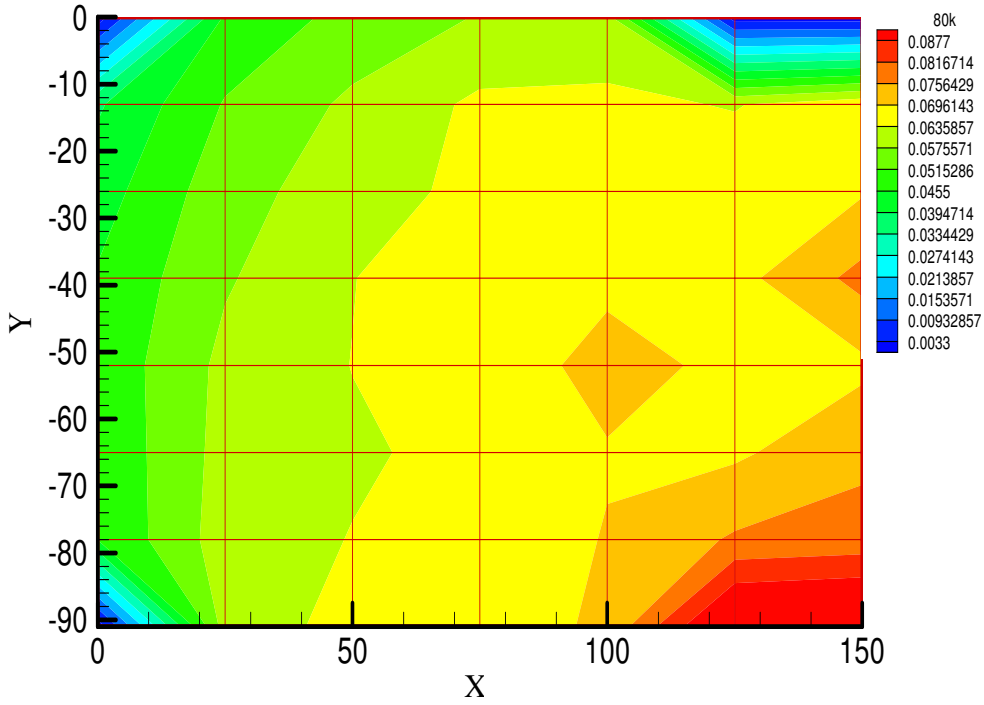

Figure 4.6: Fluctuating Pressure Coefficients (Cprms) - Contours -80 km/h

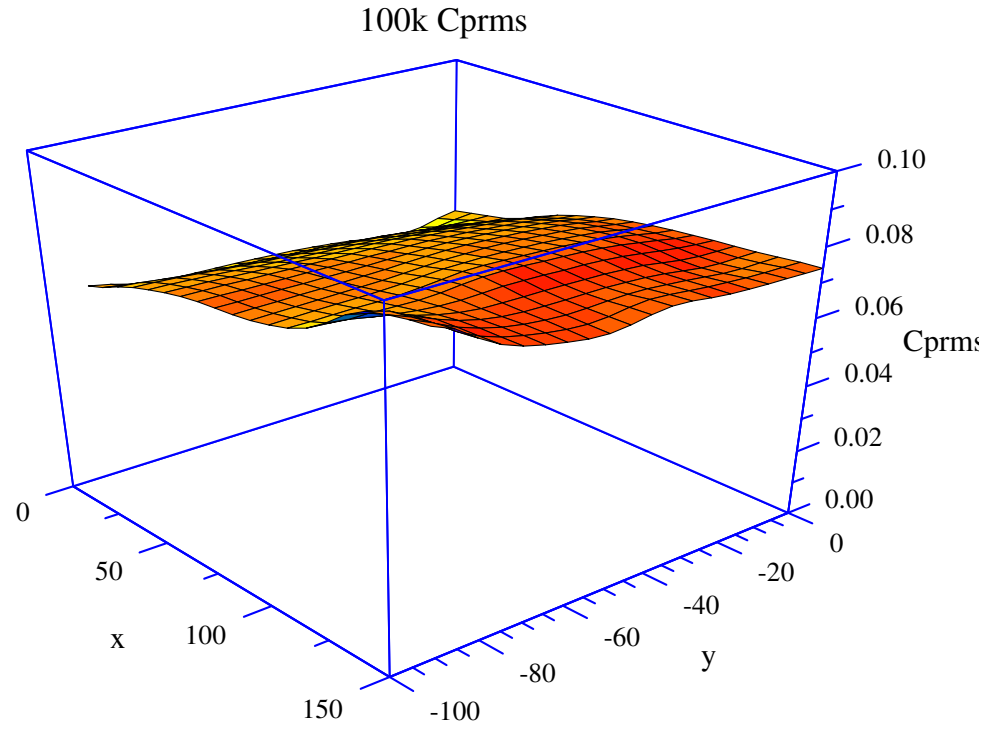

Figure 4.7: Fluctuating Pressure Coefficients (Cprms) -3D -100 km/h

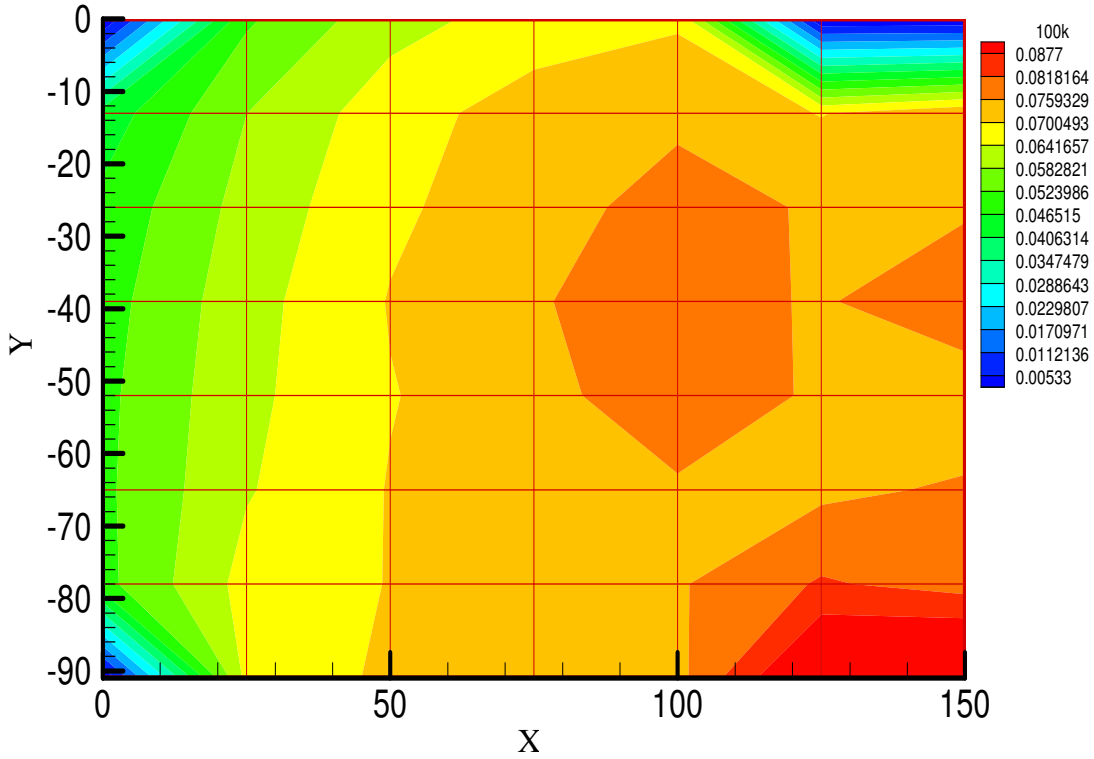

Figure 4.8: Fluctuating Pressure Coefficients (Cprms) - Contours -100 km/h

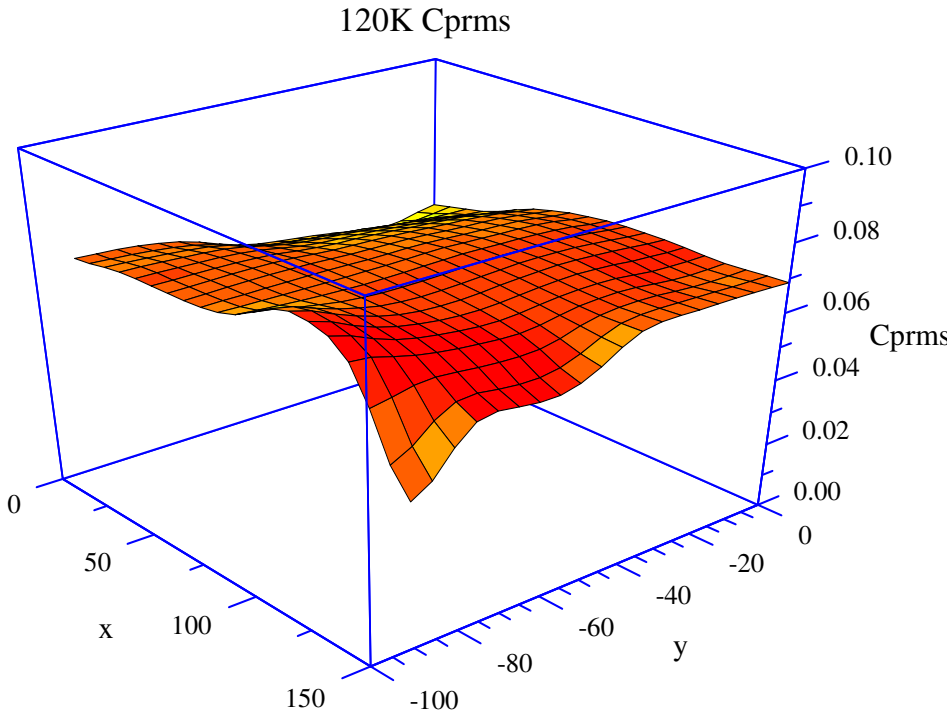

Figure 4.9: Fluctuating Pressure Coefficients (Cprms) -3D -120 km/h

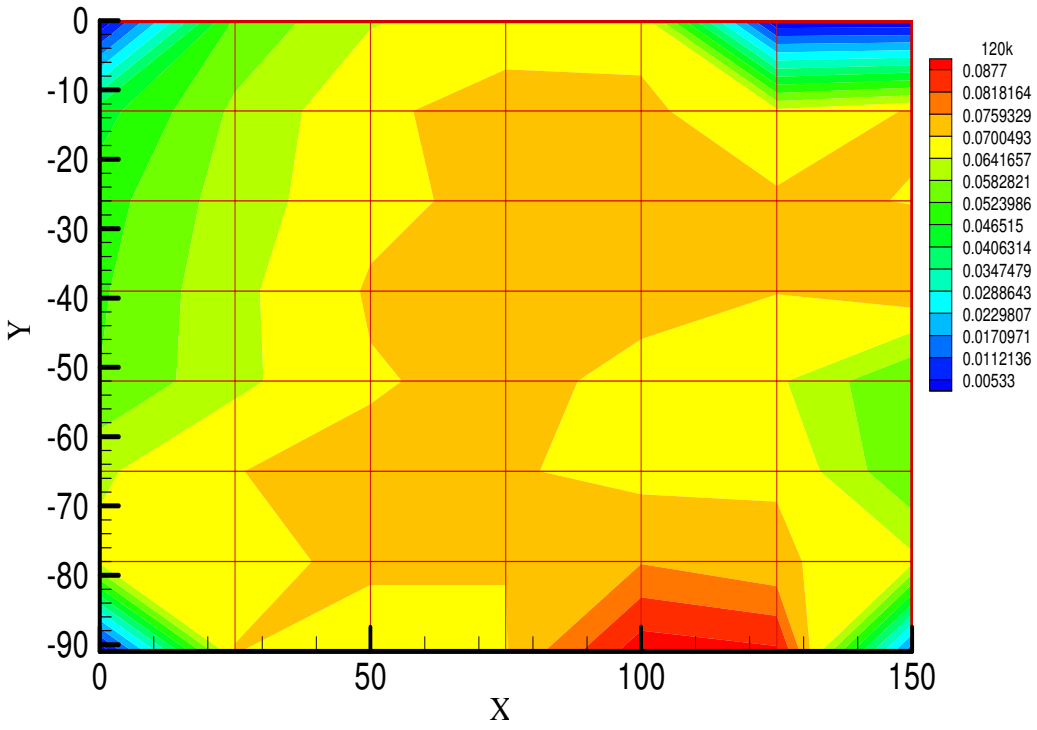

Figure 4.10: Fluctuating Pressure Coefficients (Cprms) - Contours - 120 km/h

4.4 24mm Shroud

As mentioned earlier in the section of quarter model test that a thin wooden ply was externally mounted over the mirror.

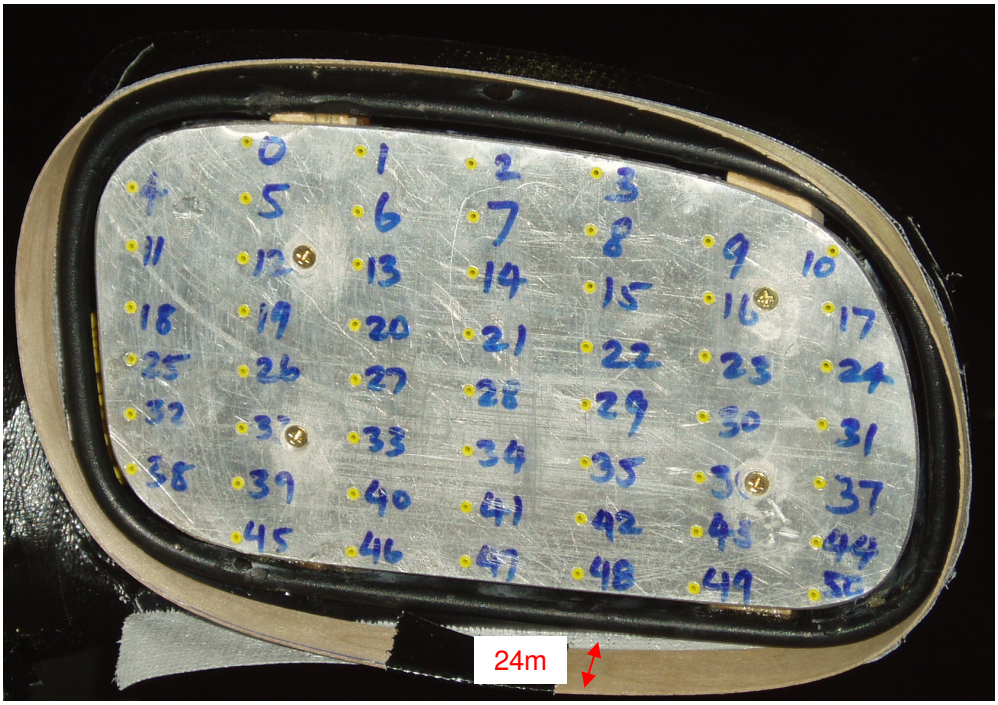

Figure 4.11 – 24mm Shroud

Figure 4.11 to Figure 4.18 show the fluctuating pressure coefficients (Cprms) for different speeds. The Figure shows the drop in the magnitude of fluctuating pressure due to the effects of shrouding. As seen before there was high magnitude in fluctuating pressure was seen on the bottom right side of the mirror face in case of standard mirror, but as the shrouding is put along the external face of the mirror, it reduces the magnitude of fluctuating pressure. The graphs showed for high speeds shows that the bottom central region causes high magnitude of fluctuating pressure when compared to that of low speeds.

4.4.1 Results of 24mm Shroud

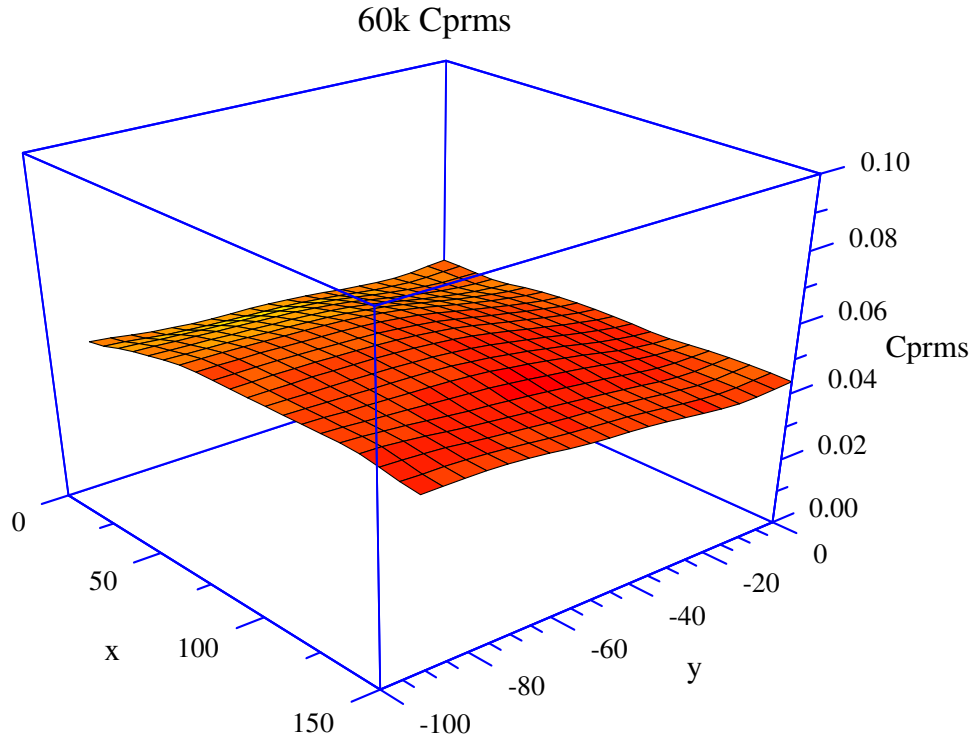

Figure 4.12: Fluctuating Pressure Coefficients (Cprms) -3D -60 km/h

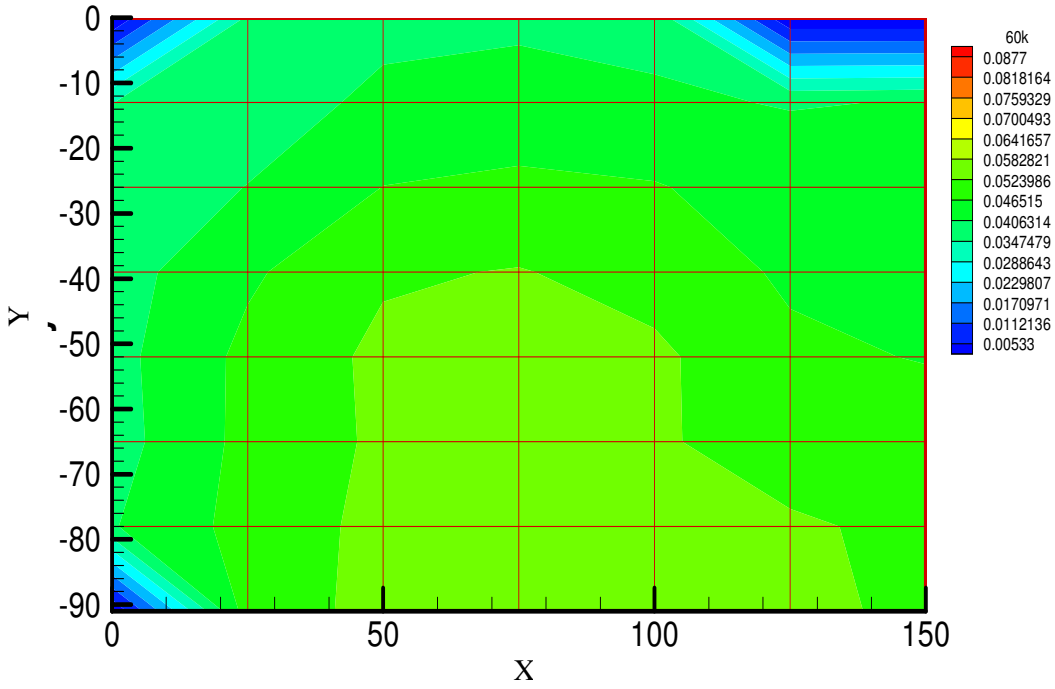

Figure 4.13: Fluctuating Pressure Coefficients (Cprms) - Contours - 60 km/h

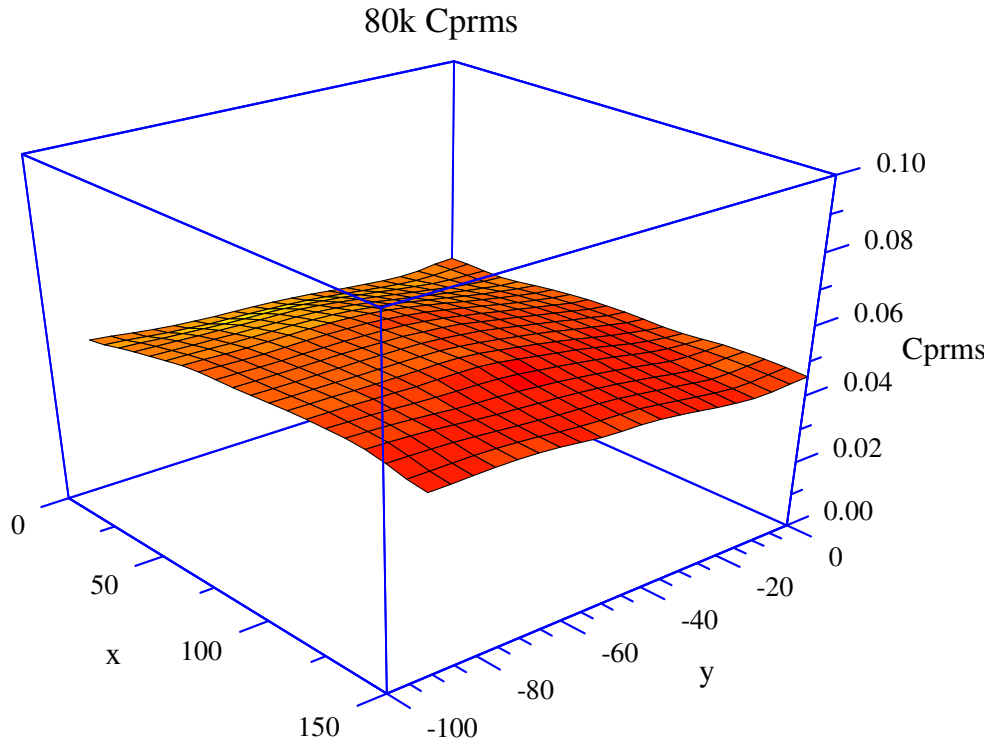

Figure 4.14: Fluctuating Pressure Coefficients (Cprms) -3D - 80 km/h

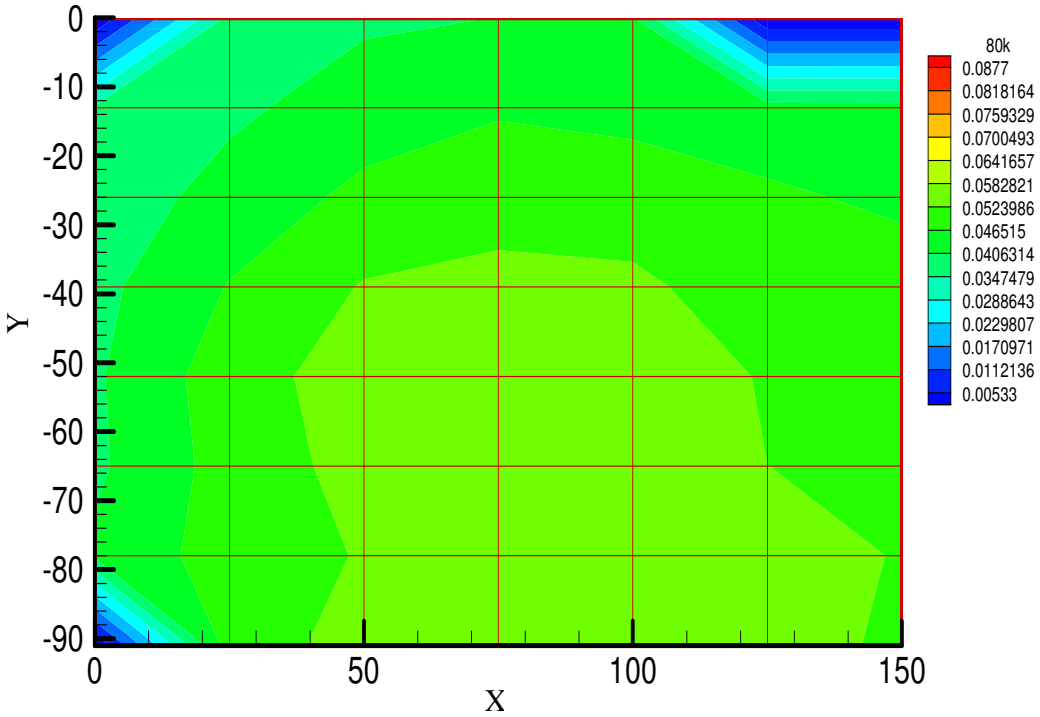

Figure 4.15: Fluctuating Pressure Coefficients (Cprms) - Contours - 80 km/h

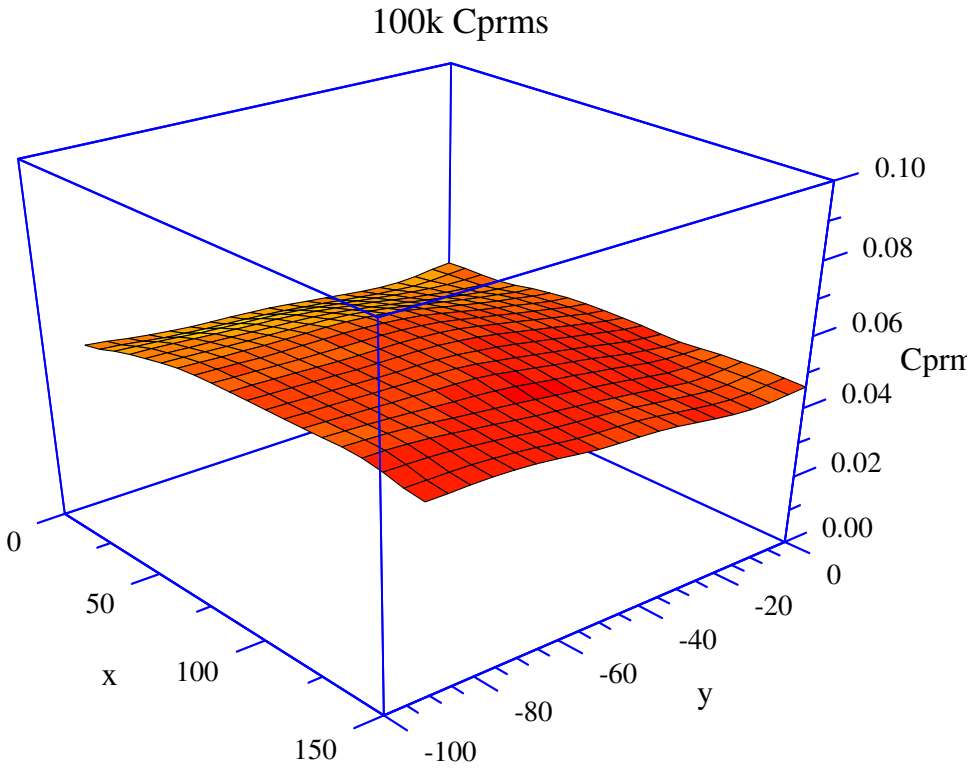

Figure 4.16: Fluctuating Pressure Coefficients (Cprms) -3D -100 km/h

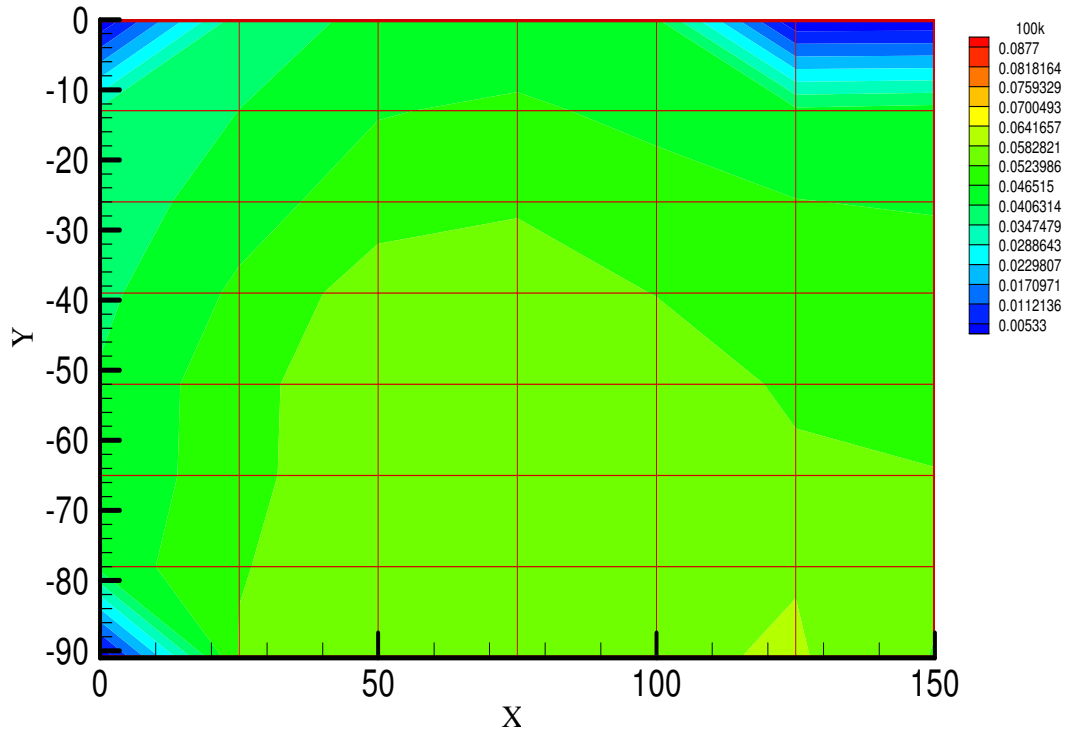

Figure 4.17: Fluctuating Pressure Coefficients (Cprms) - Contours -100 km/h

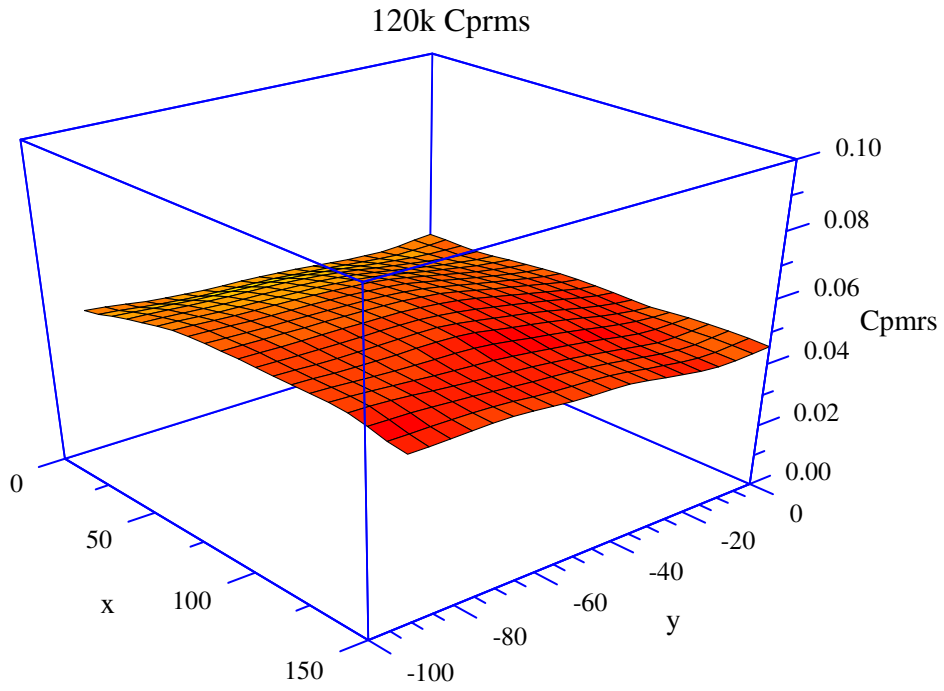

Figure 4.18: Fluctuating Pressure Coefficients (Cprms) -3D - 120 km/h

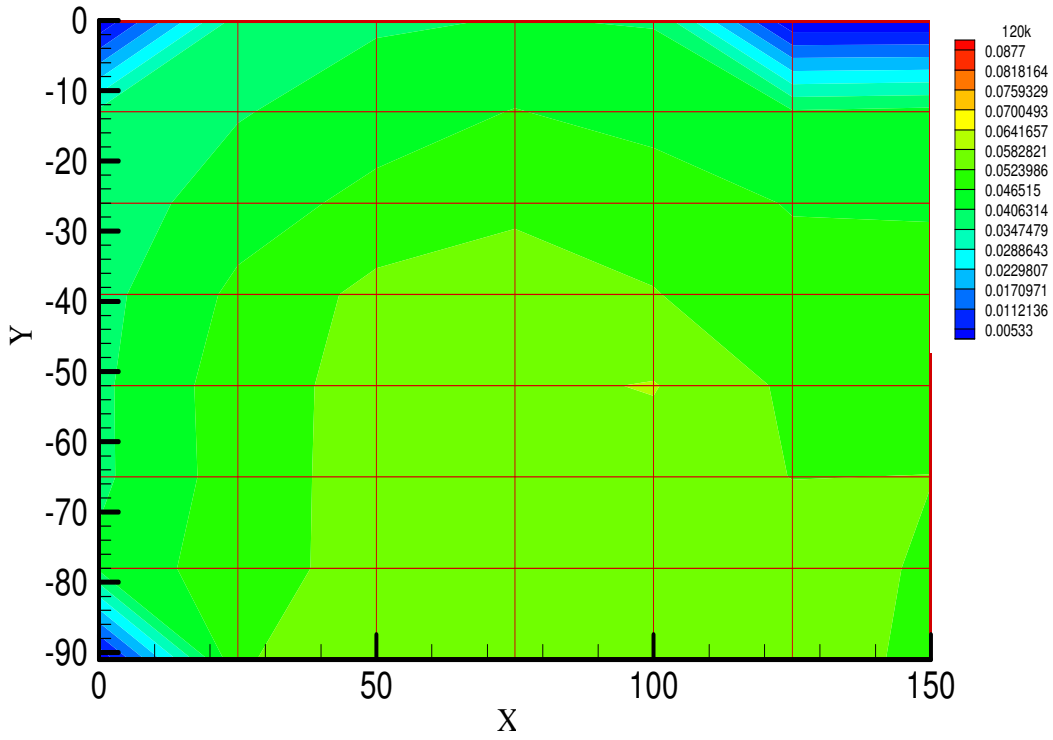

Figure 4.19: Fluctuating Pressure Coefficients (Cprms) - Contours - 120 km/h

4.5 34mm Shroud

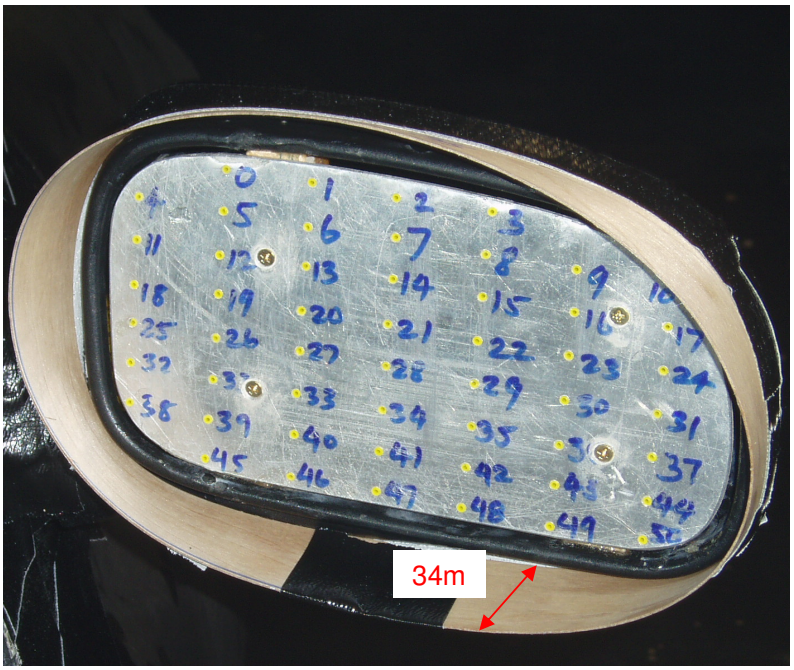

Figure 4.20: 34mm Shrouding

Figure 4.21 to Figure 4.28 show the fluctuating pressure coefficients (Cprms) for different speeds. The Figure shows further drop in the magnitude of fluctuating pressure due to the effects of increasing shrouding length. As the speed increase there is an increase in fluctuating pressure coefficients (Cprms) on the bottom section of the mirror face. However, at low speeds there not much increases in that section of the mirror face. Since there is no presence of the car body, at higher speeds some drops in pressure were noted due to absence of A-pillar flow in that region.

4.5.1 Results of 34mm Shroud

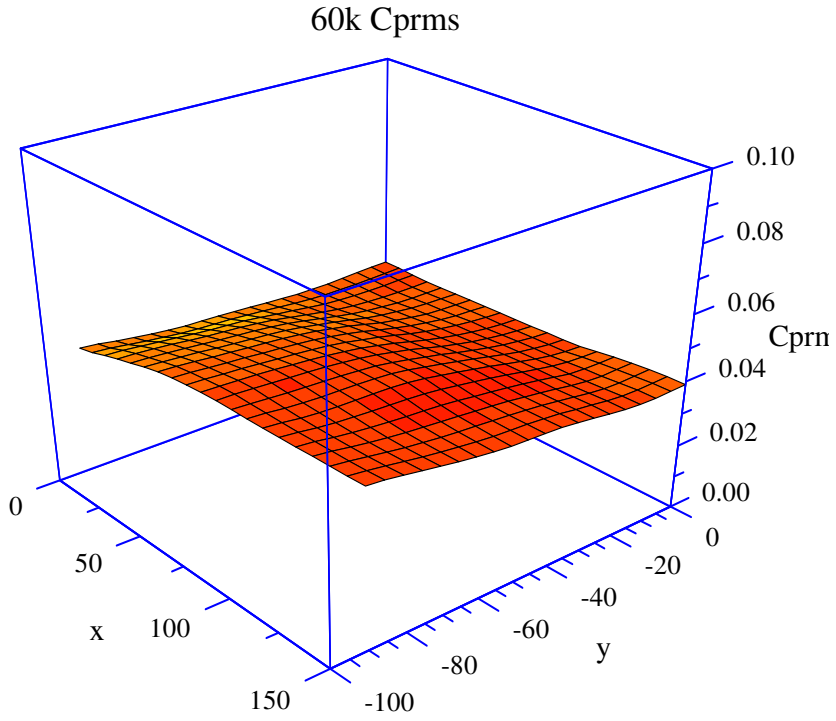

Figure 4.21: Fluctuating Pressure Coefficients (Cprms) -3D - 60 km/h

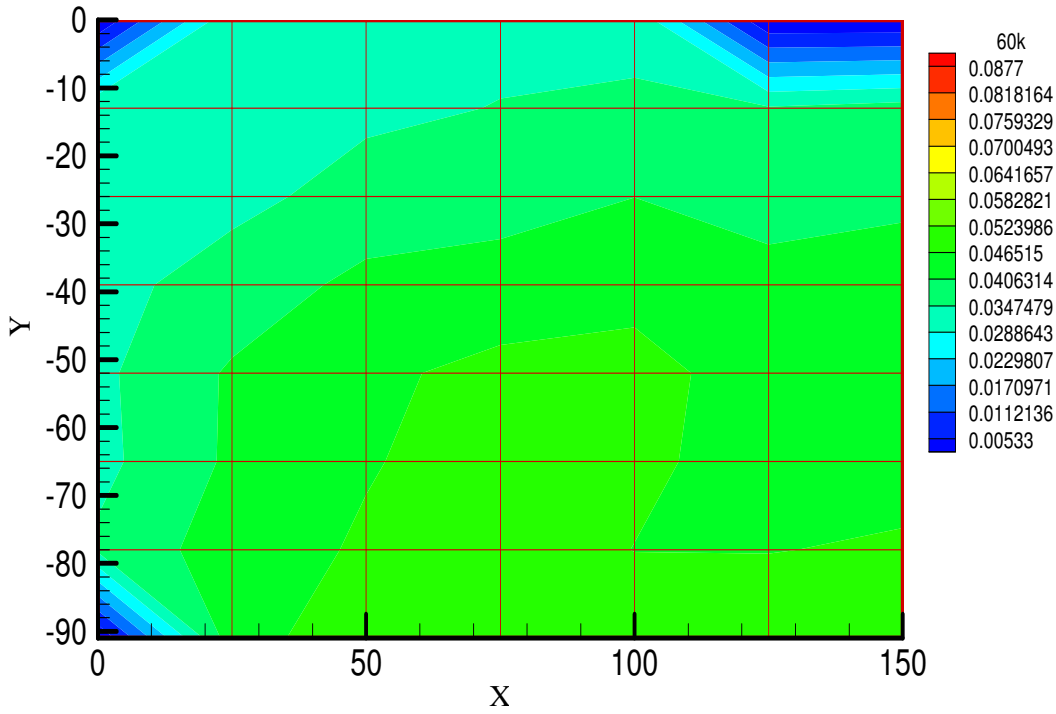

Figure 4.22: Fluctuating Pressure Coefficients (Cprms) - Contours - 60 km/h

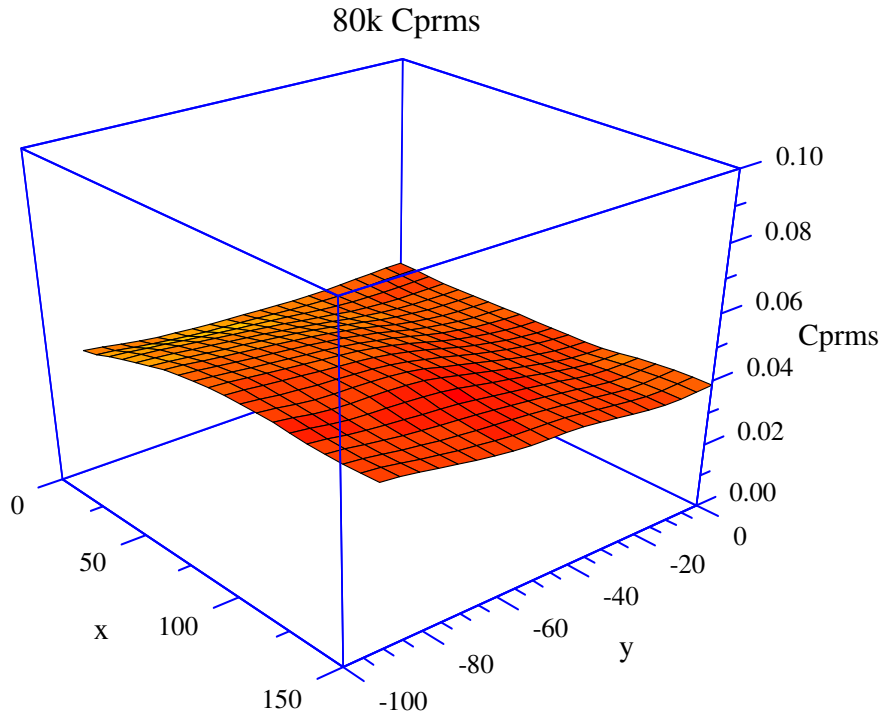

Figure 4.23: Fluctuating Pressure Coefficients (Cprms) -3D - 80 km/h

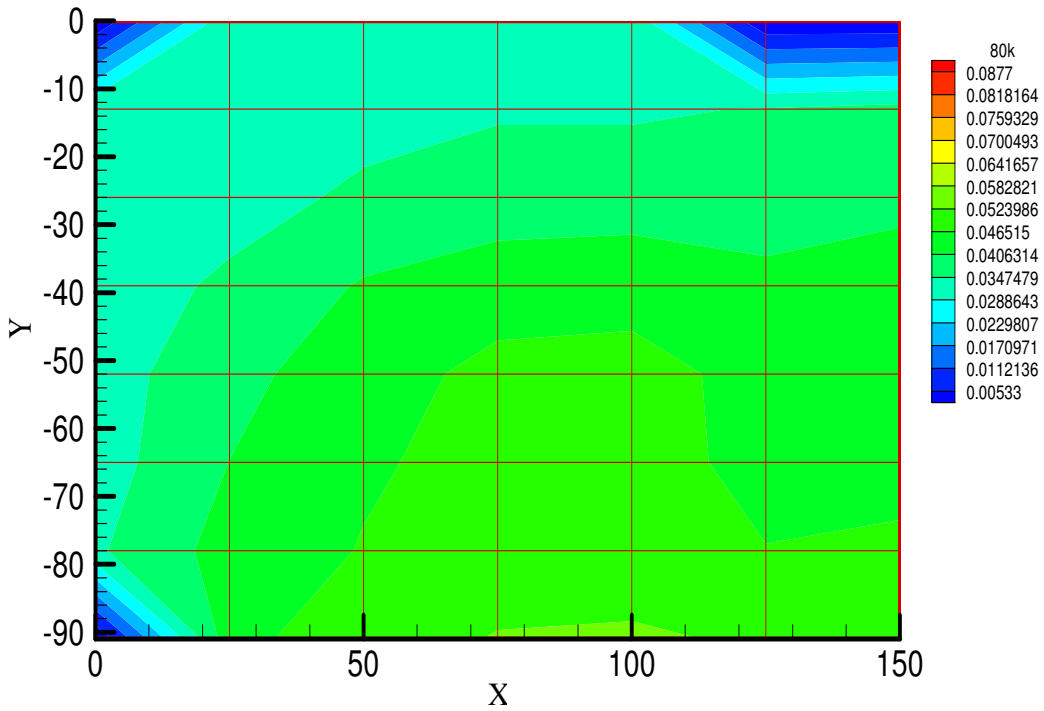

Figure 4.24: Fluctuating Pressure Coefficients (Cprms) - Contours -80 km/h

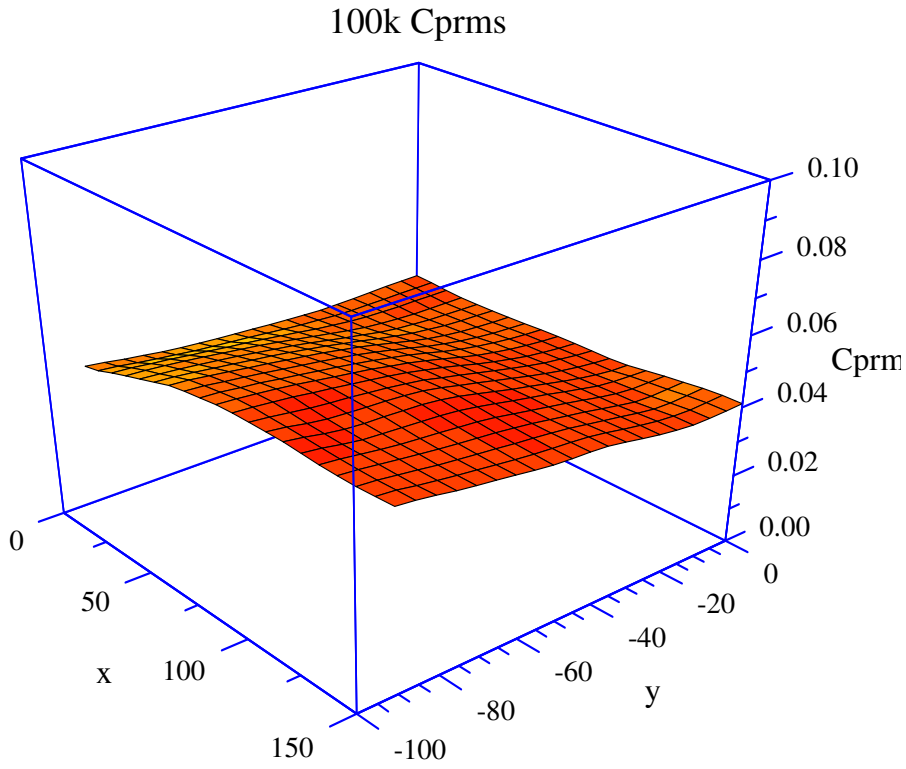

Figure 4.25: Fluctuating Pressure Coefficients (Cprms) -3D - 100 km/h

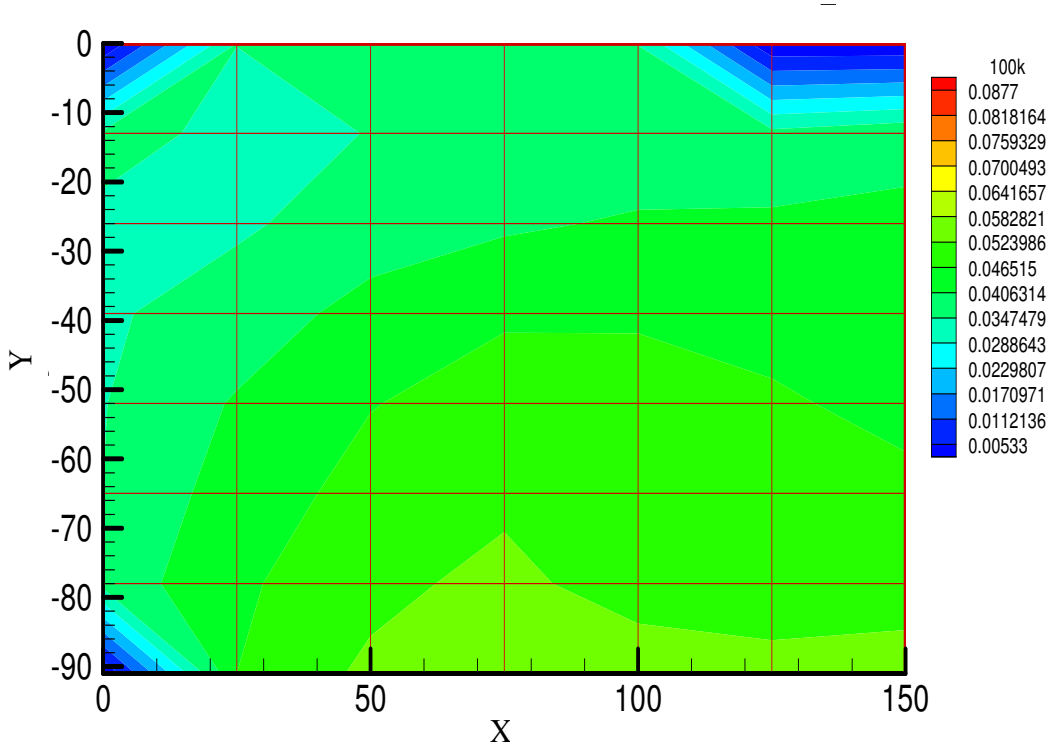

Figure 4.26: Fluctuating Pressure Coefficients (Cprms) - Contours -100 km/h

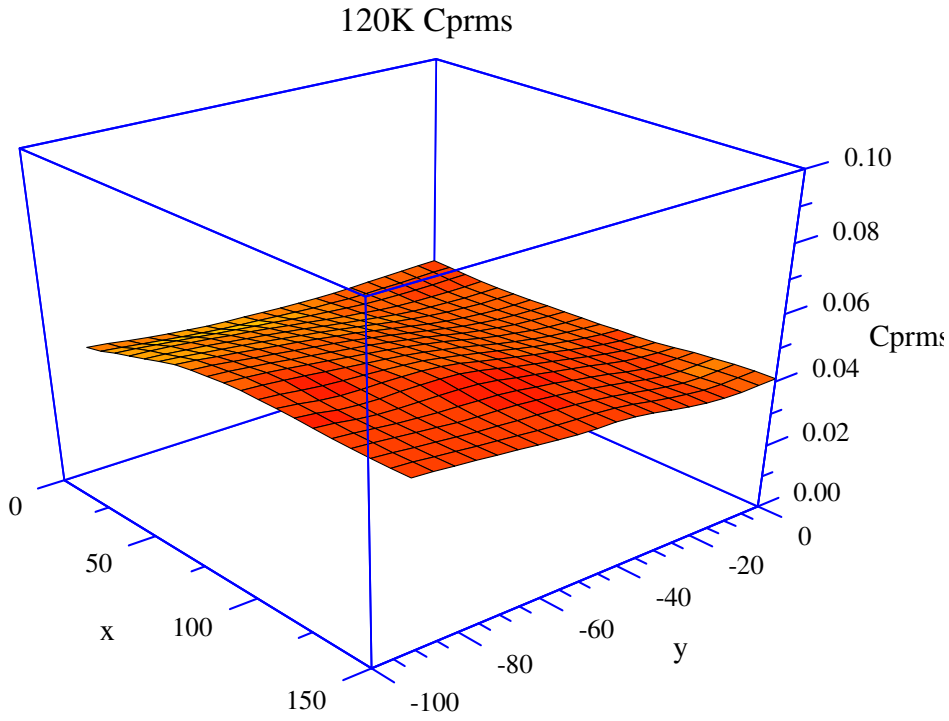

Figure 4.27: Fluctuating Pressure Coefficients (Cprms) -3D - 120 km/h

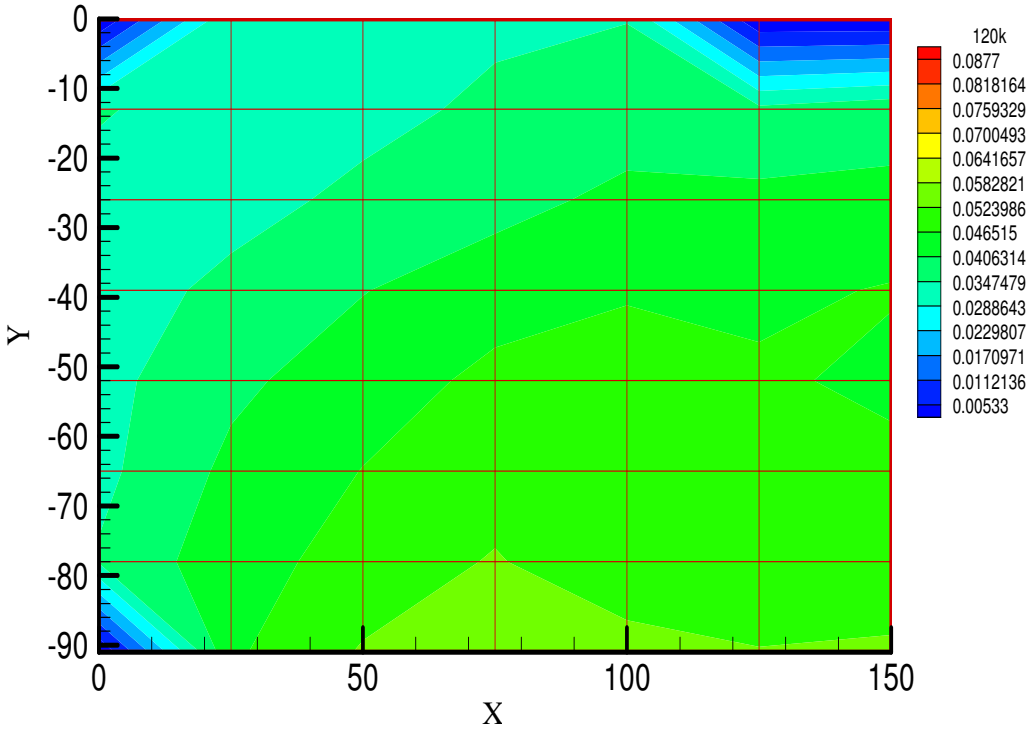

Figure4.28: Fluctuating Pressure Coefficients (Cprms) - Contours - 120 km/h

4.6 44mm Shroud

As followed before in other shrouding cases, another shroud of 44mm was attached on the external periphery of the mirror face. As seen in the case of 34mm shroud there was an increase in magnitude of the fluctuating pressure coefficients at the bottom section of the mirror surface. The results for the 44mm shroud show those high fluctuating pressure coefficients (Cprms) only at low speeds and vanish off at high speeds. This can be due to the increase in the length of shrouding which causes further drop in pressure. Figure 4.29 shows the schematic presentation of the 44mm shrouding. Figures 4.30 to Figures 4.37 show the fluctuating pressure coefficients at every speed.

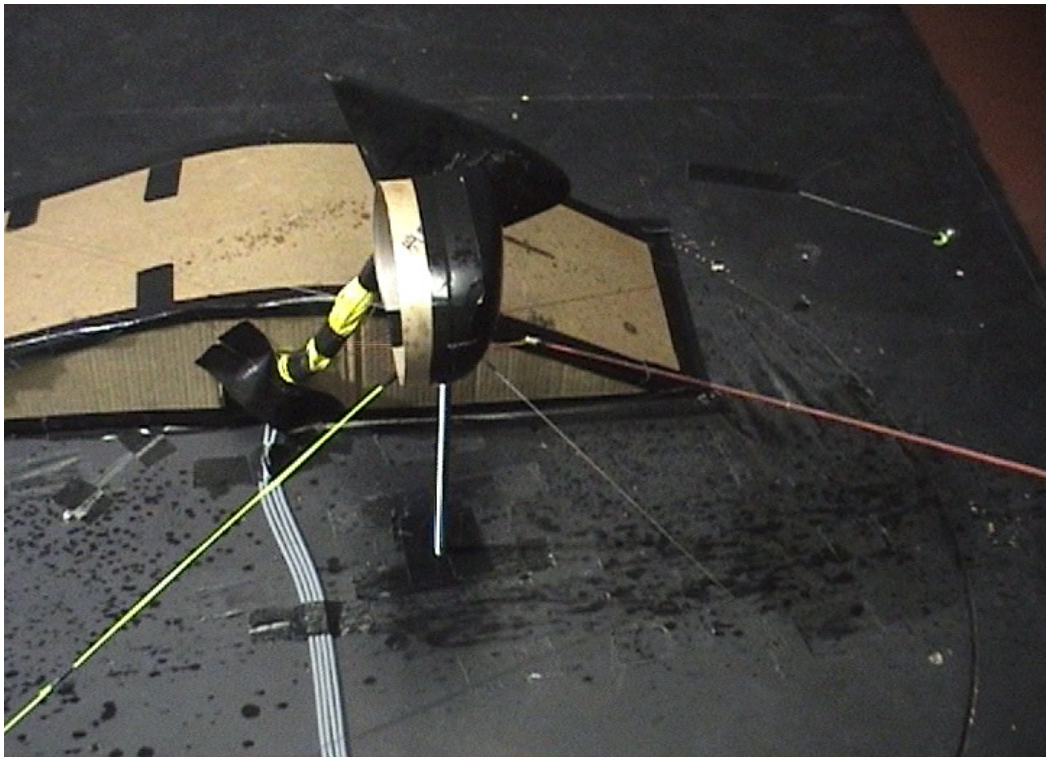

Figure 4.29: 44mm Shrouding

4.6.1 Results of 44mm Shroud

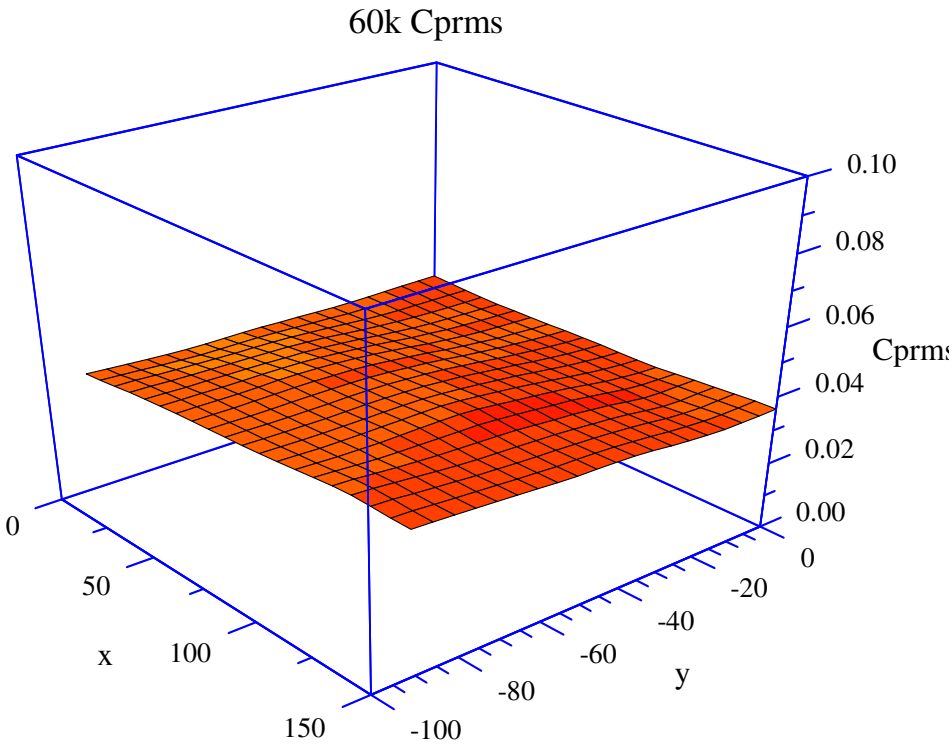

Figure 4.30: Fluctuating Pressure Coefficients (Cprms) -3D - 60 km/h

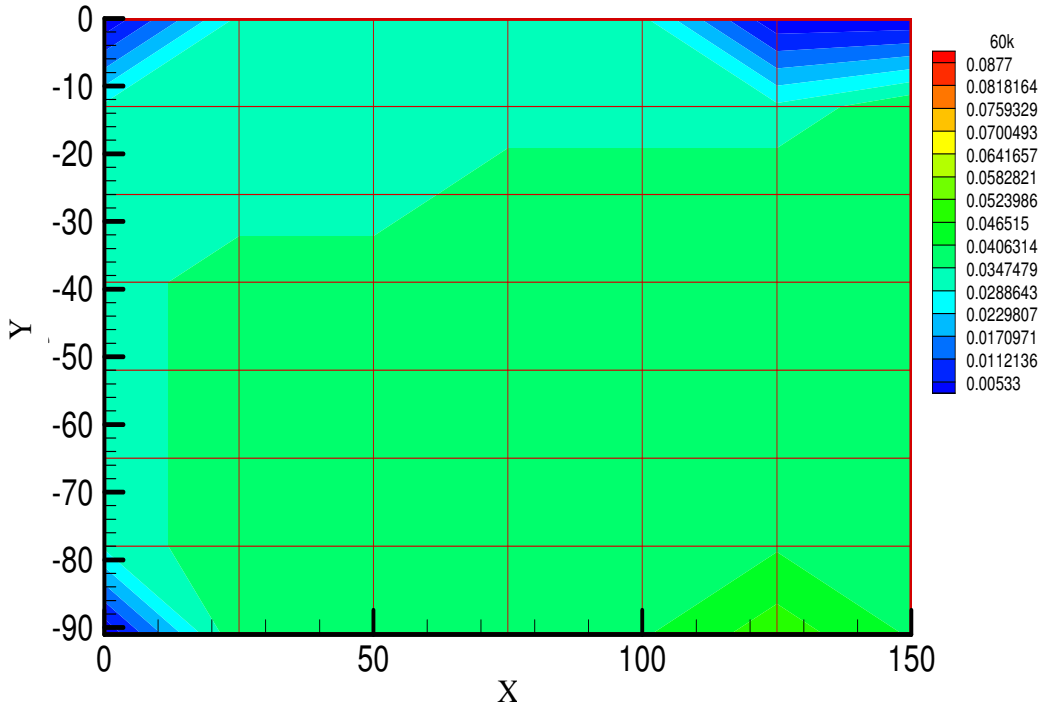

Figure 4.31: Fluctuating Pressure Coefficients (Cprms) - Contours -60 km/h

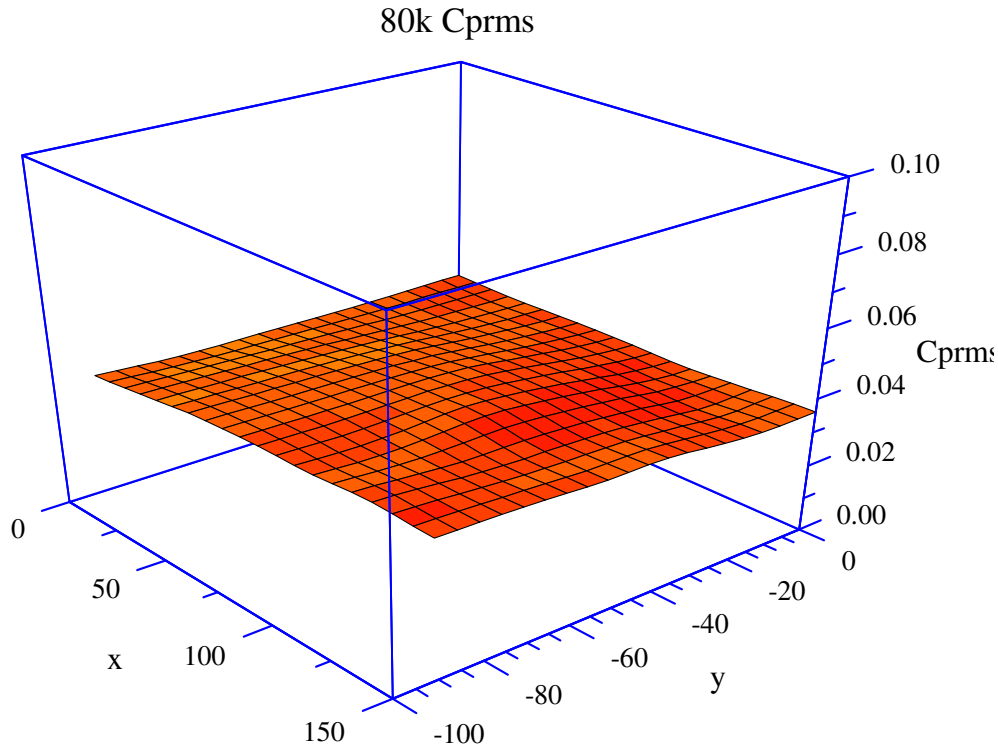

Figure 4.32: Fluctuating Pressure Coefficients (Cprms) -3D - 80 km/h

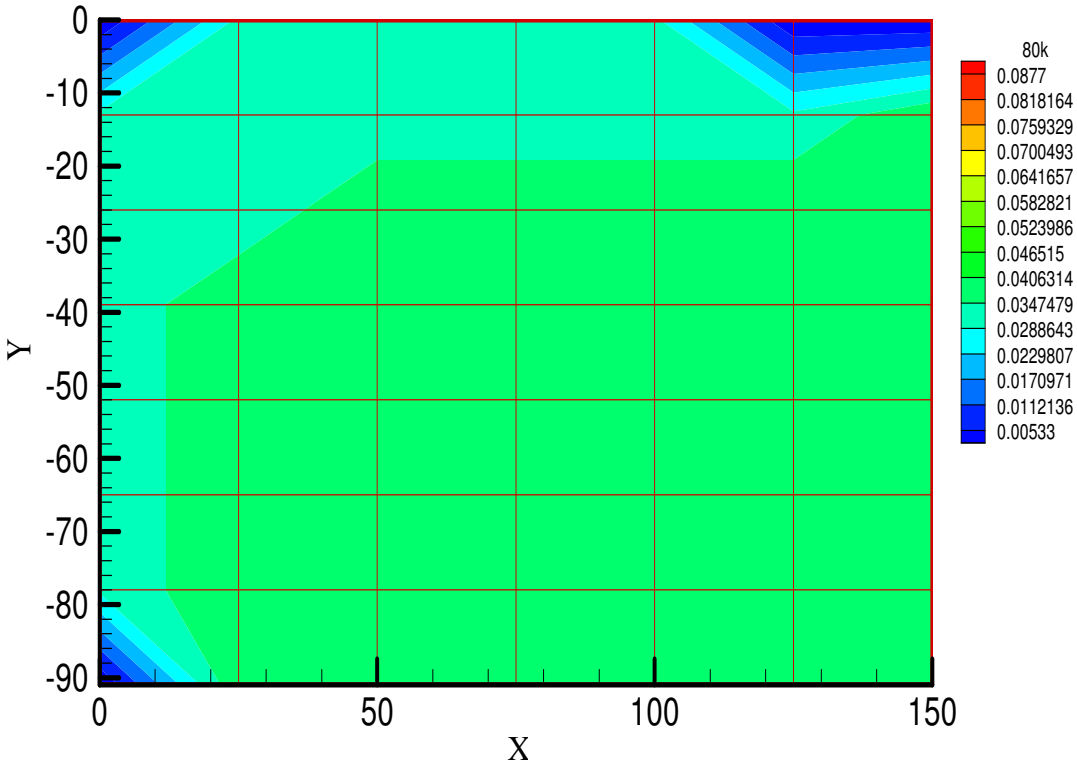

Figure 4.33: Fluctuating Pressure Coefficients (Cprms) - Contours - 80 km/h

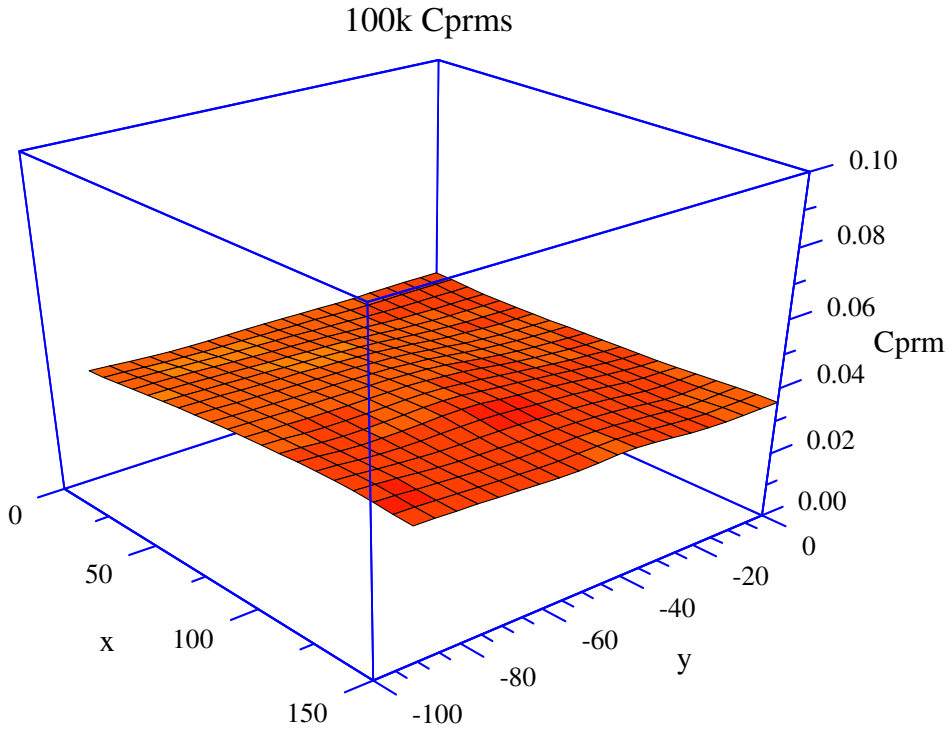

Figure 4.34: Fluctuating Pressure Coefficients (Cprms) -3D - 100 km/h

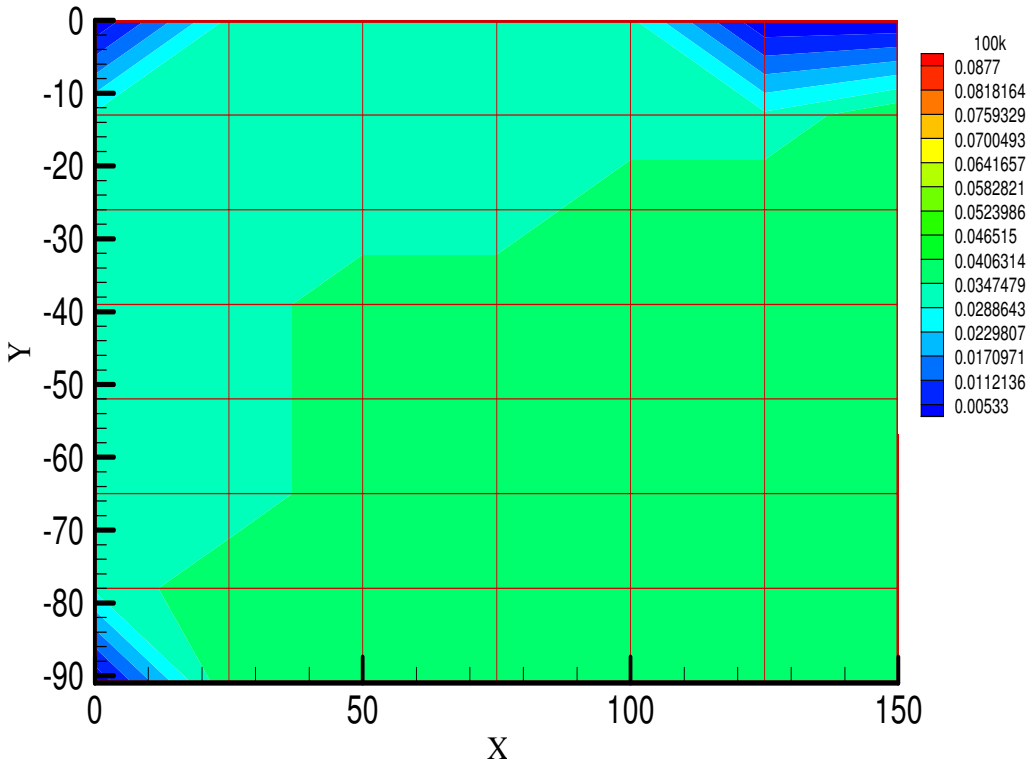

Figure 4.35: Fluctuating Pressure Coefficients (Cprms) - Contours -100 km/h

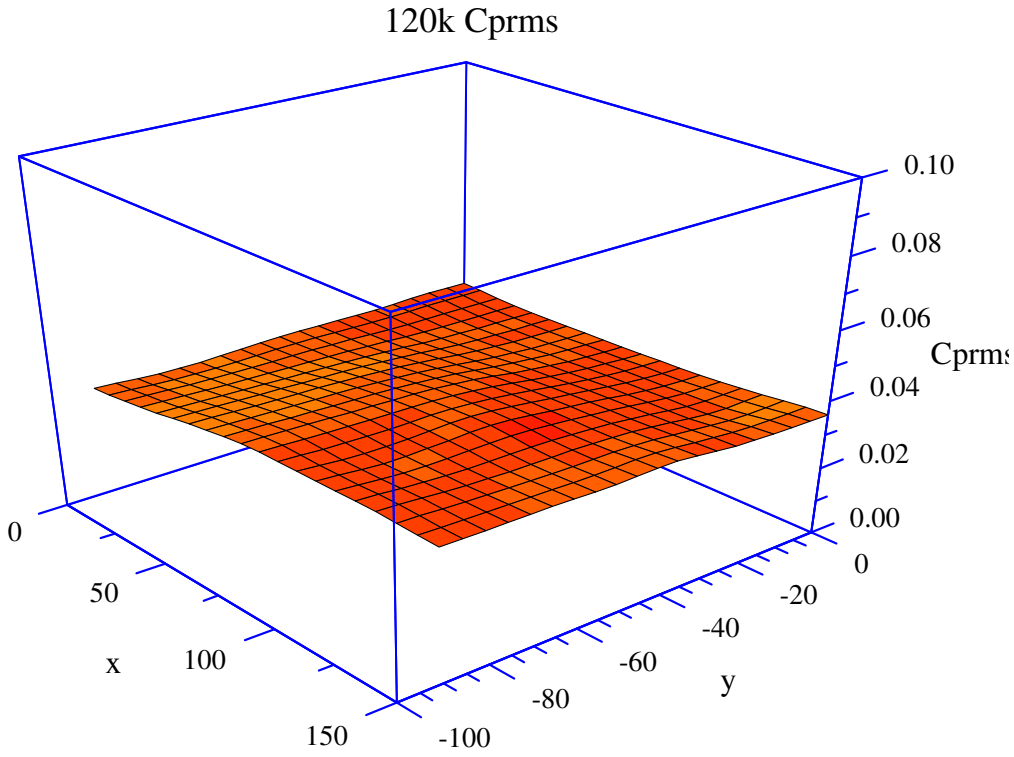

Figure 4.36: Fluctuating Pressure Coefficients (Cprms) -3D - 120 km/h

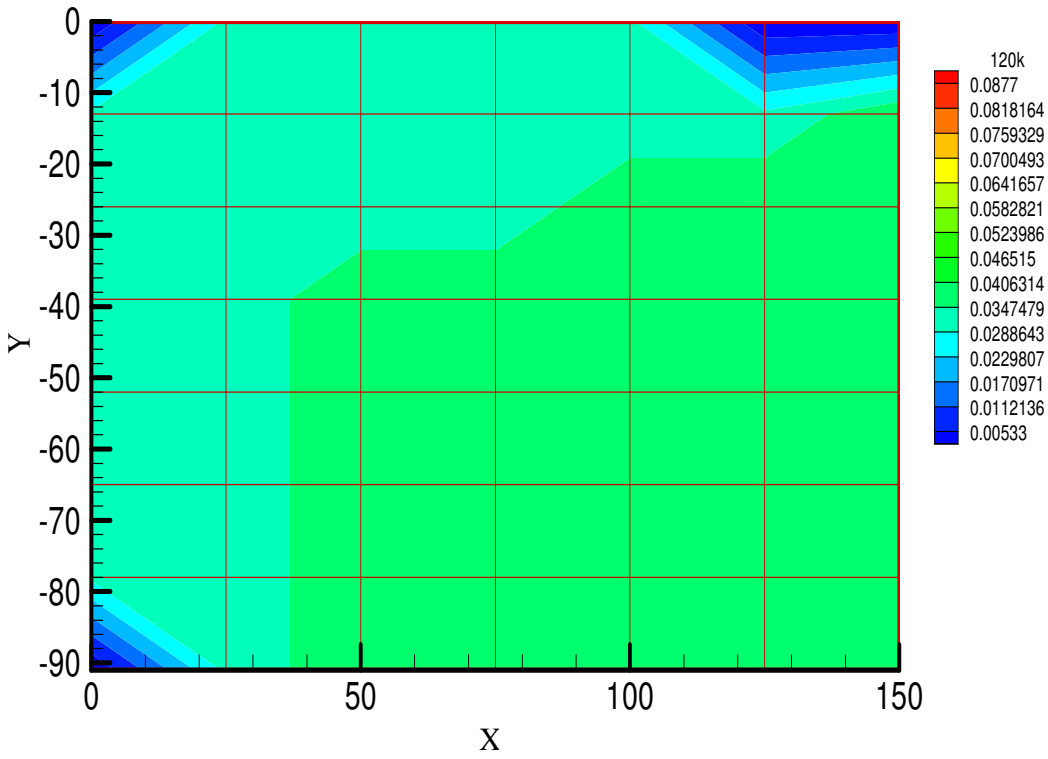

Figure 4.37: Fluctuating Pressure Coefficients (Cprms) - Contours -1200km/h

4.7 Powers Spectral Density Plot (PSD)

In this section the energy graphs of the highest fluctuating pressure are plotted for the highest fluctuating pressure coefficients for each individual case at different speeds. In case of standard mirror the maximum fluctuating pressure coefficients were observed near to bottom section of the mirror (point 50). Figure 4.40 shows the overlapping region between 200 Hz and 300Hz. The trend looks different when compared with the quarter model results due to absence of the car body, which may cause the flow to be pushed towards the mirror face. However, this was not the case when shrouding of 24mm, 34mm and 44mm were done and we can see the same trend as was seen in quarter model but with reduce magnitude. The maximum fluctuating pressure coefficients (Cpmrs) was observed in the bottom section (point 49 and 50). Figures 4.38 to 4.60 show the energy graphs at highest fluctuating pressure coefficients (Cprms) respectively. These graphs show that there is a significant energy variation in the mirror in Semi-Isolation for standard and modified mirror as the fluctuating pressure was obtained from the highest fluctuating pressure location (i.e., from different location)

Standard Mirror

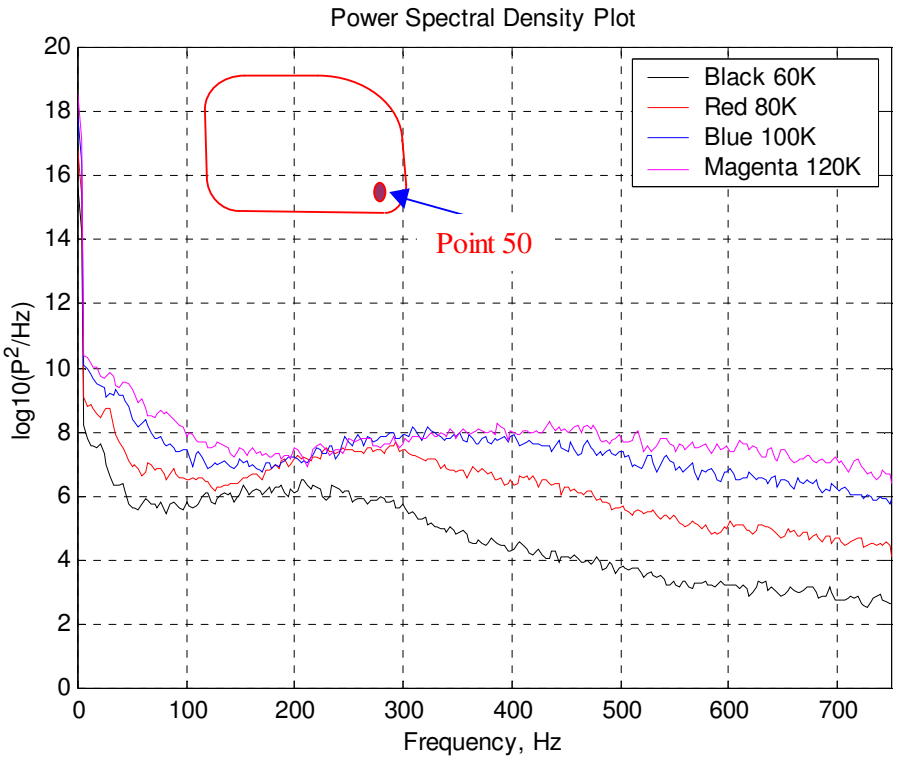

Figure 4.38: Highest Cprms at point 50

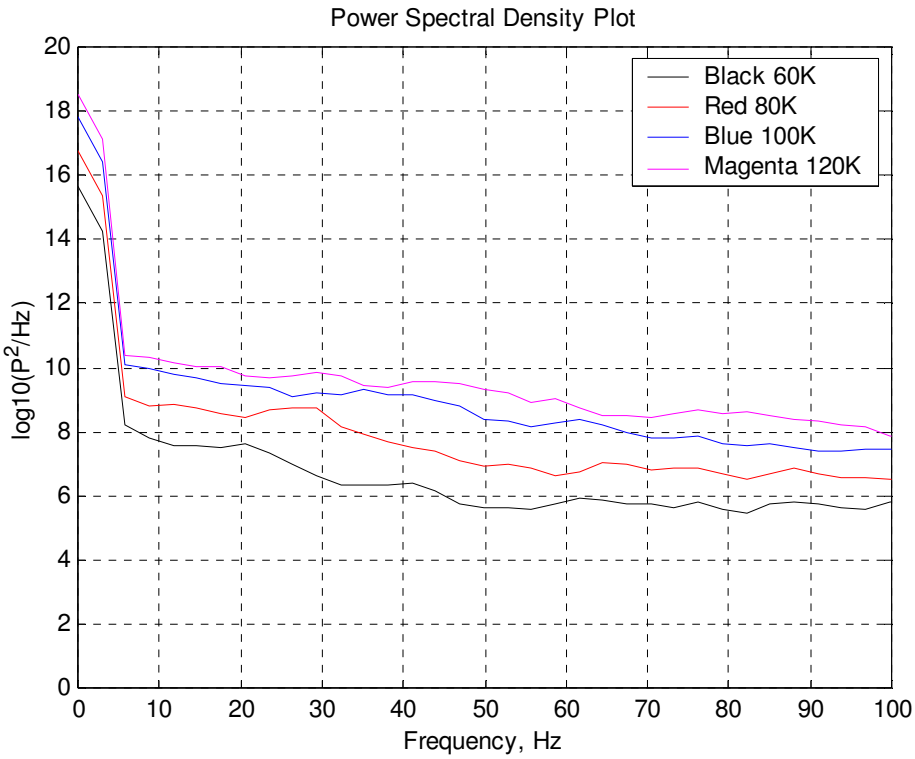

Figure 4.39: Zoom View of Highest Cprms 0-100Hz

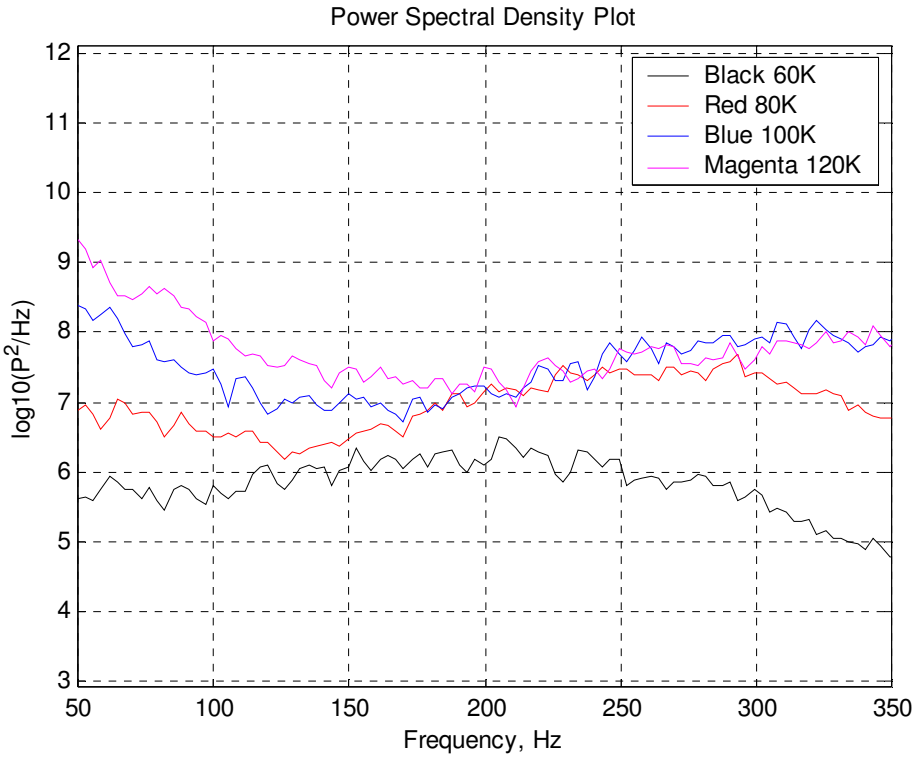

Figure 4.40: Zoom View of overlapping zones of Highest Cprms

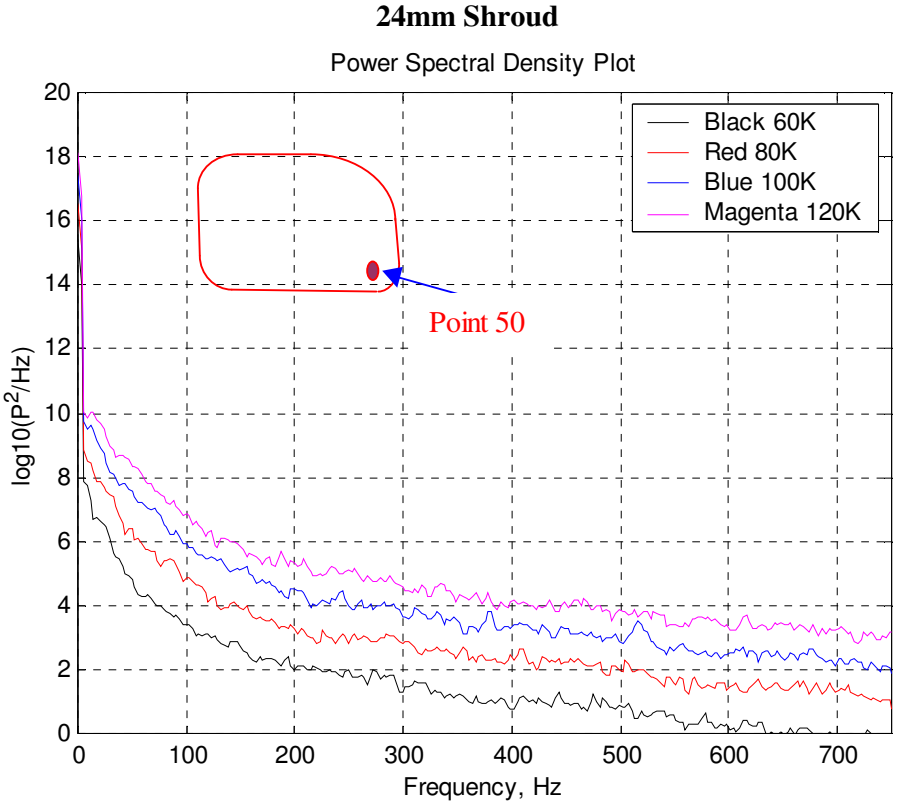

Figure 4.41: Highest Cprms at point 50

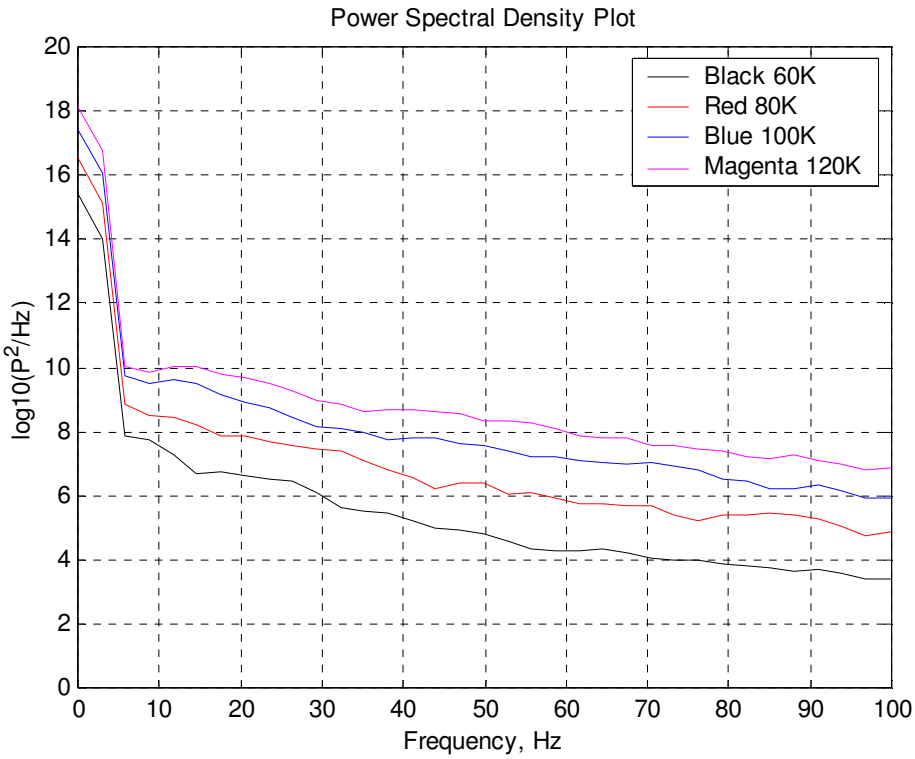

Figure 4.42: Zoom View of Highest Cprms 0-100Hz

34mm Shroud

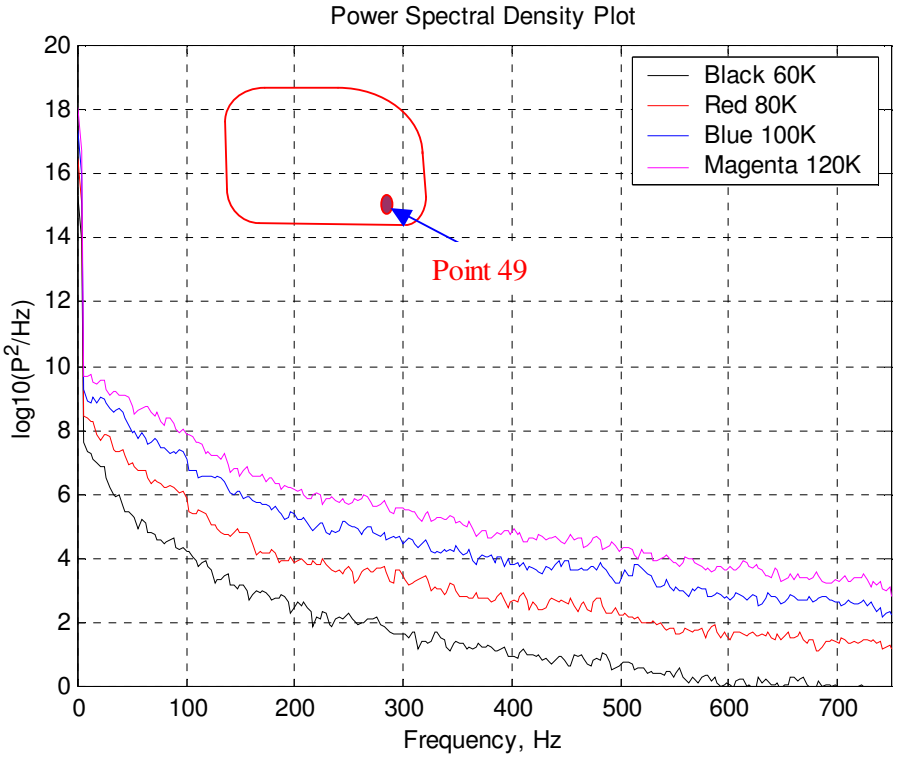

Figure 4.43: Highest Cprms at point 50

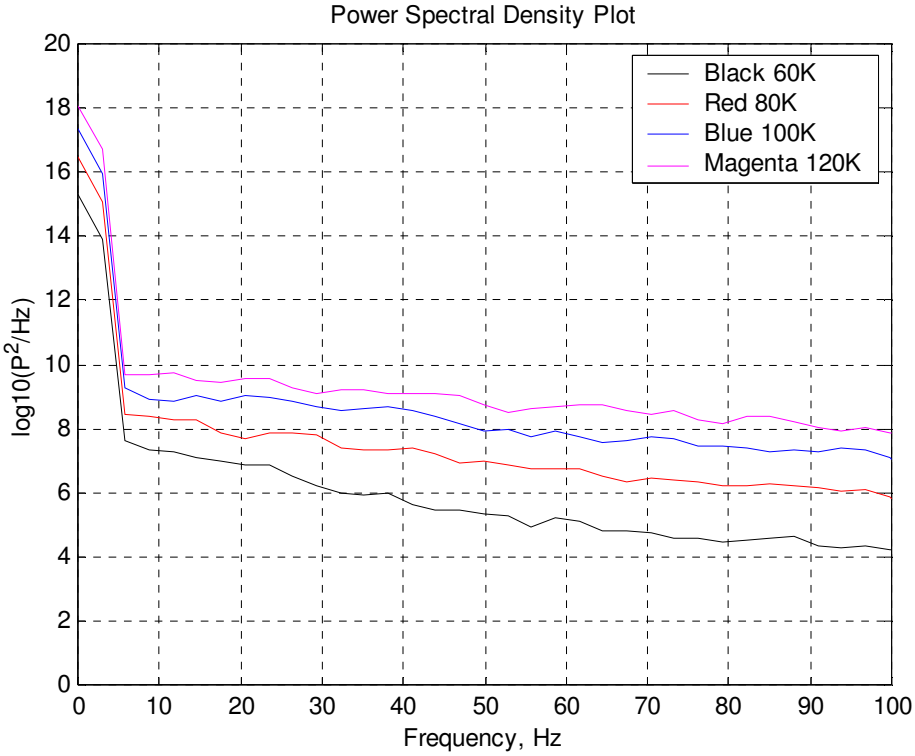

Figure 4.44: Zoom View of Highest Cprms 0-100Hz

44mm Shroud

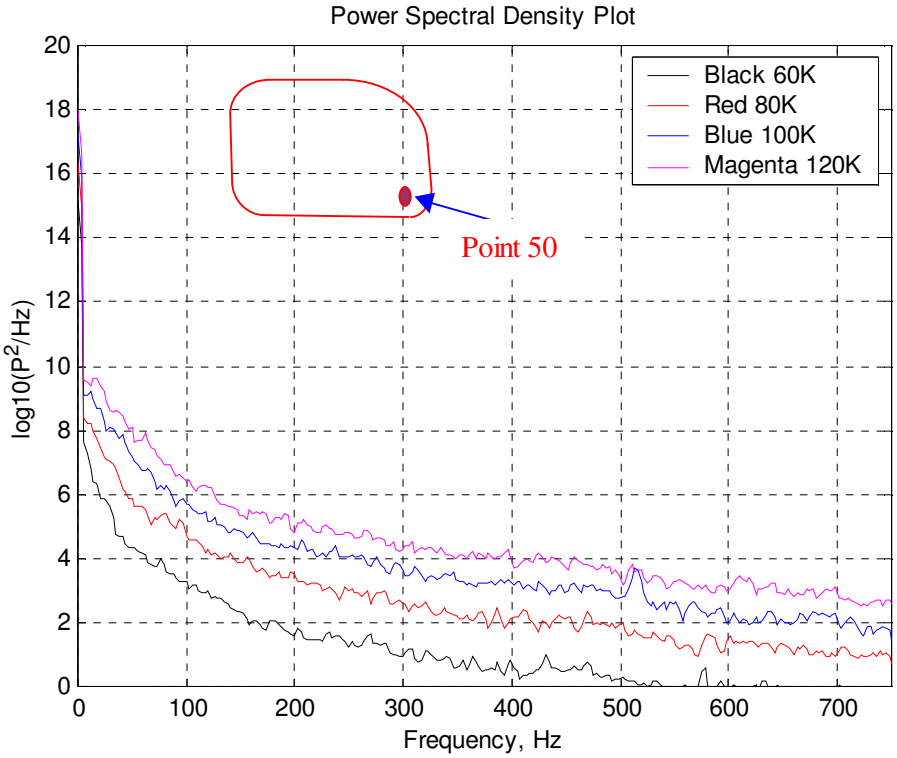

Figure 4.45: Highest Cprms at point 50

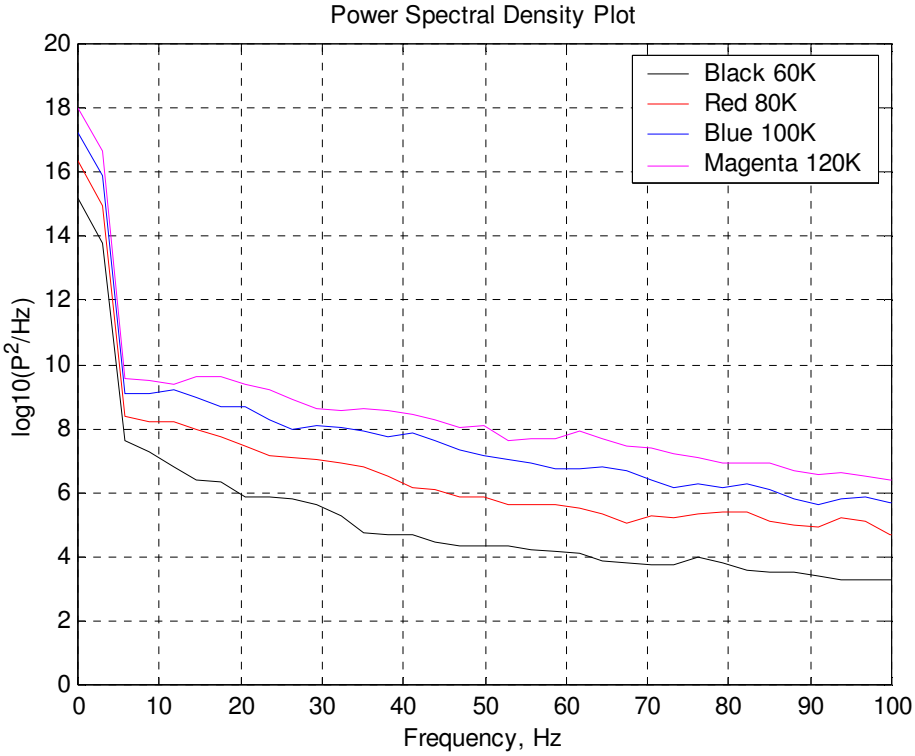

Figure 4.46: Zoom View of Highest Cprms 0-100Hz

Table 4.1 to 4.5 shows the comparison of results for the various frequency ranges (40 Hz, 50 Hz, 70Hz, 80 Hz and 90 Hz) for the data presented in the graphs above for semi-isolation condition.

Comparison of Results for Semi-Isolation at 40 Hz

Table 4.1: Energy comparison for various shrouding lengths

Speeds	Standard Mirror (Point 50)	24mm Shroud (Point 50)	34mm Shroud (Point 49)	44mm Shroud (Point 50)
60 km/h	6.25	5.50	5.75	4.75
80 km/h	6.75	6.75	7.50	6.25
100 km/h	7.75	7.75	8.30	7.75
120 km/h	8.50	8.70	9.00	8.25

Comparison of Results for Semi-Isolation at 50 Hz

Table 4.2: Energy comparison for various shrouding lengths

Speeds	Standard Mirror (Point 50)	24mm Shroud (Point 50)	34mm Shroud (Point 49)	44mm Shroud (Point 50)
60 km/h	4.75	4.50	5.25	4.25
80 km/h	6.25	6.50	7.00	5.80
100 km/h	7.70	7.75	8.00	7.25
120 km/h	8.25	8.25	8.50	8.00

Comparison of Results for Semi-Isolation at 70 Hz

Table 4.3: Energy comparison for various shrouding lengths

Speeds	Standard Mirror (Point 50)	24mm Shroud (Point 50)	34mm Shroud (Point 49)	44mm Shroud (Point 50)
60 km/h	4.10	4.10	4.75	3.80
80 km/h	5.75	5.80	6.25	5.25
100 km/h	7.00	7.00	7.80	6.25
120 km/h	7.50	7.75	8.25	6.60

Comparison of Results for Semi-Isolation at 80 Hz

Table 4.4: Energy comparison for various shrouding lengths

Speeds	Standard Mirror (Point 50)	24mm Shroud (Point 50)	34mm Shroud (Point 49)	44mm Shroud (Point 50)
60 km/h	3.75	3.90	4.25	3.75
80 km/h	5.50	5.25	6.15	5.25
100 km/h	6.25	6.50	7.75	6.15
120 km/h	7.25	7.50	8.15	7.00

Comparison of Results for Semi-Isolation at 90 Hz

Table 4.5: Energy comparison for various shrouding lengths

Speeds	Standard Mirror (Point 50)	24mm Shroud (Point 50)	34mm Shroud (Point 49)	44mm Shroud (Point 50)
60 km/h	5.75	3.75	4.15	3.50
80 km/h	6.75	5.50	6.10	5.00
100 km/h	7.80	6.25	7.50	5.75
120 km/h	825	7.25	8.05	6.75

4.7.1 Fluctuating Pressure Coefficients Comparison (Point 47)

The maximum fluctuating pressure (Cpmrs) for the quarter model testing in case of standard mirror testing was located at the bottom half of the mirror faces at point 47. However, 2-D contour and 3-D graphs shows the highest fluctuating pressure with in that region only. As a result of this, comparison is being made at the same point 47 to see the effects of the energy distribution with different shroud lengths of 24mm, 34mm, and 44mm. To see the effects in detail we have taken the same data points for each individual case with quarter model and also with semi-isolation condition for the entire frequency range. As we know that the vortex shedding occurs approximately at 50-70Hz, results were plotted for 40Hz, 50Hz and 70Hz to see the effects. Also zoomed images for the analysis up to 100Hz are provided for PSD plots graphs and are shown in Appendix C – PSD graph comparison.

4.7.1.1 Quarter Model PSD (Pint 47)

Figures C1 to C8 show the energy graph of each individual case. These Figures show the effects in the energy levels distribution are highest in case of standard mirror. However, as results of the different shrouding length of 24mm, 34mm, 44mm the energy level has dropped in magnitude. Since we have used three different lengths of shrouding we can conclude that

ideal shroud length for this particular mirror is 24mm as we can see a huge drop in magnitude with this shroud length. Table 4.6 to 4.8 shows the tabulated form of energy comparison for various shrouding lengths at different frequencies for same point location (point 47).

Comparison of Results at 40 Hz

Table 4.6: Energy comparison for various shrouding lengths

Speeds Points →	Standard Mirror Point 47	24mm Shroud Point 47	34mm Shroud Point 47	44mm Shroud Point 47
60 km/h	7.00	5.00	5.50	5.00
80 km/h	8.25	6.25	6.75	6.25
100 km/h	9.25	7.50	7.50	7.50
120 km/h	9.90	8.10	8.25	8.25

Comparison of Results at 50Hz

Table 4.7: Energy comparison for various shrouding lengths

Speeds Points →	Standard Mirror Point 47	24mm Shroud Point 47	34mm Shroud Point 47	44mm Shroud Point 47
60 km/h	6.75	5.15	4.75	4.50
80 km/h	8.25	6.15	6.25	6.00
100 km/h	9.25	7.60	7.25	7.25
120 km/h	9.90	8.00	8.10	7.95

Comparison of Results at 70Hz

Table 4.8: Energy comparison for various shrouding lengths

Speeds Points →	Standard Mirror Point 47	24mm Shroud Point 47	34mm Shroud Point 47	44mm Shroud Point 47
60 km/h	6.25	5.00	5.00	4.25
80 km/h	7.90	6.00	5.95	5.75
100 km/h	9.00	7.25	7.00	7.00
120 km/h	9.50	7.75	7.90	7.75

4.7.1.2 Semi-Isolation PSD (Point 47)

As mentioned before in the case of the quarter model testing the points having maximum fluctuating pressure coefficient (Cprms) were chosen. Similarly point 47 in case of Semi-Isolation was chosen to compare the energy distribution in case of quarter model and semi-isolation condition. This point will be used as a reference for the comparing the fluctuating pressure co-efficient for the modified mirror case (24mm, 34mm, and 44mm). Figures C8 to C15 show the PSD graphs for each individual case for the Semi-isolation condition. Table 4.7 to 4.9 shows the tabulated comparison of the energy graphs for the point 47 for mirror in Semi-Isolation condition.

Comparison of Results at 40 Hz

Table 4.9: Energy comparison for various shrouding lengths

Speeds Points →	Standard Mirror Point 47	24mm Shroud Point 47	34mm Shroud Point 47	44mm Shroud Point 47
60 km/h	5.95	5.75	5.75	5.00
80 km/h	7.25	7.00	7.00	6.50
100 km/h	9.00	8.25	8.50	8.00
120 km/h	9.75	9.15	9.15	8.50

Comparison of Results at 50 Hz

Table 4.10: Energy comparison for various shrouding lengths

Speeds Points →	Standard Mirror Point 47	24mm Shroud Point 47	34mm Shroud Point 47	44mm Shroud Point 47
60 km/h	5.80	5.25	5.00	4.75
80 km/h	7.25	7.00	7.00	6.25
100 km/h	8.25	8.15	8.15	7.25
120 km/h	9.25	8.75	9.00	8.25

Comparison of Results at 70 Hz

Table 4.11: Energy comparison for various shrouding lengths

Speeds Points →	Standard Mirror Point 47	24mm Shroud Point 47	34mm Shroud Point 47	44mm Shroud Point 47
60 km/h	5.25	5.00	4.75	4.25
80 km/h	6.75	6.25	6.25	5.75
100 km/h	8.15	7.75	7.50	7.00
120 km/h	8.75	8.60	8.25	7.75

The comparison shows that when the mirror is attached to the car model its magnitude is high for each individual case which can be due to airflow being pushed from the car body on to the mirror face and causing the flow of air to be complex due to A-pillar region. However, on the other hand for the semi-isolation condition the magnitude is lower. Moreover, we can see a significant drop in magnitude of energy level at low frequency about 40Hz, which is not same at high frequency. With an increase in speed the magnitude of energy level decreases. This can be due to the vortex shedding, which occurs at low frequency.

4.8 Flow Visualisation in Semi-Isolation

Flow visualisation was done only for case of standard mirror and 44mm shrouding. Flow visualisation was also done with the help of wool taps for the similar cases. Figure 4.47 to 4.50 shows the flow visualisation of standard mirror with the help of smoke generator inside the RMIT Industrial Wind Tunnel. Figures 4.51 to 4.54 show the flows visualisation with smoke and with wool taps for the modified mirror of 44mm shrouding. The Figures clearly show the flow separation over the mirror face and also when the shrouding is being mounted over it.

4.8.1 Standard Mirror

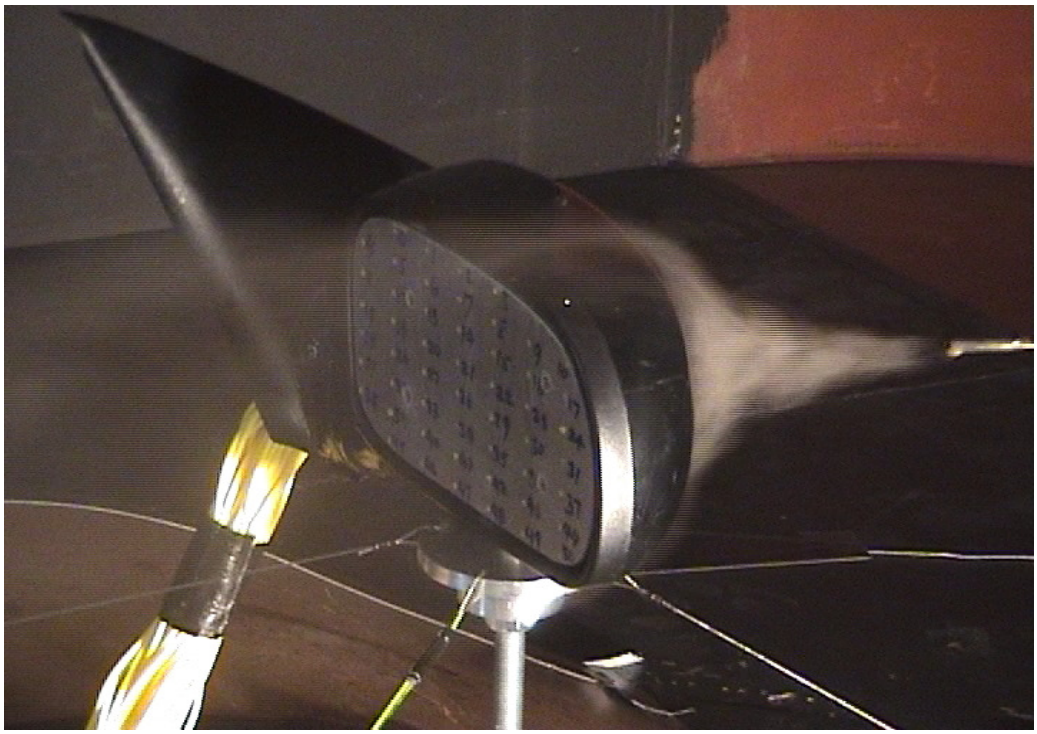

Figure 4.47: Flow Separation from the Mirror Housing (Standard Mirror)

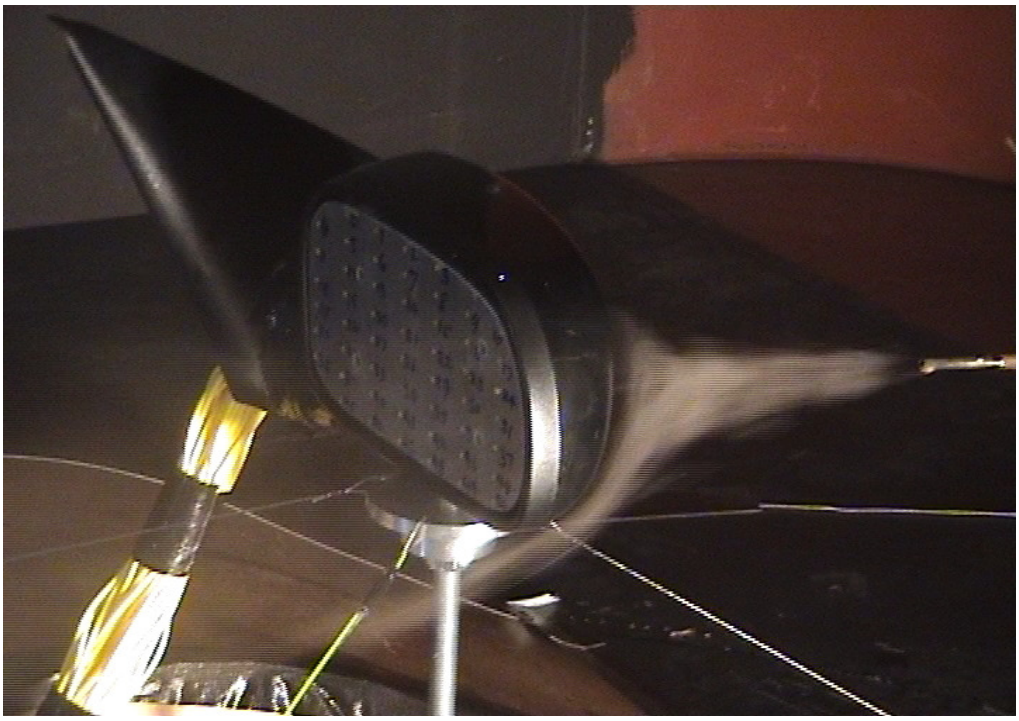

Figure 4.48: Flow Separation at the Bottom Section of Mirror Face (Standard Mirror)

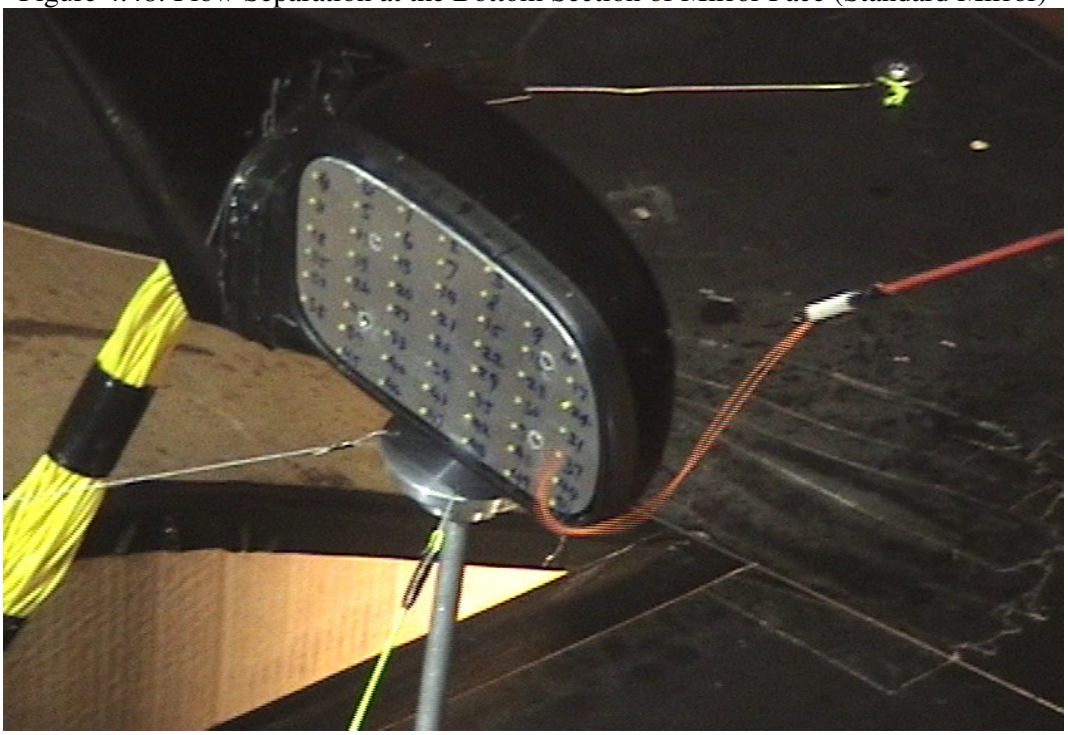

Figure 4.49: Reverse Flow on Mirror Face (Standard Mirror)

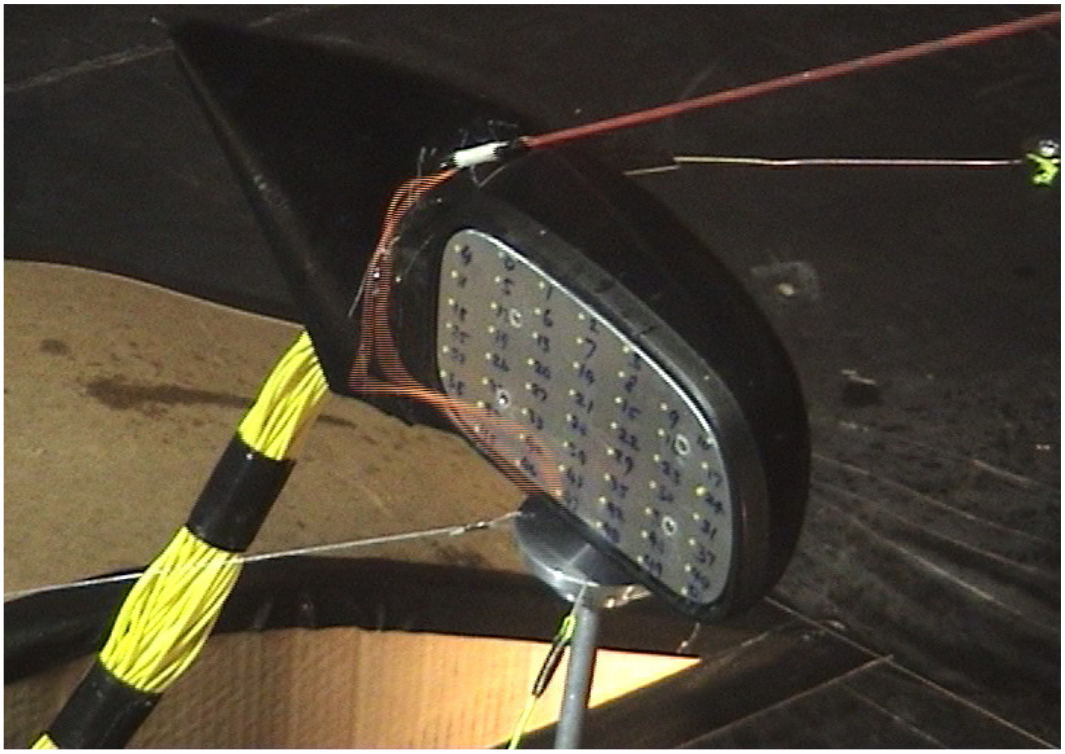

Figure 4.50: Flow through the Root of the Mirror (Standard Mirror)

4.8.2 44mm Shrouding

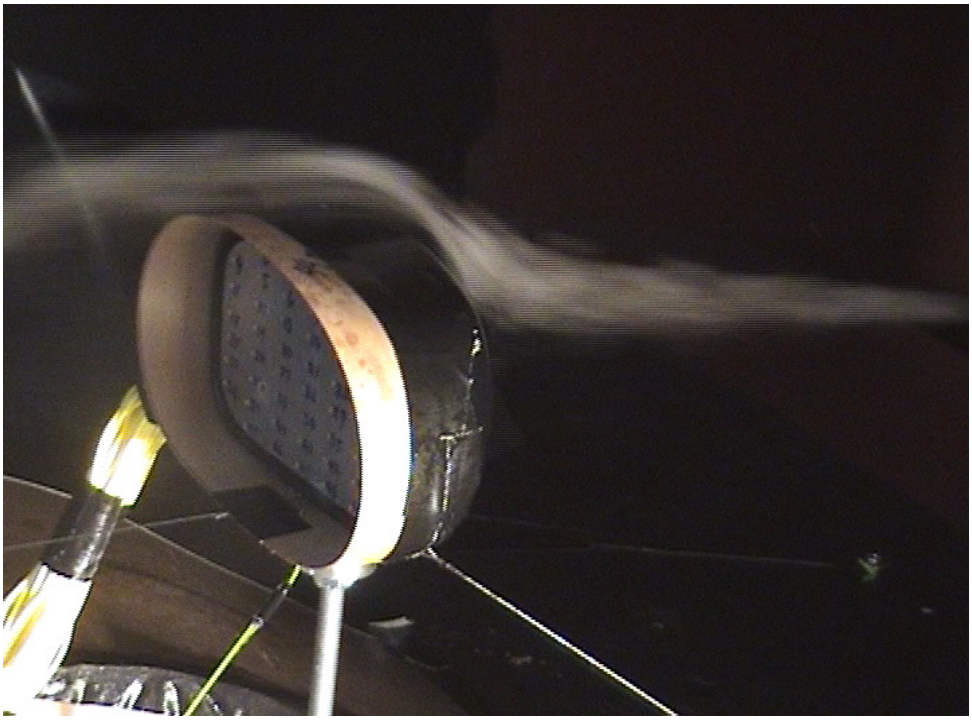

Figure 4.51: Flow Separation due to Effects of Shrouding (44mm Shroud Mirror)

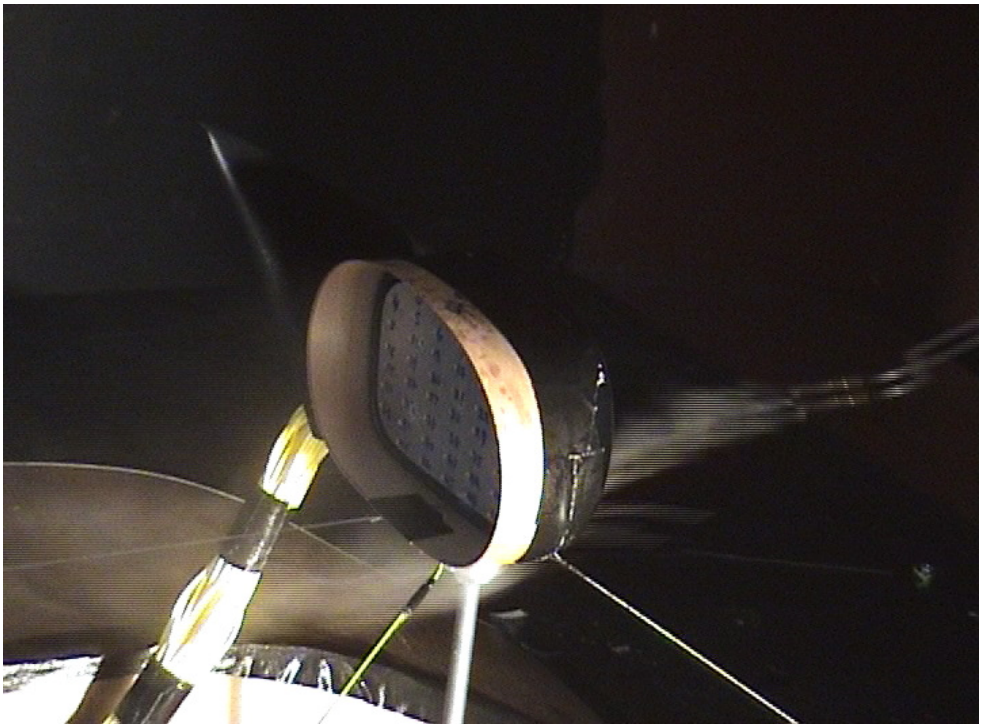

4.52: Flow Separation from the Mirror Housing

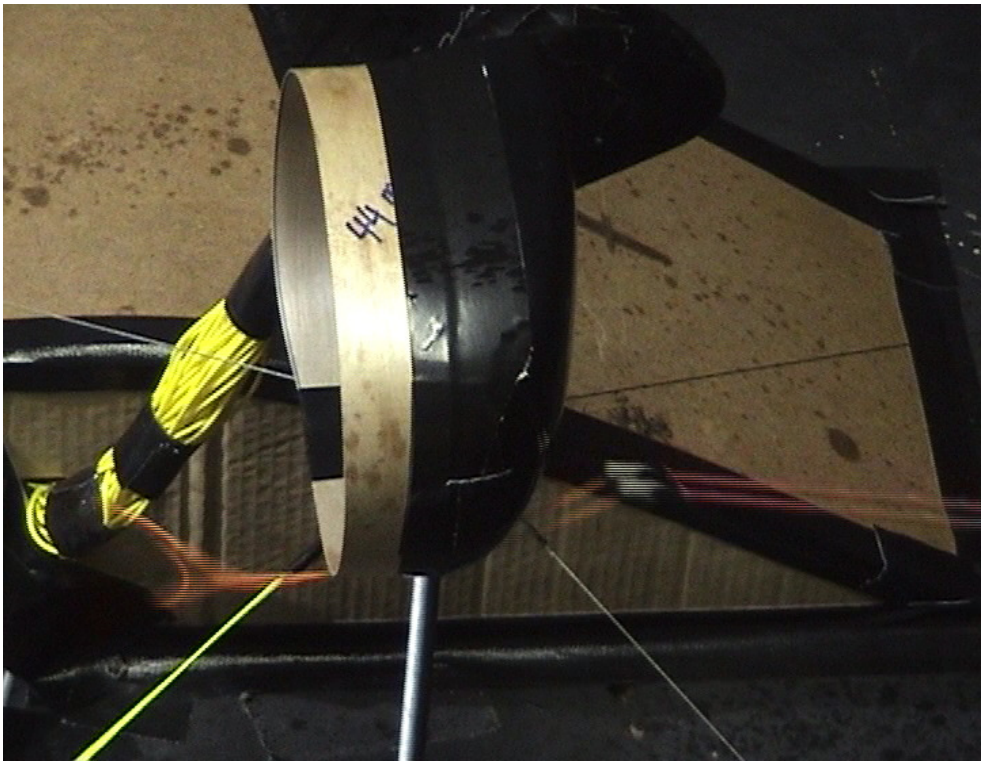

Figure 4.53: Wool Taps showing the Pressure Fluctuation at Bottom Base of Mirror

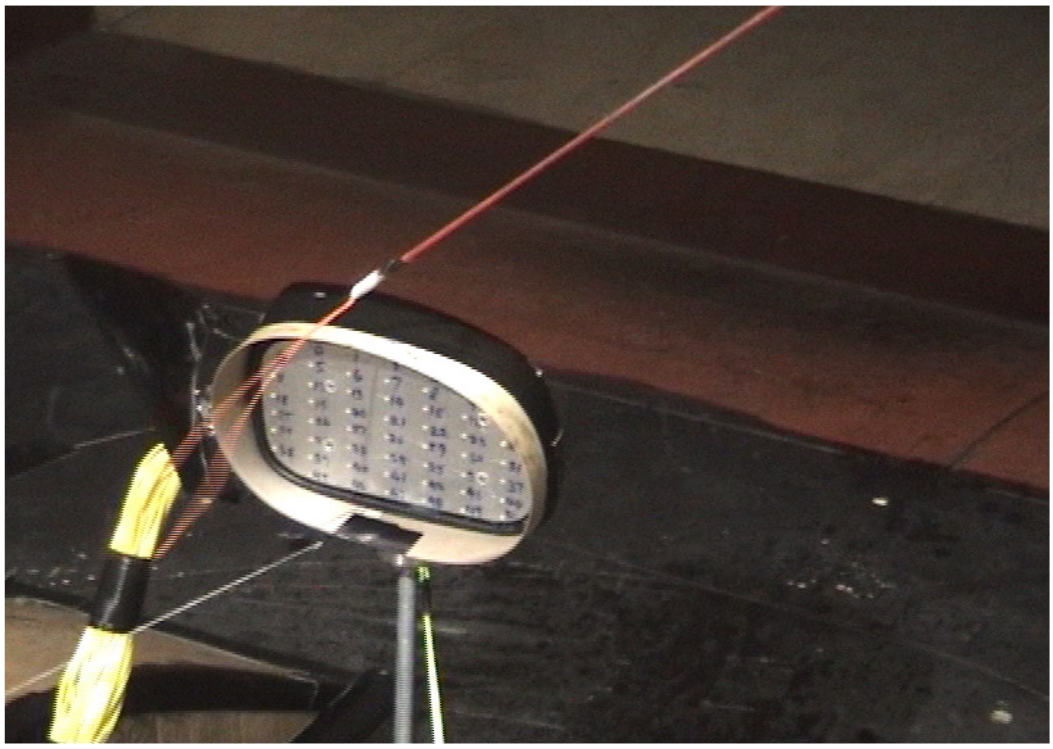

Figure 4.54: Wool Taps showing the Effects of Shrouding

Chapter 5
General Discussion

In order to understand the effects of aerodynamic inputs on mirror vibration, the time averaged mean and time dependent fluctuating pressures were measured and their non-dimensional parameters were presented and discussed in Chapter 3 and Chapter 4. All measurements were conducted for the standard mirror and modified mirror attached with a quarter model (¾) production model car. The standard and modified mirrors were also tested in isolation and the results were described in earlier chapters.

5.1 Standard Mirror with Quarter Model and in Semi-Isolation

From the test conducted for the quarter model with the mirror attached, the fluctuating pressure coefficient (Cprms) for the mirror with quarter model tends to be highest on the mirror face far away from the body of the car especially at the bottom section of the mirror face. The fluctuating pressure coefficient (Cprms) is high at 60 km/h at the extreme bottom right corner of mirror face. It is believed that fluctuating pressure coefficient shifts from extreme right corner at low speeds towards the bottom central part of the mirror face at high speeds of 120 km/h to the magnitude of 0.0818 fluctuating pressure coefficients (Cprms).

However, in semi – isolation condition the trend is not duplicated. In that the magnitude of fluctuating pressure coefficient (Cprms) is high at low speeds (0.0915) at the far right end bottom section of mirror face. This fluctuating pressure coefficient (Cprms) later moves towards the bottom central section of mirror face and drops in magnitude to 0.0850 at speed of 120 km/h.

5.2 Modified Mirror with Quarter Model and in Semi-Isolation

The location of the maximum fluctuating pressure moves from the bottom central part of the mirror face to the top central part compared to the standard mirror with the same condition. The trend for the fluctuating pressure is the same for 24 mm, 34 mm and 44 mm shroud

length. However, with an increase of shroud length, the magnitude of the fluctuating pressure decreases (0.095 for 24 mm, 0.065 for 34 mm and 0.050 for 44 mm shroud) respectively.
In semi –isolation condition, the fluctuating pressure coefficient (Cprms) is located at the bottom central section of the mirror face and measured higher compared to the modified mirror for all shroud lengths (0.060 for 24 mm, 0.050 for 34 mm and 0.043 for 44 mm shroud) respectively.

In case of bottom flange modification for 24mm shroud, it was observed that a further drop in the fluctuating pressure coefficient (Cprms) due to streamlining of the bottom flange. This also shows that the streamlining the mirror housing can have a big implication on the mirror face and can alter the pressure measurements on the mirror face.

In case of the pressure taps on mirror shell housing, tests were confined to 60 km/h, 80 km/h and 100 km/h only due to the limitation of the DPMS system. However, data analysis from 100 km/h we can see that the surface pressure measurements (Cp) is maximum near the body as compared to the far end section of the mirror housing where the pressure drops. However, the 3-D graphs show that the bottom half of the shell housing near to the mirror housing shows high fluctuating pressure coefficient (Cprms).

5.3 Phase Angle

The phase angle analysis was done for the quarter model at 100 km/h only. The phase angle of fluctuating pressures is important as they show in which direction the maximum fluctuating pressure is acting. In order to generate the differential motion of mirror glass, the fluctuating pressures of different magnitudes should act in opposite direction either in horizontally, vertically and diagonally as shown in Figure 5.1. The phase angle was calculated from the surface mean pressure data obtained for 21 seconds and only 0.25 second data has been shown in Figures 5.2 to 5.17 for different cases.

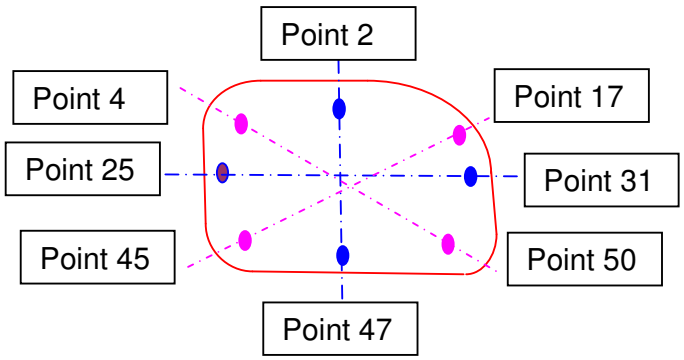

Figure 5.1: Phase Angle Representation

The fluctuating pressure for the same time length is shown in Figures 5.2 to 5.5 for the points 2 & 47, 25 & 31, 4 & 50, 17 & 45. The superimposed time history of fluctuating pressures for the standard mirror shows that the net magnitude of fluctuating pressures between the horizontal points (25 and 31) is approximately 160 Pa. The net variation of fluctuating pressures in the vertical direction of two points (2 and 47) is around 260 Pa. Diagonally the net variations between the points (4 & 50, 17 & 45) are 200 Pa and 190 Pa respectively. In all cases, the highest magnitudes of fluctuating pressures are out of phase. It may be noted that a small variation of phase could be due to time delays during data acquisition process. However, it would not affect significantly the outcomes of the phase shift. As there is a net variation in fluctuating pressures between two points and the magnitudes are generally out of phase, they will cause mirror to have rotational motion in all three directions. However, due to the highest net variation of fluctuating pressures in the vertical direction, the mirror will experience the rotation motion in the horizontal axis. Additionally, the mirror will experience

the rotational motion diagonally as well. However, the most dominant vibration will be along the horizontal axis due to the highest net pressure variation.

For the modified mirror, the fluctuating pressure for the same time length is shown in Figures 5.6 to 5.9 for the points 2 & 47, 25 & 31, 4 & 50, 17 & 45 respectively. The superimposed time history of fluctuating pressures for the modified (24 mm shroud) mirror shows that the net magnitude of fluctuating pressures between the horizontal points (25 and 31) is approximately 140 Pa. The net variation of fluctuating pressures in the vertical direction of two points (2 and 47) is around 180 Pa. Diagonally the net variations between the points (4 & 50, 17 & 45) are 150 Pa each respectively. In all cases, the highest magnitudes of fluctuating pressures are out of phase. As there is a net variation in fluctuating pressures between two points and the magnitudes are generally out of phase, they will cause mirror to have rotational motion in all three directions. However, due to the highest net variation of fluctuating pressures in the vertical direction as was seen for the standard mirror, the mirror will have the rotation motion in the horizontal axis. However, the most dominant vibration will be along the horizontal axis due to the highest net pressure variation.

The fluctuating pressure for the same time length for the 34 mm shroud length is shown in Figures 5.10 to 5.13 for the points 2 & 47, 25 & 31, 4 & 50, 17 & 45 respectively. The fluctuating pressures that the net magnitude of fluctuating pressures between the horizontal points (25 and 31) is approximately 150 Pa. The net variation of fluctuating pressures in the vertical direction of two points (2 and 47) is around 150 Pa. Diagonally the net variations between the points (4 & 50, 17 & 45) are 165 Pa and 150 Pa respectively. In all cases, the highest magnitudes of fluctuating pressures are out of phase. As there is a net variation in fluctuating pressures between two points and the magnitudes are generally out of phase, the mirror will face vibration motion. The mirror will experience the rotation motion in the horizontal axis as variation in pressures is in the vertical direction.

The fluctuating pressure for the 44 mm shroud length is shown in Figures 5.14 to 5.17 for the points 2 & 47, 25 & 31, 4 & 50, 17 & 45. The fluctuating pressures shows that the net magnitude of fluctuating pressures between the horizontal points (25 and 31) is approximately 130 Pa. The net variation of fluctuating pressures in the vertical direction of two points (2 and 47) is around 300 Pa. Diagonally, the net variations between the points (4 & 50, 17 & 45) are

170 Pa and 140Pa respectively. In all cases, the highest magnitudes of fluctuating pressures are out of phase. As there is a net variation in fluctuating pressures between two points and the magnitudes are generally out of phase, they will cause mirror to have rotational motion in all three directions. However, due to the highest net variation of fluctuating pressures in the vertical direction, the mirror will experience the rotation motion in the horizontal axis. However, the most dominant vibration will be along the horizontal axis due to the highest net pressure variation.

Table 5.1: Energy distribution comparison

Cases Points→ 100k	Horizontal Axis Point 25 & 31 (Pa)	Vertical Axis Point 2 & 47 (Pa)	Diagonal Axis-1 Point 4 & 50 (Pa)	Diagonal Axis –2 Point 17 & 45 (Pa)
Standard Mirror	160	260	200	190
24mm shroud	140	180	150	150
34mm Shroud	150	150	165	150
44mm Shroud	130	300	170	140

However, mirror will be subjected to transnational and diagonal rotation motion in all the cases described above. The magnitude of fluctuating pressures is higher for vertical axis and diagonal axis-1. However, in general we can mention that the movement of the mirror glass will be vertical and diagonalaxis-1 compared to other axis.

Standard Mirror Horizontal Axis

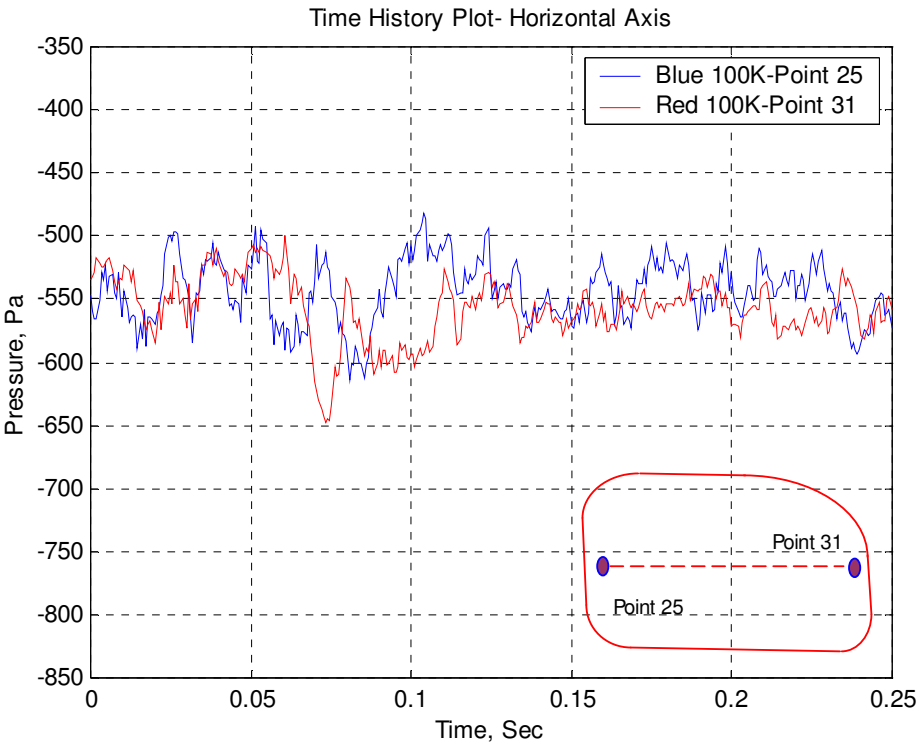

Figure 5.2: Phase angle horizontal axis

Vertical Axis

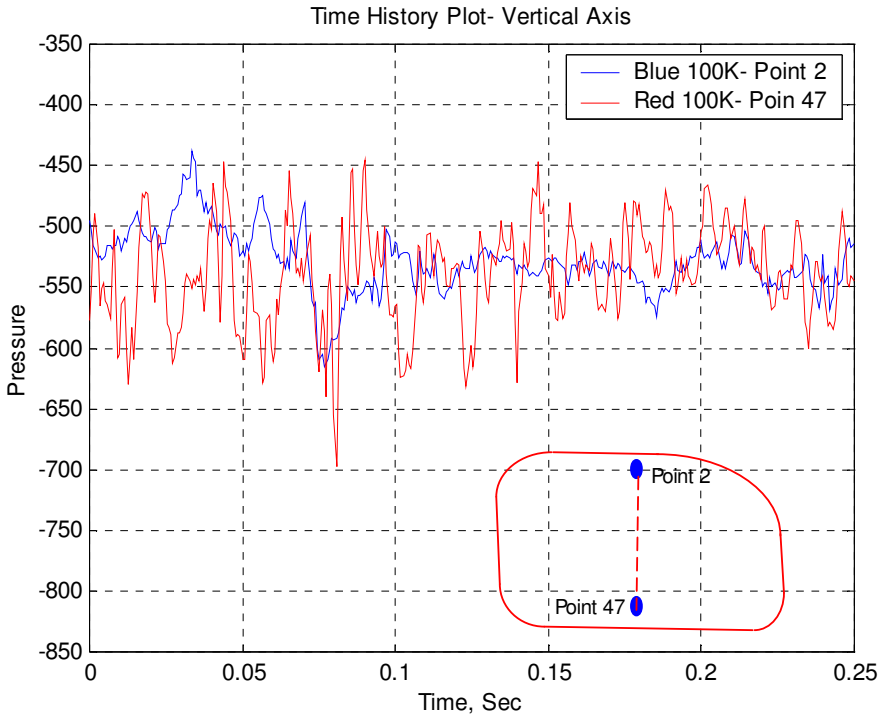

Figure 5.3: Phase angle for vertical axis

Diagonal Axis-1

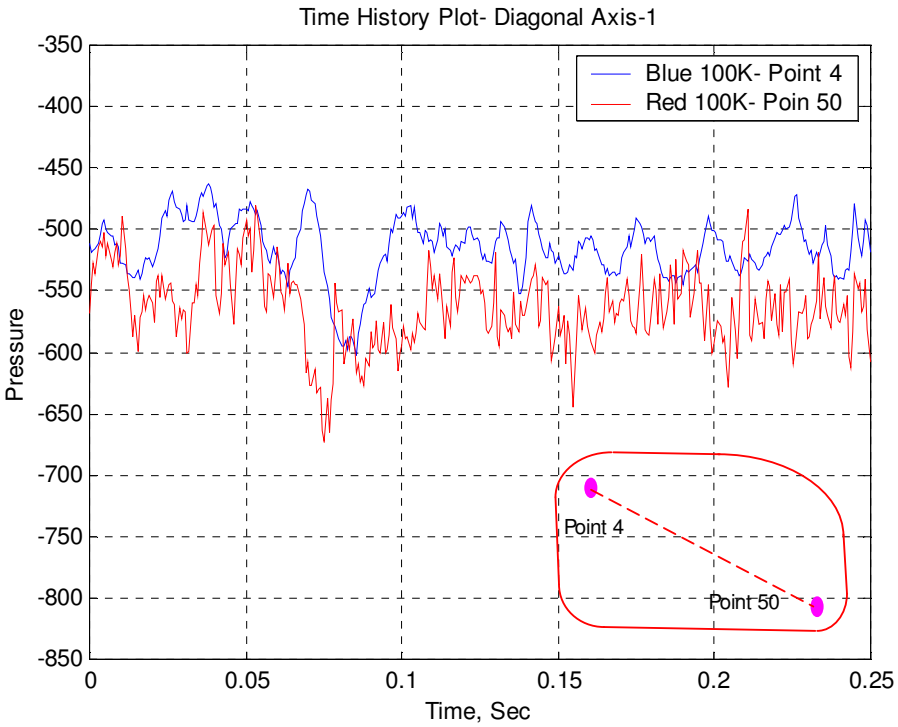

Figure 5.4: Phase angle for diagonal axis-1

Diagonal Axis-2

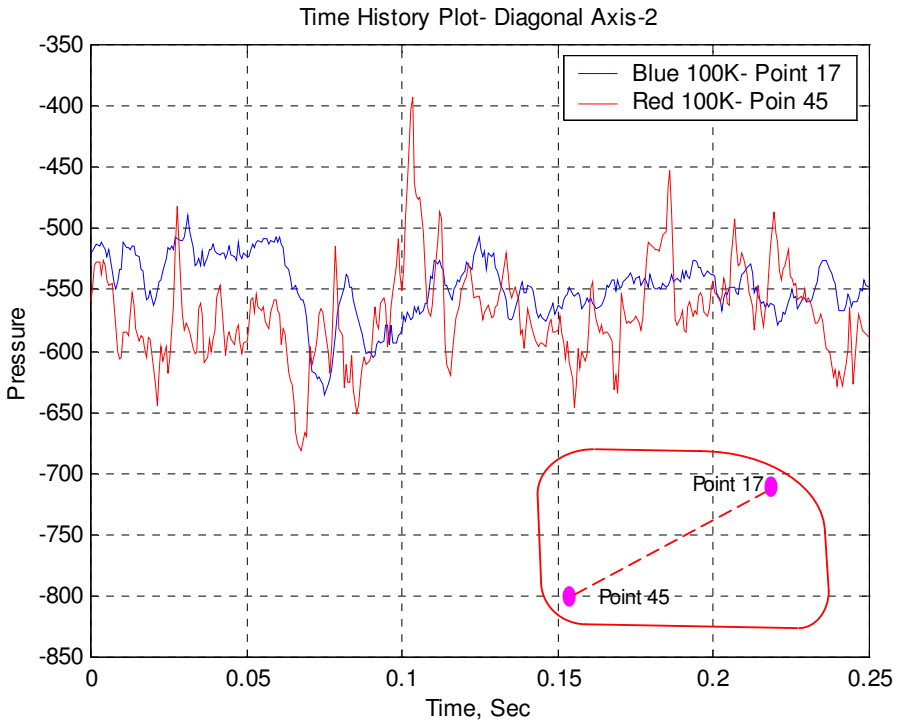

Figure 5.5: Phase angle for diagonal axis-2

24mm Shroud Horizontal Axis

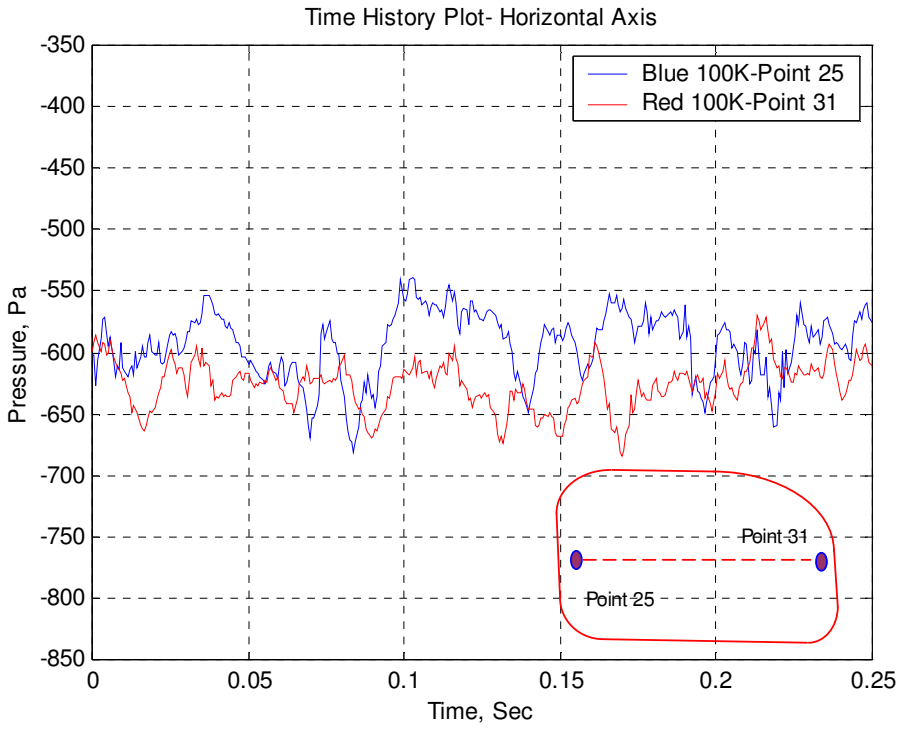

Figure 5.6: Phase angle for horizontal axis

Vertical Axis

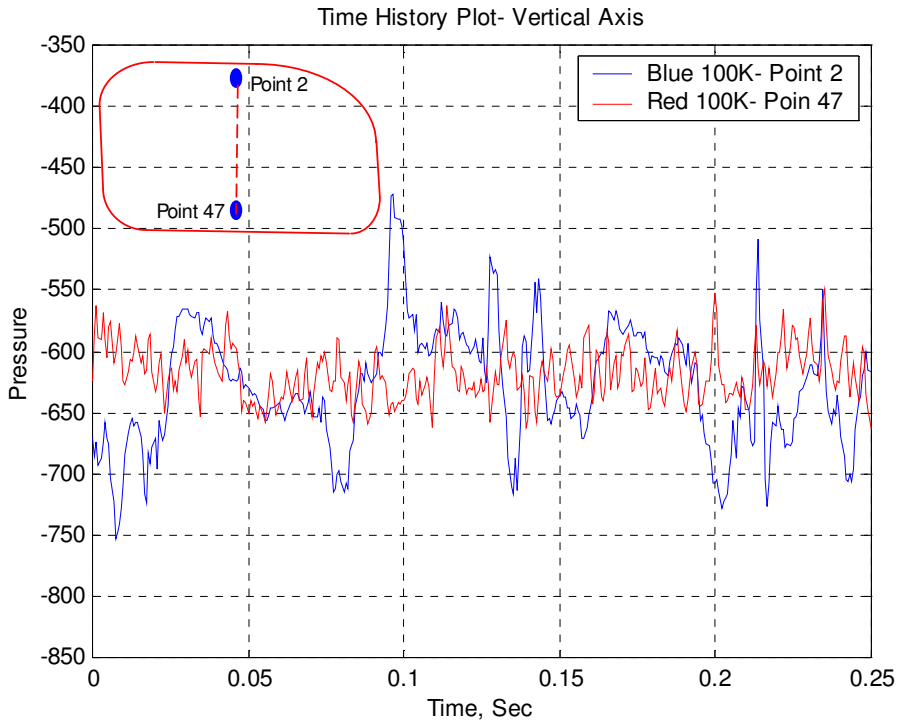

Figure 5.7: Phase angle for vertical axis

Diagonal Axis-1

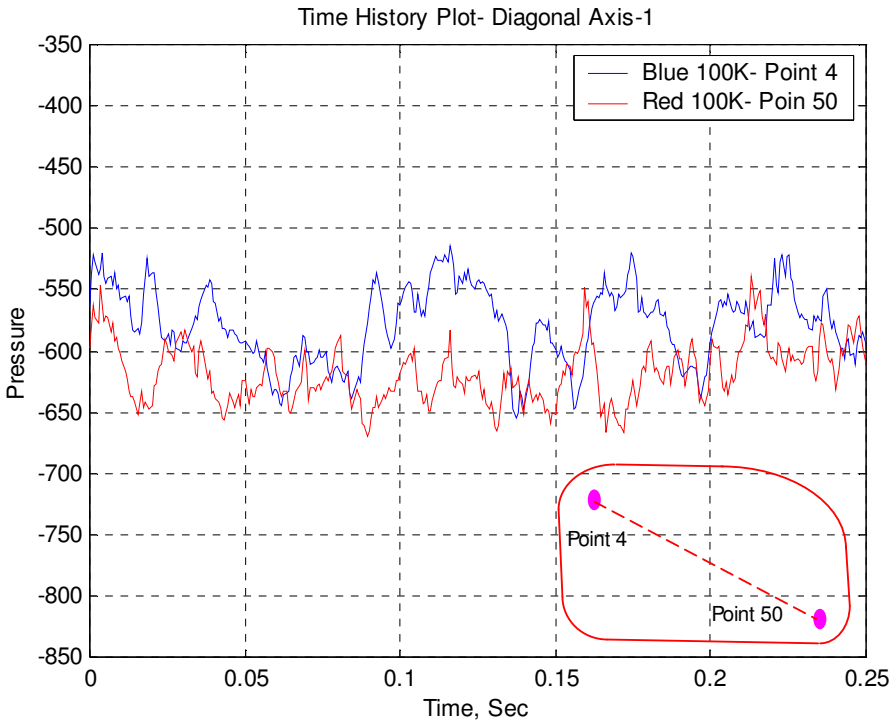

Figure 5.8: Phase angle for diagonal axis-1

Diagonal Axis-2

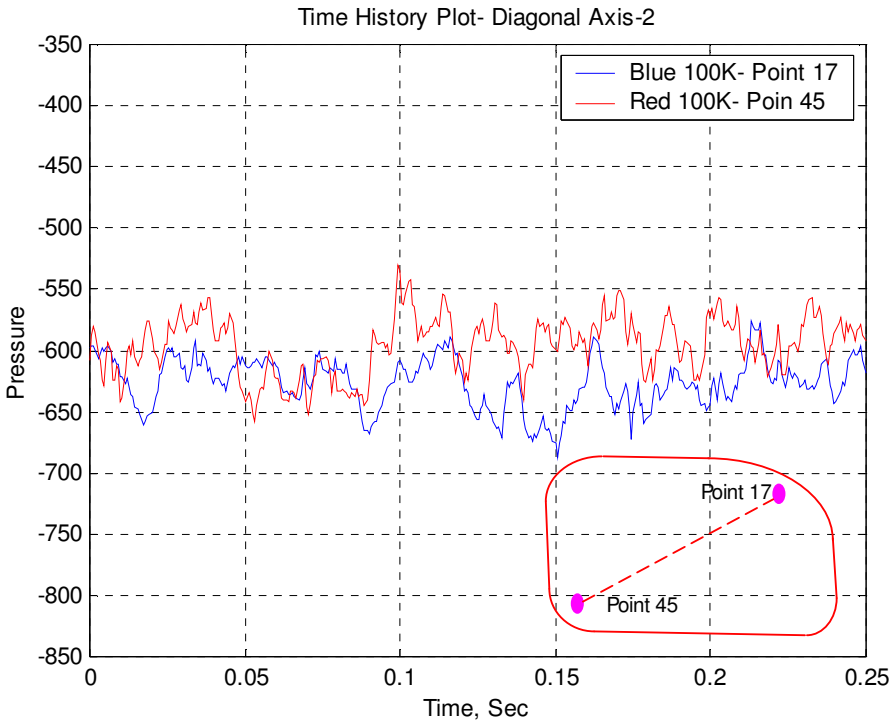

Figure 5.9: Phase angle for diagonal axis-2

34mm Shroud Horizontal Axis

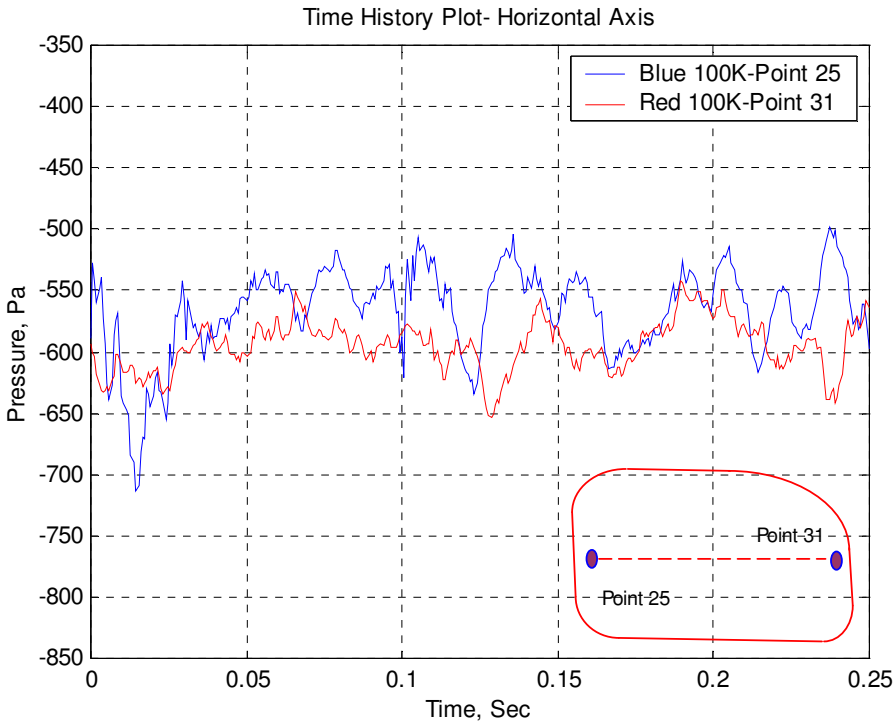

Figure 5.10: Phase angle for horizontal axis

Vertical Axis

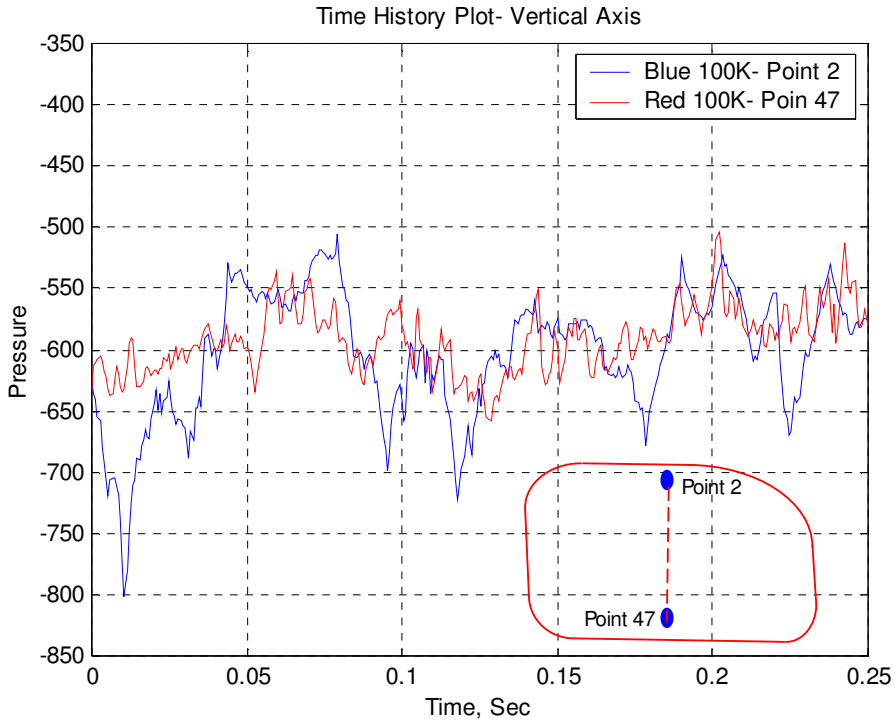

Figure 5.11: Phase angle for vertical axis

Diagonal Axis-1

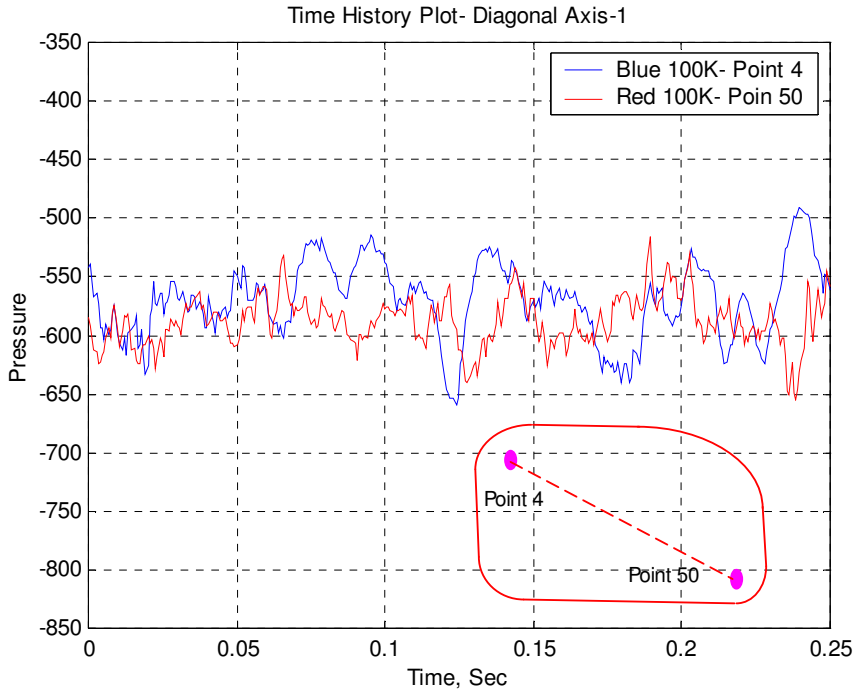

Figure 5.12: Phase angle for diagonal axis-1

Diagonal Axis-2

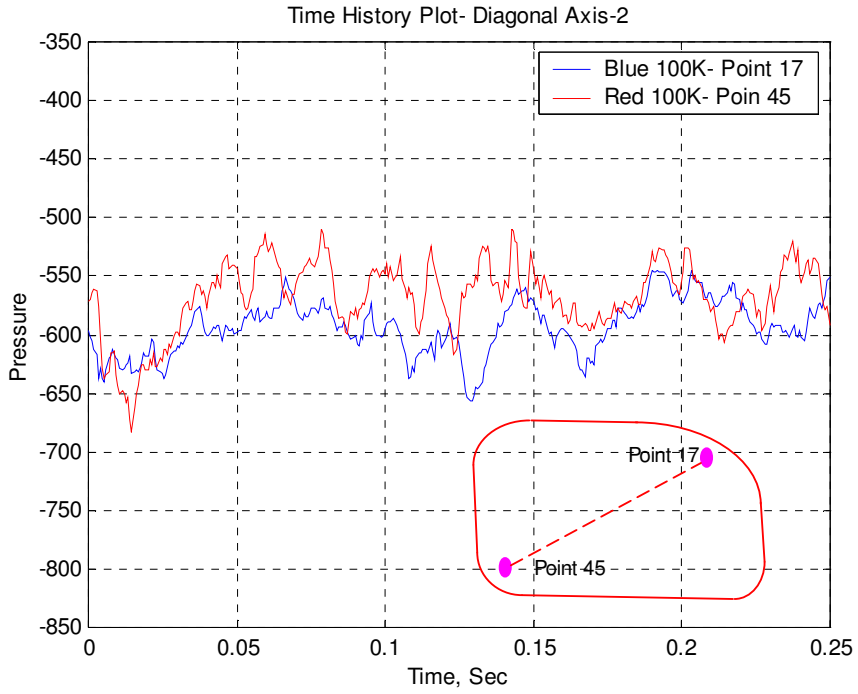

Figure 5.13: Phase angle for diagonal axis-2

44mm Shroud Horizontal Axis

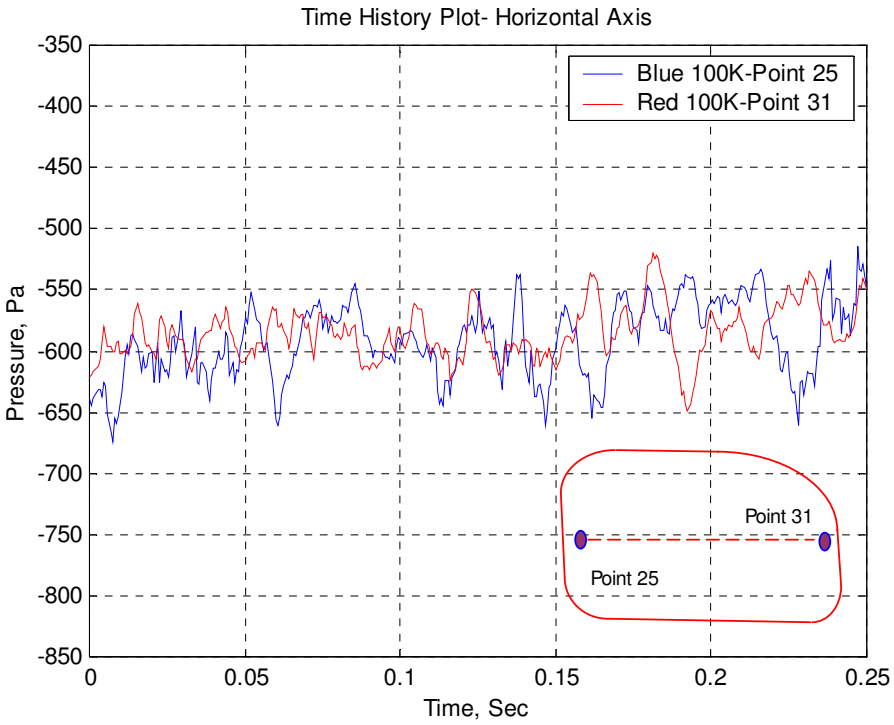

Figure 5.14: Phase angle for horizontal axis

Vertical Axis

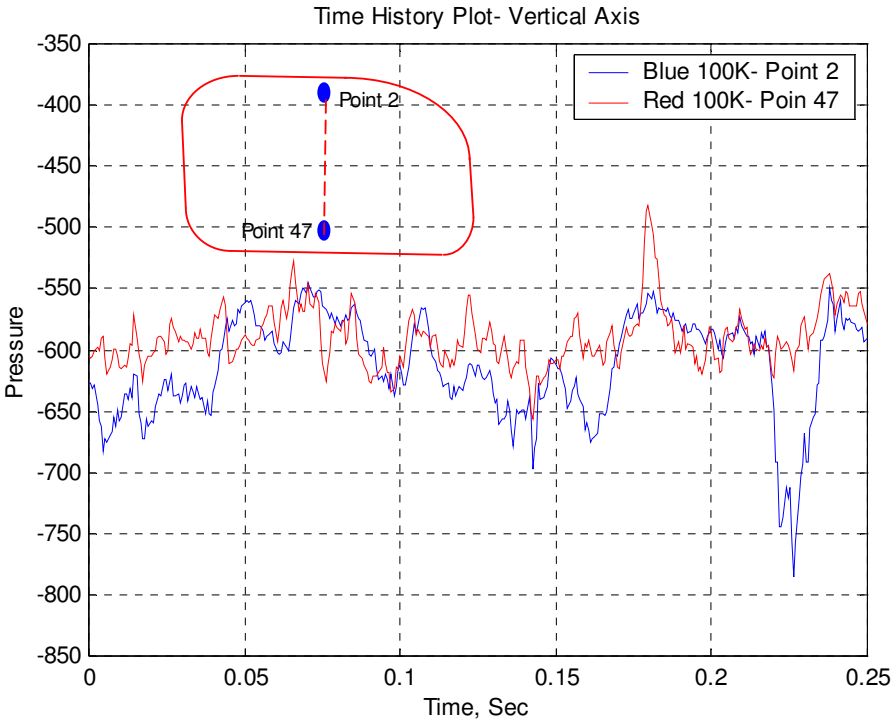

Figure 5.15: Phase angle for vertical axis

Diagonal Axis-1

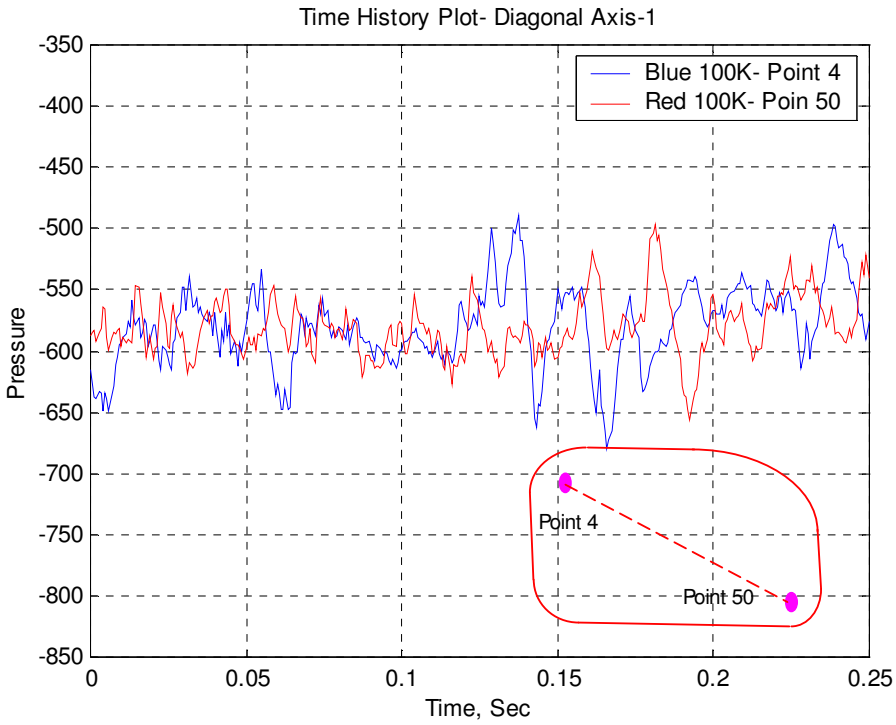

Figure 5.16: Phase angle for diagonal axis-1

Diagonal Axis-2

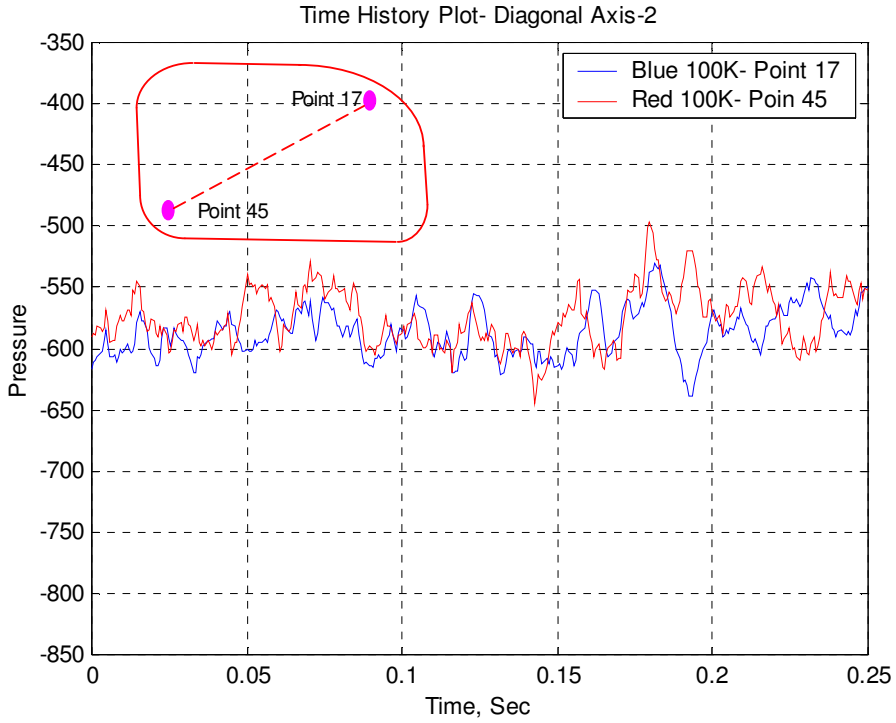

Figure 5.17: Phase angle for diagonal axis-2

Chapter 6

Conclusions

The main objective of this work was to understand the surface mean and fluctuating pressure on the rear view mirror surface of the with quarter model production car and also in semi-isolation condition. The following conclusions apply within the assumptions made in the analysis and experiments. The following conclusions were therefore drawn from this research work are presented below:

6.1 Mirrors with Quarter Model

- Fluctuating aerodynamic pressures are not uniformly distributed over an automobile mirror surface.
- The highest magnitude of fluctuating pressure (Cprms) for the standard mirror was found at the central bottom section of the mirror surface.
- The highest magnitude of fluctuating pressure (Cprms) was found at the central top section of the mirror surface for all shroud lengths. However, with an increase of shroud length, the magnitude decreases significantly. The highest reduction of fluctuating pressures was found in between 24 and 34 mm shroud length.
- At higher speeds, vibration in rear view mirror is due to the rotational motion (obtained from PSD plots) of the mirror glass. A small rotation about either its vertical or horizontal axis causes blurring of an image.

6.2 Mirrors in Semi-Isolation Model

- The highest magnitude of fluctuating pressure (Cprms) for the standard mirror was found at the bottom right section of the mirror surface.
- The highest magnitude of fluctuating pressure (Cprms) was found at the central bottom section of the mirror surface for all shroud lengths. However, with an increase of shroud

length, the magnitude decreases significantly. The highest reduction of fluctuating pressures was found in between 0 and 24 mm shroud length.

- The modification has significant effects on the magnitude of fluctuating pressures. Generally, with an increase of shrouding lengths, the magnitude of fluctuating pressures drops for the mirror in isolation case as the airflow is out of A-pillar flow influence. This trend is also noted for the mirror with quarter model except 0 to 24 mm shroud length.
- Frequency based analysis indicates that the maximum energy of the fluctuating pressure is located around 40Hz.

Chapter 7

Recommendation for further work

After completing the research work presented here and reviewing the literature, the following suggestions are made for further study:

- The effects of yaw angles also need to be considered and the testing should be conducted in a full-scale wind tunnel with a full production car model for better understanding of the airflow.
- A detailed frequency based analysis for every pressure tap is required to understand the energy characteristics of the flow paying particular attention to phase since it is the out of phase components that usually cause mirror vibration.
- Surface mean (Cp) and fluctuating pressure (Cprms) coefficients analysis should be carried out with the bottom flange modification for 34mm and 44mm shroud case for detailed analysis.
- On-road testing will provide a realistic replication of real world; however it may make the testing more complex and time consuming.
- Rear view mirror placement with respect to the A-pillar region will give more detailed information about flow. Also variation in the A-pillar height can show the better variation.
- Modifications to the A-pillar geometry and analysis of its effect on rear view mirror vibrations will further improve understanding of airflow within this region.
- Modifications to the mirror housing will further improve understanding of airflow within this region, and provide suggestions to how the turbulent wake behind the mirror housing may be reduced.
- Measuring the air speeds closer to the rear view mirror, for both on-road and wind tunnel testing, will provide a more accurate analysis of how the changes in airflow affect rear view mirror vibrations.

References/Bibliography

- Alam, F., "The Effects of Car A-pillar and Windshield Geometry on Local Flow and Noise", Ph.D. Thesis, Department of Mechanical and Manufacturing Engineering, RMIT University, Melbourne, Australia, 2000.
- Arter, N. H., "Aerodynamically Induced Vibration of Automotive External Rear View Mirror", 4th year thesis, RMIT University, 1999.
- Bannister, M., "Drag and Dirt Deposition Mechanisms of External Rear View Mirrors and Techniques Used for Optimisation", SAE Paper No. 2000-01-0486, also in SP- 1524, SAE World Congress, March, Detroit, USA, 2000.
- Buresti, G., " Bluff Body Aerodynamics", University of Pisa, Italy, June 2000
- Chi-Hao. "An Investigation into the Vibrational Characteristics of Automotive Rear View Mirror", 4th. Year Thesis, RMIT University, Melbourne, Australia, 2003.
- Gerrad, J.H., " the mechanics of the formation region of vortices behind bluff bodies", Journal of Fluid Mechanics, Vol.l25, pp 401-413, 1966.
- Hamel, T. A. and Ahuja, K. K., "Wind Noise Measurements on an Automobile Side Glass with A-Pillars of Different Height", AIAA Journal, 1996
- Haruna, S., Nouzawa, T. & Kamimoto, I., 'An Experimental Analysis and Estimation of Aerodynamic Noise Using a Production Vehicle', Society of Automotive Engineering International (SAE) Technical Paper, No.900316, 1990.
- Heisler H. " Advanced Vehicle Technology" – Second Edition, 2002
- Hucho, W. H., "Aerodynamics of Road Vehicles: From Fluid Mechanics to Vehicle Engineering", 4th edn. Society of Automotive Engineers, USA, 1998.
- Jaitlee, R., Alam. F., and Watkins. S., "Pressure Measurements on an Automobile Side Rear View Mirror" 15th Australasian Fluid Mechanics Conference, The University of Sydney, Sydney, Australia, 13-17 December 2004.
- Jaitlee. R., Alam. F., and Watkins. S., "Vibration of Automobile Side View Mirror Due to Aerodynamic Inputs" 6th International Conference on Mechanical Engineering (ICME2005), Dhaka, Bangladesh, December 2005.

- Joachim H and Clausen S., "The Visibility Distance of a Car-Driver in Driving Situation" Society of Automobile Engineers SAE 82041, 1982.
- Kosnar, D., **"**Vibration to Automotive External Rear view Mirrors**"**, 4th. Year Thesis, RMIT University, Melbourne, Australia, 1999.
- Kulikowski J. "What Really Limits Vision? Conceptual Limitations to the Assessment of Visual Function and the Role of Interacting Channels" - Vision and Visual Dysfunction, Macmillan Press, USA, vol 5 pp 286-323, 1991.
- Lee, A., "Wing Mirror Vibration" 4th year thesis, RMIT University, 1998.
- Mourant R.R., Donohue R. J., "Mirror Sampling Characteristics of Drivers" - Society of Automotive Engineers SAE 740964, 1974.
- Nagata M. and Kuriyama H., "Drivers Visual Behaviour with Door and Fender Mirror Systems" - Society of Automotive Engineers SAE 850330, 1985.
- Narain. M., and Homsi E., "Vibration Control of Body-Mounted Plastic Mirror Design", SAE Paper No. 982312, 1998.
- Norton, M. P., "Fundamentals of Noise and Vibration Analysis for Engineers", Cambridge University Pres, Cambridge,U.K., 1989.
- Popat, B.C., "Study of Flow and Noise Generation from A-pillar", PhD Thesis, Department of Aeronautics, Imperial College of Science, Technology and Medicine, The University of London, U.K,1991.
- PSI Plot software online http://www.polysoftware.com/plot.htm
- SAE 1995, 'Vision Factors Considerations in Rear-view Mirror Design', Society of Automotive Engineering International (SAE) Technical Paper, No.J985 JUN95, 1995
- SAE Driver Vision Standards Committee, Vision Factors Considerations In Rear-view Mirror Design, Society of Automotive Engineers (SAE) Technical Paper, SAE J985, December, 2002.
- Smith and Gulick , "Visual Contours and Movement Perception", 1956.
- Watanabe, M., Harita, M., and Hayashi, E. The Effect of Body Shapes on Wind Noise', Society of Automotive Engineering International (SAE) Technical Paper, No.780266, 1978.

- Watkins, S. & Oswald, G., 'The Flow Field of Automobile Add-ons – with Particular Reference to the Vibration of External Mirrors', Journal of Wind Engineering and Industrial Aerodynamics, Vol.83, pp541-554, 1999.
- Watkins, S., "On The Causes of Image Blurring in External Rear View Mirrors", SAE Papers 2004-01-1309, SP- 1874, Detroit, Michigan, USA, 2004.
- Watkins, S., Oswald, G. and Czedel, R., "Aerodynamically Induced Noise and Vibration of Automobile Add-Ons- External Mirrors, Aerials and Roofracks", The 9th International Pacific Conference on Automotive Engineers, Bali, Indonesia, 1997.
- White F., "Fluid Mechanics", 2003
- Yunus A. C. and Robert H.T., "Fundamental of Theral – Fluid Sciences", 2001.

Appendix A

Quarter Model Results

Standard Mirror

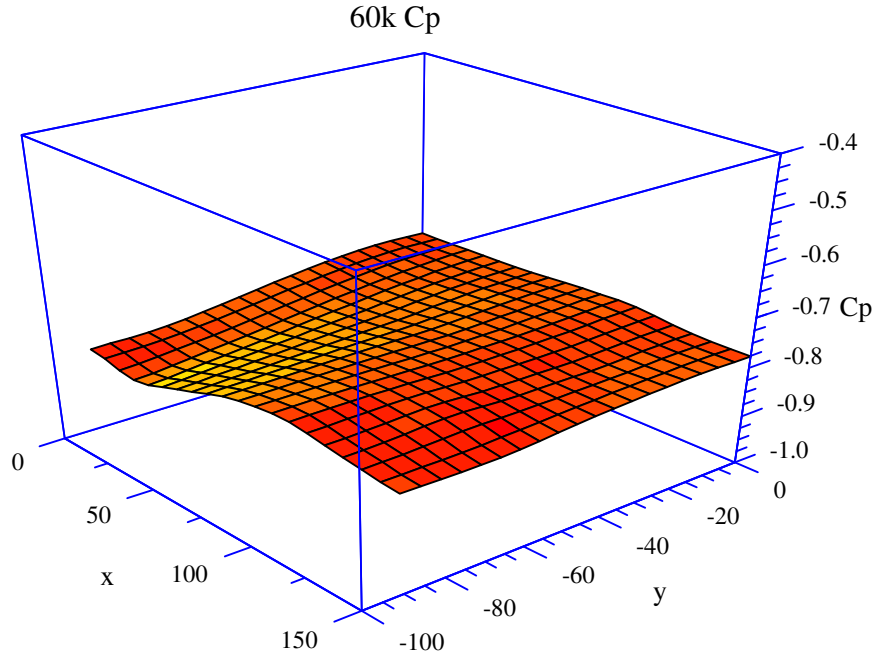

Figure A1: Surface Pressure Coefficients (Cp) - 3D- 60 km/h

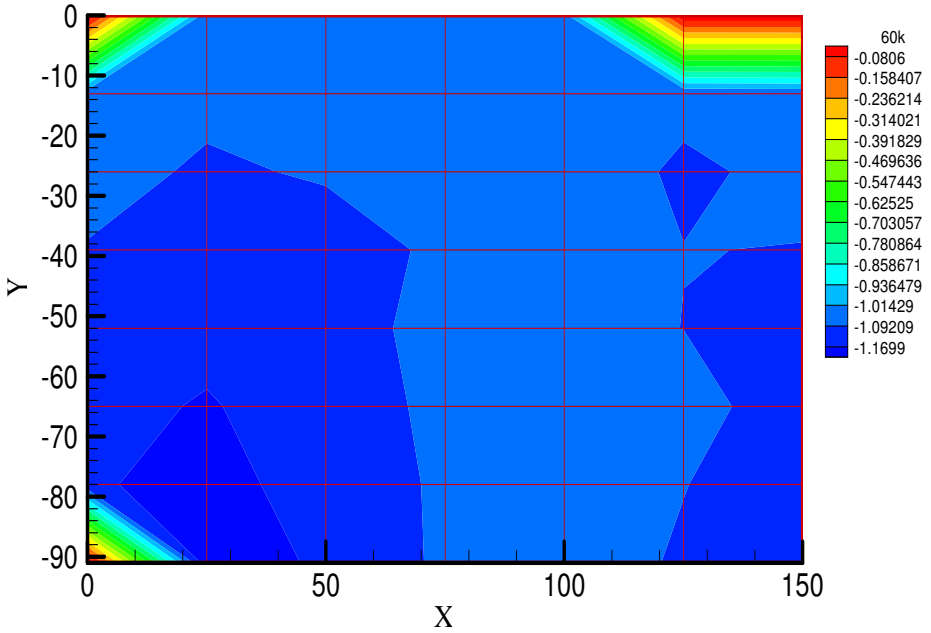

Figure A2: Surface Pressure Coefficients (Cp) - Contours - 60 km/h

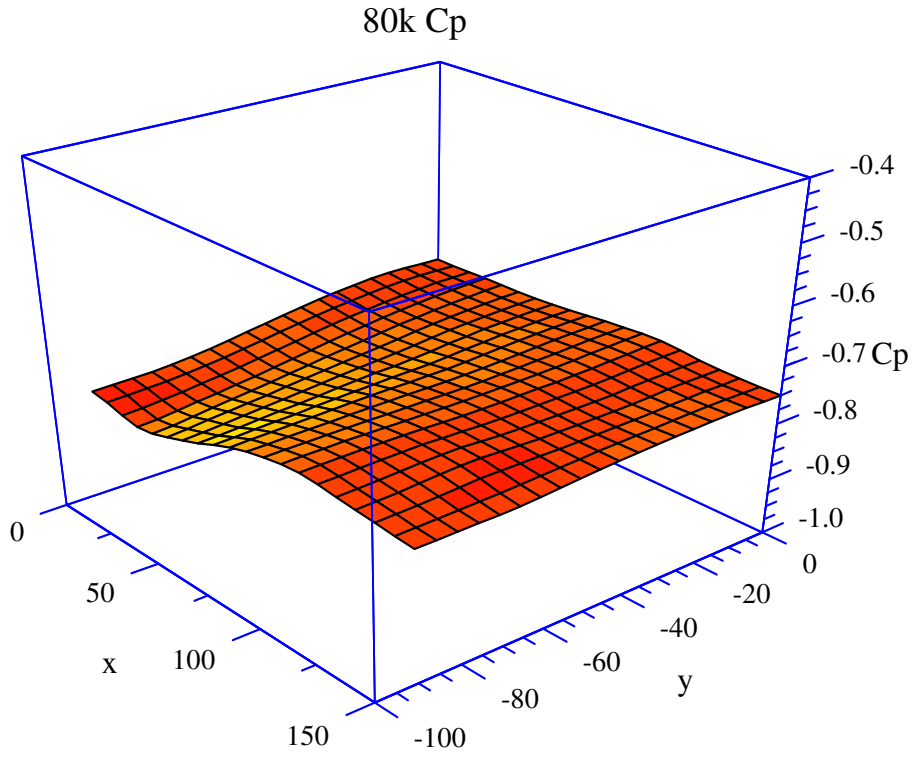

Figure A3: Surface Pressure Coefficients (Cp) - 3D-80 km/h

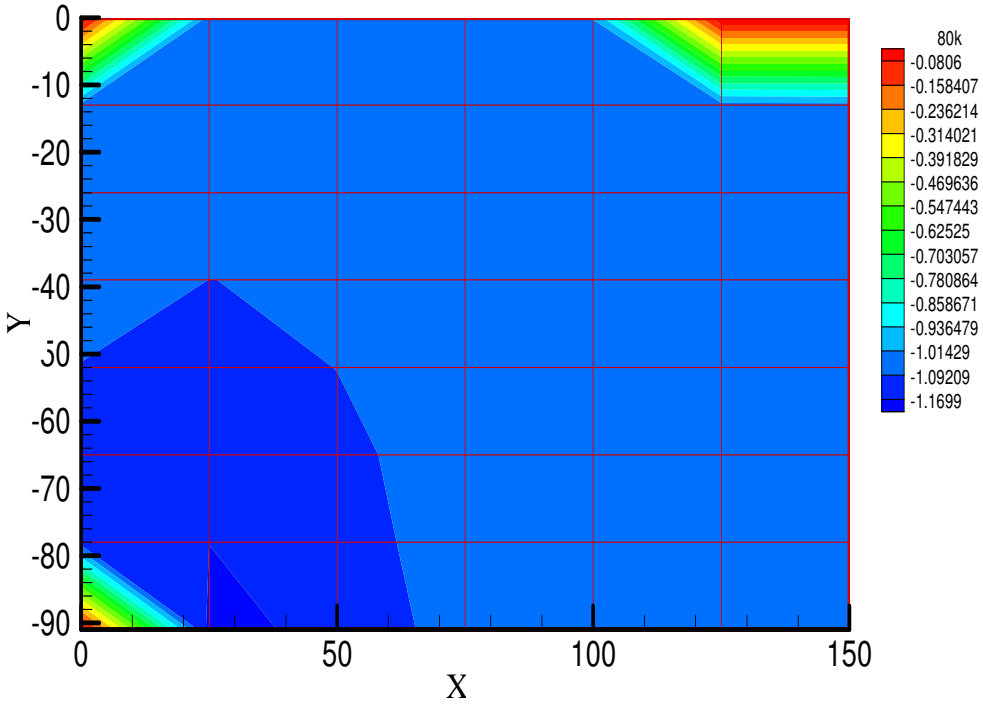

Figure A4: Surface Pressure Coefficients (Cp) - 3D-80 km/h

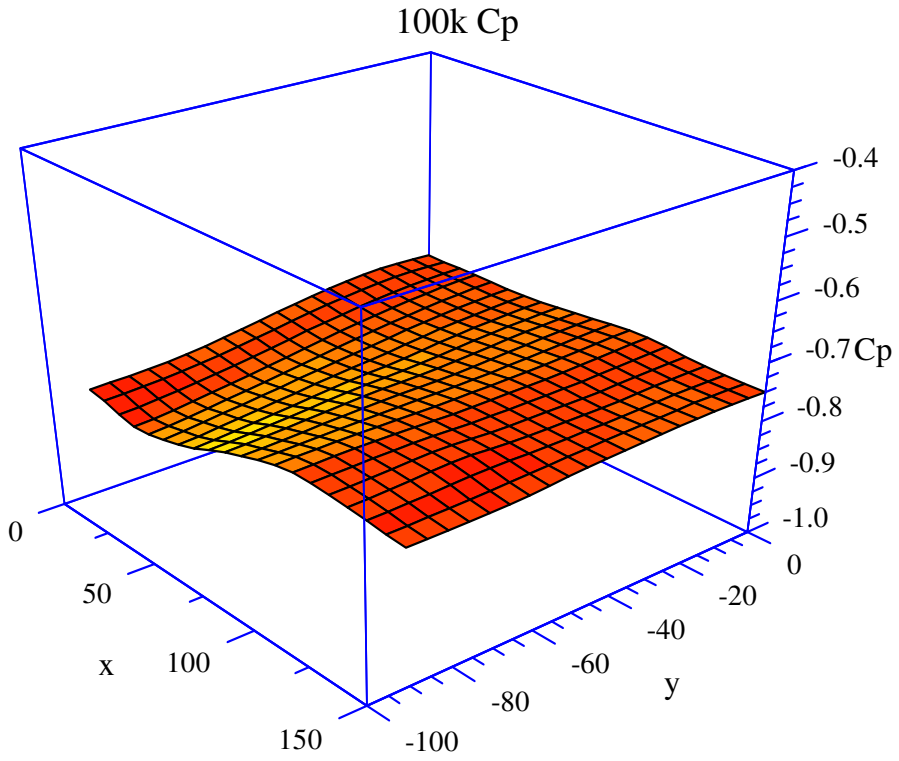

Figure A5: Surface Pressure Coefficients (Cp) - 3D-100 km/h

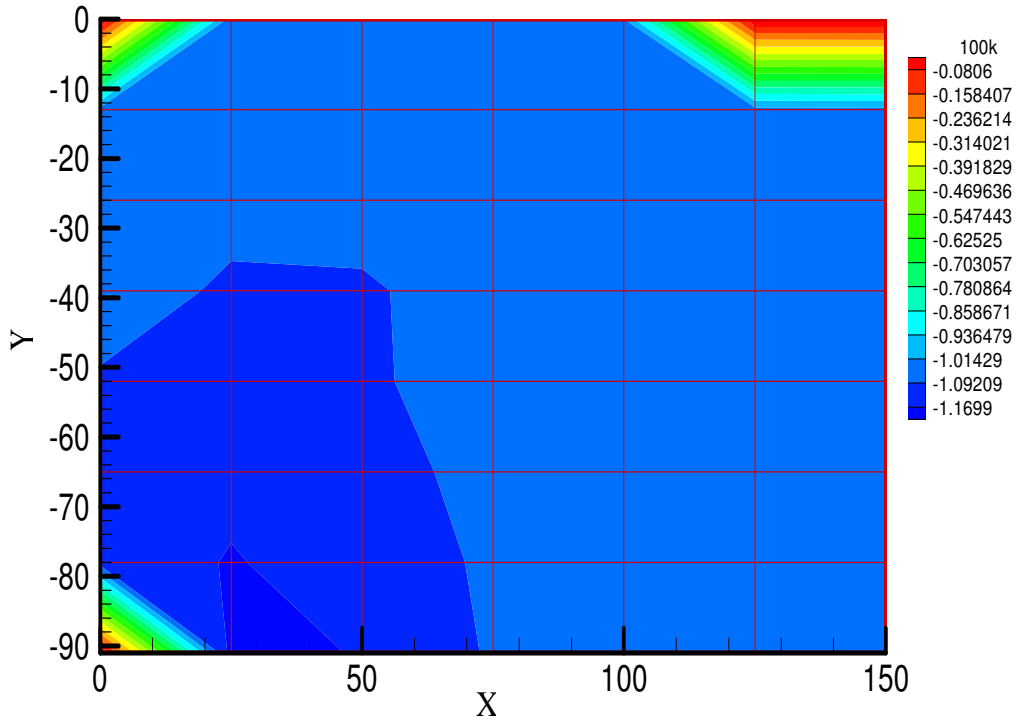

Figure A6: Surface Pressure Coefficients (Cp) - Contours -100 km/h

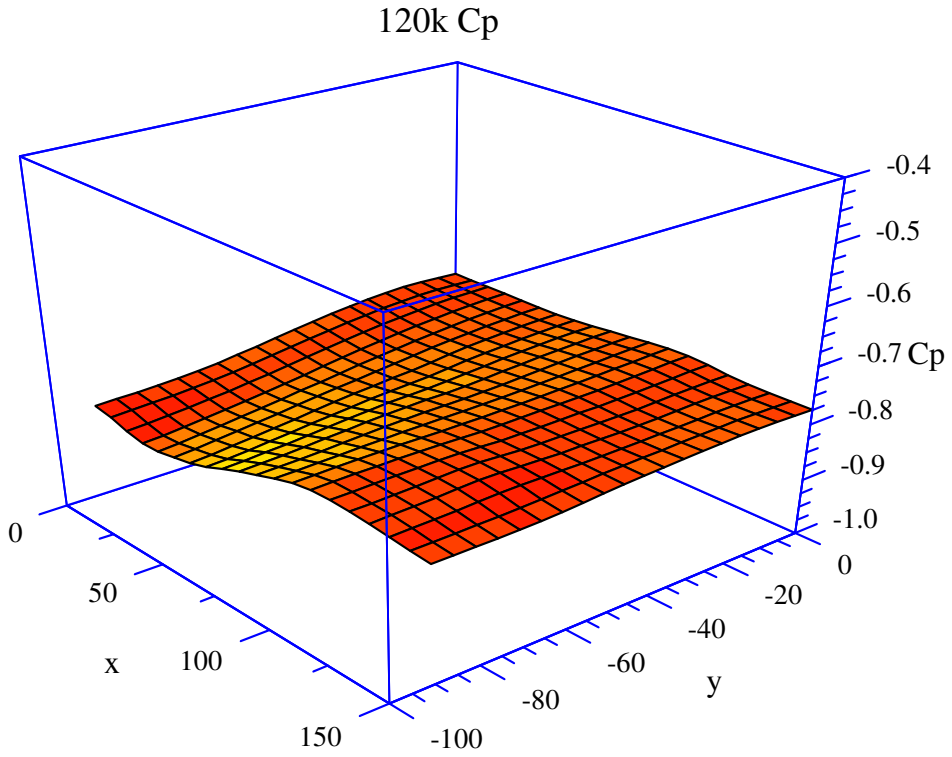

Figure A7: Surface Pressure Coefficients (Cp) - 3D-120 km/h

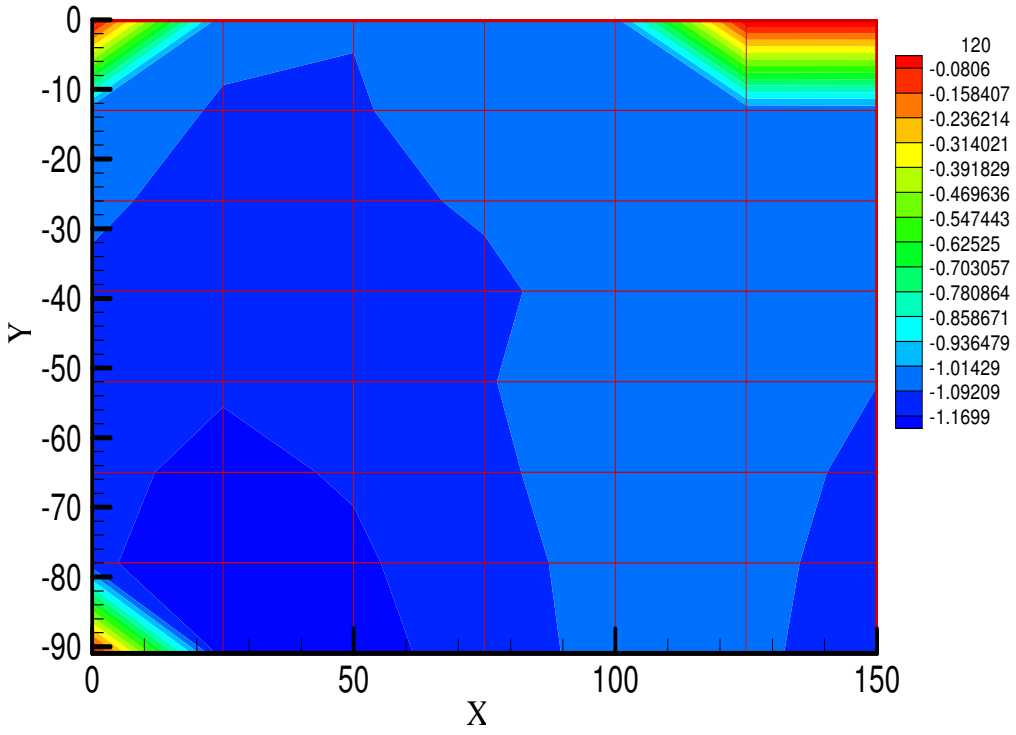

Figure A8: Surface Pressure Coefficients (Cp) - Contours - 120 km/h

24 mm Shroud

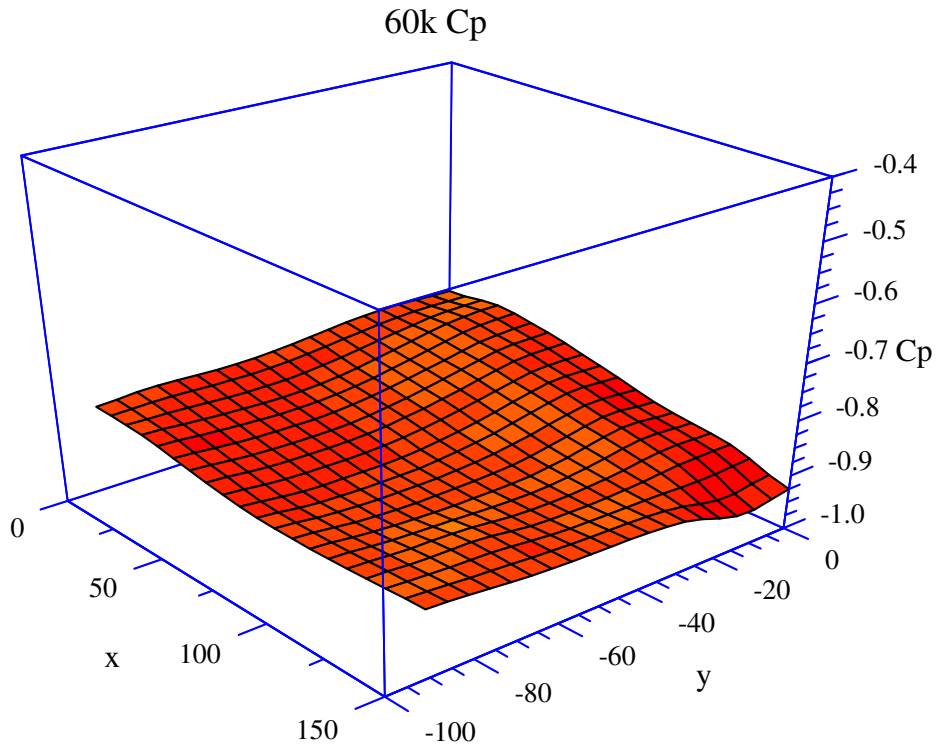

Figure A9: Surface Pressure Coefficients (Cp) - 3D- 60 km/h

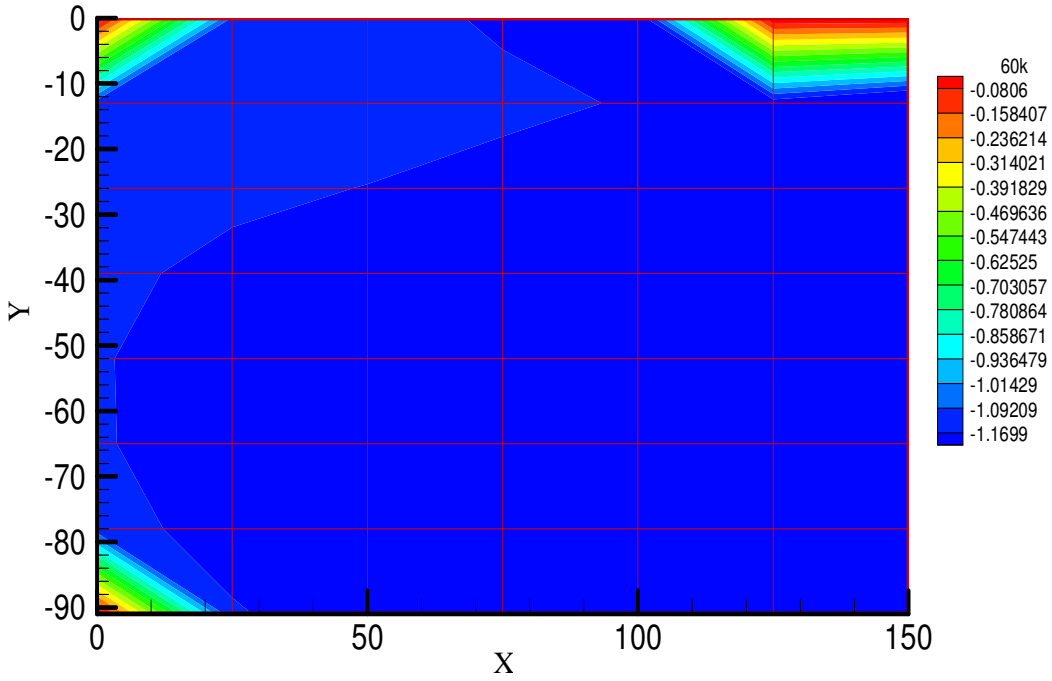

Figure A10: Surface Pressure Coefficients (Cp) - Contours - 60 km/h

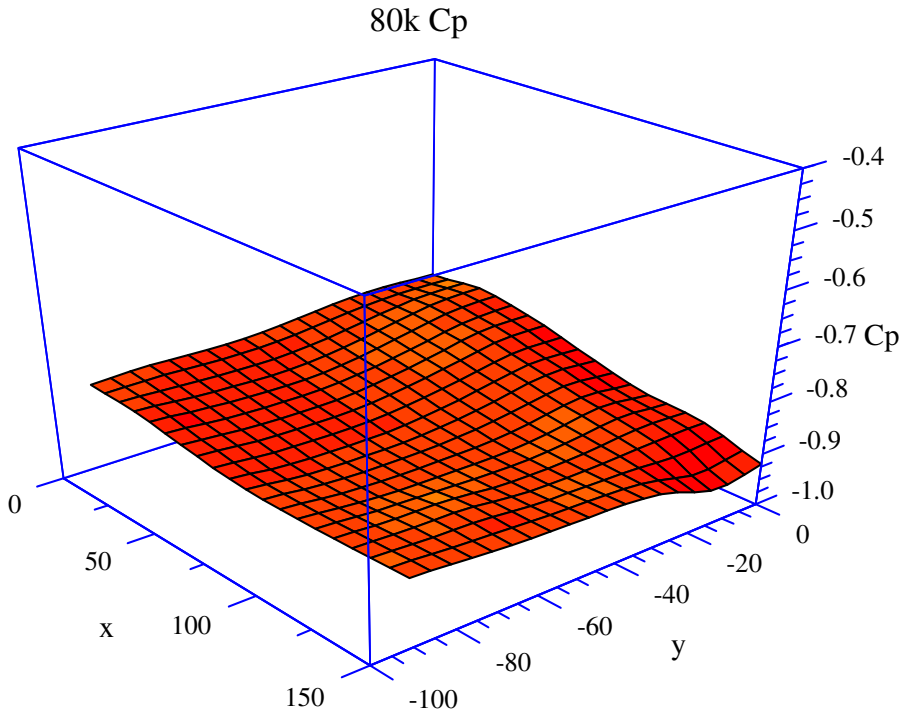

Figure A11: Surface Pressure Coefficients (Cp) - 3D- 80 km/h

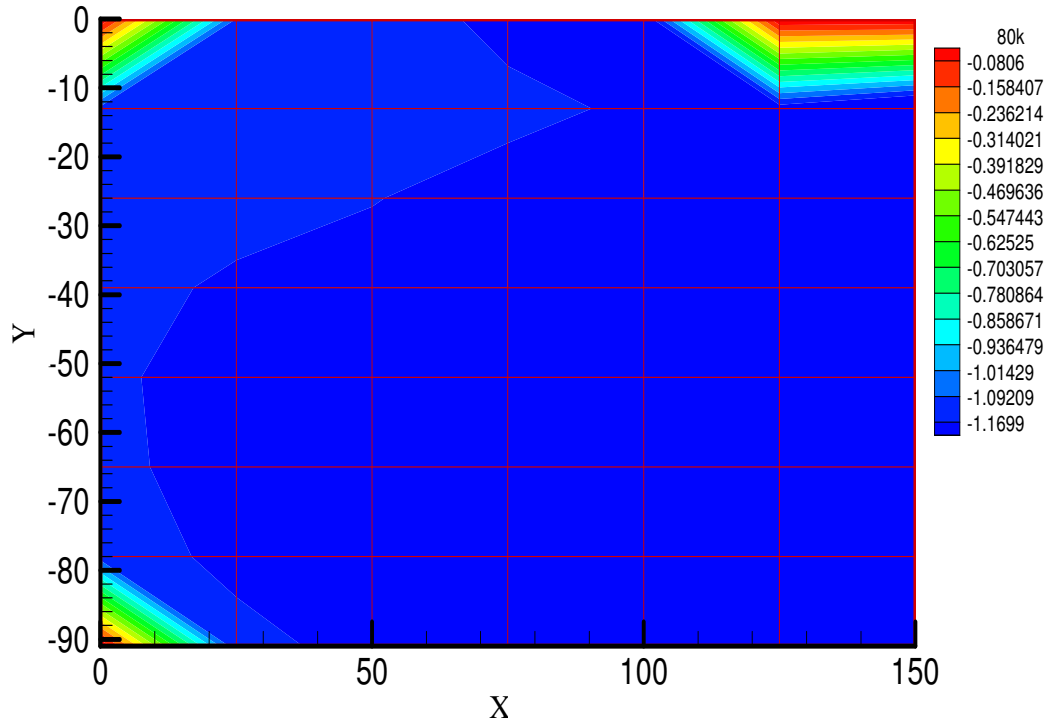

Figure A12: Surface Pressure Coefficients (Cp) - Contours -80 km/h

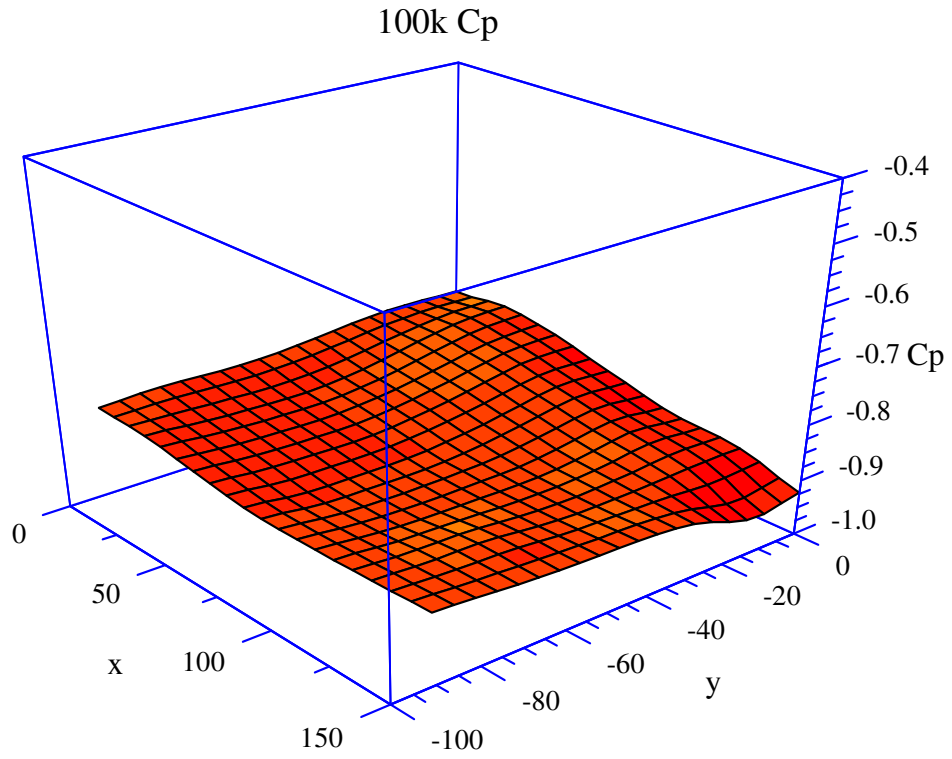

Figure A13: Surface Pressure Coefficients (Cp) - 3D-100 km/h

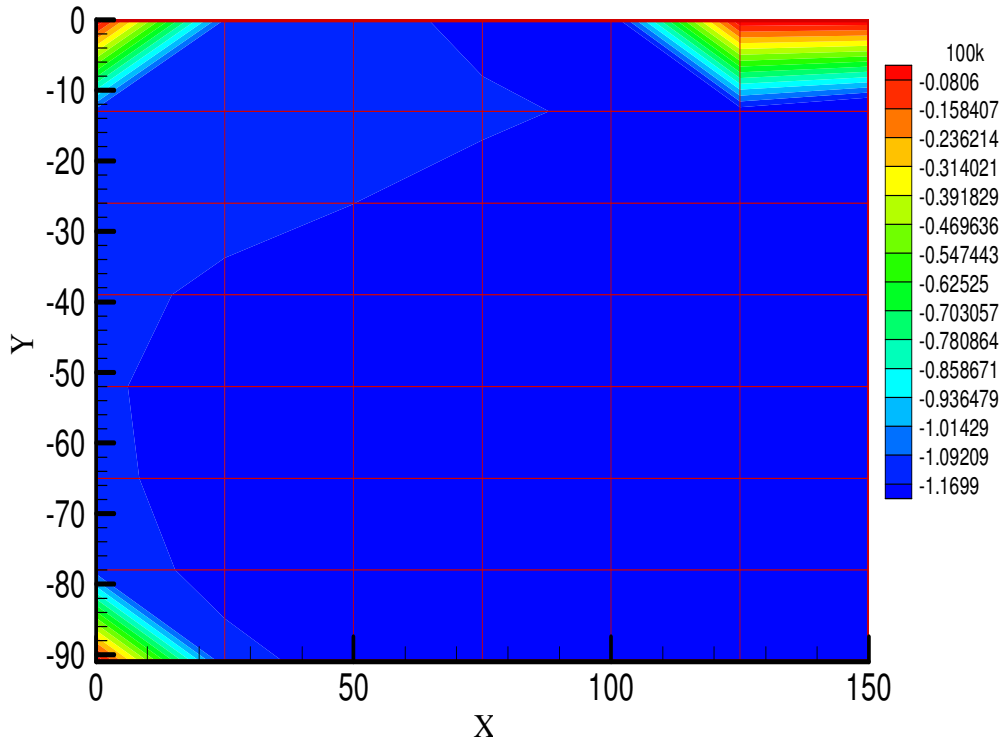

Figure A14: Surface Pressure Coefficients (Cp) - Contours - 100 km/h

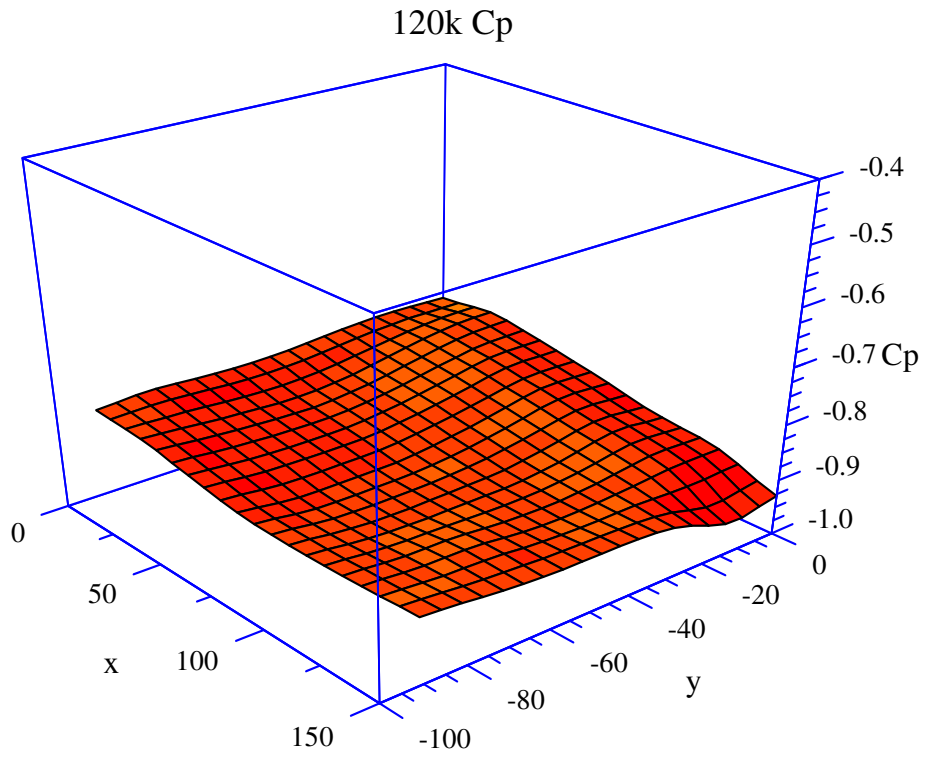

Figure A15: Surface Pressure Coefficients (Cp) - 3D-120 km/h

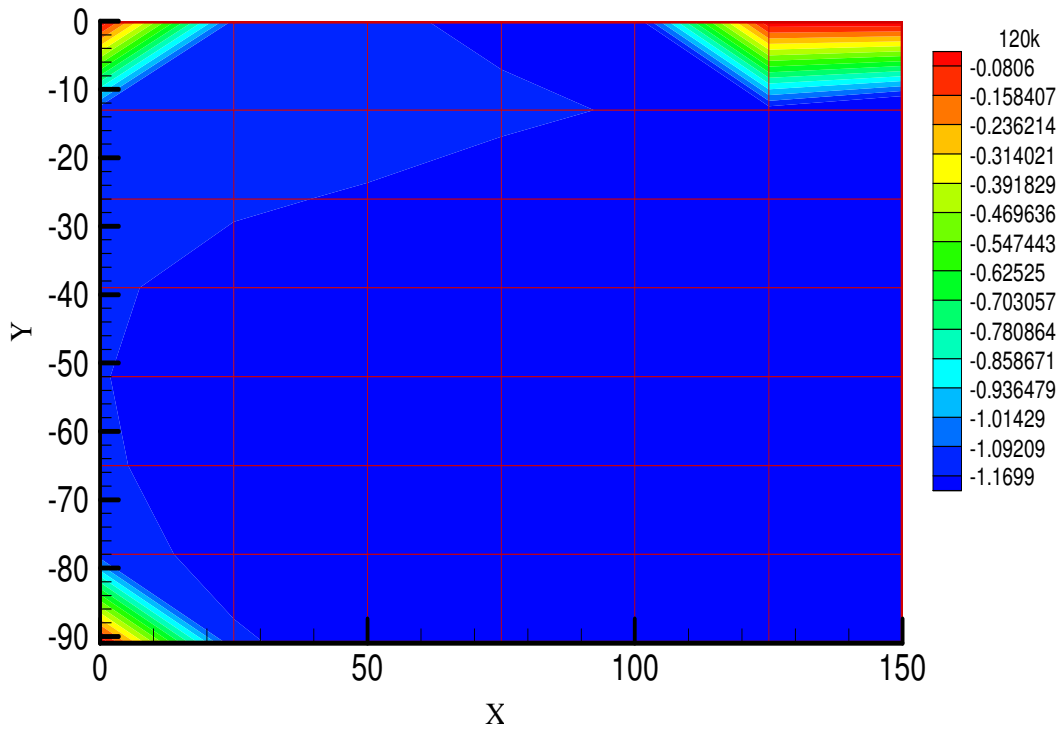

Figure A16: Surface Pressure Coefficients (Cp) - Contours -120 km/h

34mm Shroud

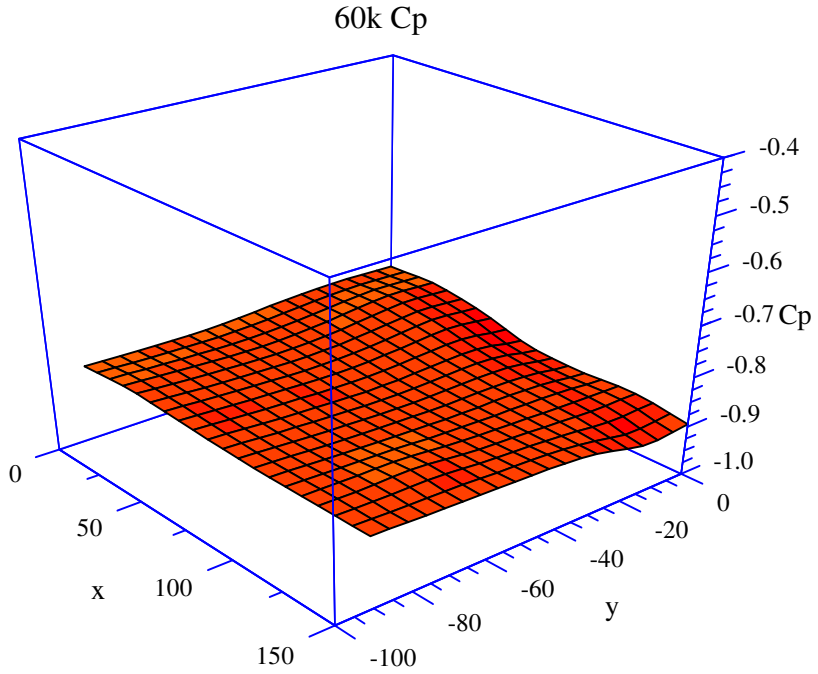

Figure A17: Surface Pressure Coefficients (Cp) - 3D- 60 km/h

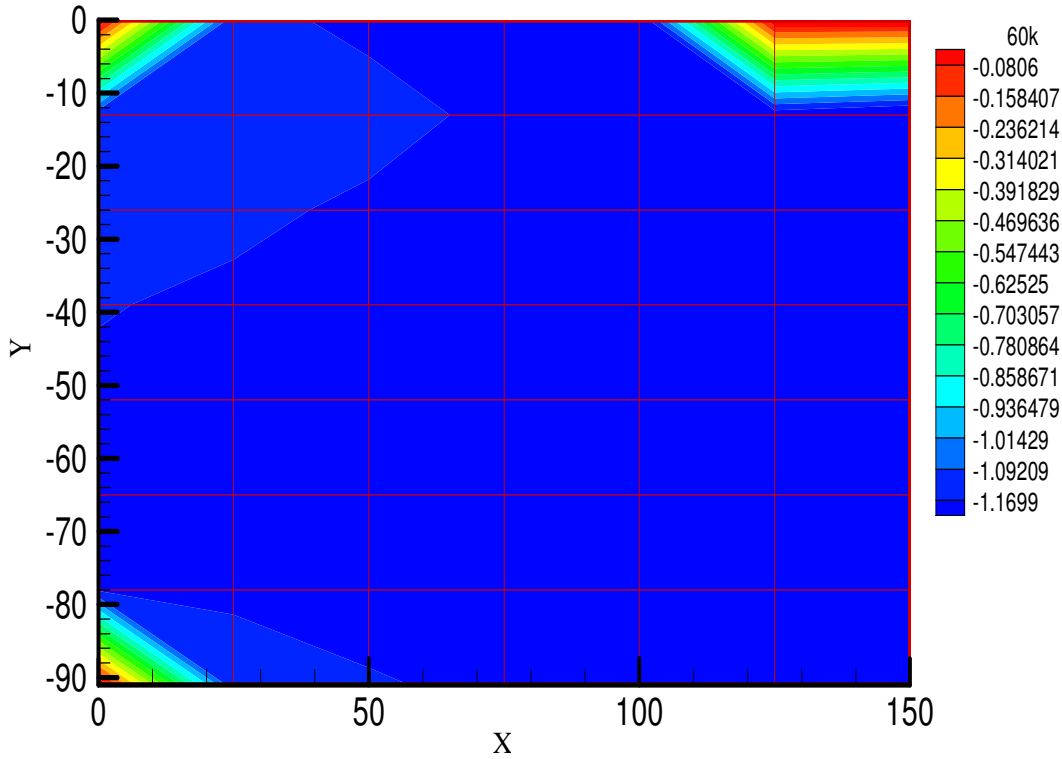

Figure A18: Surface Pressure Coefficients (Cp) - Contours - 60 km/h

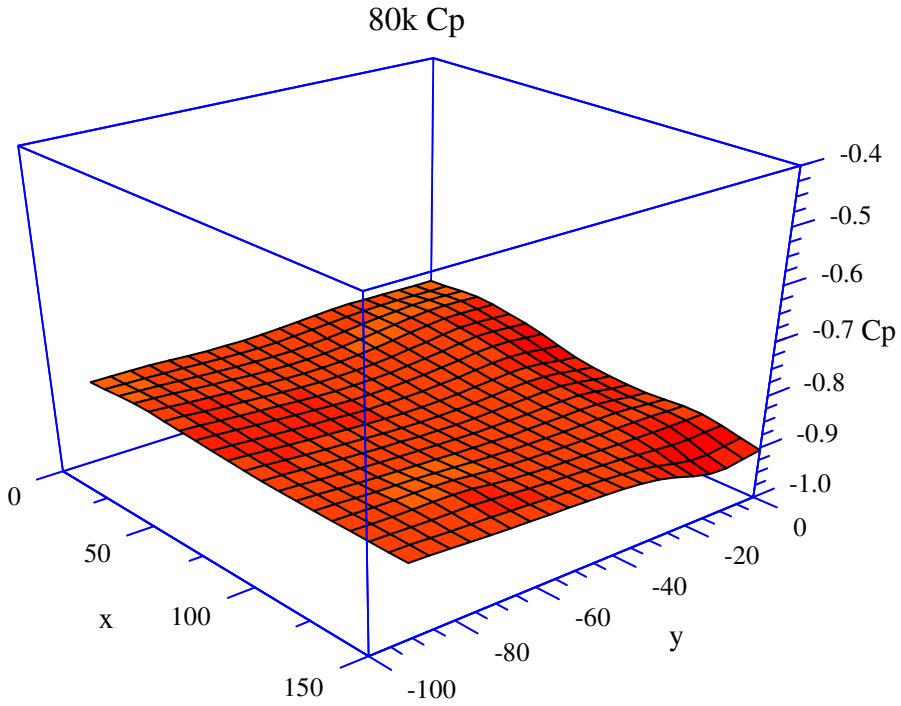

Figure A19: Surface Pressure Coefficients (Cp) - 3D- 80 km/h

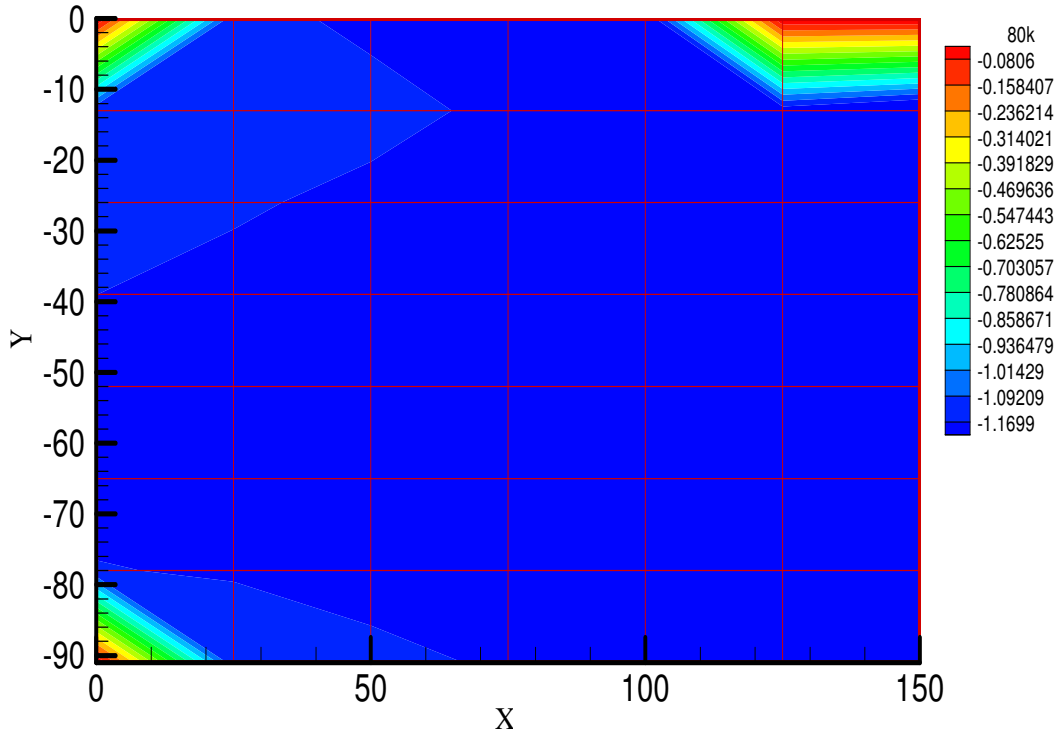

Figure A20: Surface Pressure Coefficients (Cp) - Contours - 80 km/h

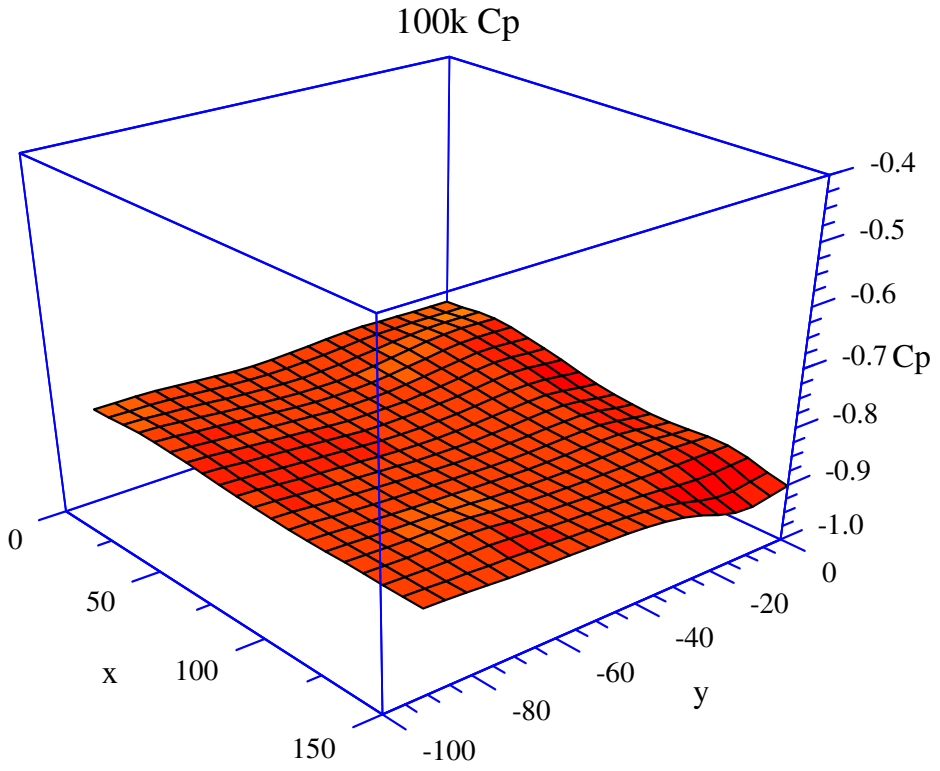

Figure A21: Surface Pressure Coefficients (Cp) - 3D-100 km/h

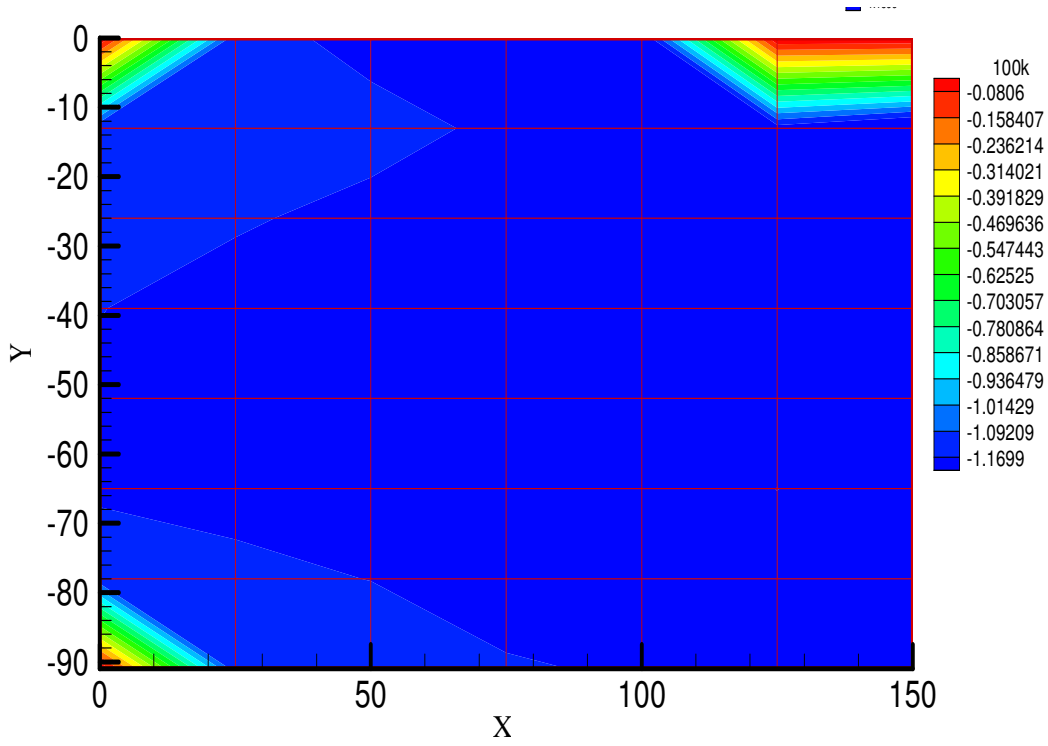

Figure A22: Surface Pressure Coefficients (Cp) - Contours - 100 km/h

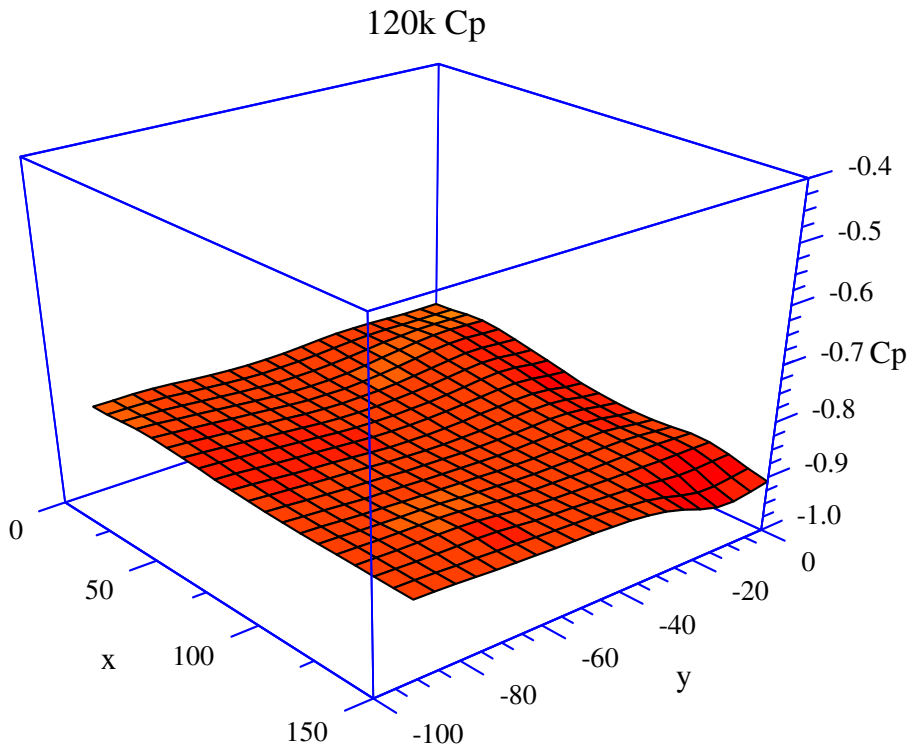

Figure A23: Surface Pressure Coefficients (Cp) - 3D-120 km/h

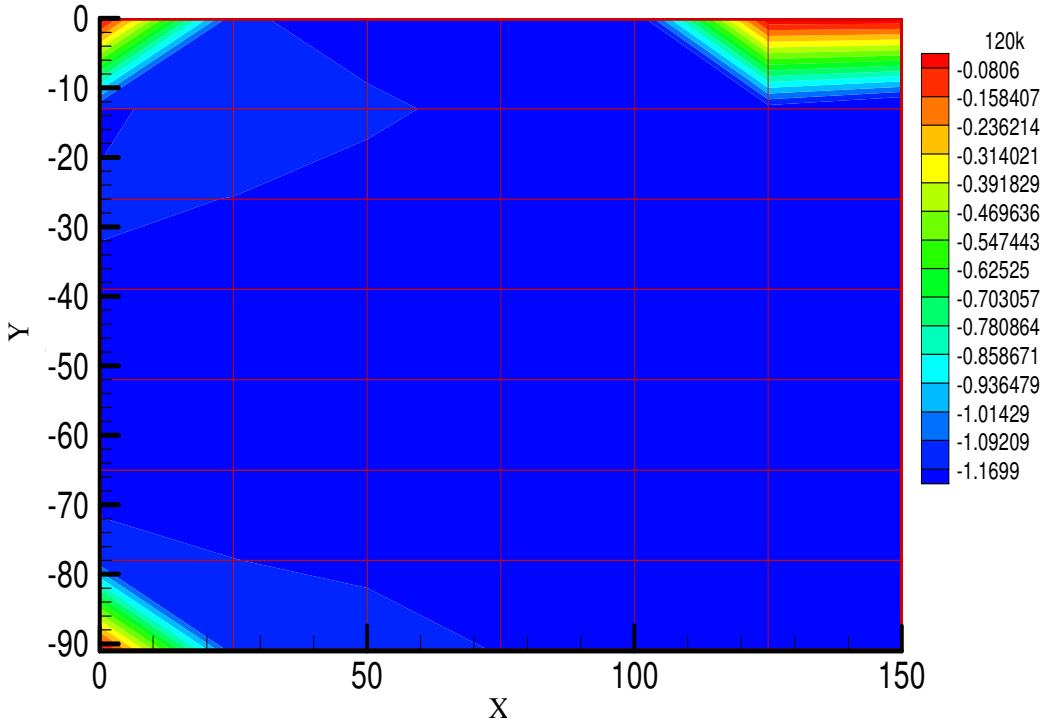

Figure A24: Surface Pressure Coefficients (Cp) - Contours -120 km/h

44mm Shroud

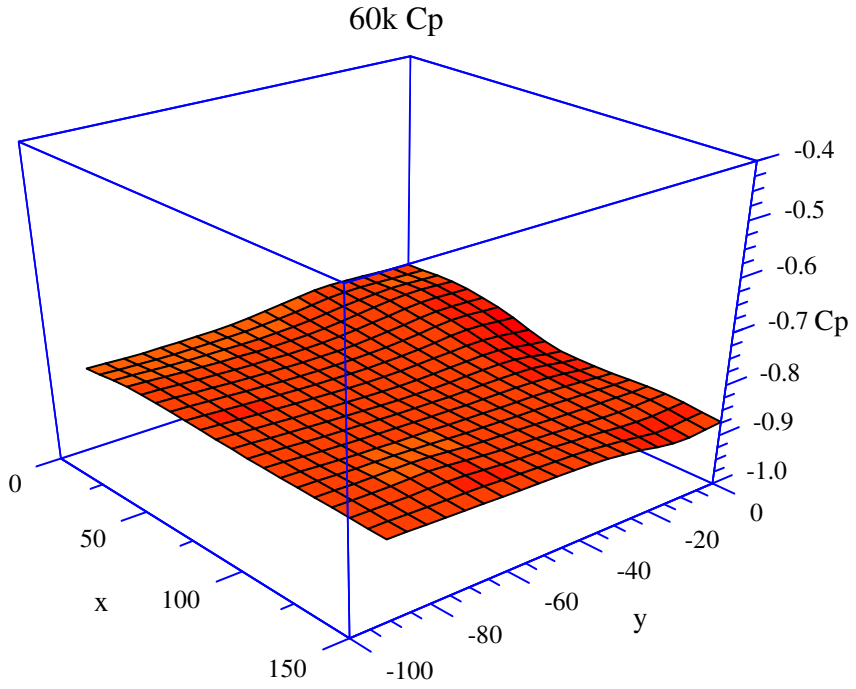

Figure A25: Surface Pressure Coefficients (Cp) - 3D- 60 km/h

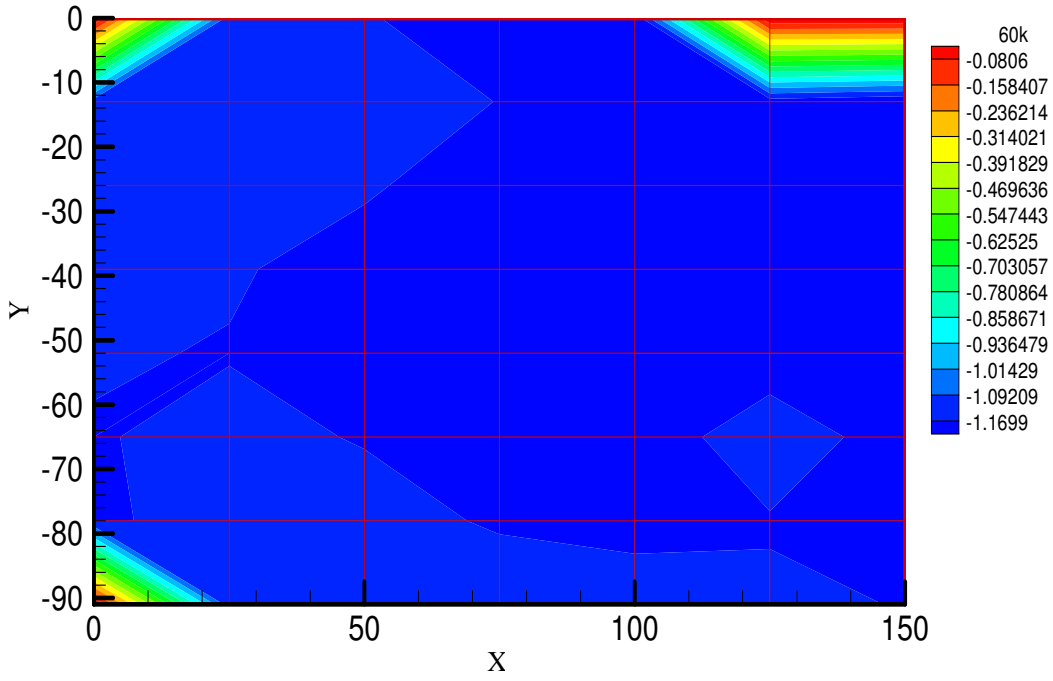

Figure A26: Surface Pressure Coefficients (Cp) - Contours - 60 km/h

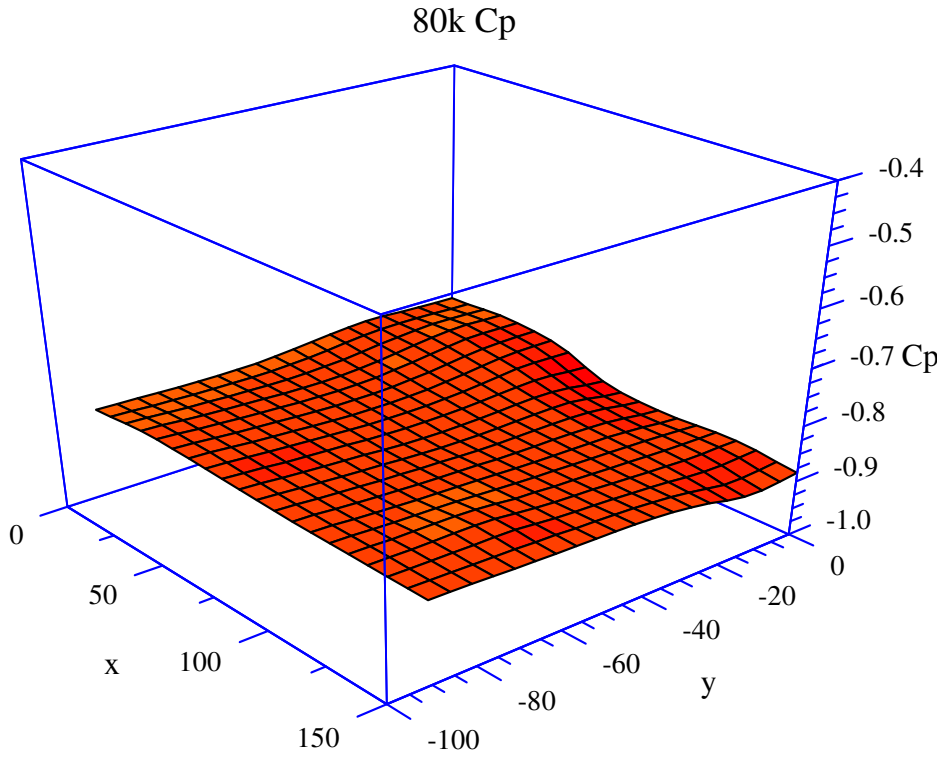

Figure A27: Surface Pressure Coefficients (Cp) - 3D-80 km/h

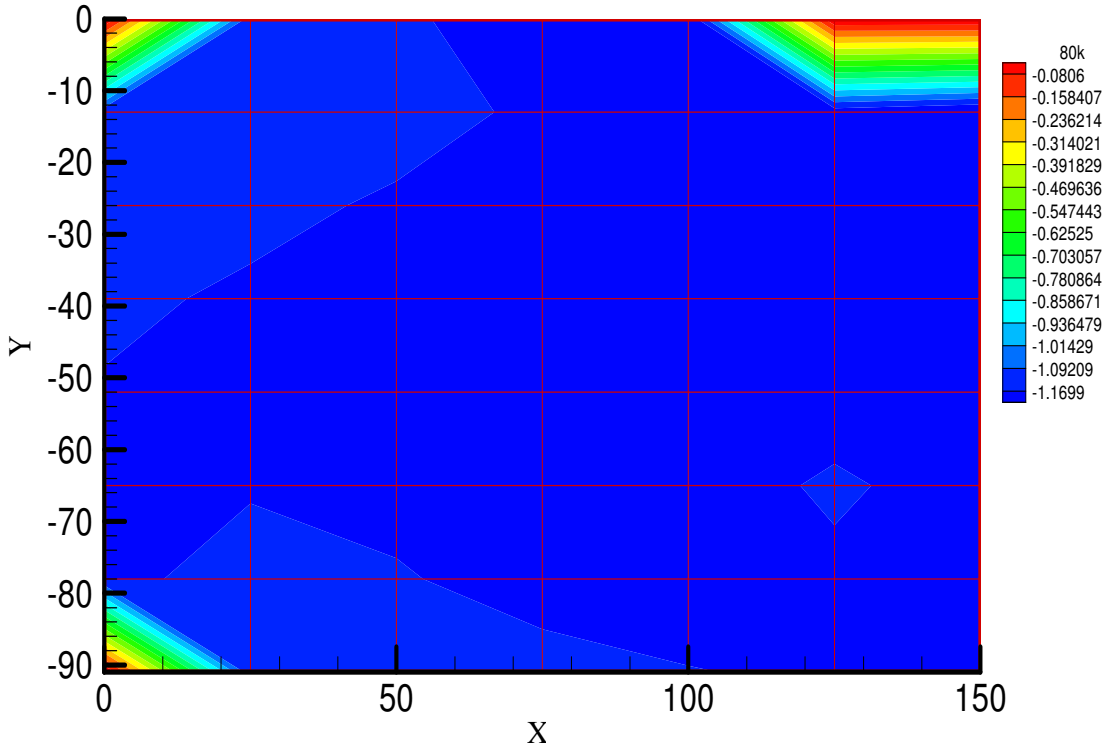

Figure A28: Surface Pressure Coefficients (Cp) - Contours - 80 km/h

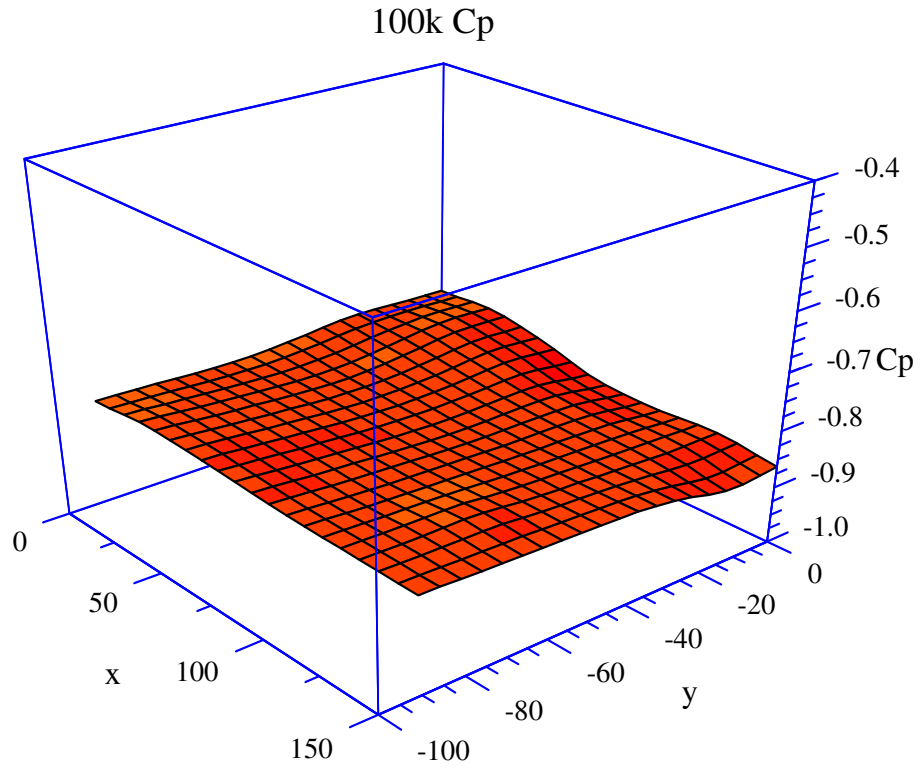

Figure A29: Surface Pressure Coefficients (Cp) - 3D- 100 km/h

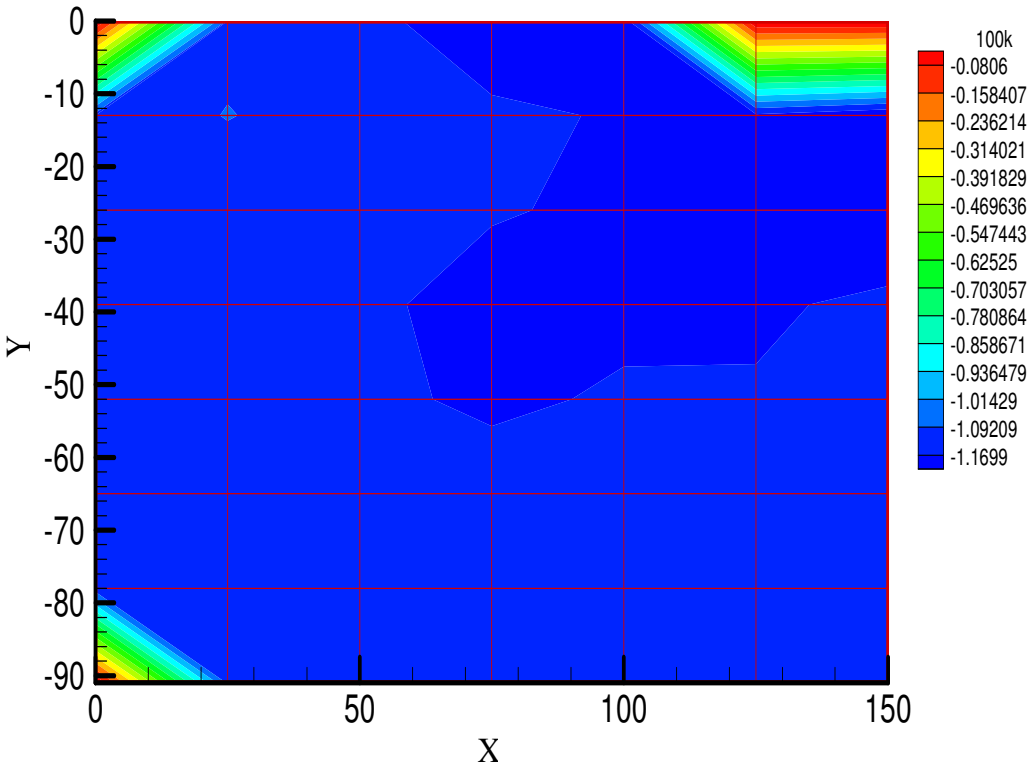

Figure A30: Surface Pressure Coefficients (Cp) - Contours -100 km/h

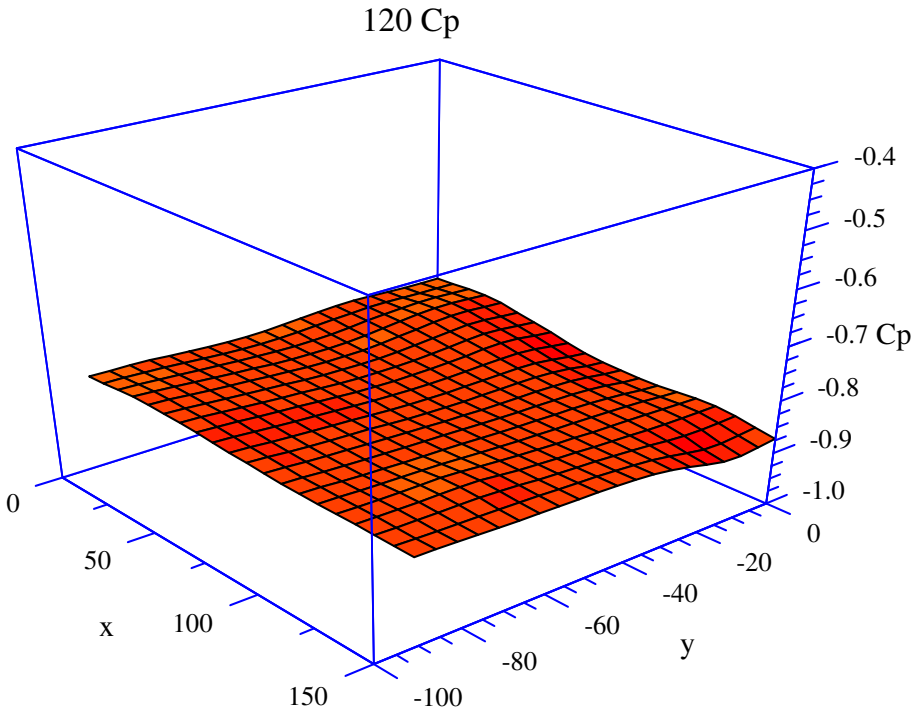

Figure A31: Surface Pressure Coefficients (Cp) - 3D- 120 km/h

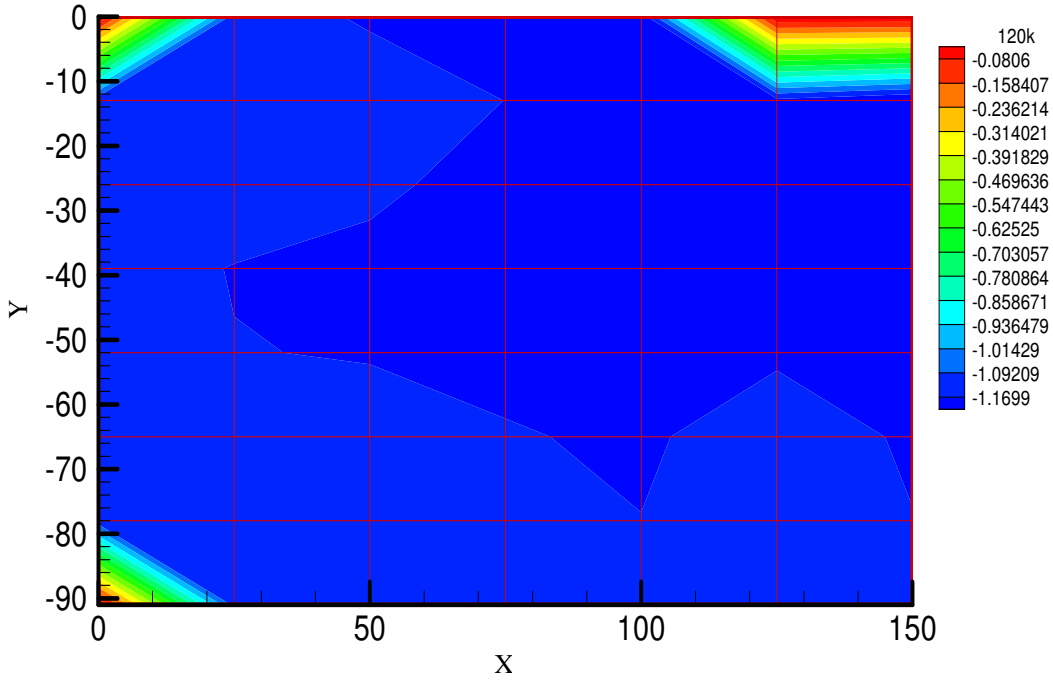

Figure A32: Surface Pressure Coefficients (Cp) - Contours - 120 km/h

Appendix B

Mirror in Semi-Isolation

Standard Mirror

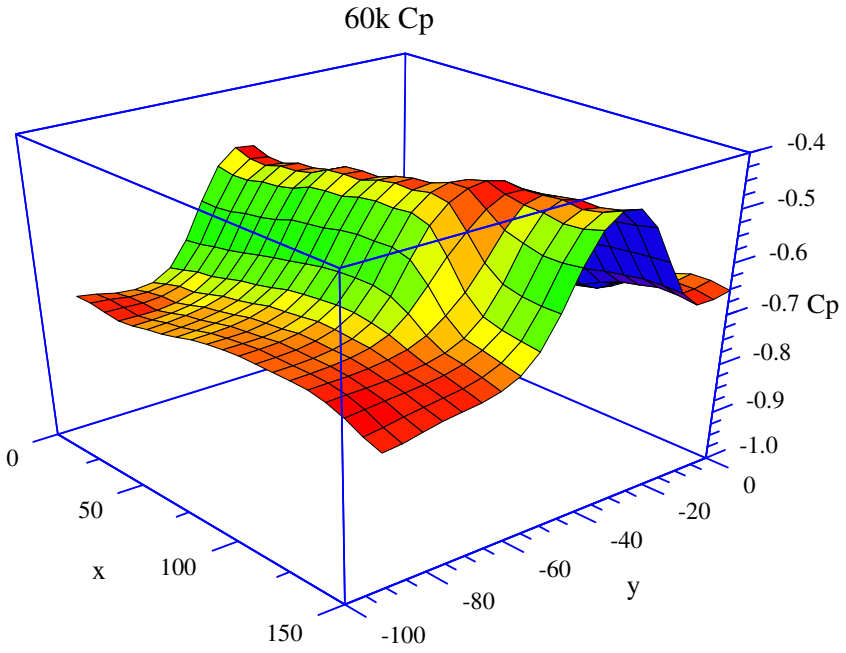

Figure B1: Surface Pressure Coefficients (Cp) - 3D- 60 km/h

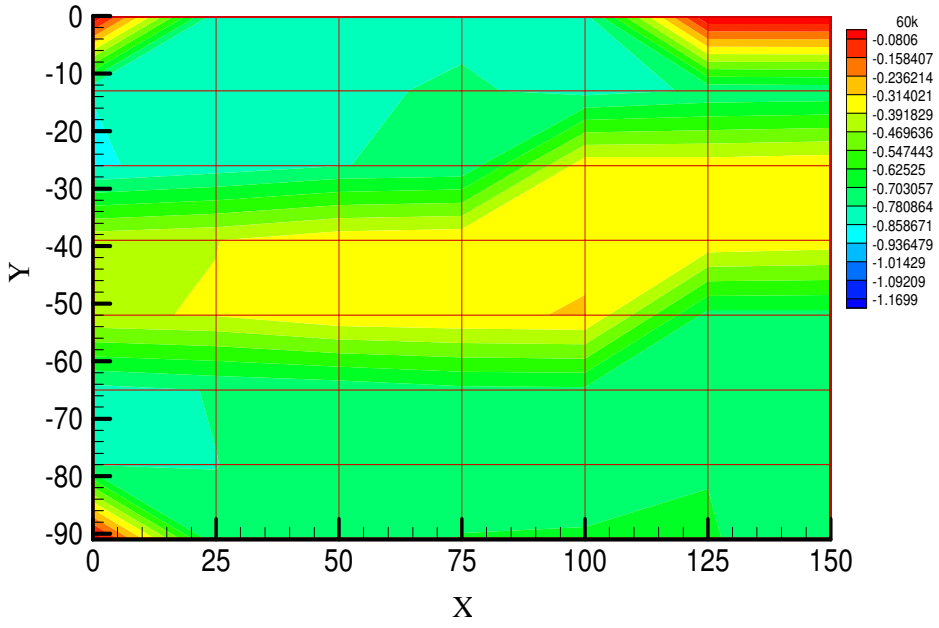

Figure B2: Surface Pressure Coefficients (Cp) - Contours - 60 km/h

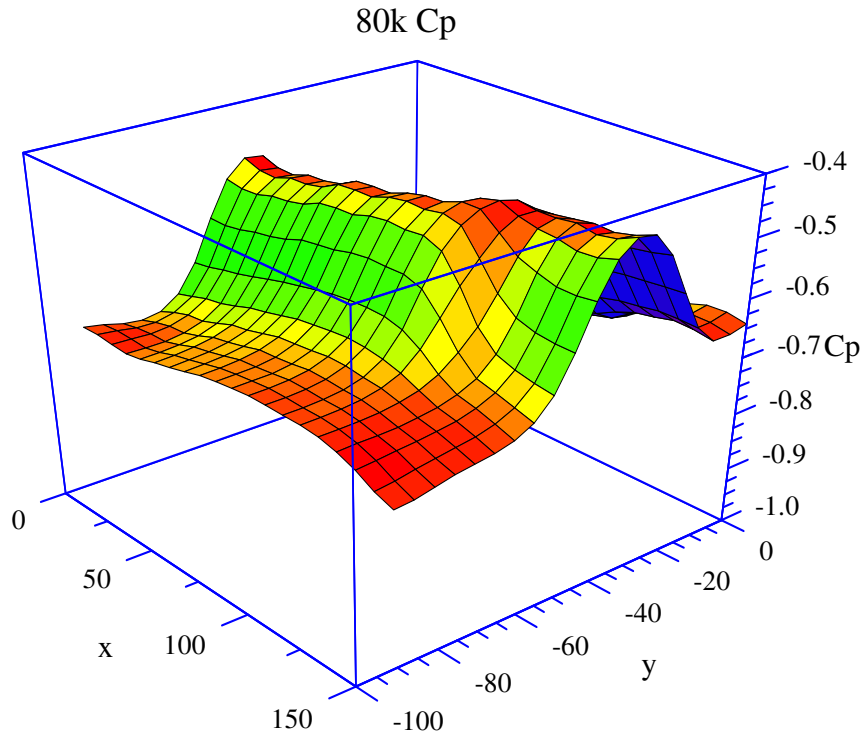

Figure B3: Surface Pressure Coefficients (Cp) - 3D-80 km/h

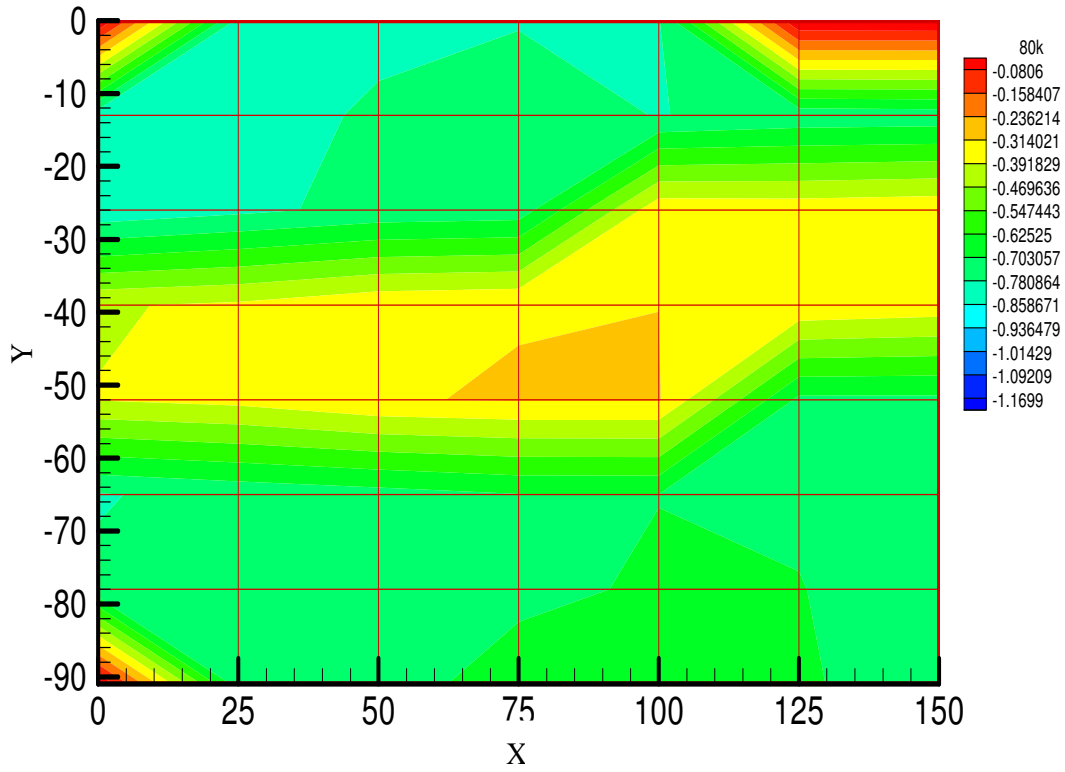

Figure B4: Surface Pressure Coefficients (Cp) - Contours - 80 km/h

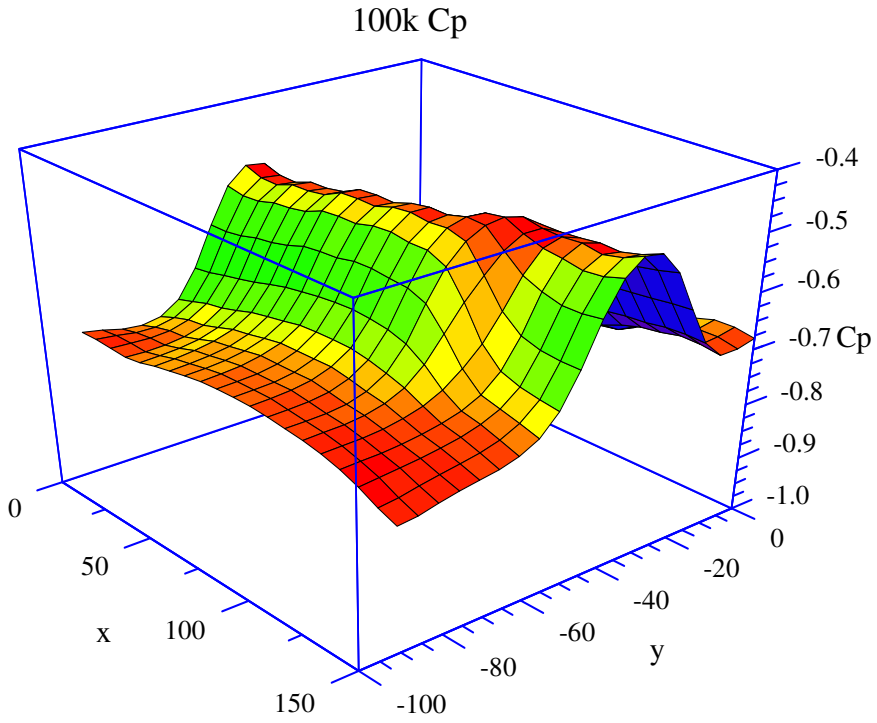

Figure B5: Surface Pressure Coefficients (Cp) - 3D-100 km/h

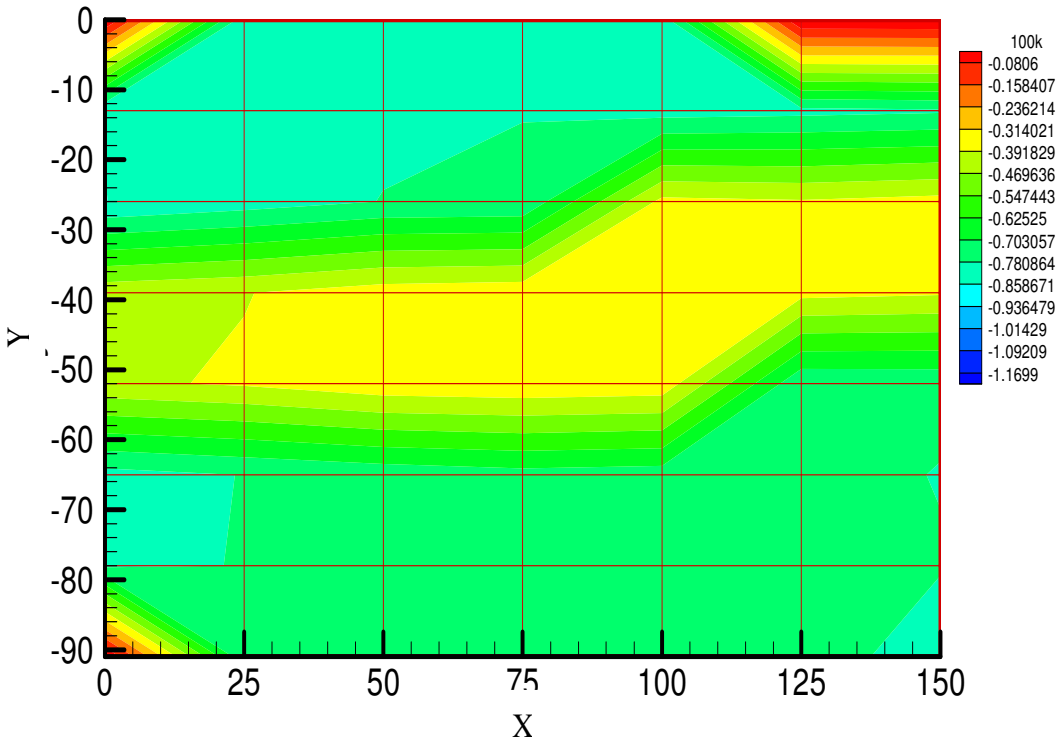

Figure B6: Surface Pressure Coefficients (Cp) - Contours -100 km/h

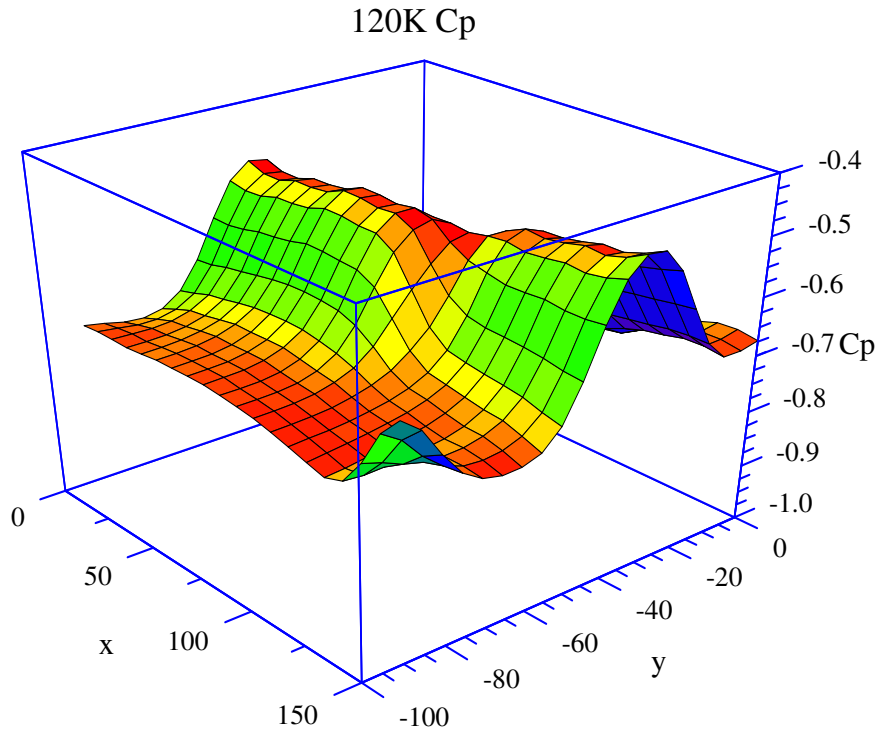

Figure B7: Surface Pressure Coefficients (Cp) - 3D-120 km/h

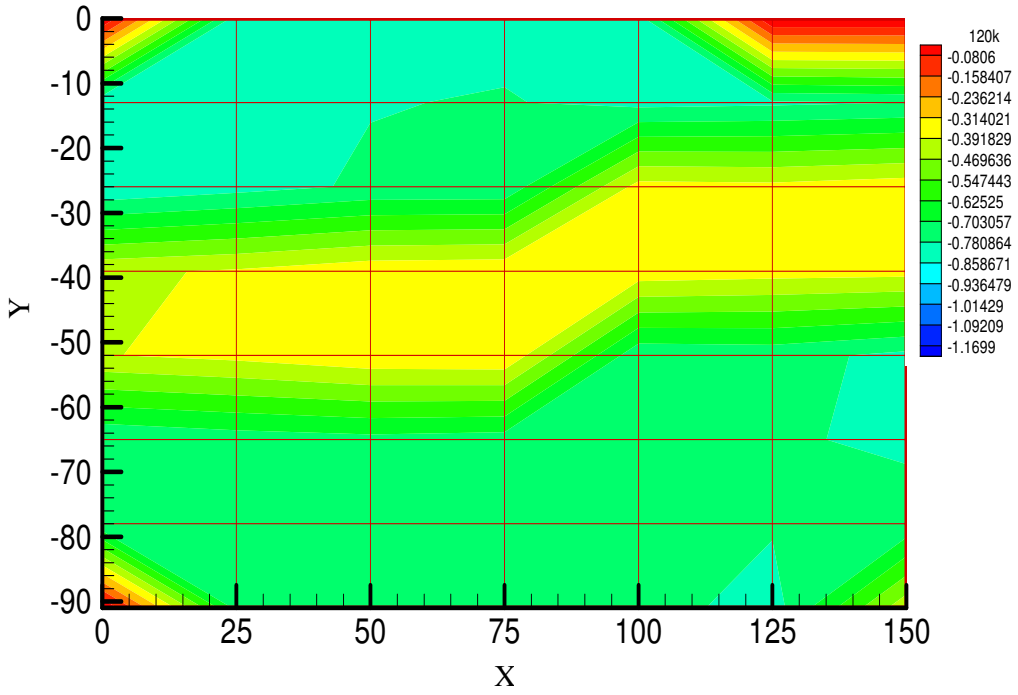

Figure B8: Surface Pressure Coefficients (Cp) - Contours - 120 km/h

24mm Shroud

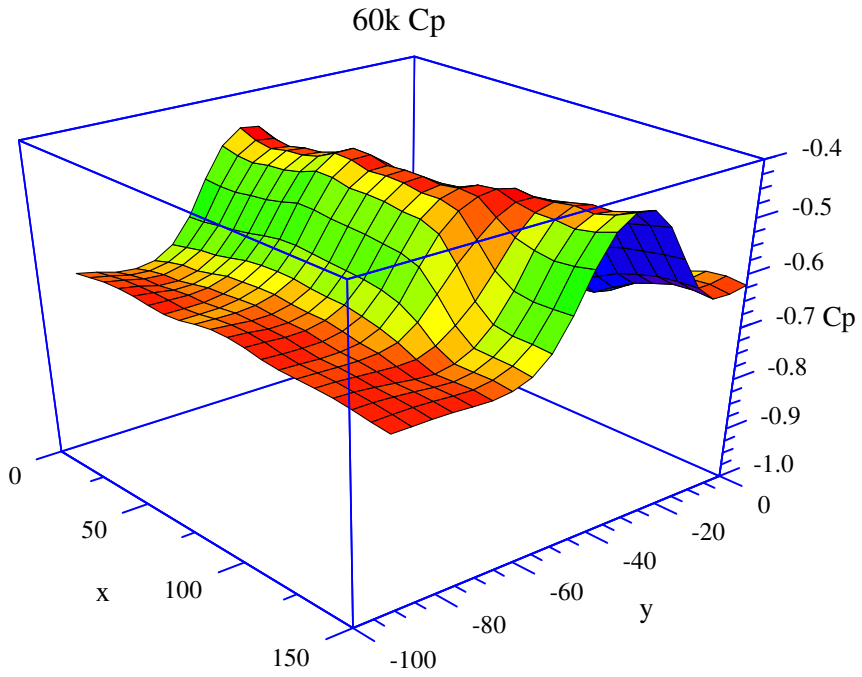

Figure B9: Surface Pressure Coefficients (Cp) - 3D- 60 km/h

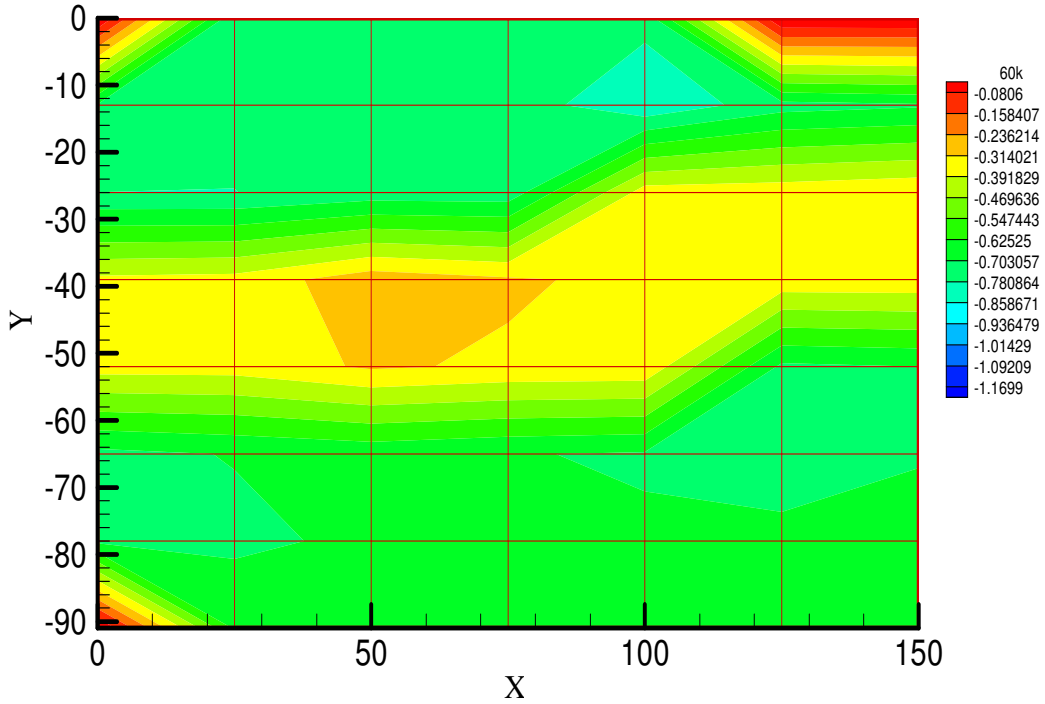

Figure B10: Surface Pressure Coefficients (Cp) - Contours - 60 km/h

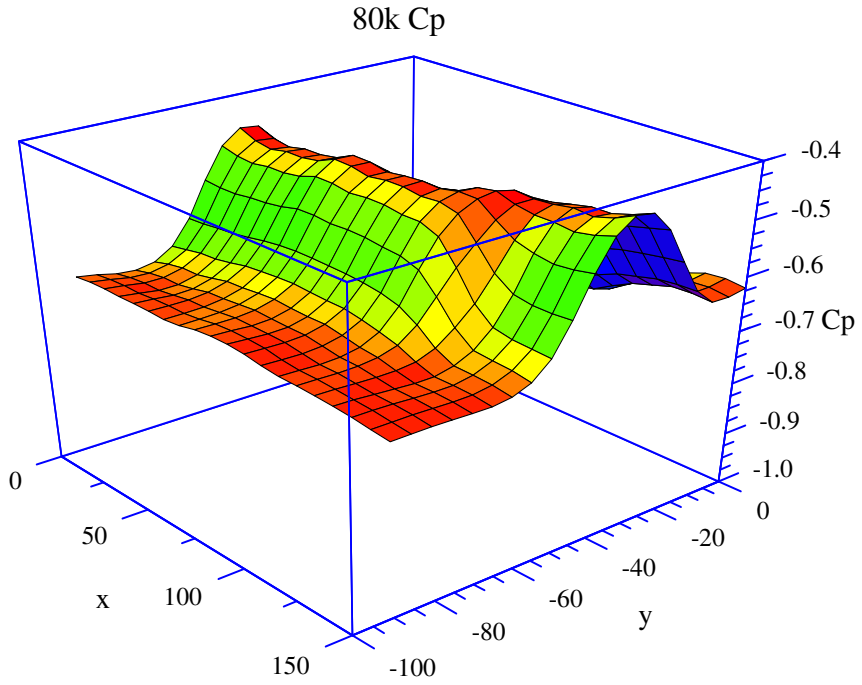

Figure B11: Surface Pressure Coefficients (Cp) - 3D- 80 km/h

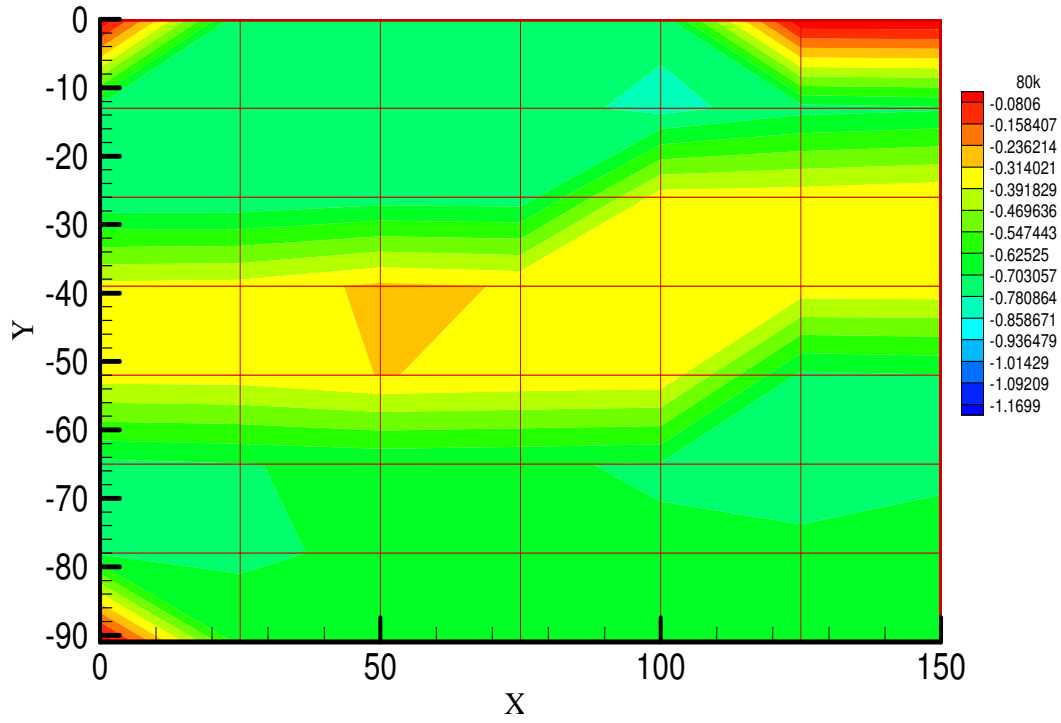

Figure B12: Surface Pressure Coefficients (Cp) - Contours -80 km/h

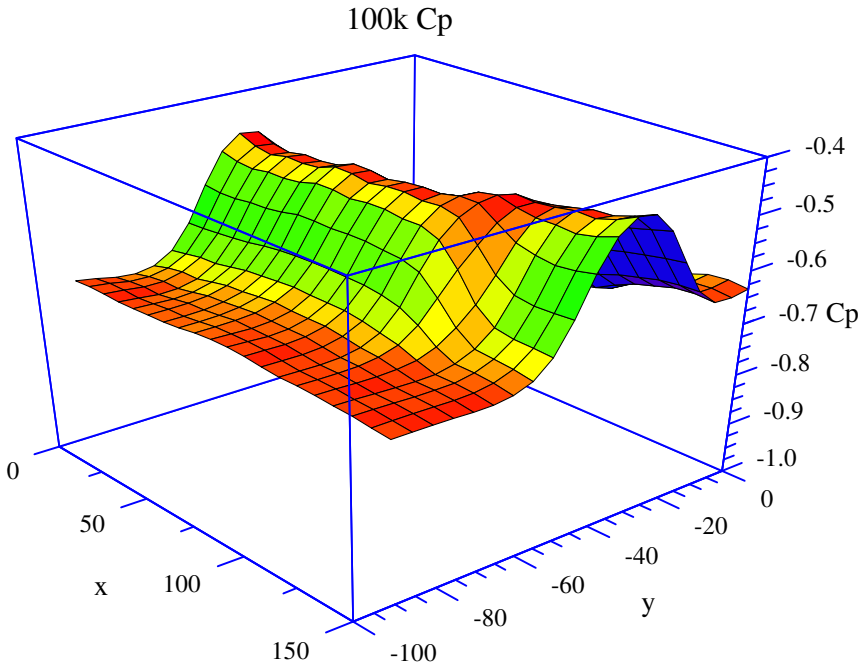

Figure B13: Surface Pressure Coefficients (Cp) - 3D-100 km/h

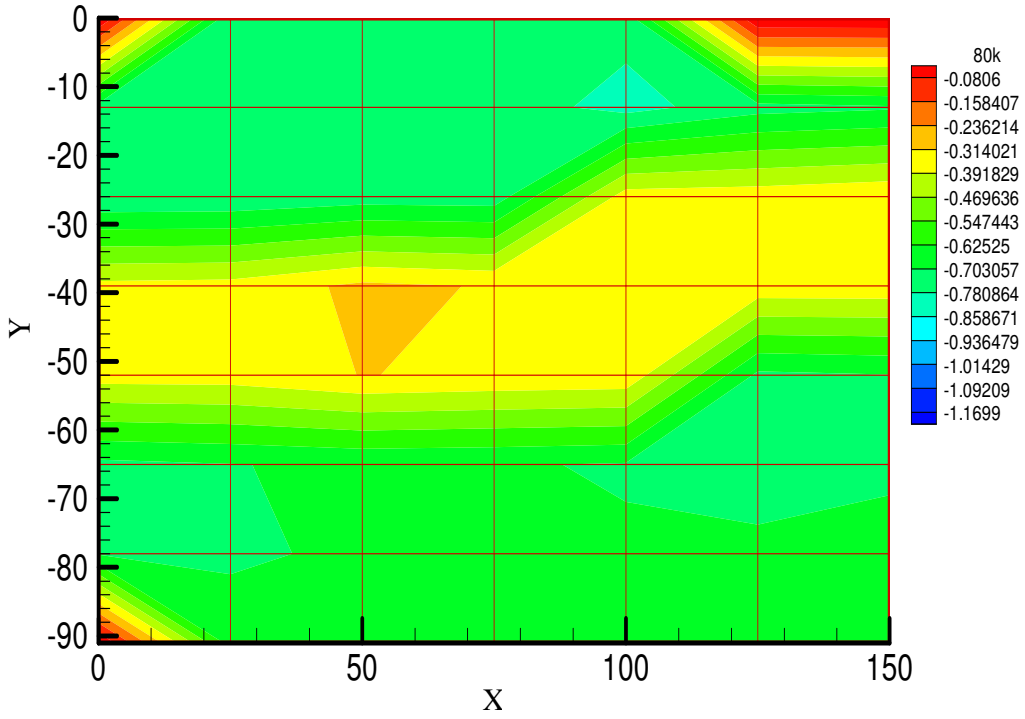

Figure B14: Surface Pressure Coefficients (Cp) - Contours - 100 km/h

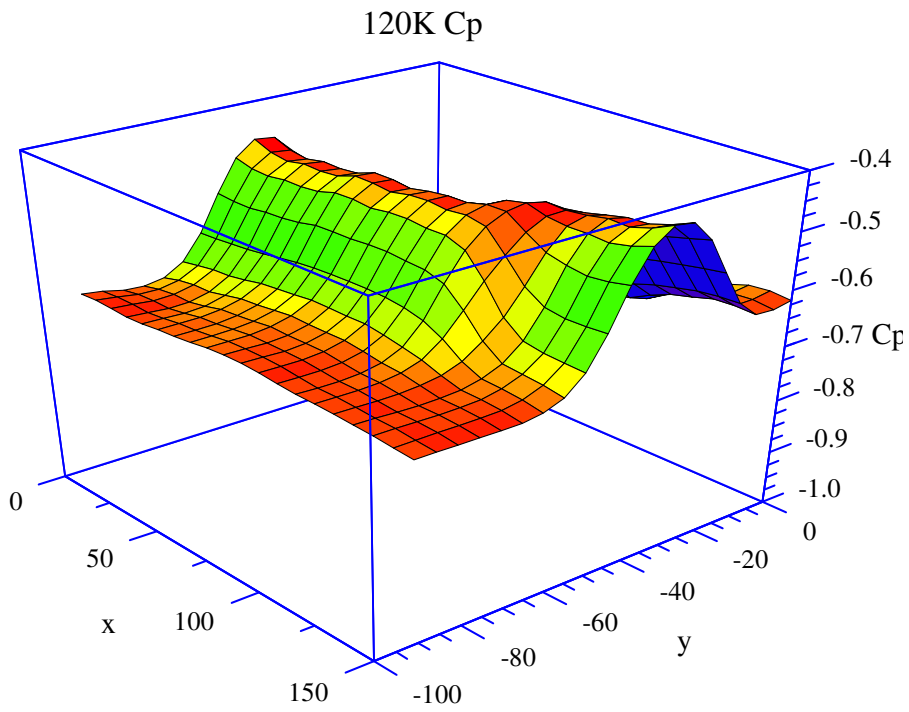

Figure B15: Surface Pressure Coefficients (Cp) - 3D-120 km/h

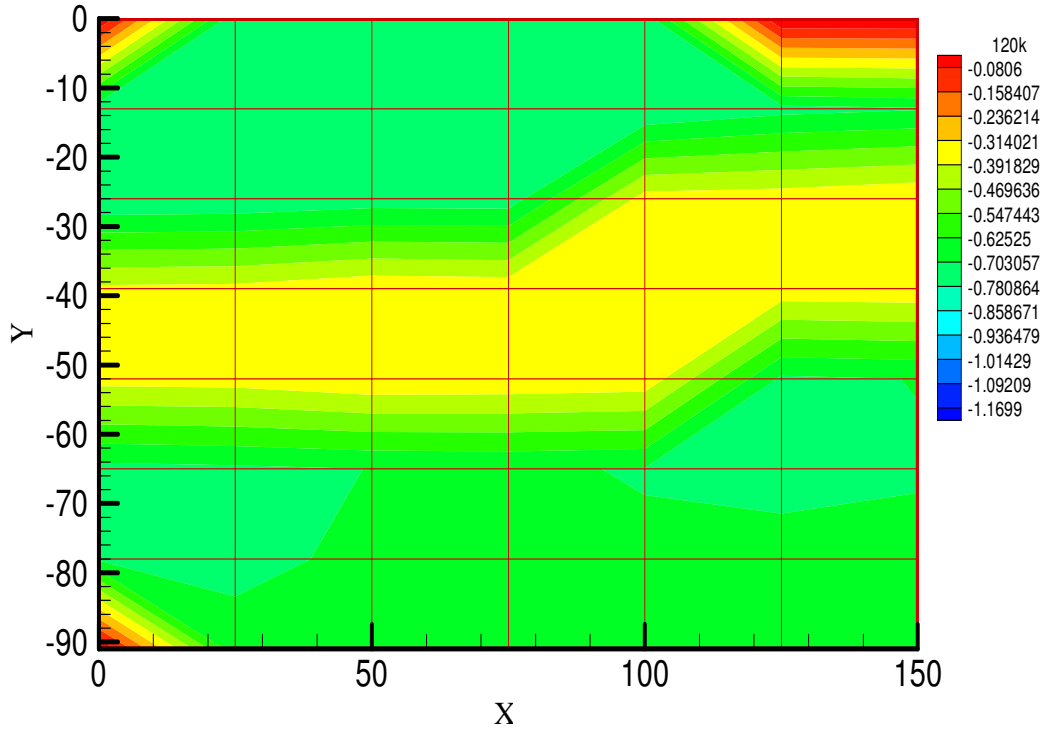

Figure B16: Surface Pressure Coefficients (Cp) - Contours -120 km/h

34mm Shroud

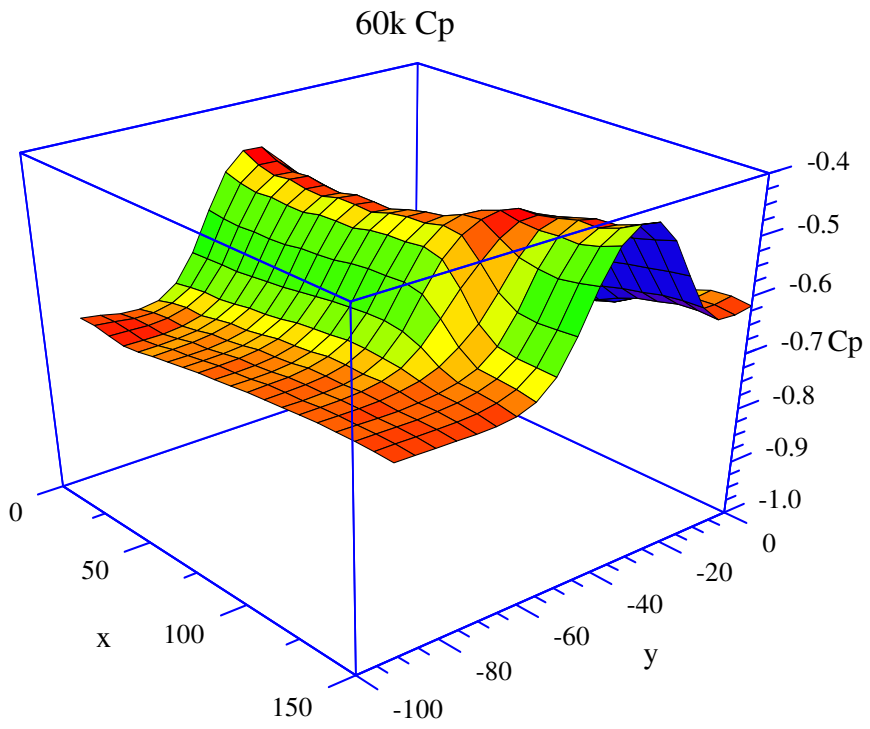

Figure B17: Surface Pressure Coefficients (Cp) - 3D- 60 km/h

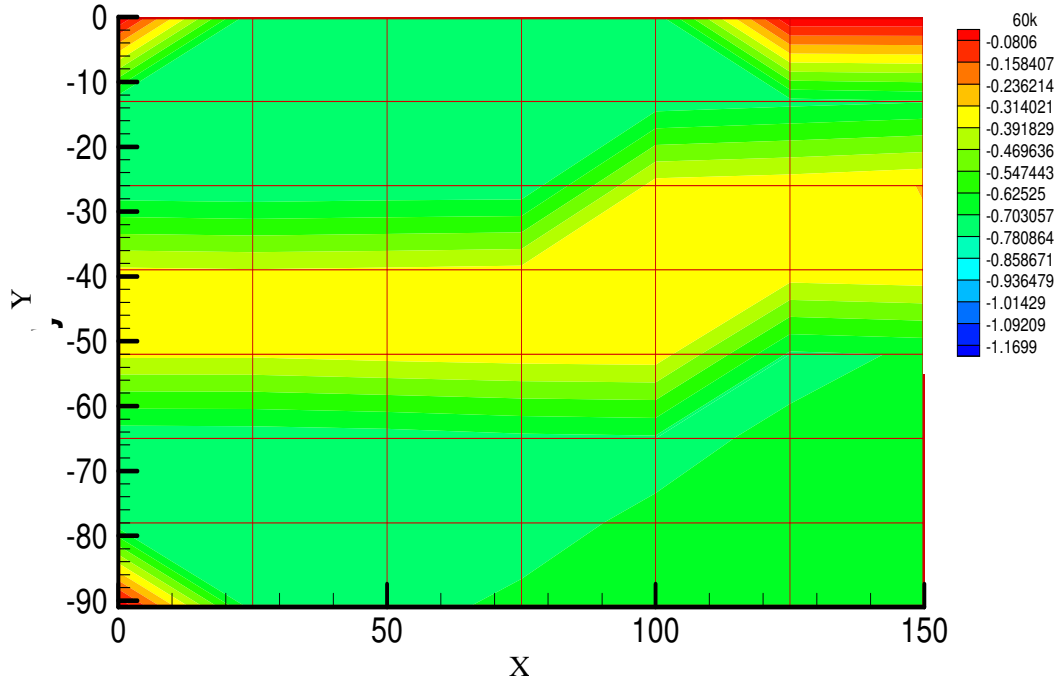

Figure B18: Surface Pressure Coefficients (Cp) - Contours - 60 km/h

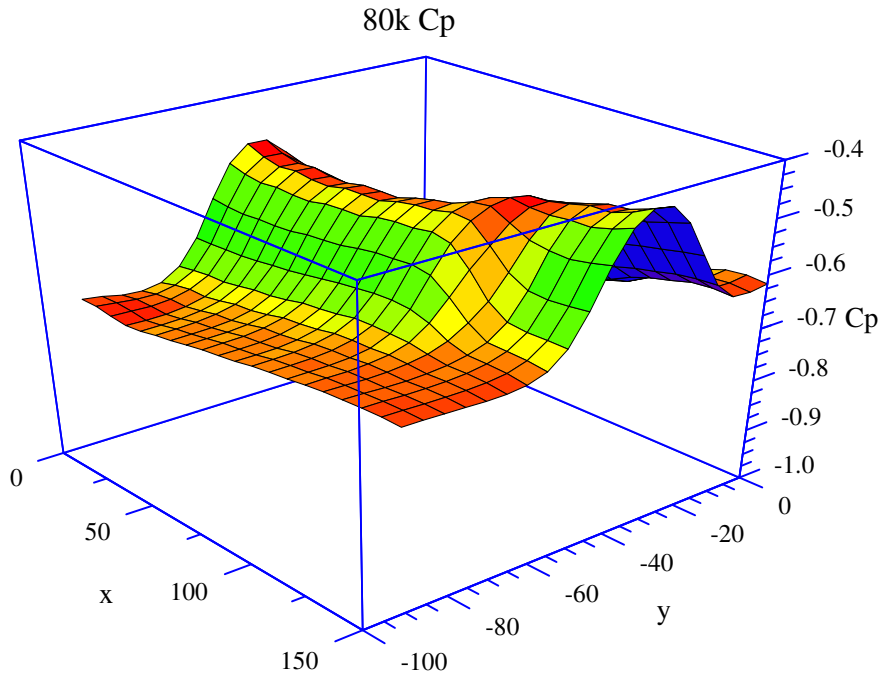

Figure B19: Surface Pressure Coefficients (Cp) - 3D- 80 km/h

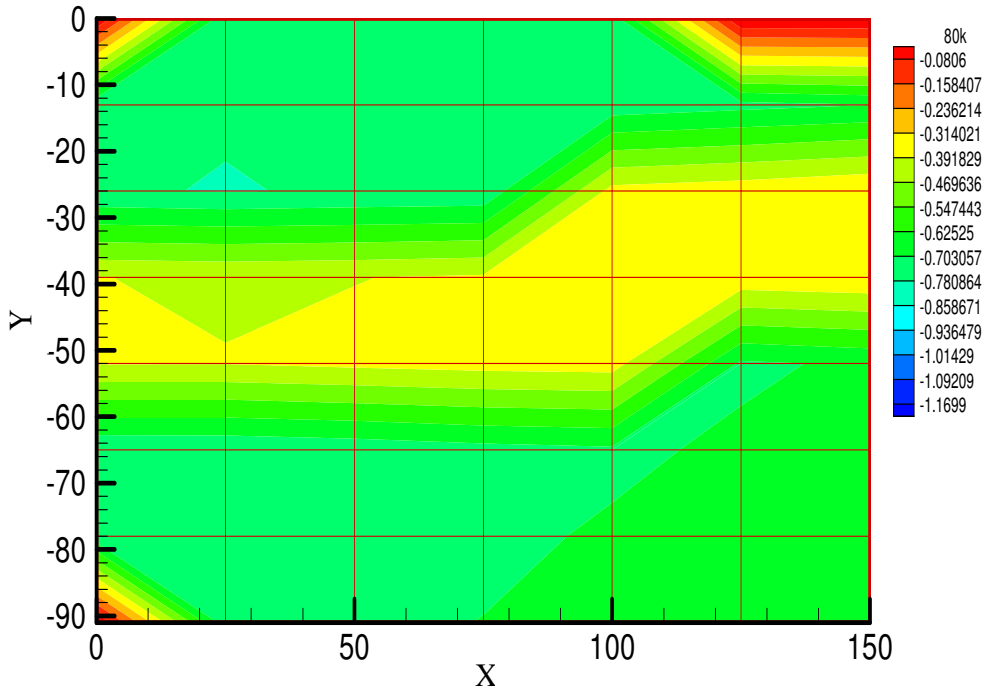

Figure B20: Surface Pressure Coefficients (Cp) - Contours - 80 km/h

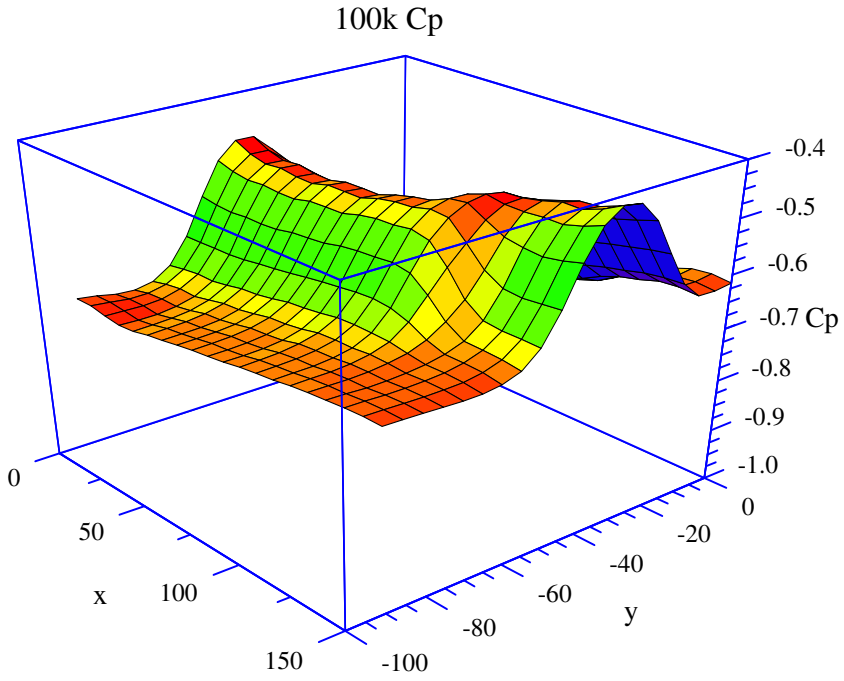

Figure B21: Surface Pressure Coefficients (Cp) - 3D-100 km/h

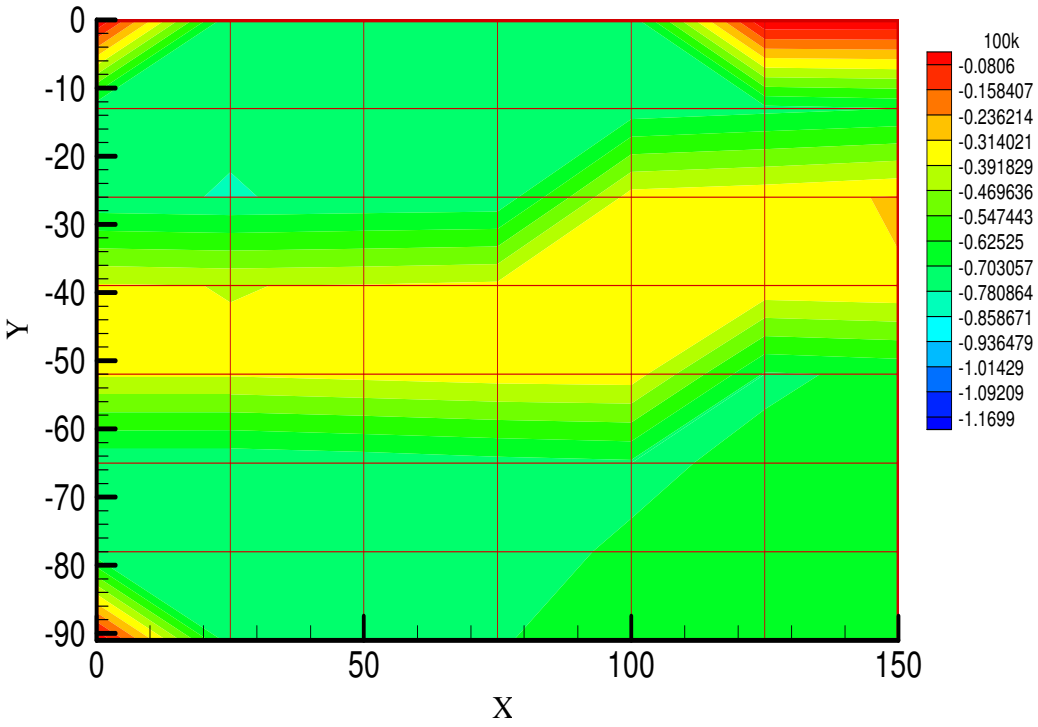

Figure B22: Surface Pressure Coefficients (Cp) - Contours - 100 km/h

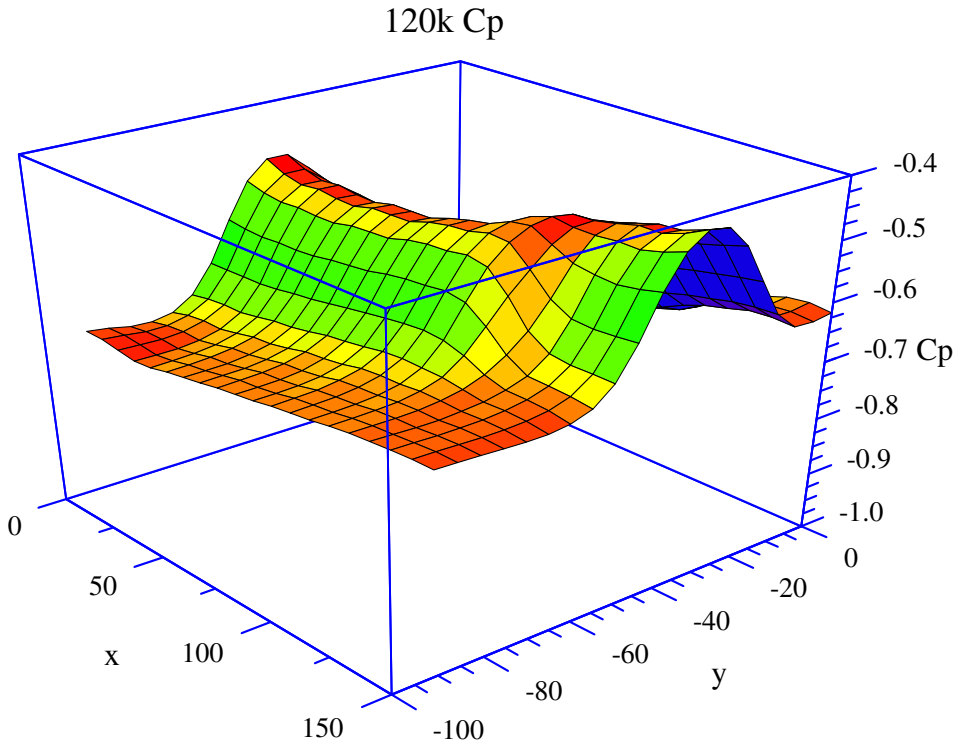

Figure B23: Surface Pressure Coefficients (Cp) - 3D-120 km/h

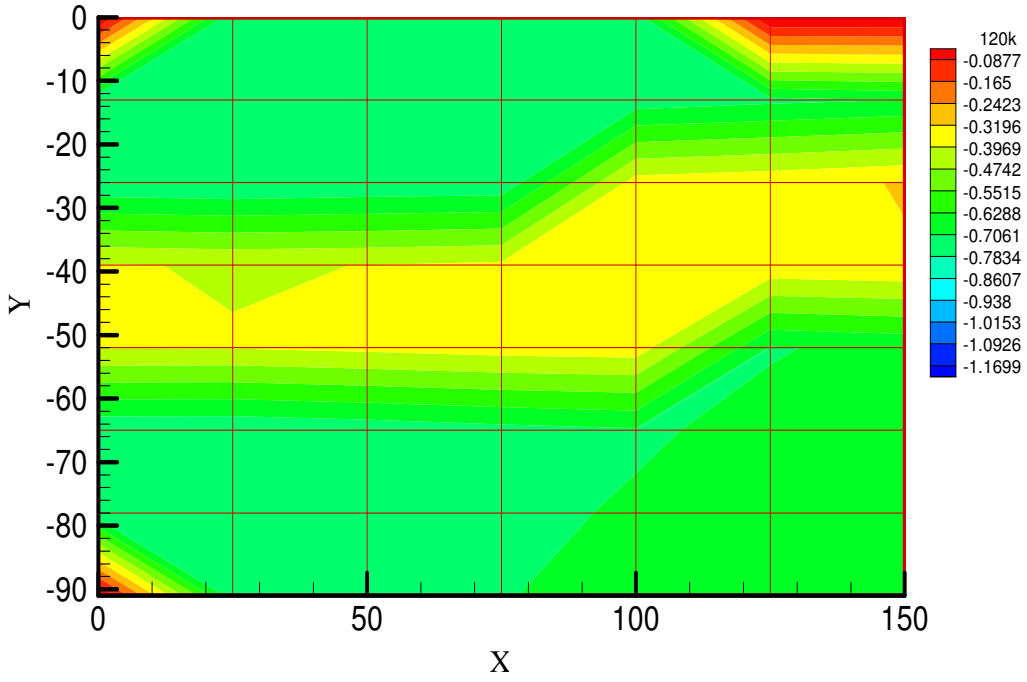

Figure B24: Surface Pressure Coefficients (Cp) - Contours -120 km/h

44mm Shroud

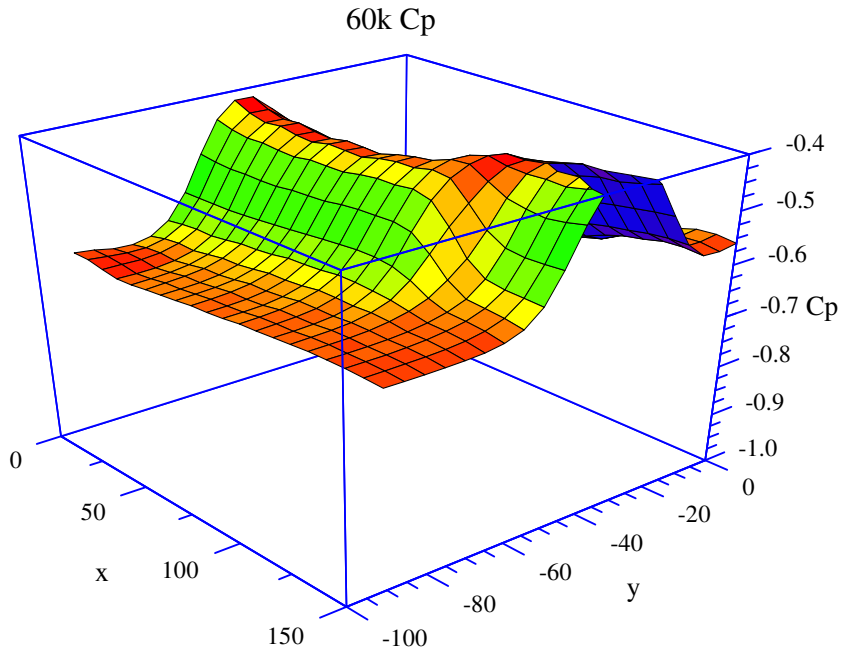

Figure B25: Surface Pressure Coefficients (Cp) - 3D- 60 km/h

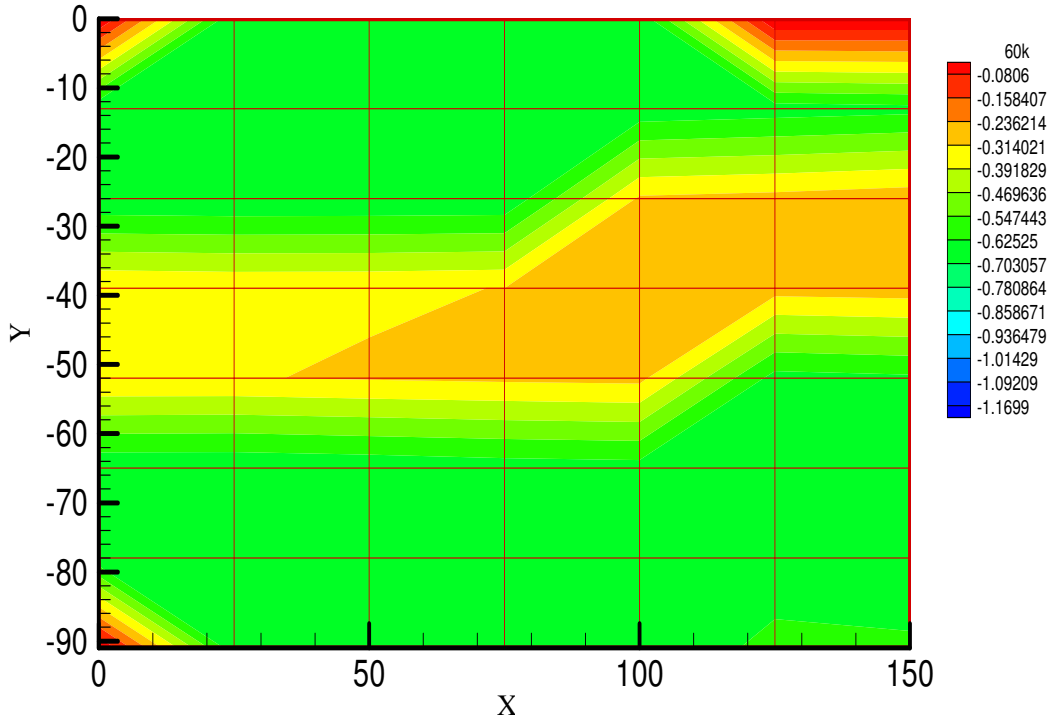

Figure B36: Surface Pressure Coefficients (Cp) - Contours - 60 km/h

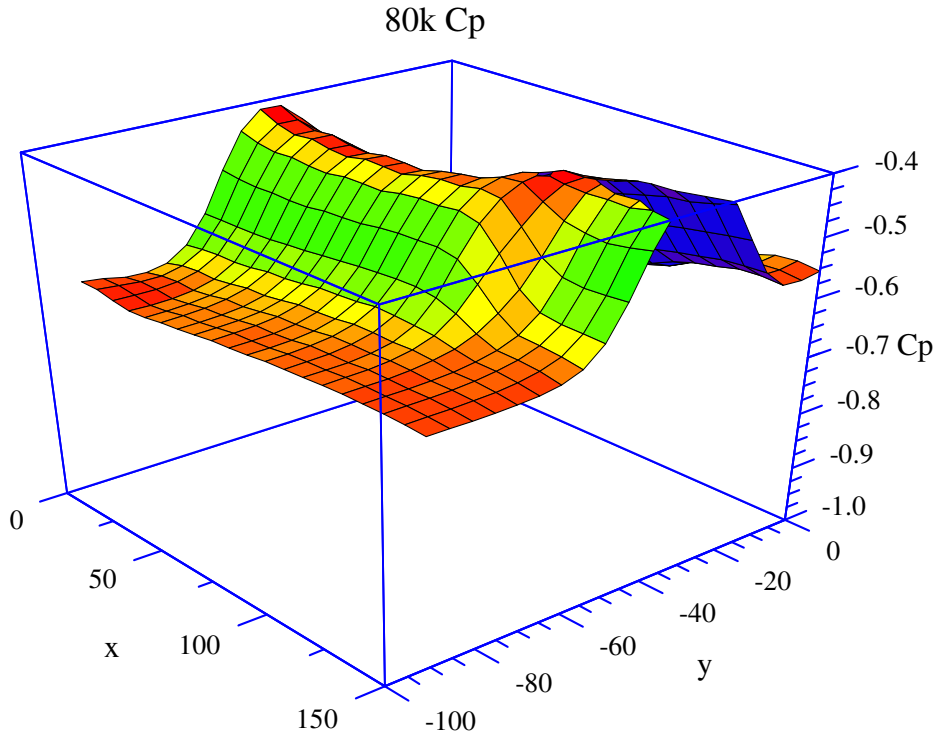

Figure B27: Surface Pressure Coefficients (Cp) - 3D-80 km/h

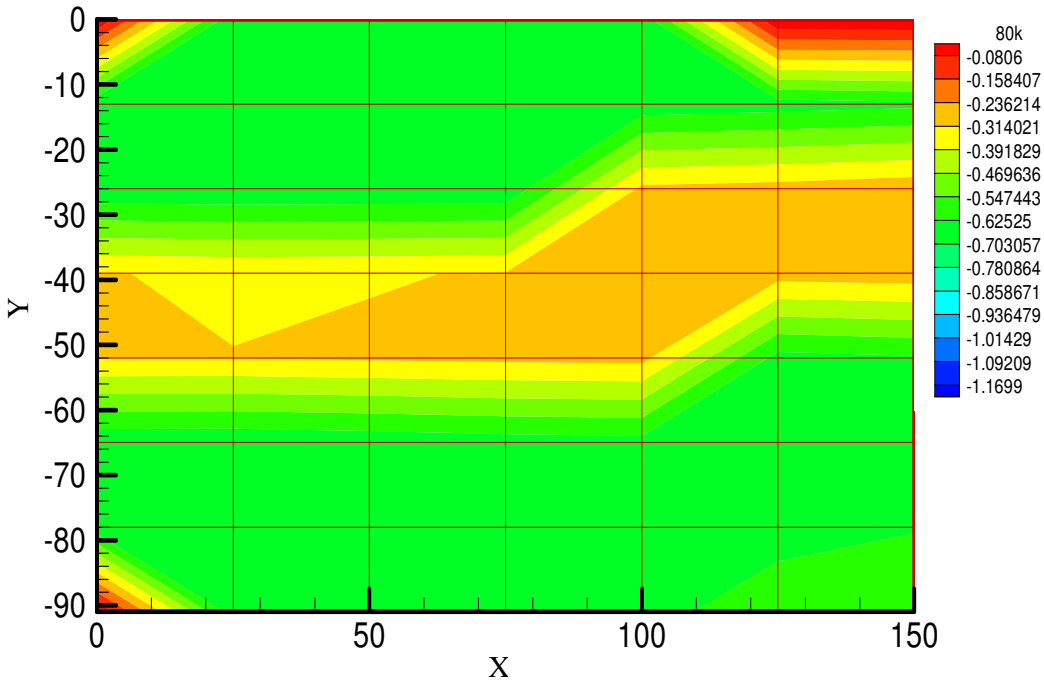

Figure B28: Surface Pressure Coefficients (Cp) - Contours - 80 km/h

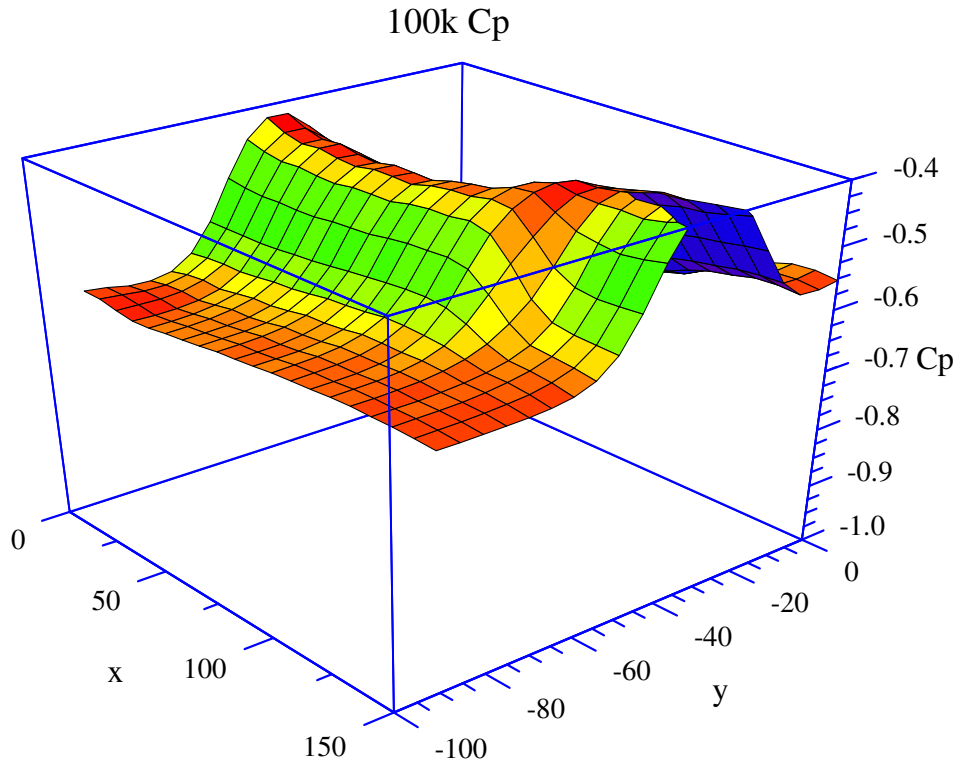

Figure B29: Surface Pressure Coefficients (Cp) - 3D- 100 km/h

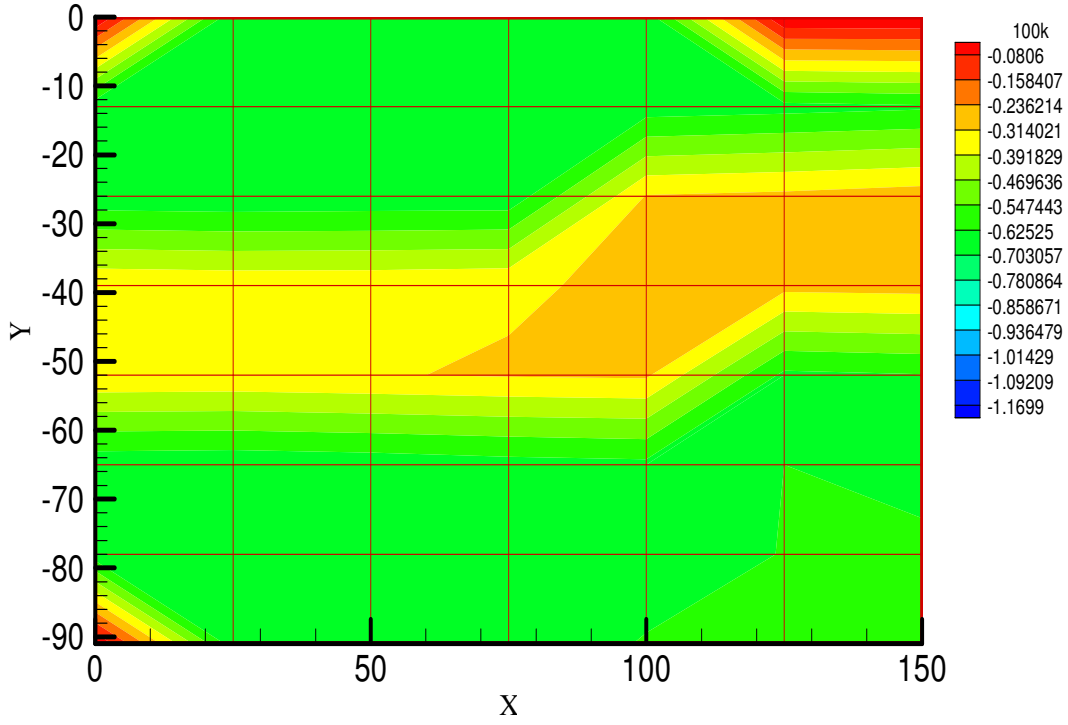

Figure B30: Surface Pressure Coefficients (Cp) - Contours -100 km/h

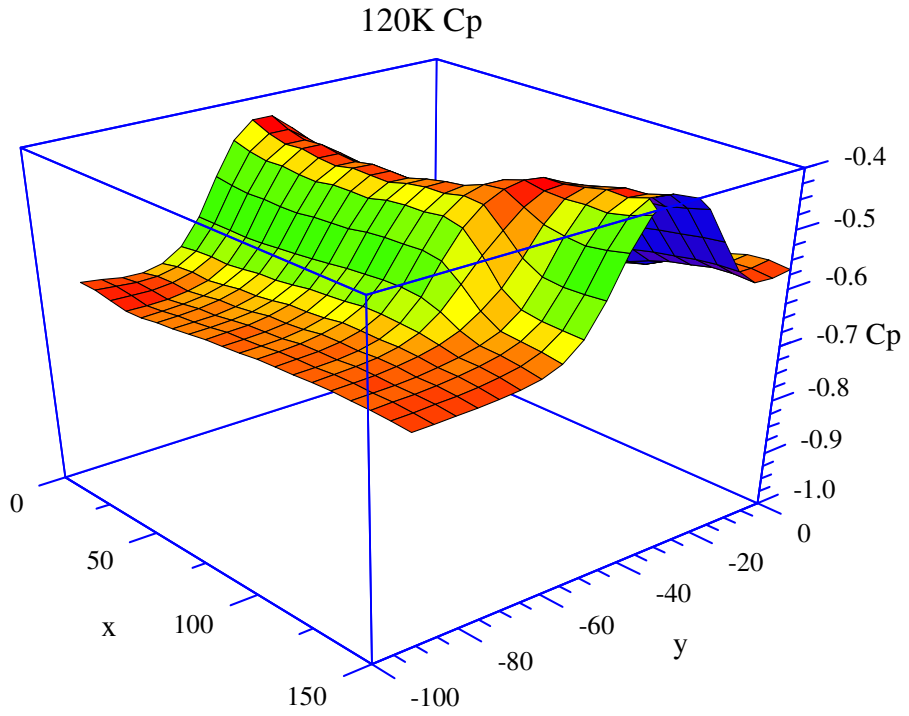

Figure B31: Surface Pressure Coefficients (Cp) - 3D- 120 km/h

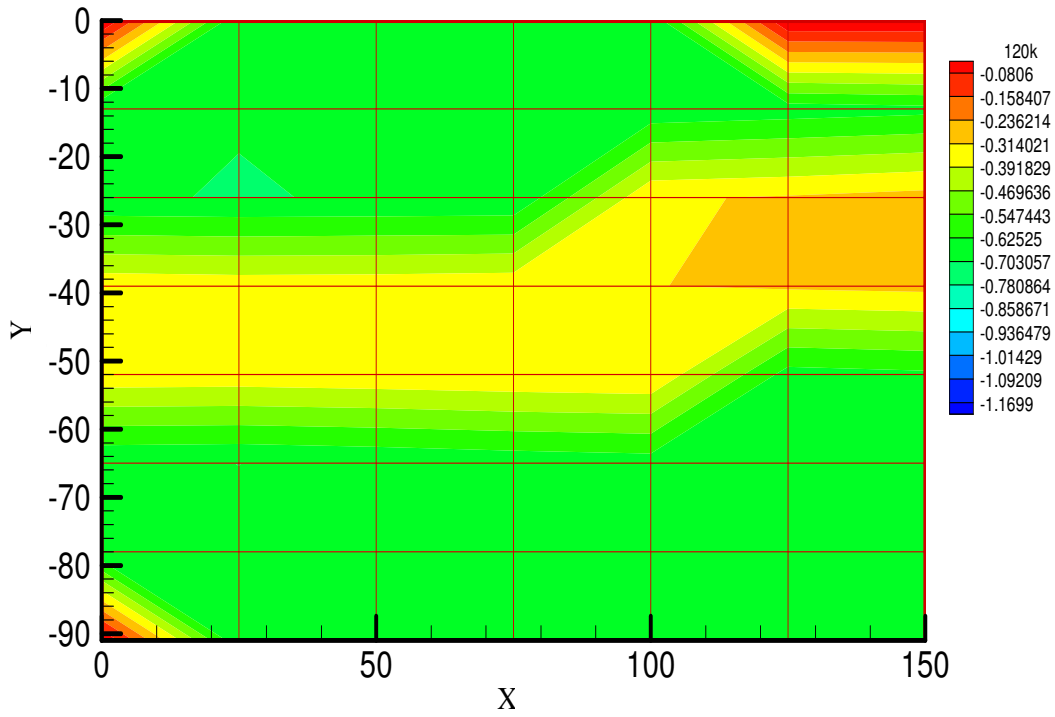

Figure B32: Surface Pressure Coefficients (Cp) - Contours - 120 km/h

Appendix C

PSD Comparison for Point 47

Quarter Model (Standard Mirror)

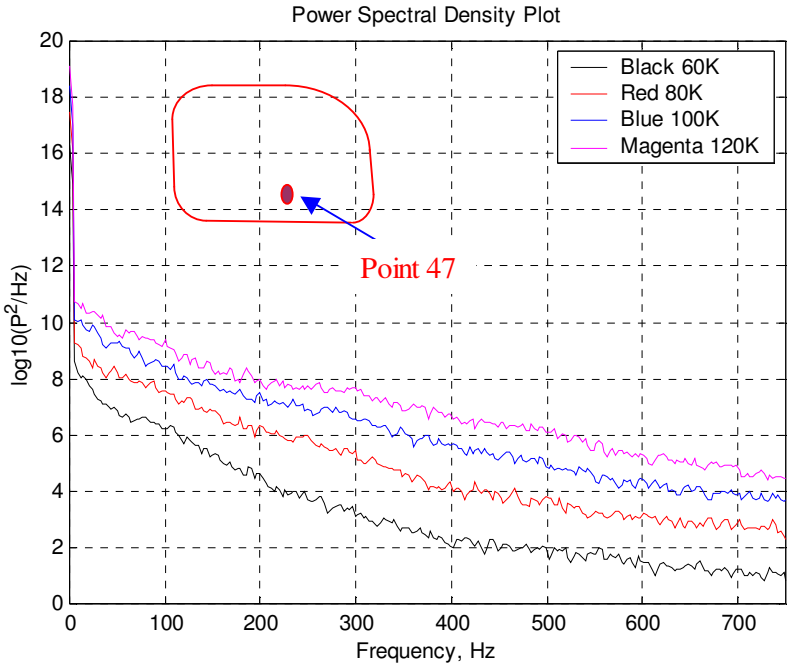

Figure C1: Highest Cprms at Point 47

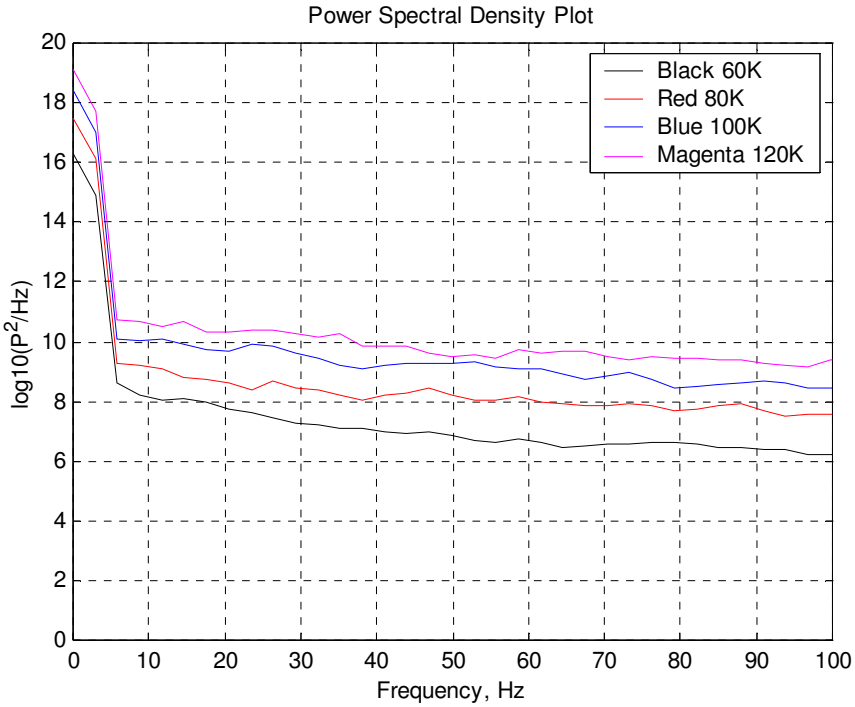

Figure C2: Zoom View of Highest Cprms 0-100Hz

24 mm Shroud

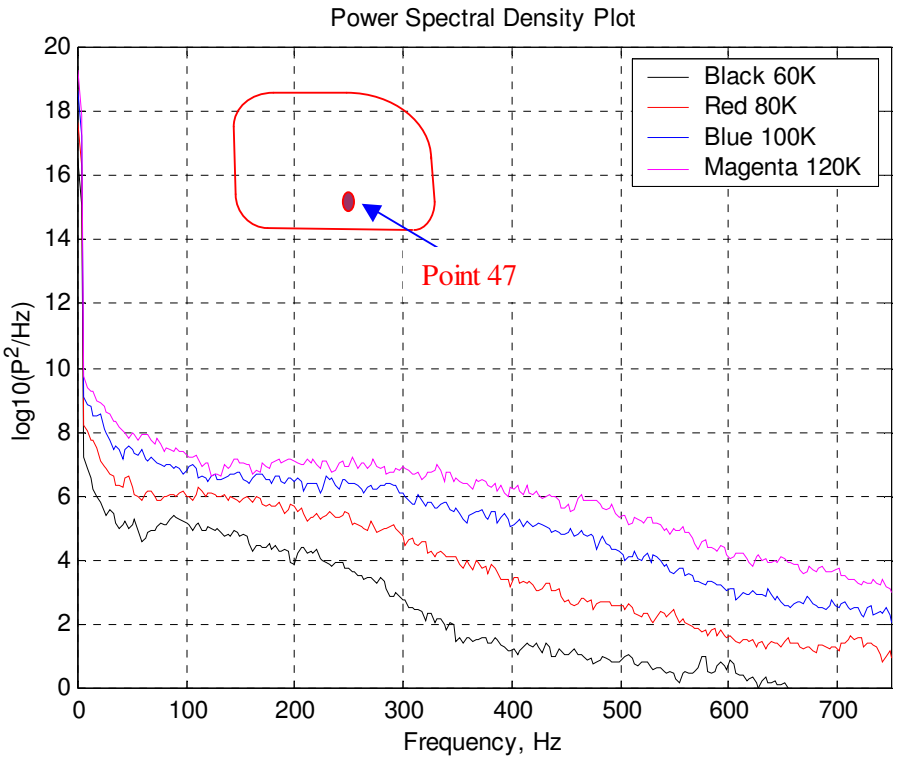

Figure C3: Highest Cprms at Point 47

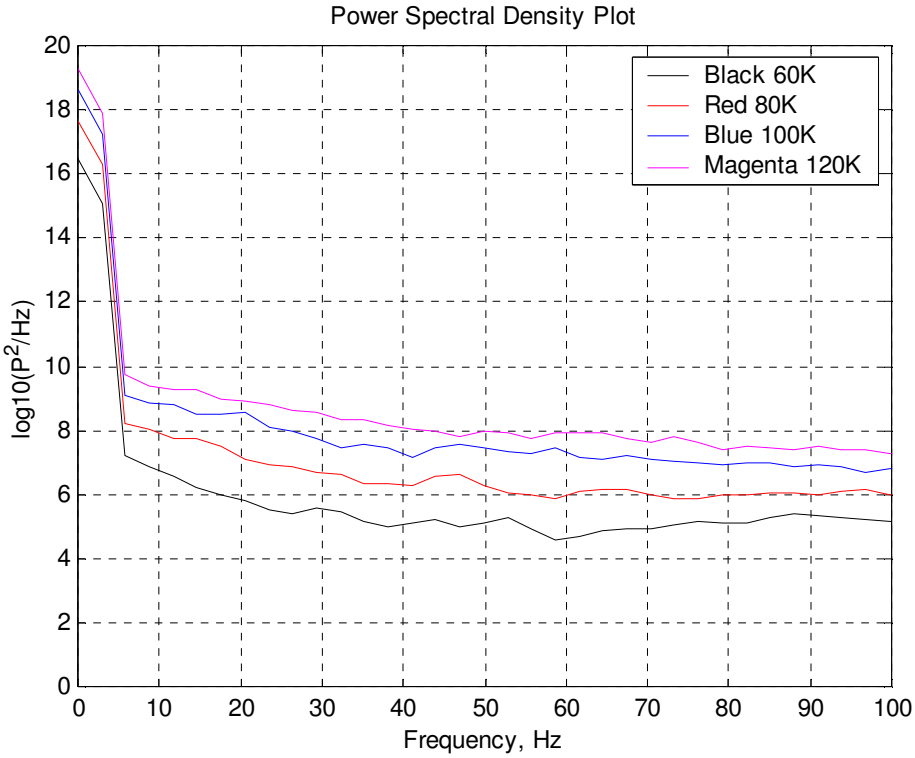

Figure C4: Zoom View of Highest Cprms 0-100Hz

34mm Shroud

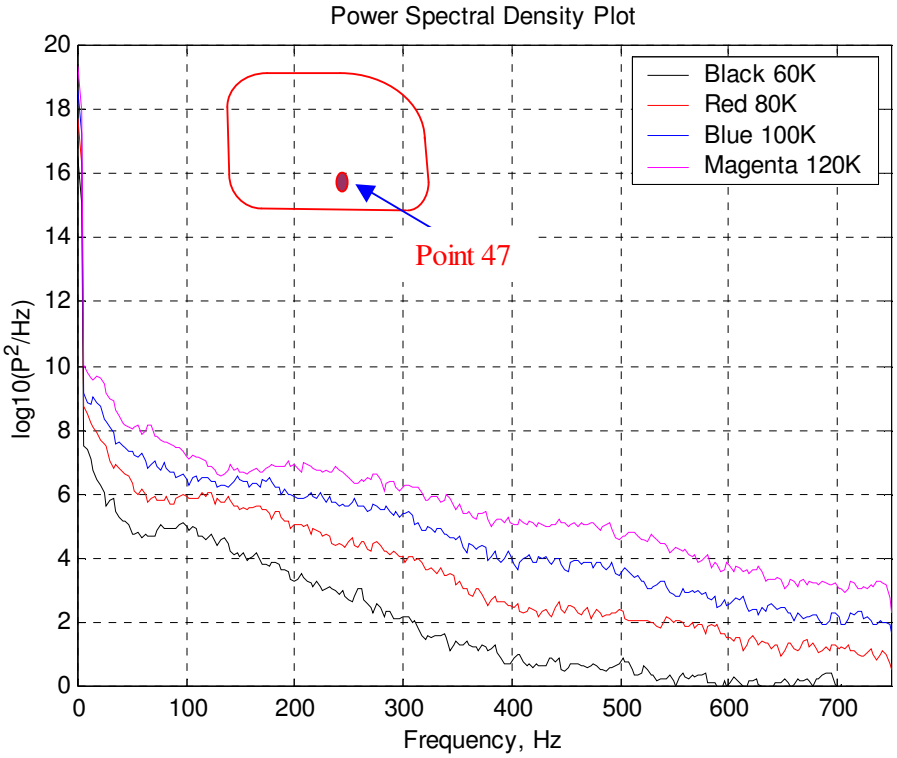

Figure C5: Highest Cprms at Point 47

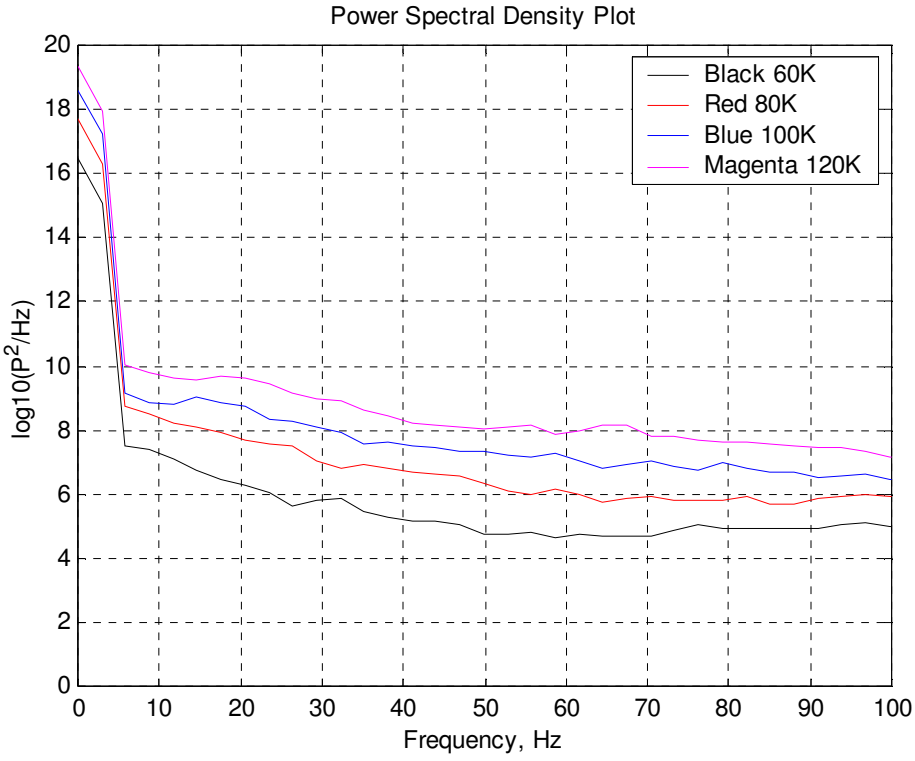

Figure C6: Zoom View of Highest Cprms 0-100Hz

44mm Shroud

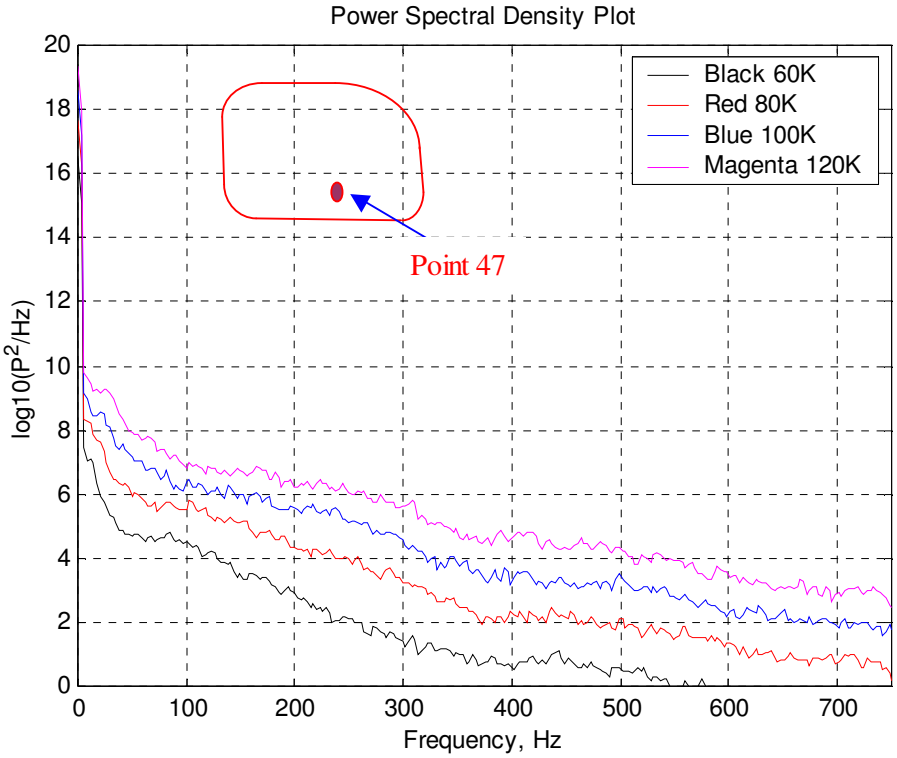

Figure C7: Highest Cprms at Point 47

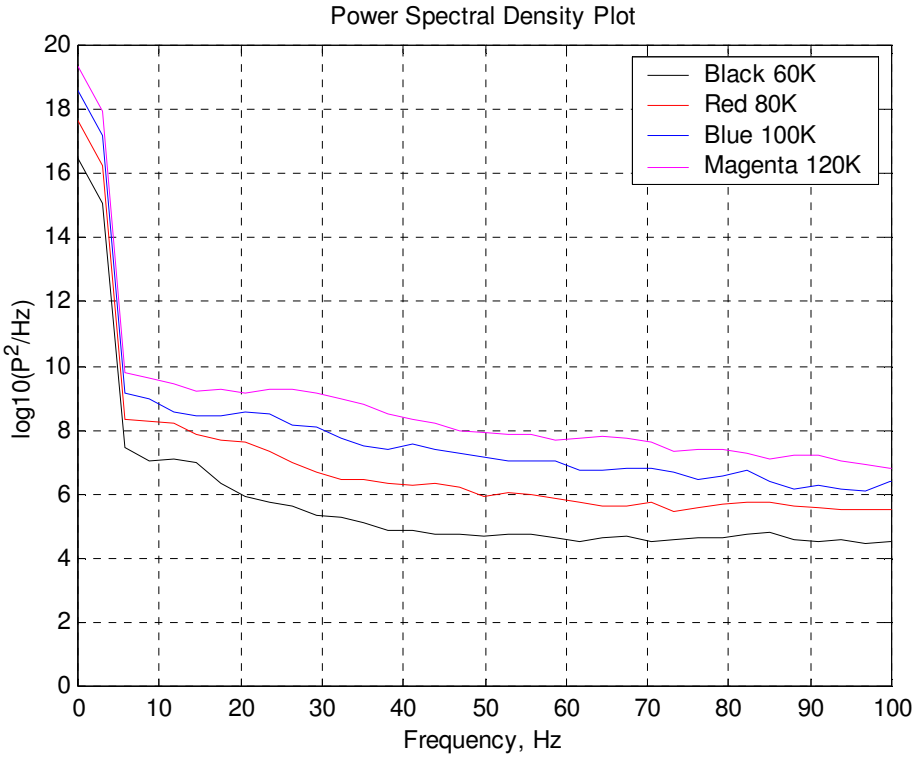

Figure C8: Zoom View of Highest Cprms 0-100Hz

Semi – Isolation (Standard Mirror)

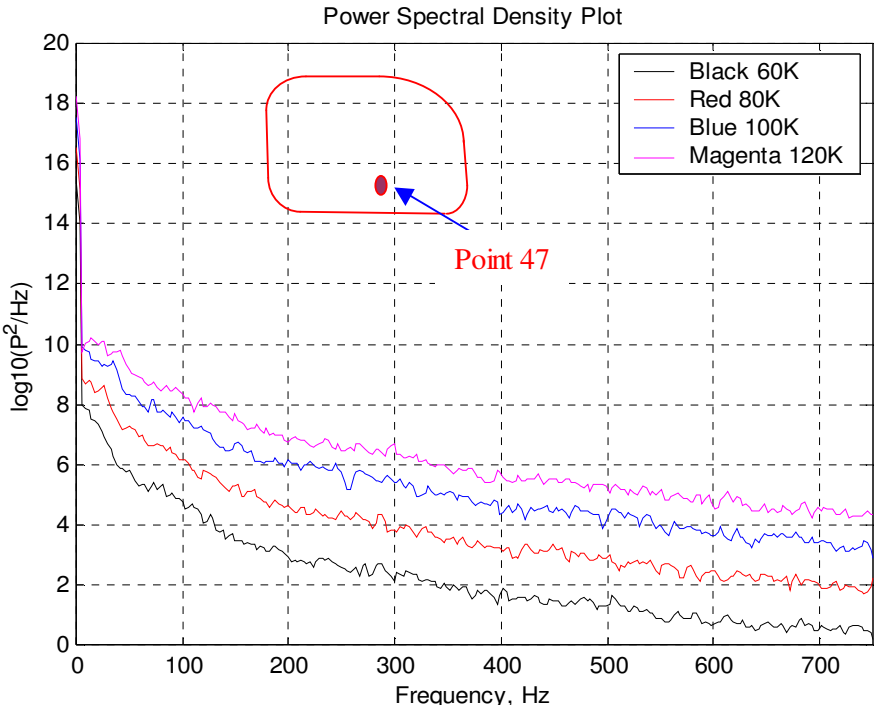

Figure C9: Highest Cprms at Point 47

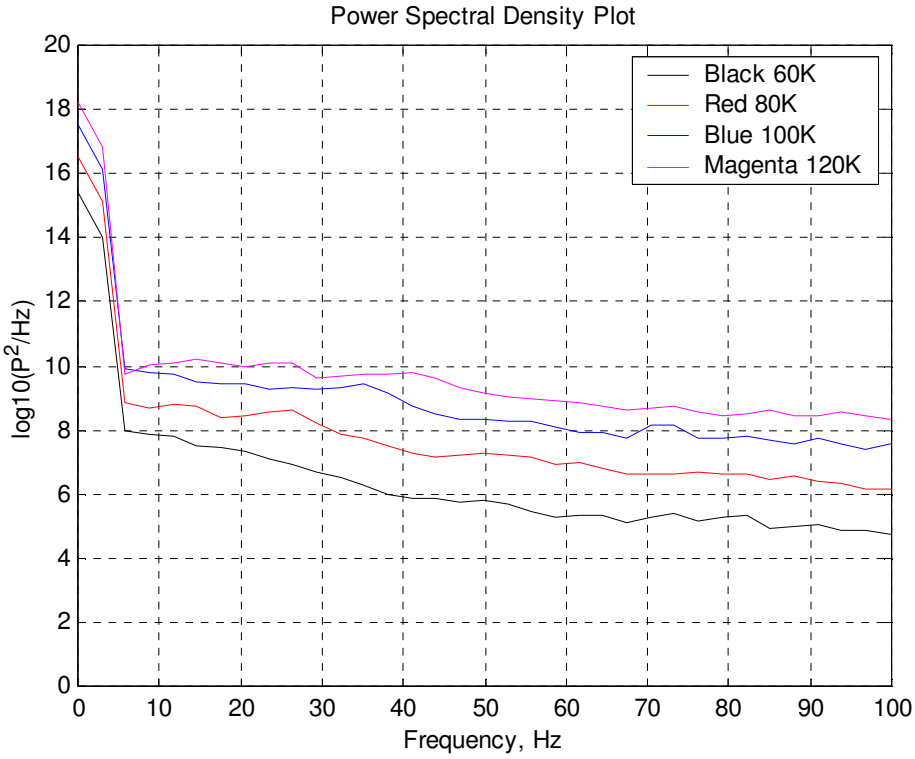

Figure C10: Zoom View of Highest Cprms 0-100Hz

24mm Shroud

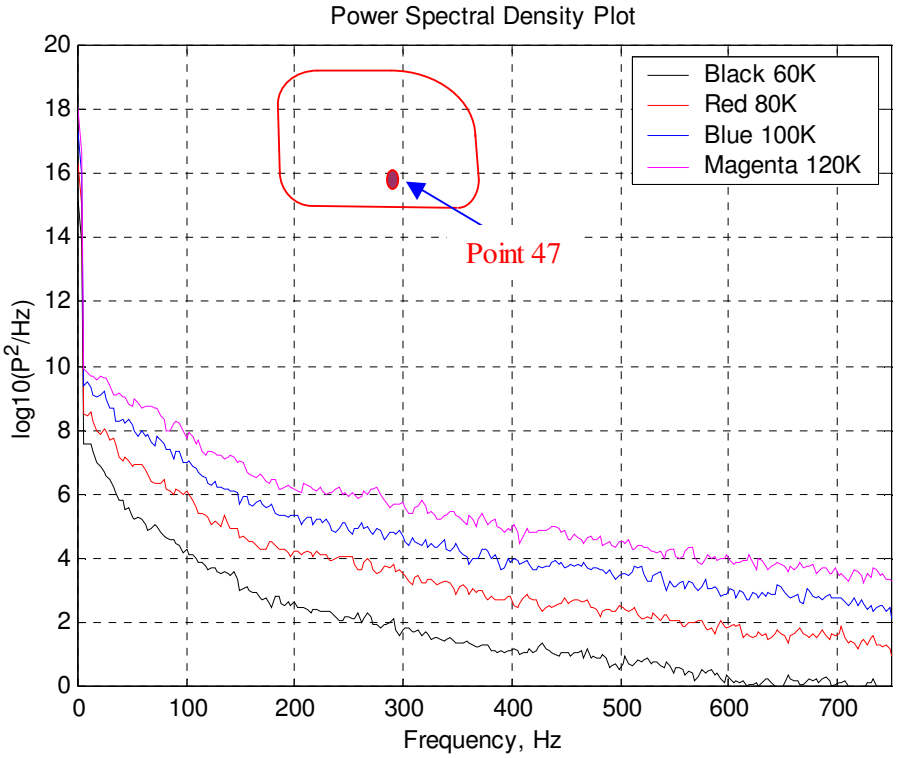

Figure C11: Highest Cprms at Point 47

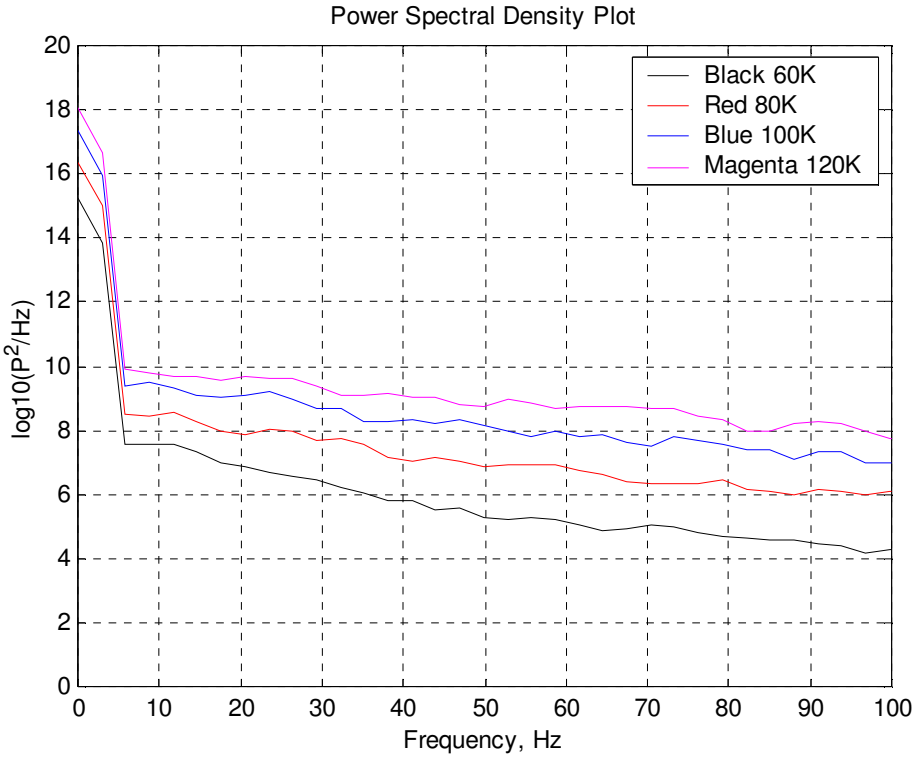

Figure C12: Zoom View of Highest Cprms 0-100Hz

34mm Shroud

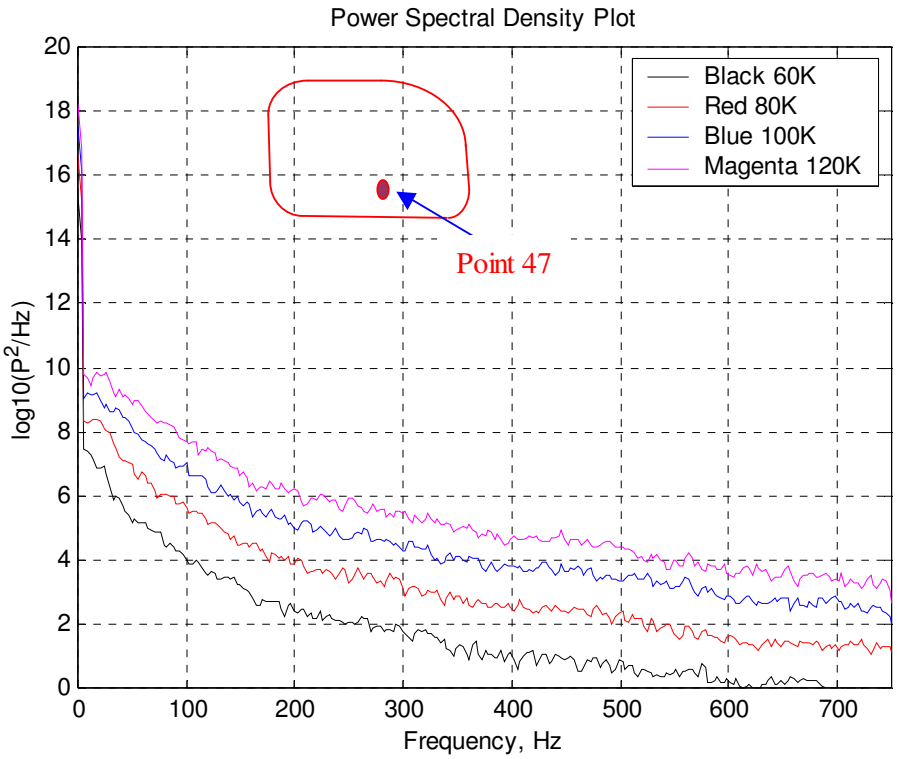

Figure C13: Highest Cprms at Point 47

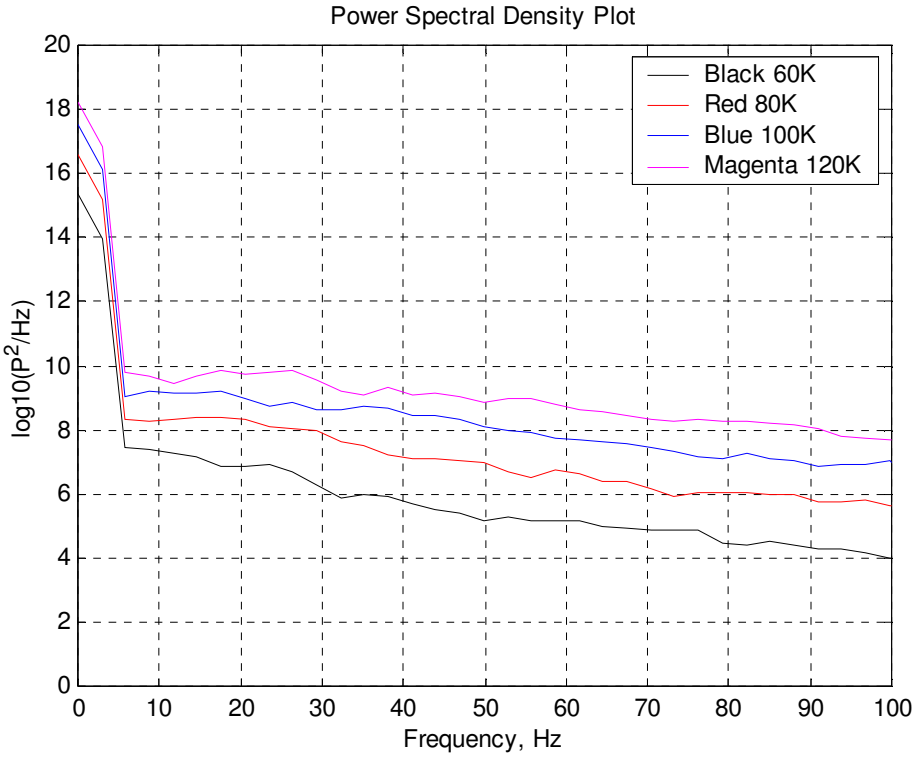

Figure C14: Zoom View of Highest Cprms 0-100Hz

44mm Shroud

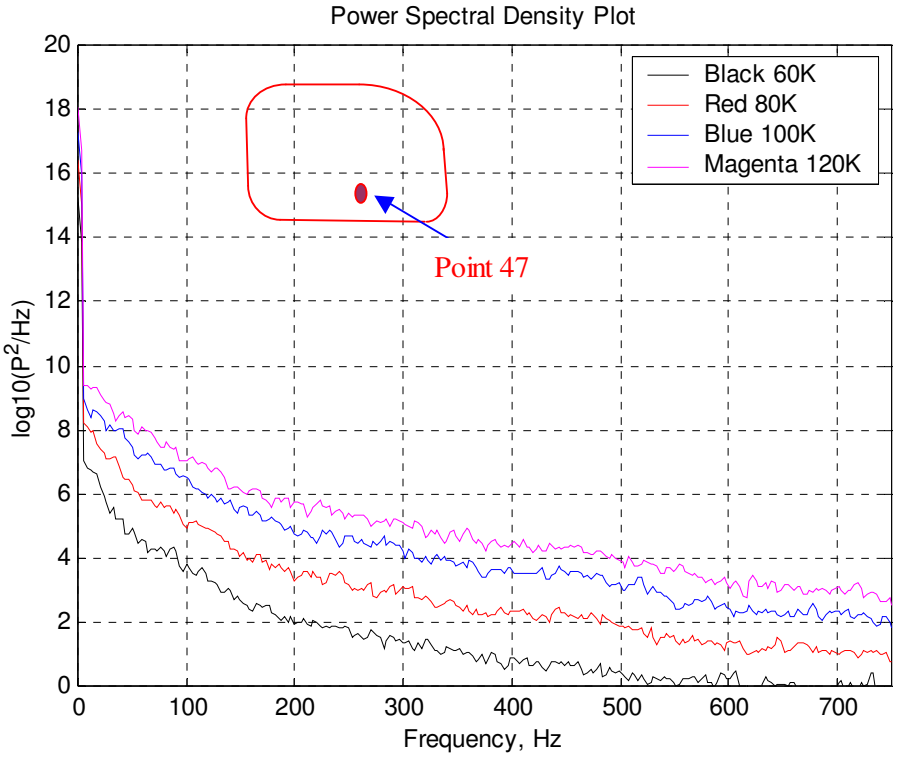

Figure C15: Highest Cprms at Point 47

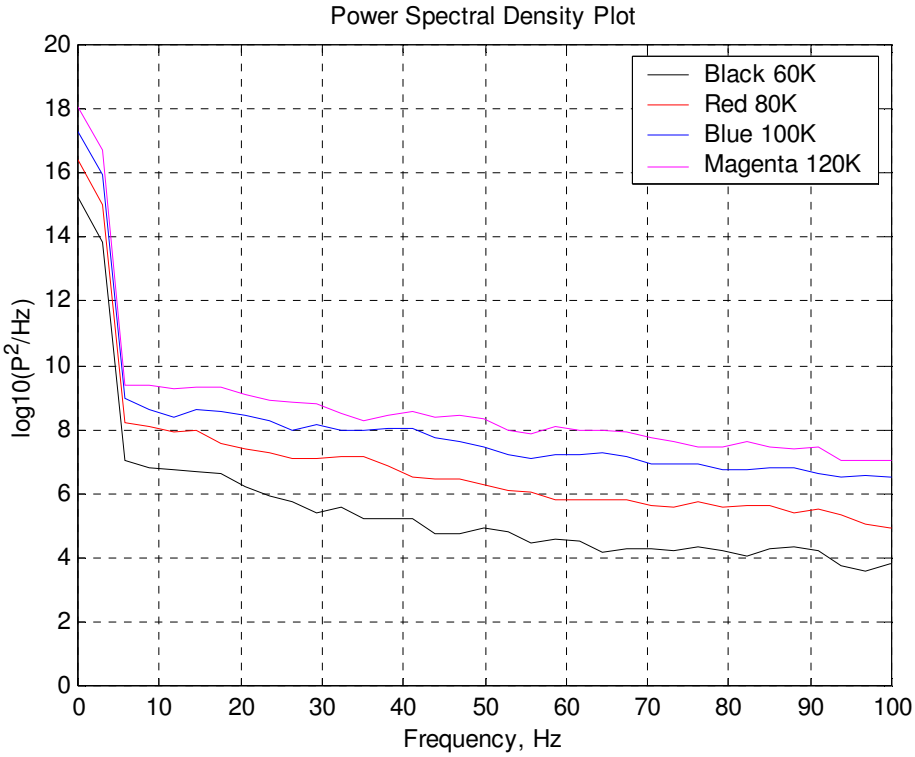

Figure C16: Zoom View of Highest Cprms 0-100Hz

Appendix D

Comments on Calibration and Accuracy

As all experimental work in this research was conducted on quarter model and semi-isolation condition in wind-tunnel, experimental errors will be discussed separately in the next subsection.

D1. Wind Tunnel Tests

During the surface mean and fluctuating pressure measurements using the RMIT Industrial Wind Tunnel random errors might have occurred for a variety of reasons such as location errors, slow changes in tunnel speed. However, these errors can be assessed by degree of data repeatability.

D2. Repeatability of Results

The data was first zeroed in the wind tunnel before test in order to reduce the voltage offset. This was done in order to measure the electrical and electro-magnetic influence due to wind tunnel controllers and power supplies with no physical inputs from the airflow inside the wind tunnel onto the pressure transducers. However, data were acquired several times to check for the repeatability.

D3. Wind Tunnel Speed Errors

During the test inside RMIT Industrial wind tunnel and the air speed was measured with a Pitot static tube connected to the Baratron-reference pressure transducer. It is estimated that there is ±0.9% error involved with the wind tunnel speed

D4. Dynamic Pressure Measurement Systems (DPMS)

Typical characteristics may include: (provided by manufacturer)

- up to 256 channels/module (with a total of 1024 channels/A/D card)
- 0 Hz - several kHz frequency response

- 0.3% FS accuracy over 0° - 50°C
- ±2% accuracy for frequency amplitude (dependant on tube dimensions)

Transducer sensitivity: 300Pa V (nominal)

Transducer Sensitivity: <0.3%

Transducer output range: ± 10V

Linearity and hysteresis: 0.25%

Measured error: ±5.2% (based on minimum measured pressure)

D5. Solid Blockage Correction for Quarter Model

The RMIT Industrial wind tunnel is a closed loop and due to it and presence of tunnel walls causes the flow around the vehicle reduces the area through which the air flows as compared to free flow of air in absence of the quarter model. This is called solid blockage and expressed as the ratio of projected frontal area to the wind tunnel test section area. This blockage can affect the mean static pressure distribution over the surface.

Blockage Ratio of the Quarter Model

Area of Quarter Model (A1) = (0.83* h*w)

Height of car (h) = 1.36

Width of car 0.96 (w) = 1.3056

Total Area of Car (A1) = 1.083648

Area of Wind Tunnel (A0) = 6 m^2

Blockage (E = A1/A0) = 0.180608

$Q = (1+E)^2 = (1+0.180608)^2$

Q= 1.393835

D6. Conclusion on Errors

After careful consideration of relevant error estimation, we can conclude that none of the conclusions made in this work will be affected by any instrumental or procedural errors.

Appendix E

Mirror Housing Surface Mean Pressure Coefficient (Cp)

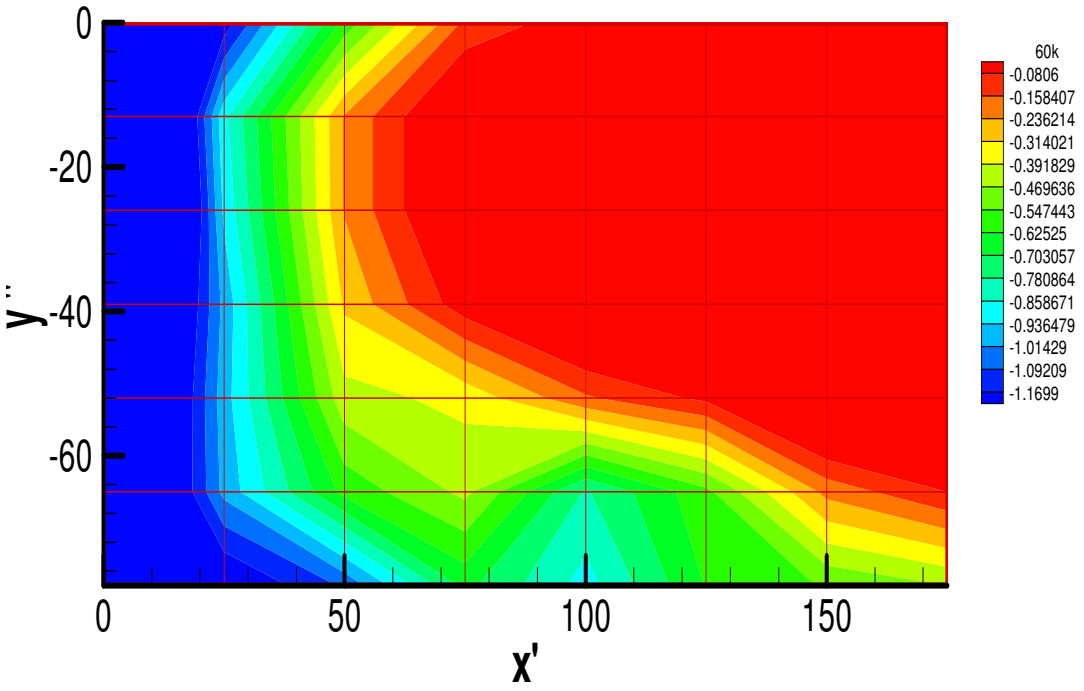

Figure E1: Surface Mean Pressure Coefficient (Cp) for 60 km/h

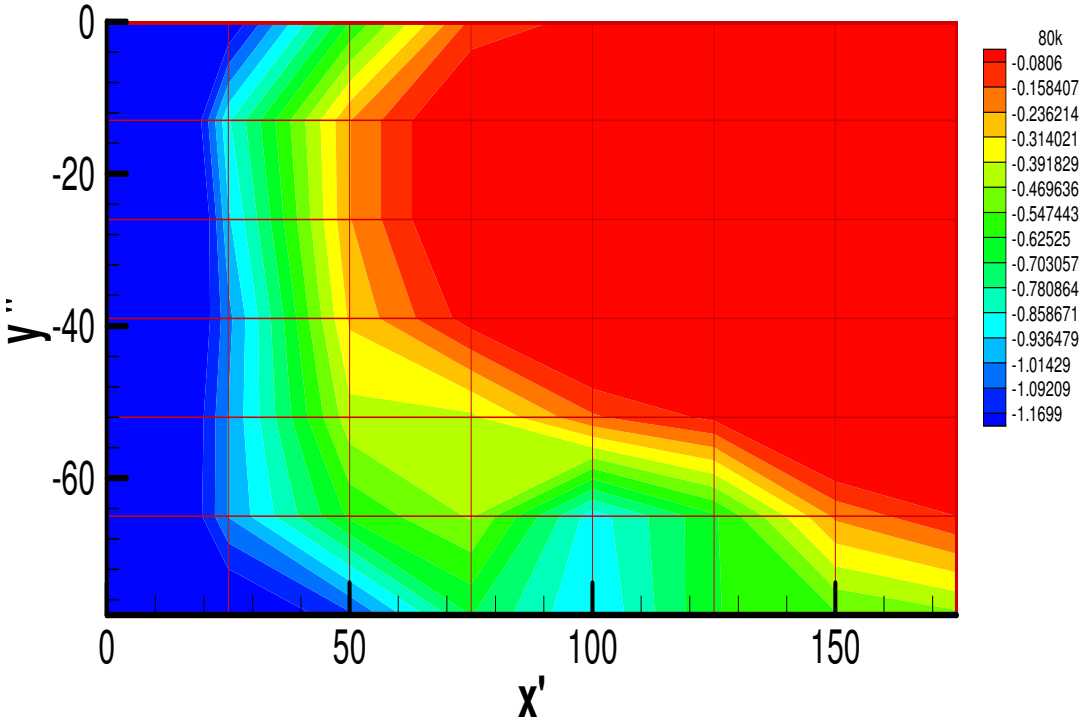

Figure E2: Surface Mean Pressure Coefficient (Cp) for 80 km/h

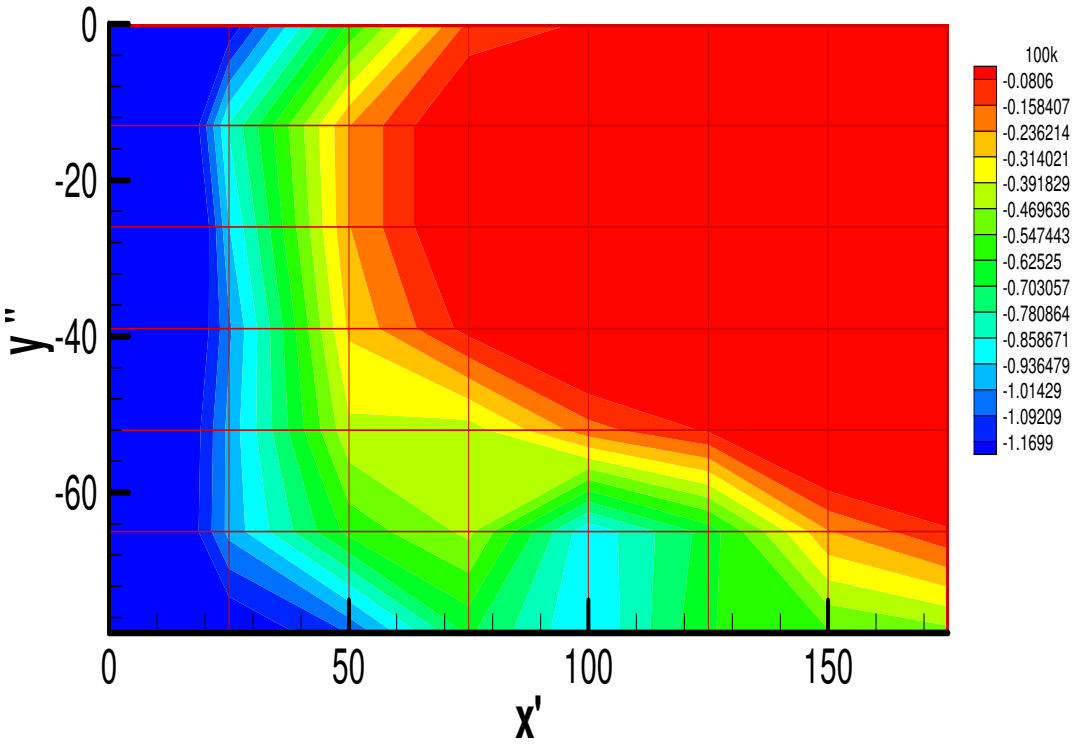

Figure E3: Surface Mean Pressure Coefficient (Cp) for 100 km/h

Appendix F

Surface Mean Pressure Coefficient (Cp)

For Bottom Flange Streamline

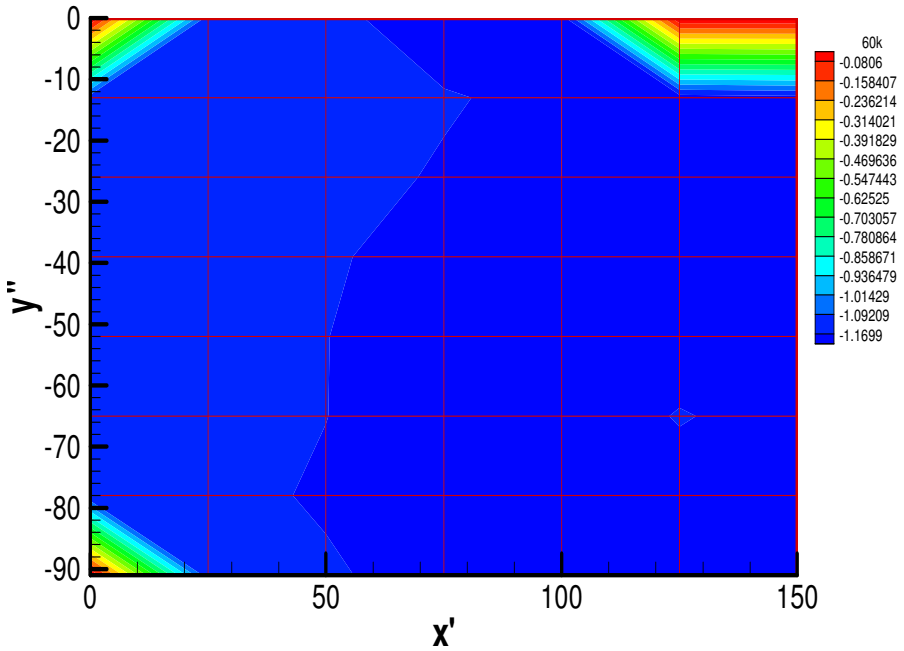

Figure F1: Surface Mean Pressure Coefficient (Cp) for 60 km/h

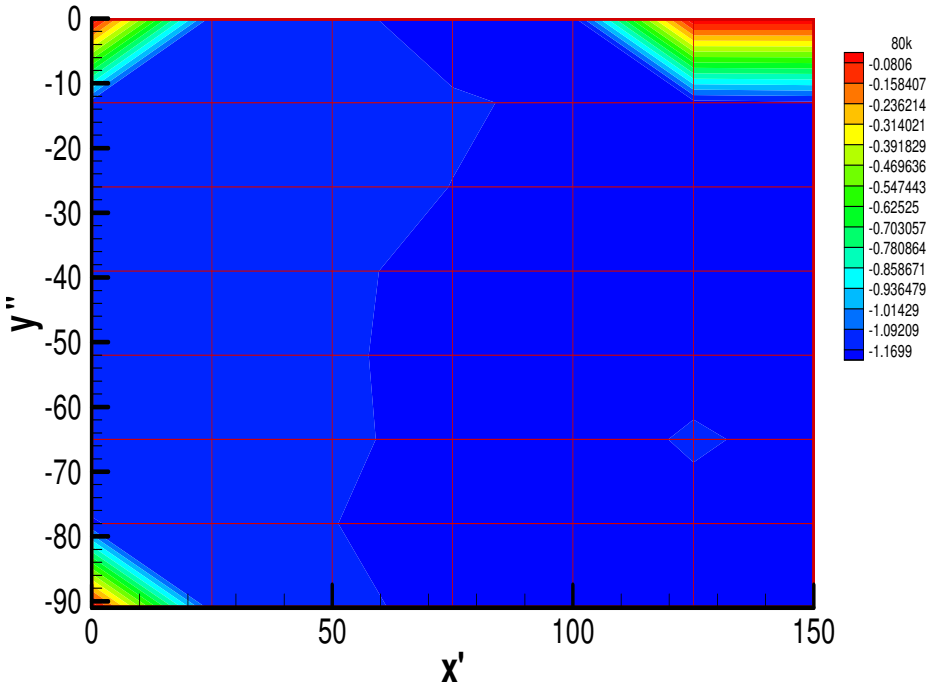

Figure F2: Surface Mean Pressure Coefficient (Cp) for 80 km/h

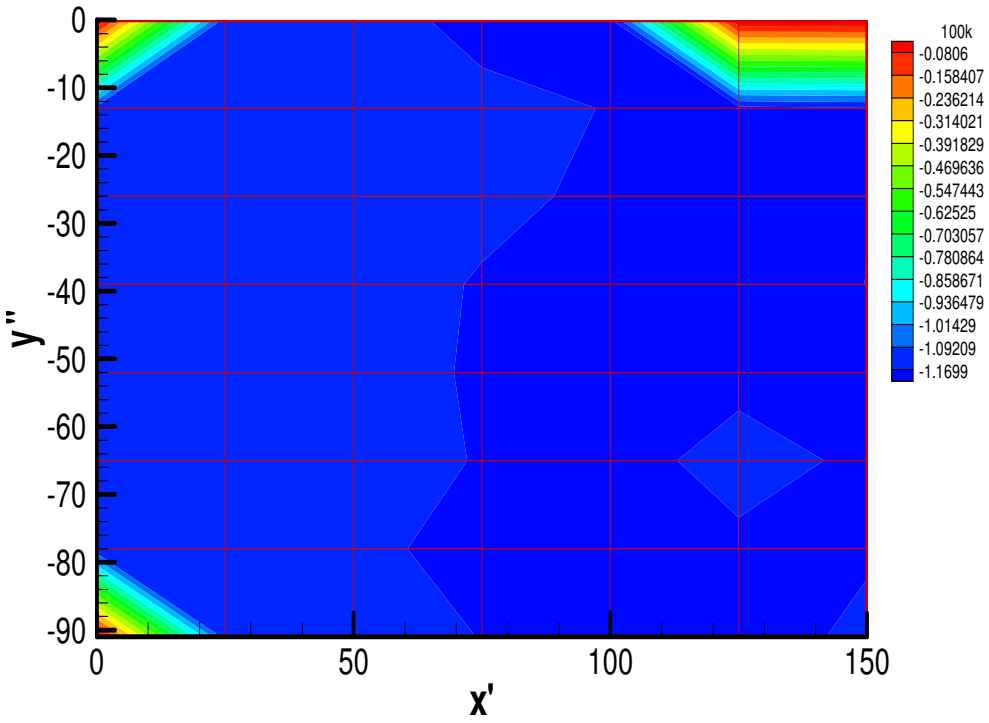

Figure F3: Surface Mean Pressure Coefficient (Cp) for 100 km/h

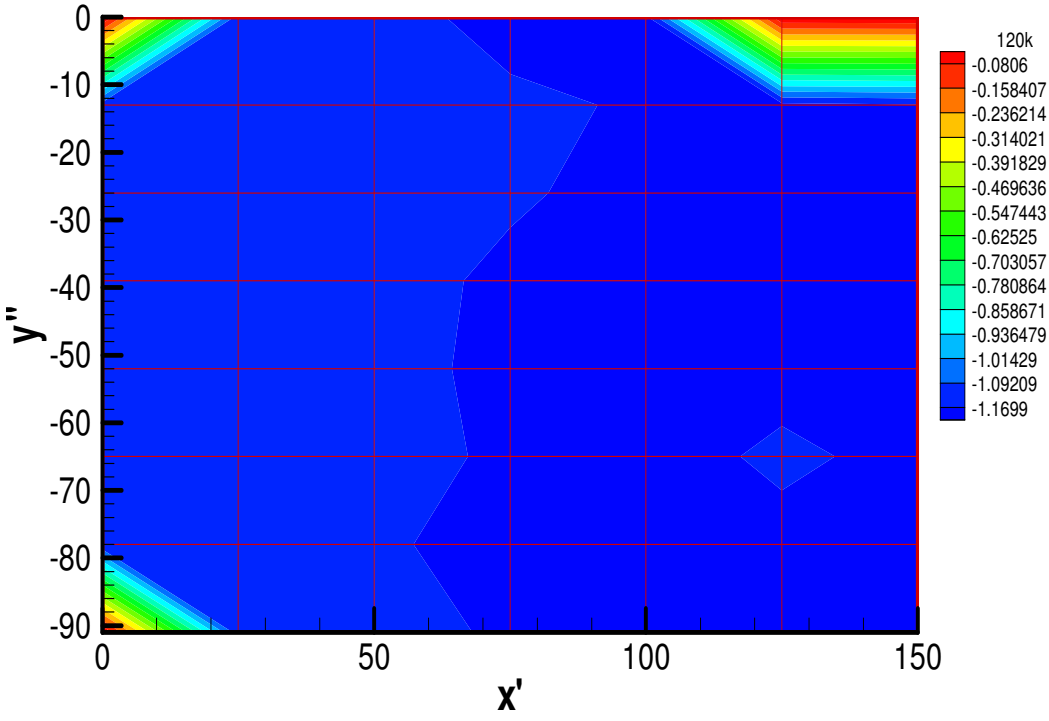

Figure F4: Surface Mean Pressure Coefficient (Cp) for 120 km/h